Investigations into Avian Cornea Development and the Influence of Chondroitin Sulphate Proteoglycans on Keratocyte Phenotype

A thesis submitted to Cardiff University for the degree of Doctor of Philosophy

January 2022

Kiranjit Kaur Bains

Structural Biophysics Group
School of Optometry and Vision Sciences
Cardiff University

Supervisors:

Professor Andrew J. Quantock
Dr Elena Koudouna
Dr Robert D. Young

Advisor:

Dr Matt J. Dunn

Acknowledgements

Firstly, I want to thank my supervisors Professor Andrew J. Quantock, Dr Elena Koudouna, and Dr Robert D. Young. Your support, guidance, and expertise throughout this journey is immeasurable and I am truly grateful for the time and energy you've devoted towards moulding me into a scientist over these past four years.

I would also like to thank all the members of the Structural Biophysics Group, who helped me throughout my studies. In particular, I would like to thank Sean Ashworth for his efforts in purifying chondroitin sulphate substrates and sharing them with me, in addition to his guidance for optimising their use in my experiments. I would also like to thank Dr Philip Lewis for his time and expertise in teaching me how to navigate the Amira-Azizo software.

I am also grateful to Dr Duncan Muir for helping me in the acquisition of SEM images for the developing and adult avian cornea and Dr Graham Bottley for going above and beyond in helping me grasp the fundamentals of flow cytometry, developing an experimental design, and interpreting my data. I would also like to extend my gratitude to Dr Nikita J. Thomas for her help with navigating R and JASP.

Moreover, I would also like to thank Tanyaradzwa J. Mutingwende for being a wonderful friend, you have kept me sane and laughing over the past four years.

Finally, I would like to dedicate this thesis to my family. Your love and support throughout this whole experience has been a true blessing. You have helped me to remain focused and level-headed when experiments and life weren't going my way – your sacrifices have laid the foundation for me to achieve my goals and for that I am beyond grateful. I love you all very much and I am excited to see what new challenges and opportunities will come from this experience.

List of Publications

Bains, K.K., Fukuoka, H., Hammond, G.M., Sotozono, C. and Quantock, A.J. (2019). Recovering vision in corneal epithelial stem cell deficient eyes. *Contact Lens and Anterior Eye* **42**(4), pp.350-358.

Ashworth, S., Harrington, J., Hammond, G.M., **Bains, K.K**., Koudouna, E., Hayes, A.J., Ralphs, J.R. *et al.* (2021). Chondroitin sulfate as a potential modulator of the stem cell niche in cornea. *Frontiers in Cell and Developmental Biology* **8**.

Abstract

In the cornea, a population of stem/progenitor cells is known to reside in the putative limbal stem cell niche. The aim of research described in this thesis, using the avian eye as an experimental model, was to investigate a postulated role for chondroitin sulphate *(CS)* proteoglycans *(PGs)* in regulating the proliferation and differentiation potential of corneal stem/progenitor cells, as previously proposed for articular cartilage.

To investigate the effects of CSPGs on progenitor cells, the thesis presents the first attempts to optimise a protocol for flow cytometric analysis of keratocytes cultured on different CS-based substrates to quantify changes in expression of putative stromal stem cell *(PSSC)* markers which found that the expression profile of PSSC markers changed towards a less-differentiated phenotype.

A novel investigation was also undertaken to characterise the extracellular matrix distribution of CS, in addition to cellular and anatomical features of the avian stem cell niche using immunohistochemistry, scanning electron microscopy, transmission electron microscopy, and serial block-face scanning electron microscopy *(SBF-SEM)*. The avian cornea labelled positively for CS sulphation-specific motifs with variations in regional distribution noted between motifs and developmental stages. Moreover, marked differences were discovered in the presumptive limbal stem cell niche of the avian eye from that in the human, whilst also confirming some shared characteristics. In SBF-SEM serial image 3D reconstructions, distinct undulating projections of epithelium and stroma similar in appearance to palisades of Vogt and limbal crypts were observed. Parts of the presumptive niche were shown to host cells morphologically similar to putative stem cells, have stromal-epithelial cell interactions, and be in close proximity to localised forms of CS. These findings suggest that CS may indeed have a role in regulating the potential of stem/progenitor cells within the presumptive stem cell niche in the avian cornea which could broaden the potential for future applications in tissue engineering strategies.

Table of Contents

List of Figures

List of Tables

Abbreviations

APC	Allophycocyanin
AF	Autofluorescence
BSE	Backscattered electrons
BMP	Bone morphogenetic protein
BSA	Bovine serum albumin
CNS	Central nervous system
CS	Chondroitin sulphate
C4st1	Chondroitin-4-sulfotransferase 2
ChABC	Chondroitinase ABC
CX43	Connexin 43
CESC	Corneal epithelial stem cell
CCSC	Corneal stromal stem cell
CLET	Cultured limbal epithelial transplantation
COMET	Cultured oral mucosal epithelial transplantation
DS	Dermatan sulphate
DMEM	Dulbecco Modified Eagle Medium
D-PBS	Dulbecco's Phosphate-Buffered Saline
eTAC	Early transient amplifying cell
EB	Embryonic bodies
E	Embryonic day
ESC	Embryonic stem cell
ECM	Extracellular matrix
FBS	Fetal bovine serum
FACIT	Fibril-associated collagens with interrupted triple helices
FITC	Fluorescein isothiocyanate
FSP	Focal stromal projection
FSC	Forward scatter
FSC-H	Forward scatter height
FSC-A	Forward side scatter area
Gal	Galactosamine
G6ST	Galactose 6-O sulphotransferase
GlcA	Glucuronic acid
GlcAT-I	Glucuronyltransferase-I
GAG	Glycosaminoglycan
HS	Heparan sulphate
Hep	Heparin
HMDS	Hexamethyldisilazane
hLM	Human limbal melanocyte
HA	Hyaluronan
IdoA	Iduronic acid
Ig	Immunoglobulin
KS	Keratan sulphate
K-SFM	Keratinocyte serum-free medium
LC	Limbal crypt
LEC	Limbal epithelial crypt
LESC	Limbal epithelial stem cell
MedFI	Median fluorescence intensity
MSC	Mesenchymal stem cell
mAb	Monoclonal antibody
GalNAc	N-Acetylgalactosamine
GlcNAc	N-acetylglucosamine
Gn6ST	N-Acetylglucosamine 6-O sulphotransferase
Nsph	Neurosphere
nMedFI	Normalised median fluorescence intensity
OCT	Optimal cutting temperature
PoV	Palisades of Vogt
PFA	Paraformaldehyde
PBS	Phosphate buffered saline
PG	Proteoglycan
PSSC	Putative stromal stem cell
RPM	Revolutions per minute
SEM	Scanning electron microscopy
SHG	Second harmonic generation
SE	Secondary electrons
SEAM	Self-formed ectodermal autonomous multi-zones
RT-PCR	Reverse-transcription polymerase chain reaction
SI	Separation Index
SBF-SEM	Serial block face scanning electron microscopy
P	Serial Passage
Ser	Serine
SSC	Side scatter
SSC-A	Side scatter area
SLRP	Small leucine-rich proteoglycans
SCM	Stem cell medium
SM	Sulphation motifs
TAC	Transient amplifying cell
TEM	Transmission electron microscopy

Chapter 1: Introduction

1.1 The Layers of the Cornea

The cornea is a transparent, avascular tissue layer located along the anterior surface of the eye. Its fundamental roles are to supply two-thirds of the eye's optical power in addition to acting as a protective shield from external dangers such as dust, pathogens, bacteria, and debris (Tsubota et al. 1999; Meek et al. 2003). As seen in Figure *1.1*, this highly specialised structure consists of five distinct layers: a stratified epithelium, Bowman's layer, stroma, Descemet's membrane, and endothelium; all of which are–contiguous with surrounding structures at a junction called the limbus.

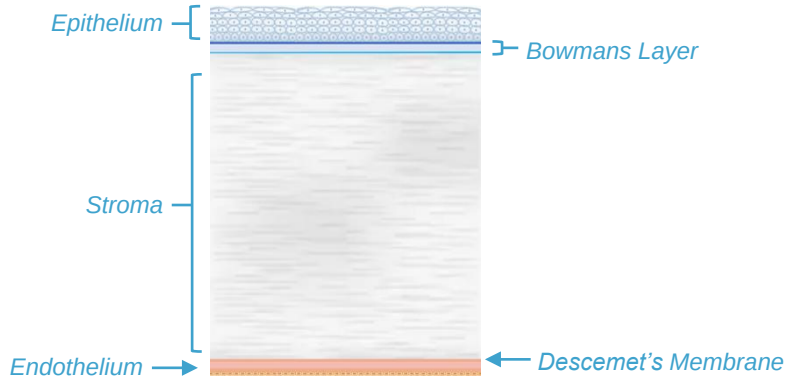

Figure 1.1: Cross-section depicting the five distinct layers of the cornea with the anterior most layer at the top.

1.1.1 Epithelium

The stratified corneal epithelium of non-keratinizing cells constitutes the outermost cellular layer of the eye (Oyster 2006; Kitazawa et al. 2017). Looking closer at the composition of the epithelial layers, the strata are formed of three morphologically distinguishable cells (*basal, wing, and squamous*). The whole of the stratified epithelium is recycled within ten days, starting with the posterior-most epithelial cells *(basal)* migrating anteriorly to become wing cells, before maturing into squamous cells (Wei et al. 1996; Lavker et al. 2003). This recycling of cells is necessary because cell loss across the ocular surface is inevitable due to mechanical and environmental factors, however these desquamated cells are continuously replenished from holoclone limbal epithelial stem cell *(LESC)* colonies residing in the superior and inferior basal zones of the limbal palisades of Vogt *(PoV)* at the transitional zone between the cornea and bulbar conjunctiva (Nishida et al. 1995; Kinoshita et al. 2001; Shortt et al. 2007a). It is within the heavily undulating folds of the LESC niche that stem cell properties are nurtured for the purposes of maintaining homeostasis. Specifically, an

asymmetrical stem cell division aids in self-renewal and production of daughter transient amplifying cells *(TACs)*. With slow cell cycle division taking place, two stem cells are generated with one remaining in the limbal niche to repopulate the stem cell pool**,** while the other cell, an early transient amplifying cell *(eTAC)*, is translocated from the niche in order to subsequently divide into a TAC. As seen in Figure *1.2*, migration occurs superficially from the limbus towards the basal layer of the central cornea. As TACs continue along their path of finite differentiation, they will become post-mitotic, terminally differentiated cells which in turn contribute to the maintenance of corneal integrity (Kinoshita et al. 1981; Tseng 1989; Secker and Daniels 2009).

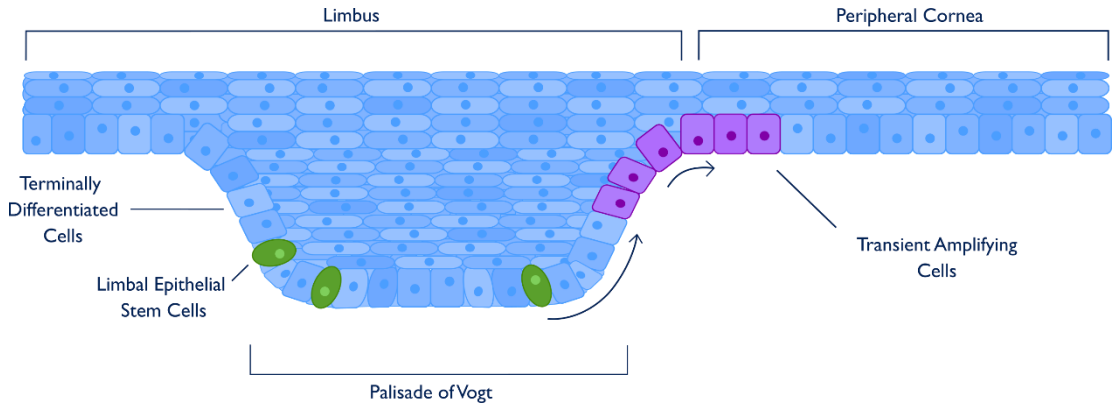

Figure 1.2: Schematic representation of corneal epithelium at the limbal zone. The schematic illustrates the flow of transient amplifying cells migrating out of the limbal Palisades of Vogt towards the central corneal surface.

1.1.2 Bowman's Layer

Subjacent to the epithelium is an acellular band of fibrillar material (*type I, III, and V collagen fibrils)* 8-12 µm thick that naturally acts as a boundary separating the epithelium from the stroma (Nakayasu et al. 1986; Gordon et al. 1994). Functionally, the Bowman's layer is thought to provide a strong attachment point for the epithelium to be able to counter abrasive forces experienced from eyelid interaction and external environmental factors (Gordon et al. 1994; Beuerman and Pedroza 1996; Linsenmayer et al. 1998). However, some researchers also believe it has an adjunct role in inhibiting any potential breach by pathogens into the posterior-most layers of the cornea (Wilson and Hong 2000).

1.1.3 Stroma

The stroma is a highly organised collagenous tissue that contributes to 90% of the cornea's overall thickness (Du and Funderburgh 2010). The complex interactions occurring in the extracellular matrix *(ECM)* between stromal constituents is principally responsible for maintaining the

transparency of the cornea (Komai and Ushiki 1991; Meek and Fullwood 2001; Moller-Pedersen 2004). One of the two major components in the stromal ECM are collagen fibrils which have a diameter of 25-35 nm; these fibrils are regularly spaced and run parallel to each other forming flat lamellae (Komai and Ushiki 1991; Meek and Fullwood 2001). As seen in Figure *1.3*, lamellae are stacked to form a collagen matrix comprised of multiple layers of varying width *(about 0.5-250 μm)* and thicknesses *(about 0.2-2.5 μm)* (Komai and Ushiki 1991). Embedded within the matrix are proteoglycans, macromolecules composed of a "core protein" covalently attached to one or more glycosaminoglycan *(GAG)* chains, that promote stromal hydration to maintain corneal transparency (Komai and Ushiki 1991). The other major ECM component is corneal fibroblast cells *(keratocytes)*, which are responsible for the synthesis of collagen and stromal repair (Muller et al. 1995; West-Mays and Dwivedi 2006; Oyster 2006). Both components will be discussed in greater detail in Sections 1.2.1 and 1.2.2.

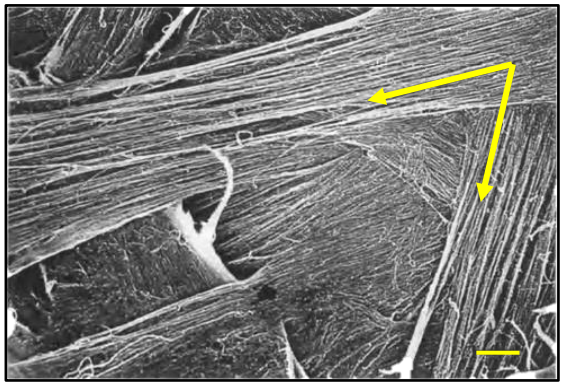

Figure 1.3: Mid-stroma corneal lamellae viewed with scanning electron microscopy. Yellow arrows indicate angled crossing between lamellae. Scale bar = 10 μm. *Taken from:* Meek and Fullwood (2001).

1.1.4 Descemet's Membrane

Interposed between the stroma and endothelium is a thick, basal lamina called the Descemet's membrane (Waring et al. 1982; Beuerman and Pedroza 1996). It is secreted by the endothelium and is therefore, considered to be its basement membrane. The function of this membrane is to provide mechanical strength and it has been found to uniformly increase from 2 μm to 10 μm in thickness with age (Beuerman and Pedroza 1996; Oyster 2006).

1.1.5 Endothelium

The posterior-most layer of the cornea, the endothelium, is a monolayer of hexagonal cells resembling a mosaic with an approximate cell density at birth of 3000 cells/mm^2 arranged in a continuous layer 4-6 μm thick (Vogt 1977; Waring et al. 1982; Oyster 2006). Functionally, the endothelium is responsible for maintaining the movement of aqueous humour throughout the

cornea[1] (Bonanno 2012). Loss of endothelial cells due to age, mechanical trauma, or genetics can disrupt the mechanism leading to oedema, loss of transparency and consequently, impairment of vision (Maurice 1981; Bonanno 2012).

1.2 Corneal Stromal Ultrastructure and Function

1.2.1 Keratocytes

As previously discussed, keratocytes are found within the corneal stroma embedded in the ECM between collagen lamellae (Figure *1.4*). They are a population of quiescent cells arranged sparsely throughout the stroma with an estimated human corneal density between $4.6x10^4$ and $6.2x10^4$ cells/mm^3 (Moller-Pedersen and Ehlers 1995; Moller-Pedersen 1997; Quantock et al. 2010). Through the interactions between their dendritic processes, keratocytes are able to form an active network of intercellular communication spanning the whole of the stromal layer (Muller et al. 1995; West-Mays and Dwivedi 2006).

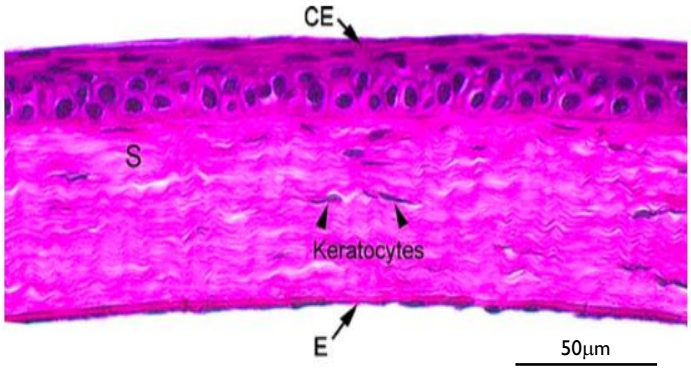

Figure 1.4: Corneal cross-section. Keratocytes are interspersed throughout the stroma *(arrowheads)* between collagen lamellae. Corneal epithelium (CE), Stroma (S), Endothelium (E). *Taken from:* West-Mays and Dwivedi (2006).

1.2.1.1 Origins and Plasticity

Keratocytes are neural crest-derived mesenchymal cells that appear after the formation of the primary stroma[2] in the developing avian cornea (Hay and Revel 1969). There are two waves of mesenchymal cell migrations, the first forming the endothelium and the second resulting in the invasion of cells to populate the primary stroma with presumptive keratocytes. At the stage of

[1] Applying "Pump-Leak" mechanism that utilises active transport in order to facilitate an osmotic gradient that shifts water across the cellular layer leading to hydration and maintenance of corneal transparency.
[2] Day 5 of development (stage 27).

eyelid opening, keratocytes will have entered into G_o phase, withdrawing from the cell cycle and thereby inhibiting complete terminal differentiation (Lwigale et al. 2005; West-Mays and Dwivedi 2006).

Lwigale and colleagues determined that keratocytes were not stem cells, but rather, partially restricted progenitor cells able to maintain plasticity and multi-potentiality (Lwigale et al. 2005). As a result, in the presence of corneal injury, keratocytes have the ability to undergo apoptosis or transition into an "activated" repair phenotype *(fibroblast or myofibroblast[3])* (Wilson et al. 2003; West-Mays and Dwivedi 2006). Specifically, keratocytes adjacent to the wound undergo apoptosis, while neighbouring keratocytes become activated several hours later *(post-wound)* for the purposes of migrating to the site of injury, to repair damaged matrix and replenish the depleted population through mitosis, before reverting to a quiescent state (Wilson et al. 2003; Fini and Stramer 2005; West-Mays and Dwivedi 2006). Studies looking at the turnover rate of keratocytes revealed they did not regularly enter the cell cycle in which DNA repair was initiated, suggesting they could go without replacement for decades in the absence of corneal injury (Giglia-Maria et al. 2011). The benefit of this attribute means the DNA repair response is reasonably controlled to limit the potential of accumulated DNA damage brought on by metabolising processes[4] (Funderburgh 2010; Giglia-Maria et al. 2011).

1.2.1.2 Function

As previously suggested, keratocytes play a key role in facilitating corneal wound healing, but they are also essential for the deposition and maintenance of the stroma in terms of synthesising and secreting matrix elements[5] that preserve the structural integrity and transparency of the cornea (Hart 1976; Hay et al. 1979; Linsenmayer et al. 1983; 1986; Funderburgh et al.1986; Lwigale et al. 2005; Funderburgh 2010). Incidentally, it is the high accumulation of crystallin[6] within keratocytes that is a contributing factor to the cornea's overall transparency (Funderburgh 2010). Indeed, the measured response to localised damage would not be possible without an advanced network of interconnected processes allowing for broad stromal communication to initiate the relevant signalling cascades.

[3] Phenotypic activation in response to disturbance of the corneal basement membrane.
[4] Such as oxidative stress and UV radiation resulting in replication errors and/or uncontrolled recombination leading to loss of genomic integrity (Giglia-Maria et al. 2011).
[5] Keratan sulphate and collagen type I, V, and VI (West-Mays and Dwivedi 2008).
[6] Water-soluble structural proteins that limit light scatter.

1.2.2 Collagen

The mechanical resistance to tensile forces exerted on the cornea is in part achieved by the assembly of collagen fibrils within lamellae sheets. The precise nature and arrangement of the striated collagen fibrils is what allows them to act as the principal load-bearing component of the stroma in addition to being conducive to corneal transparency (Linsenmayer et al. 1998; Meek and Knupp 2015).

1.2.2.1 Structure and Assembly of Collagen Fibrils

There are two characteristics common to all collagen molecules. Firstly, they are composed of three parallel alpha peptide chains[7] (Figure *1.5*) which are wrapped around one another *(with a one-residue stagger)* to form a rope-like structure[8] (Linsenmayer et al. 1998). Secondly, they have a minimum of one domain where the alpha chains are arranged in a triple-helical conformation[9] (Gross 1974; Kuhn 1987; Linsenmayer et al. 1998; Ihanamaki et al. 2004; Gordon and Hahn 2010). Other collagens have a non-triple-helical region incorporated into the terminal end of the molecule, but many also have them interspersed between triple-helical regions resulting in an extension of functional capacity (Linsenmayer et al. 1998; Ihanamaki et al. 2004; Gordon and Hahn 2010).

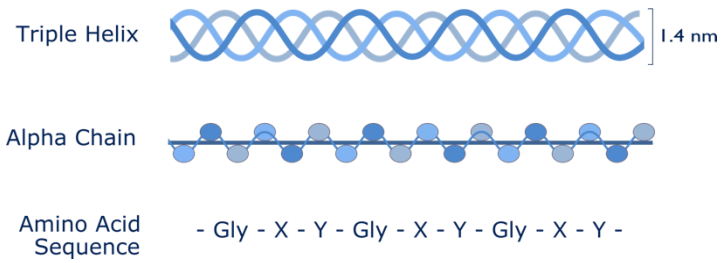

Figure 1.5: Structural breakdown of a collagen microfibril. Each rope-like triple helix molecule *(top)* is comprised of three α-peptide chains *(middle)* which is made up of a specific sequence or repeating amino acids (-Gly-X-Y-) *(bottom)*. Glycine = Gly.

As seen in Figure *1.6*, collagen molecules in the corneal stroma self-assemble in an axially staggered manner to form a collagen microfibril consisting of five molecules which in turn coil together into a 30 nm diameter collagen fibril (Meek and Holmes 1983; Meek and Boote 2004). Overall, each collagen fibril contains about 300-400 triple helical molecules (Meek and Leonard 1993; Holmes

[7] Each of the three chains being a coil itself are collectively wound into a left-handed helix conformation (Linsenmayer et al. 1998).
[8] Right-handed triple helix conformation.
[9] A triple-helical domain is formed of a repeating sequence of glycine, alanine or proline, and hydroxyproline amino acids.

and Kadler 2005; Meek and Knupp 2015). Collagen fibrils within the stroma are the building blocks that form lamellae sheets. In the central cornea of humans, there are approximately 200 lamellae stacked one on top of the other with anterior lamella being thinner *(0.2-1.2 μm thick)* than posterior lamella *(1.0-2.5 μm thick)* (Polack 1961; Komai and Ushiki 1991; Bron 2001; Meek and Knupp 2015). Similarly, each lamella lies angled from its neighbour at approximately 0-90 degrees to create a distinct shift in orientation of collagen fibrils (Meek and Boote 2004). Anatomically, there are differences in lamellae throughout the cornea. Anterior lamellae are characterised as being highly interwoven (Radner et al. 1998, Meek 2009), possessing a 50% greater density than more posteriorly situated layers (Bergmanson et al. 2005; Meek 2009). Posterior lamellae also have less interlacing as a result of greater hydration (Radner and Mallinger 2002; Meek 2009; Meek and Knupp 2015).

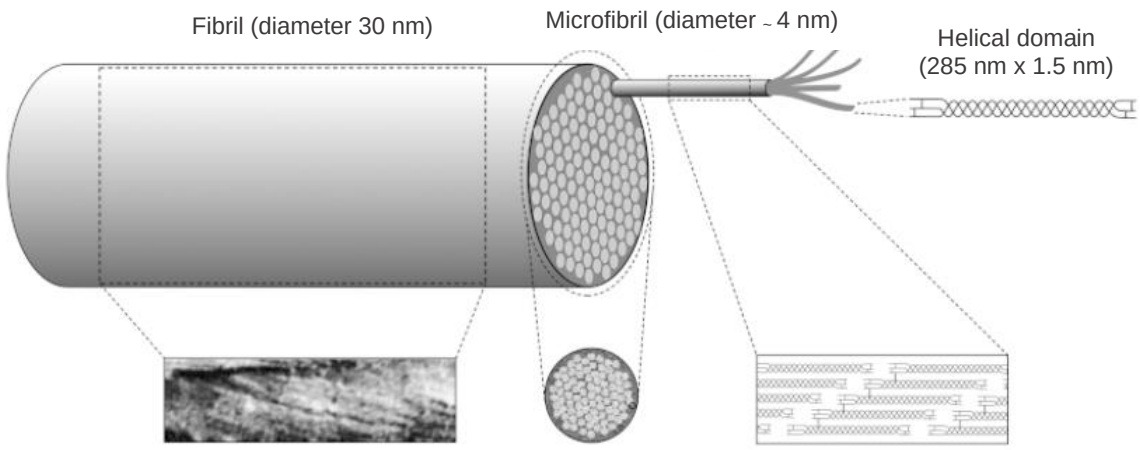

Figure 1.6: Structural hierarchy of a collagen fibril. Triple helical molecules *(top right)* self-assemble in a staggered array *(bottom right)* to form a microfibril consisting of five molecules within its coiled structure. 300-400 microfibrils combine together to form a single fibril with a diameter of 30 nm *(top left)*. *Taken from:* Meek and Knupp (2015).

1.2.2.2 Collagen Types

Using protein and genetic analyses[10], 28 different collagen types have been identified, half of which were documented in the cornea alone (Quantock and Young 2008). By convention, collagen types are numbered to reflect the chronological order of their discovery and are designated with Roman numerals. Table *1.1* categorises collagen into three distinct groups or classes: fibril-forming collagens, fibril-associated collagens with interrupted triple helices *(FACITs)*, and non-fibrillar

[10] Allows for differentiation on the basis of structure, function, size, domain structure, and supramolecular organisation.

collagens, whereas Table *1.2* summarises the different collagen types found thus far in vertebrate corneas (Michelacci 2003).

Table 1.1: Summary of collagen types sub-divided into their respective families. *Adapted from:* Michelacci (2003).

	Collagen Types
Fibril Forming	I, II, III, V, XI
FACIT	IX, XII, XIV, XVI, XIX
Non-Fibrillar	
Short Chain	VIII, X
Basement Membrane	IV
Anchoring Fibrils	VII
Microfibrillar	VI
Other Collagens	XIII, XV, XVII, XVIII, XX, XXI, XXII, XXIII, XXIV, XXV, XXVI, XXVII, XXVIII

Fibril-forming collagen[11] is the most abundant ECM protein of the three categories (Kuhn 1987; Linsenmayer et al. 1998). The domain sequence is composed of over 1000 amino acid residues forming a classic striated collagen structure (Gordon and Hahn 2010). In other words, the arrangement is such that individual molecules are staggered nearly one-quarter in length resulting in a short space between terminal ends of adjacent molecules[12] (Linsenmayer et al. 1998). The resultant spaces allows for the penetration of various enzymes necessary in forming aldehyde-derived crosslinking to stabilise the fibril structure (Linsenmayer et al. 1998). Within the cornea, type I collagen is the most abundant molecular form. Previous reports have shown collagen type I exists as a hybrid *(heterotypic)* assembly with collagen type V such that the minor collagen limits the number of molecules that can self-assemble within the collagen fibril (Birk et al. 1986; Meek and Knupp 2015). For that reason, it is recognised as one of the mechanisms responsible for modulating fibril diameter and in part responsible for regulating collagen fibril formation (Birk et al. 1990).

Unlike fibril-forming collagens, FACIT collagens do not produce fibrils themselves, rather they are cross-linked to the surfaces of fibril-forming collagens and other matrix components at regular intervals to modulate the biomechanical properties of the tissue as a whole (Wu et al. 1992; Wu and Eyre 1995; Linsenmayer 1998). Flexible molecular interactions are a result of the structural

[11] Over 95% of the molecule is a continuous triple helical domain.
[12] Specifically, the NH_2-terminus of one molecule and the COOH-terminus of the other.

configuration of each FACIT molecule[13] which contains one or more surface domains that anchor the molecule to underlying fibrillar collagens[14] while other domains project outwards from the molecule to promote interactions with ECM components or neighbouring collagen fibrils (Wu et al. 1992; Wu and Eyre 1995; Linsenmayer 1998).

Comparatively, nonfibrillar collagen[15], like the ones listed in Table *1.1* are expressed in small quantities to form three-dimensional networks[16] that influence the shape and thickness of type I collagen fibrils and anchor the fibrils to one another and surrounding components (Gordon and Hahn 2010; Yamakoshi 2014). As such, they are a prominent feature within basement membranes, microfibrils, and anchors with notable expression in the corneal epithelium/endothelium *(type IV collagen)* and Descemet's membrane *(type IV and VIII collagens)* (Michelacci 2003; Yamakoshi 2014).

Table 1.2: Summary of different collagen types found throughout the vertebrate cornea. *Adapted from:* Michelacci (2003).

Type	Localization
I	Stroma
II	Developing Stroma *(Epithelium)*
III	Inflammation, wound healing
IV	Basement membranes
V	Stroma
VI	Stroma
VII	Basement Membrane *(Epithelium)*
VIII	Basement Membrane *(Descemet's)*
IX	Developing Stroma *(Epithelium)*
XII	Stroma *(Endothelial origin)*
XIII	Stroma *(Posterior two thirds)*
XIV	Stroma
XVII	Developing Stroma *(Hemi-desmosomes)*
XVIII	Basement Membrane *(Epithelium)*

[13] Each FACIT molecule is made up a pair of conserved cysteine residues separated by four amino acids at the C-terminus in addition to two interrupted triple helices within the repeating disaccharide domain (Fitzgerald and Bateman 2001).
[14] Cross-linked by covalently oxidised lysine residues.
[15] Rich in glycine, proline, and hydroxyproline amino acids that form short, interrupted helical units.
[16] Cross-linked by cysteine disulfide bonds primarily within the C-terminus of the molecule.

1.2.2.3 Corneal Transparency

One of the key characteristics of the cornea is its inherent transparency, which until recent years, was considered to result primarily from the architecture of the collagen fibrils, specifically their uniform diameter and regular spacing between adjacent fibrils (Meek and Knupp 2015). Initial proposals by Maurice (1957) suggested fibrils were embedded in an adherent "ground substance" assumed to have a difference in refractive index causing light scatter. He further ascertained that corneal transparency resulted from the destructive interference of scattered wavelengths that could only be achieved if the collagen fibril arrangement was a lattice formation with uniformity in fibril size (Maurice 1957; Freegard 1997). However, it was determined by Goldman and Benedek (1967) that an exact lattice arrangement of collagen fibrils was not necessary for the cornea to be transparent. In actuality, it was sufficient for just adjacent fibrils to possess short-range order, that is, a fibrillar arrangement that causes deconstructive interference of backwards radiation resulting in only forward radiation being transmitted through the cornea (Lewis et al. 2010; Meek and Knupp 2015).

1.2.3 Proteoglycans and Glycosaminoglycans

Proteoglycans *(PGs)* are a fundamental component of connective tissue, extracellular matrix, and many cell surfaces. They possess a diverse set of biological functions throughout vertebrates; however, within the corneal stroma their primary role is to regulate fibrillogenesis[17] in addition to regulating cellular migration, adhesion, and hydration of the stroma to ensure maintenance of corneal transparency (Hedbys 1961; Scott 1975; Meek et al. 2003). The basic composition of PGs includes a core protein covalently bonded to one or more GAG chains (Michelacci 2003). The chain itself is a heterogenous polysaccharide containing linear repeating disaccharide units known to occupy a large volume of space (Scott 1995; Ho et al. 2014). Moreover, the disaccharide units are made up of a sequence of: (1) an amino acid sugar *(glucosamine or galactosamine (Gal))* and (2) either a galactose or a uronic acid *(iduronic acid (IdoA) or glucuronic acid (GlcA))* (Caterson 2012; Lindahl et al. 2015-2017). Carboxyl and sulphate ester groups are also located at specific sites throughout the GAG chain which confer a highly negative charge to the molecule; this negative charge is what facilitates stromal hydration by drawing water into the collagen architecture (Bettelheim and Plessy 1975; Scott 2001; Ho et al. 2014). Together the structure of the core protein, the composition of the GAG chain, and the distribution of the PGs throughout the ECM

[17] More accurately, proteoglycans provide one of the mechanisms in place to maintain collagen fibril diameter and uniform spacing.

collectively influence the biological activities related to each individual PG (Lindahl et al. 2015-2017).

1.2.3.1 Classification of Glycosaminoglycans

As seen in Figure *1.7*, there are four main subgroups of GAGs found in mammals: keratan sulphate *(KS)*, chondroitin/dermatan sulphate *(CS/DS)*, heparin/heparan sulphate *(Hep/HS)*, and hyaluronic acid or hyaluronan *(HA)* (Caterson 2012). Each subgroup differs with respect to the monosaccharide composition, linkage and variations in stereo-chemical position of carboxyl and sulphate groups on oligosaccharides (Caterson 2012). In the corneal stroma, the primary GAGs, in order of abundance, are KS followed by CS/DS (Blochberger et al. 1992; Dunlevy et al. 2000), both of which belong to the small leucine-rich proteoglycans *(SLRP)* superfamily (Lindahl et al. 2015-2017). The characteristic feature of SLRPs is a repeating leucine residue flanked by cysteine clusters at either side of the central domain (Iozzo 1998; Heinegård 2009; Esko et al. 2009).

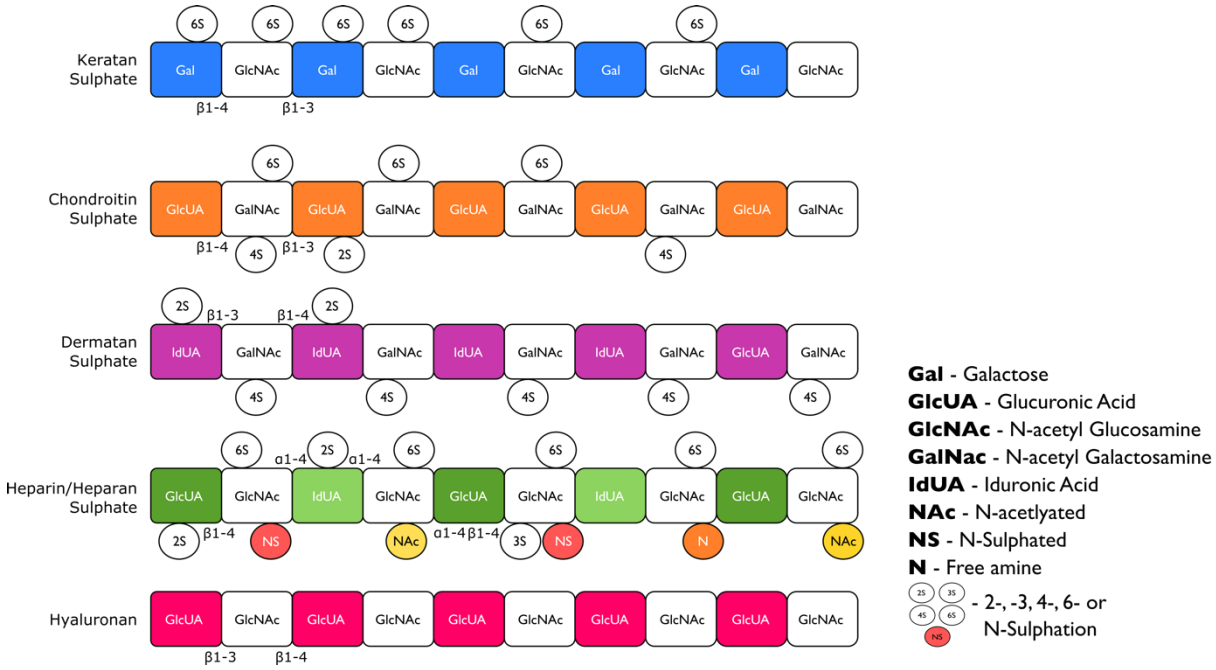

Figure 1.7: Two-dimensional depiction of glycosaminoglycans keratan sulphate, chondroitin sulphate, dermatan sulphate, heparin/heparan sulphate, and hyaluronan. *Adapted from:* Caterson (2012).

1.2.3.1.1 Keratan Sulphate

KS GAGs are predominantly localised within the mature corneal stroma and contribute 50% of the total GAG volume (Suzuki 1939; Funderburgh 2000; Bron et al. 2001; Quantock et al. 2010; Ho et al. 2014). Within the stromal layer, KS is thought to regulate collagen fibril diameter in

addition to maintaining uniform spacing[18] of type I collagen fibrils (Scott and Haigh 1988; Chakravarti et al. 1998; Esko et al. 2009; Akhtar et al. 2010; Quantock 2010). Structurally, KS is a linear polymer of N-acetyllactoasmine disaccharides joined by β1-3 linkages *(lactosaminoglycan)* with sulphation occurring on the 6-carbon of both the sugar moieties (Funderburgh 1986; 2002; Lindahl et al. 2015-2017). In humans, there are two distinct isoforms[19] of KS: (1) KS I, found in but not limited to the corneal stroma, and (2) KS II, found in skeletal tissue (Funderburgh 2000). As seen in Figure *1.8*, KS I is a N-glycan core structure linked to a protein through an asparagine residue, whereas KS II is an O-glycan core structure linked to a protein through a serine *(Ser)* or threonine residue (Funderburgh 2000; 2002; Esko et al. 2009).

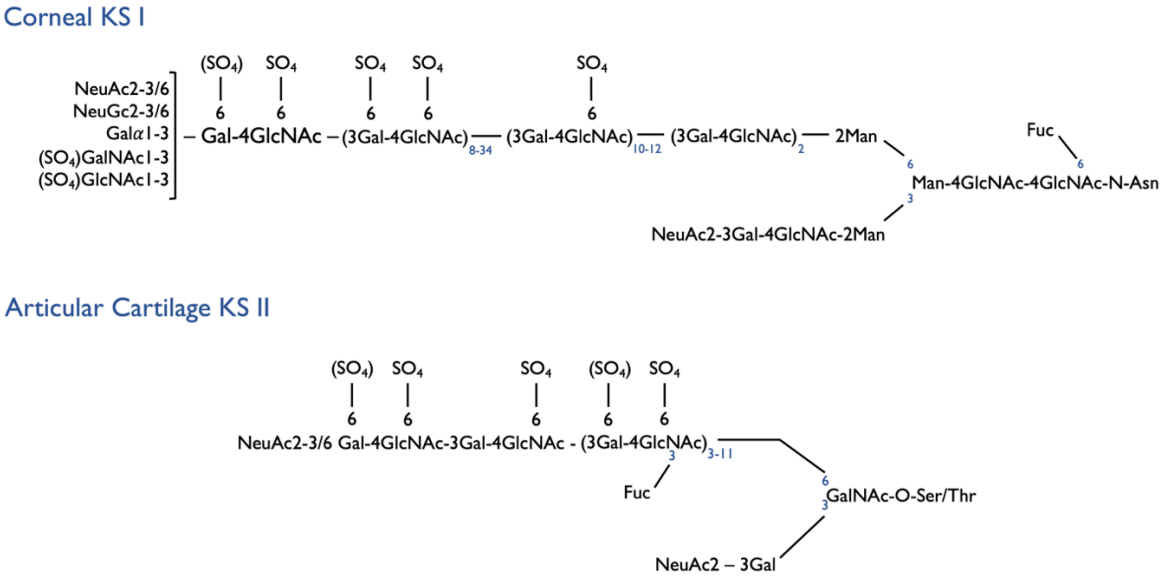

Figure 1.8: Structure of glycosaminoglycans keratan sulphate isoforms I *(corneal)* and II *(articular cartilage).* Ser = Serine, Thr = theronine, Asn = asparagine. *Adapted from:* Funderburgh (2000).

Corneal Keratan Sulphate Proteoglycans

As discussed in Section 1.2.3.1, one of the major GAGs in the cornea is KS; its sulphate chains are linked to core proteins such as keratocan, lumican, or mimecan to form a few of the primary SLRPs found in the corneal stroma (Blochberger et al. 1992; Michelacci 2003). Expression of keratocan, lumican, and mimecan mRNA is not restricted to the corneal stroma, rather it is detected to a lesser extent in other non-ocular regions; with respect to keratocan, it is also expressed in ligaments, cartilage, striated muscles, skin, and arteries (Liu et al. 1998; Dunlevy et al. 2000). Moreover, the molecular mass of keratocan is roughly 38 kDa (Liu et al. 1998) and consists of three major domains: a variable N-terminal region, six conserved cysteine residues, and 11

[18] To prevent scattering of light as it passes through the cornea.
[19] KS isoforms differ in the nature of their structural linkage of oligosaccharides to a core protein.

leucine-rich repeats; it plays an important role in maintaining the transparency of the cornea (Corpuz et al. 1996). Lumican on the other hand is also found in the lungs and kidneys. It has a molecular weight of roughly 40 kDa and structurally is comprised of four major domains: (1) a negatively charged N-terminal consisting of disulphide bonds and sulphated tyrosine, (2) C-terminal domain containing two conserved cysteine residues, (3) 6-10-residue long signal peptide, and (4) leucine-rich repeats (Kobe and Kajava 2001; Nikitovic et al. 2008). It has a supposed functional role in regulating fibril organisation, corneal transparency, and tissue repair. Mimecan, like keratocan and lumican, is extensively expressed in various other tissues like bone and lung as a non-sulphated glycoprotein, however, with respect to stromal composition, mimecan is found in lower quantities than its other two counterparts, with a notably lower molecular weight of 25 kDa (Corpuz et al. 1996; Funderburgh et al. 1997; Cao et al. 2015).

Keratan Sulphate Biosynthesis

KS polymer elongation occurs during the polypeptide synthesis-coupled translocation at the rough endoplasmic reticulum where there is transfer of high-mannose oligosaccharide clusters onto nascent core proteins (Quantock et al. 2010). This bi-antennary core structure uses four substrate specific enzymes to synthesise linear KS-GAG carbohydrates: (1) β1,3-N-acetylglucosaminyltransferase, (2) β1,4-galactosyltransferase, (3) N-acetylglucosamine 6-O sulphotransferase *(Gn6ST)*, and (4) galactose 6-O sulphotransferase *(G6ST)* which transfer a sugar molecule to a non-reducing terminus of the carbohydrate chain (Oeben et al. 1987; Quantock et al. 2010). Sulphation of the KS-GAG is achieved by two sulphotransferase enzymes: corneal Gn6ST and KS G6ST which transfer sulphate onto the 6-O position of N-acetylglucosamine *(GlcNAc)* and Gal, respectively (Fukuta et al. 1997; Akama et al. 2001; Quantock et al. 2010). Both sulphotransferase enzymes exhibit substrate specificity with corneal Gn6ST sulphating the non-reducing terminal GlcNAc, whereas KS G6ST sulphates both the internal and non-reducing terminal Gal (Fukuta et al. 1997; Akama et al. 2002; Quantock et al. 2010).

1.2.3.1.2 Chondroitin Sulphate/Dermatan Sulphate

CS and DS are found to a lesser extent than KS in the corneal stroma. Structurally, CS is primarily composed of repeating sequences of disaccharides *(GlcA and GlcNAc residues)*, whereas in DS, as seen in Figure *1.7,* the repeating disaccharide sequence contains IdoA in place of GlcA. Moreover, proteoglycan chains can be either non-sulphated or differentially sulphated; in the case of CS, sulphation occur across the 4- or 6- position of the Gal unit, whereas, in DS, sulphation occurs at

either the 2- or 4- positions on the Gal unit (Caterson et al. 1990b; Lauder et al. 2000; Lamari and Karamanos 2006; Sugahara and Mikami 2007; Mantovani et al. 2016).

The discovery of non-sulphated and differentially sulphated CS was determined through the use of monoclonal antibodies *(mAbs)* following chondroitinase ABC *(ChABC)* digestion *(mechanism of ChABC discussed in Section 1.2.3.1.2.1)* which enabled the specific recognition of different "native" sulphation motifs/epitopes that make up the CS isotypes (Caterson et al. 1985; 1990; 2012, Hayes et al. 2008). Consequently, these mAbs have since been used to identify spatio-temporal expression patterns of CS sulphation motifs that occur in numerous embryonic/adult tissues and recently, have been utilised to investigate their association within stem/progenitor cell niches (Caterson et al. 2012; Hayes et al. 2008; 2016). Moreover, it has facilitated decades of research that has gone into determining the important and necessary role of CSPGs within the body.

Corneal Chondroitin Sulphate/Dermatan Sulphate Proteoglycans

Decorin and biglycan are the two other main core proteins in the SLRP superfamily to which chondroitin sulphate and dermatan sulphate chains are linked. The difference between decorin and biglycan is that decorin is linked to a single glycosaminoglycan chain on either CS or DS, whereas biglycan is linked to two (Scott 1991; Bock et al. 2001). They both have a diverse number of processes but are mainly responsible for the regulation of collagen fibrillogenesis (Vogel et al. 1984; Reed and Iozzo 2002; Iozzo and Schaefer 2015).

Corneal Chondroitin Sulphate/Dermatan Sulphate Biosynthesis

The polymerization of CS/DS first requires the synthesis of the tetrasaccharide linkage region *(GlcA-Gal-Gal-Xylose)* that bridges the core protein and the chondroitin/dermatan polymer (Calabro et al. 2000; Silbert and Sugumaran 2002). The construction of the oligosaccharide linkage occurs once the core protein is transferred from the rough endoplasmic reticulum to the cis-Golgi, initiating the transfer of xylose, by enzyme xylosyltransferase, onto the hydroxyl group of the core proteins Ser residue to form xylosylserine (Lohmander et al. 1989; Vertel et al. 1993; Calabro et al. 2000). Subsequent formation of the linkage region occurs by sequential addition of sugar residues via galactosyl transferase I/II and GlcA. Chain polymerization is initiated with the addition of an GalNAc residue onto the end of the newly formed linkage region by GalNAc transferase followed by the addition of a GlcA residue by GlcA transferase; thereafter, continued addition of alternate GlcA and GalNAc residues is carried out. DS, a derivative of CS, results from epimerases converting a proportion of glucuronic acid residues in the growing chain to IdoA residues via

epimerization of the five-carbon. Sulphation of distinct locations on the polymer's backbone structure is achieved by multiple sulfotransferases utilising phosphoadenosinephosphosulfate to add sulphoesters to either the 4- and 6- position of GalNAc or both, whereas, for DS, the addition of sulphoesters is done to either the 2- or 4- position of IdoA (Calabro et al. 2000).

1.2.3.1.2.1 Functional and Biological Roles of Chondroitin Sulphate Proteoglycans

Over the past few years, there has been growing interest into the study of CS, specifically in relation to the sulphation motif sequences within the CS chain structure. Overwhelming evidence has shown that CS sulphation motifs are a source of significant biological information to cells and their surrounding environment as they have been shown to interact with a wide spectrum of bioactive molecules like growth factors, cytokines, chemokines, enzyme inhibitors, and structural components within the extracellular milieu – implicating CS in an assortment of signalling pathways that modulate cellular behaviours including proliferation, differentiation, matrix synthesis, migration, and pluripotency (Nandini and Sugahara 2006; Caterson 2012; Hayes et al. 2018). Consequently, through these motif interactions, CSPGs have played a role in the maintenance of growth, morphogenesis, development, tissue remodelling, and disease (Hayes et al. 2018).

Strategies for Assessing Chondroitin Sulphate Proteoglycan Function

Recent literature focussing on both the positive and negative aspects of CSPG expression in various tissue structures has shed light on its biological and functional roles by way of experimental reduction in CS expression or degradation of existing CSPGs to induce observable changes to the system *(i.e., disease or injury)*; a small sample of said literature has been summarised in Table *1.3* to provide insight into the diverse role of CS in vertebrates (Haylock-Jacobs et al. 2011).

The strategies used to reduce the amount of complete CSPG released into the media is achieved by way of inhibitors targeting the glycosaminoglycan side chains (Schwartz 1977; Haylock-Jacobs et al. 2011). In brief, this is done by:

(a) Utilising an analogue *(i.e., fluorinated glucosamine)* which acts to inhibit an enzyme necessary for the elongation of the polysaccharide chains. (Nigro and Wang 2009; Haylock-Jacobs et al. 2011)

(b) Using xylose-conjugated organic molecules *(i.e., xyloside)* to interfere with GAG synthesis machinery from attaching the polysaccharide chains to the CSPG core protein. (Silbert and Sugumaran 2002; Schwartz 1977; Victor et al. 2009; Haylock-Jacobs et al. 2011)

Similarly, a more direct approach to altering the function of CSPG is accomplished by using ChABC, a bacteria-derived enzyme that acts by cleaving the CS disaccharides from its core proteins which in turn prevents the necessary interactions with receptors (Campbell et al. 1990; Bradbury et al. 2002; Haylock-Jacobs et al. 2011). The benefit to this strategy is that it can alter CSPGs already excreted into the ECM, making it the most common method used to degrade CSPGs, whereas xyloside is the preferred method for inhibiting CSPG biosynthesis (Duan and Giger 2010; Haylock-Jacobs et al. 2011). The subsequent section will delve deeper into a few selected studies that used an assortment of tissue sources to substantiate the biological roles of CSPGs.

Table 1.3: The negative and beneficial roles of chondroitin sulphate proteoglycans in various pathologies. *Adapted from:* Haylock-Jacobs et al. (2011).

Negative Roles of Chondroitin Sulphate Proteoglycans		**References**
Arthritis	▪ Breakdown of aggrecan leads to irreversible ECM loss and chronic disability.	(Flannery et al. 1992; Sandy et al. 1992; Caterson et al. 2000; Huang 2008)
	▪ Breakdown is mediated by ADAMTS proteins.	(Stanton et al. 2005; Song et al. 2007)
	▪ Anti-aggrecan cell-mediated immune response.	(Panayi et al. 1992; Angyal et al. 2010)
CNS Trauma	▪ Highly expressed in glial scar.	(Tang et al. 2004; Sandvig et al. 2004;)
	▪ Block axonal regeneration.	(McKeon et al. 1991; Davies et al. 1997; Jones et al. 2003; Sandvig et al. 2004; Galtrey and Fawcett 2007)
	▪ Increase collapse of growth cones.	(Monnier et al. 2003; Gopalakrishnan et al. 2008)
Immunity	▪ CSPGs bind chemokines *(homeostatic and pro-inflammatory).*	(Petersen et al. 1998; Hirose et al. 2001)
	▪ CSPGs can bind to and activate CD44.	(Kawashima et al. 2000; Rolls et al. 2008a)
	▪ CSPGs can interact with cell trafficking molecules *(L- and P-selectin).*	(Kawashima et al. 2000)
Multiple Sclerosis	▪ Present at edges of multiple sclerosis lesions.	(Sobel and Ahmed 2001)
	▪ CS GAGs ↑ Th1 and Th17 differentiation and worsen experimental autoimmune encephalomyelitis.	(Rolls et al. 2006; Zhou et al. 2010)
Beneficial Role of Chondroitin Sulphate Proteoglycans		
CNS Trauma	▪ CSPGs can regulate microglia and enhance a regulatory phenotype at early time points post spinal cord injury	(Rolls et al. 2008b; Rolls et al. 2009)
Multiple Sclerosis	▪ CS disaccharides ↓ T cell migration and encephalomyelitis pathogenesis.	(Rolls et al. 2006; Zhou et al. 2010)

1.2.3.1.2.2 Chondroitin Sulphate Proteoglycan Function in Other Biological Tissues/Systems

As alluded to earlier, there have been many experimental studies conducted to show the potentials of CS throughout the body. Evidently, there appears to be a skew towards investigating the biological/functional roles of CS in the central nervous system *(CNS)*, possibly due to a spike in interest over the last few decades with regards to enhancing our understanding of neurodegenerative disease. Nevertheless, this section will provide an overview of selected literature, justifying the relevance and importance of this thesis topic.

Central Nervous System

Cells in the nervous system are broadly categorised into two groups: glial cells and neuronal cells. Some CSPG isotypes are expressed only by a single cell group whereas others are expressed by both. For example, *NG2*, a typical glial CSPG is expressed by oligodendrocyte progenitor cells in the CNS (Nishiyama et al. 1996; Levine et al. 1996; Oohira et al. 2000), whereas neurocan is secreted mainly by neuronal cells (Engel et al. 1996; Oohira et al. 2000). In contrast, phosphocan is produced by both glial cells (Engel et al. 1996; Canoll et al. 1996; Oohira et al. 2000) and neural cells (Shintani et al. 1998; Oohira et al. 2000); suggesting that CSPGs have a spatiotemporal expression pattern that involves it in various developmental events in the brain.

Neurocan has been found to have a high affinity for binding with molecules, such as:

- ***Growth Factors:*** bFGF (Milev et al. 1998b) pleiotrophin/HB-GAM and amphoterin (Milev et al. 1998a; Oohira et al. 2000).
- ***Cell Adhesion Molecules:*** TAG-1/axonin-1 (Milev et al. 1996; Oohira et al. 2000), and N-CAM/ Ng-CAM/L1 (Friedlander et al. 1994; Oohira et al. 2000).
- ***ECM Glycoproteins:*** tenascin-R (Aspberg et al. 1997; Milev et al. 1998a; Oohira et al. 2000), and tenascin-C (Grumet et al. 1994; Oohira et al. 2000).

Similarly, as in the case of phosphocan, a high affinity for binding exists with molecules such as:

- ***Growth Factors:*** pleiotrophin/HB-GAM (Maeda et al. 1996, Milev et al. 1998a; Oohira et al. 2000), midkine (Maeda et al. 1999; Oohira et al. 2000), amphoterin (Milev et al. 1998a; Oohira et al. 2000), and bFGF (Milev et al. 1998b; Oohira et al. 2000)

- ***Cell Adhesion Molecules:*** TAG-1/axonin-1 (Milev et al. 1996; Oohira et al. 2000), N-CAM and Ng-CAM/L1 (Milev et al. 1994; Oohira et al. 2000), contactin/F11/F3 (Peles et al. 1995; Oohira et al. 2000)
- ***ECM Glycoproteins:*** Tenascin-C (Grumet et al. 1994; Oohira et al. 2000), and tenascin-R (Grumet et al. 1994; Xiao et al. 1997; Oohira et al. 2000)

Suggesting the CS moieties in these two major nervous tissues are involved in modulating, to some degree, cellular events including pathfinding in brain development, cell proliferation, migration, adhesion, and neurite outgrowth (Oohira et al. 2000).

The inferences drawn from studies pre-dating the 21st century have therefore, established a foundation for future investigators to strive to provide supporting data experimentally. With this in mind, Ida and colleagues set out to investigate the location and functional roles of CSPGs in the brain primordium by excising the telencephalon region of a mouse foetus via mechanical dissociation, with the aim of forming a single-cell expansion of floating neurospheres *(Nsph)* in culture (Ida et al. 2005). Immunohistochemical analysis found nestin-positive expression *(a marker of neural/stem progenitor cells)* and an abundance of CS throughout the cerebral tissue, specifically, neurocan, phosphocan, and NG2 – indicating a niche of neural stem/progenitor cells containing these brain-specific CSPGs. Experimental treatment of samples with ChABC to digest CS isotypes of varying sulphation *(4-O-sulphate, 6-O-sulphate, and 4,6-O-disulfate)* resulted in evident loss of brain-specific CS immunoreactivity *(as expected)*; suggesting that neural stem/progenitor cells have a role in synthesis and deposition of CS into their surrounding niche (Ida et al. 2005; Canning et al. 2015; Tribble et al. 2018). Furthermore, to clarify the functional role of CS, its effect on cell proliferation was examined by comparing growth of neural stem cells in the presence of various GAGs such as HA, KS, and highly sulphated CS; results found that CS potentiated the activity of proliferation by about 20% more than controls, whereas, HA and KS did not exert an effect on the growth of neural stem cells – thus demonstrating for the first time that CS can modulate the growth of neural stem/progenitor cells at an early developmental stage (Ida et al. 2005).

Similarly, a study conducted by Sirko et al. (2007) investigated the role of CS-GAGs in the regulation of growth and differentiation factors for neuronal stem cells. This was done by treating isolated embryos from pregnant mice in a defined media containing growth factors to facilitate the formation of Nsph culture suspensions; parallel sets were also treated with ChABC. This resulted in the compromised generation of Nsphs with almost complete settling of Nsphs onto the

substrate of the culture dish. Parallel experiments were performed using keratanase, a KS digesting enzyme, to assess the resultant effects on Nsph formation and adherence; compared to the control, Nsph formation was indistinguishable, forming no adherence with underlying substrate. These findings suggest that CS-GAGs are necessary for the maintenance of Nsphs in a free-floating state as well as the neural stem/progenitor cell niche. Furthermore, two independent investigations were undertaken to assess ChABC on neurogenesis and gliogenesis. Results demonstrated that when immunoselected Nsph cell populations containing radial cells were cultivated in ChABC-containing medium, a significant decrease in neurogenesis in both cortex and stratum derived Nsphs was observed (Sirko et al. 2007). Furthermore, there was a proportional increase in the number of astrocytes, supporting the idea that CS-GAGs are crucial components involved in proliferation and lineage determination of neural precursor cells (Sirko et al. 2007).

Likewise, Izumikawa et al. (2010) generated glucuronyltransferase-I *(GlcAT-I)* knock-out mice by gene targeting to inhibit the synthesis of CS and HS in early embryogenesis. GlcAT-I was used to diminish the synthesis of CS as it initiates the formation of CS disaccharide chains. Results showed that without the presence of CS, embryos died before the eight-cell stage due to failure of cytokinesis. Furthermore, two-cell embryos were independently treated with chondroitin sulphatase leading to death of 67% samples between two-cell and eight-cell stages. Collectively, these results indicate that CS is involved in controlling embryonic cell division and cytokinesis (Izumikawa et al. 2010). Izumikawa and colleagues went on to use the same knock-out model to determine the role of CS in mouse embryonic stem cell *(ESC)* self-renewal and differentiation. Controls were able to form embryonic bodies *(EBs)*, showing upregulations of key markers in all three germ layers: endoderm (*Gata4*), ectoderm (*Nestin*), and mesoderm (*Tbx6, Foxc1, and Brachyury*). Also, the downregulation of pluripotent genes such as Nanog and Oct4 was observed. In contrast, the GlcAT-I knock-outs showed none of the germ layer markers and were able to maintain high expression of *Nanog* and *Oct4*. In summary, CS is required to maintain the pluripotency of ESCs and promote initial ESC commitment to differentiation *(*Izumikawa et al. 2014).

Cartilage

Cartilage, like cornea, a collagen-rich material, is a highly specialised tissue responsible for bearing compressive loads in joints (Watanabe et al. 1998). Similar to the studies done to investigate the role of CS in the CNS, there has also been an increase in desire to understand the role of CS in cartilage as a result of increased incidence of severe joint disorders like osteoarthritis stemming from cartilage's limited repair capacity (Watanabe et al. 1998; Sakai et al. 2007). Previously,

Dowthwaite et al. (2004) reported the existence of chondroprogenitor cell populations within the surface of articular cartilage. With this, Matsumoto et al. (2006) went on to discover the presence of versican aggregates, minimally sulphated CSPGs, within that cartilage region (Dowthwaite et al. 2004; Matsumoto et al. 2006).

Using this knowledge, Klüppel et al. (2005) went on to implement a gene knock-out model for bone morphogenetic protein *(BMP)*-induced chondroitin-4-sulfotransferase 2 *(C4st1)*; responsible for encoding the enzyme tasked with sulphation of 4-O-position in CS. Analysis of the cartilage growth plate in mutant mice showed that loss of *C4st1* resulted in abnormal localization of CS, leading to the upregulation of TGF-β signaling *(important for cartilage morphogenesis)*, and down-regulation of BMP signaling *(responsible for regulating hypertrophy and chondrocyte proliferation)*. These defects caused abnormal chondrocyte orientation within the growth plate, leading to disturbance in plate morphogenesis as well as leading to abnormal chondrocyte differentiation. Specific isotypes of CS were thus shown to be required for appropriate CS localisation, modulation of signaling pathways, and growth plate morphogenesis within the stem/progenitor niche (Klüppel et al. 2005).

Furthermore, a study by Sauerland et al. (2003) sought to show how structural alterations of CS could result from accumulated impact on load bearing joints, mimicking a phenomenon that occurs during aging. One of two sets of tissue was subjected to cyclic compressive pressure whereas the other was not, serving as a control. In the final hours of the experiment, samples were radiolabelled, and full-thickness cartilage explants were removed from the weight-bearing area of the articulating cartilage discs. Explants were then treated with ChABC enzyme and samples were analysed using high-performance anion-exchange chromatography. It was determined that accumulated mechanical loading had an effect on synthesis of highly sulphated CS, but not minimally sulphated. Also, intermittent cycles of mechanical loading appeared to elongate the CS chain. These findings provide evidence that compressive stress on articular cartilage can impact the normal composition of CS in the ECM. With the observable decrease in highly sulphated CS, an overall drop in net-negative charge can be inferred, which can heavily wain on CS's ability to draw in water, which can in turn compromise the resilience cartilage needs to sustain compressive loading. Overall, this suggests a possible link between CS and the development of degenerative joint disease, as well as implicating CS as a key player in maintenance of cartilage function (Sauerland et al. 2003).

1.2.3.1.2.3 Chondroitin Sulphate Proteoglycans in Therapeutics

As pointed out earlier, there has been a growing interest in developing our understanding of both the functional and biological roles of CS to serve as a catalyst for potential application in therapeutics. CS has been implicated in an assortment of modulated signalling pathways that make it a player in proliferation, differentiation, and matrix synthesis, to name a few (Hayes et al. 2018). This section will summarise articles that illustrate the direction and future of therapeutic as a result of investigative interest in CSPGs.

Central Nervous System Disorders

Growing knowledge about the role of stem cells and the mechanisms that govern their proliferative and differentiation potential, coupled with research about CSPGs, has led to avenues of investigation via niche-modifications to aid in the regeneration of morphological and functional properties of the CNS (Sato and Oohira 2009). As shown previously, CS is involved in the proliferation and neurogenesis of neural stem/progenitor cells. As in the case of Parkinson's disease, a neurodegenerative disease resulting in the progressive loss of dopamine containing neurons, treatment strategies have focused on restoration deficiencies by transplant therapy of human fetal mesencephalic tissue rich with dopamine neurons. On the whole, treatment outcomes have been variable and the problem of insufficient tissue samples available for transplantation still remains to be solved, to enable assessment with large cohorts of patients (Sato and Oohira 2009). Recently, there has been a rise in the number of studies aiming to enhance the number of dopamine neurons generated by stem cells. Parish et al. (2008) were able to expand and culture mice ventral brain neurospheres with specific growth factors, which when transfected with Wnt5a and transplanted into Parkinson's disease mice showed a 10-fold increase in dopamine neurons with notable functional recovery (Parish et al. 2008; Sato and Oohira 2009).

Similarly, in the case of multiple sclerosis, where there is a systematic demyelination of neurons, several studies have gone on to address the benefits of administering CSPG in affected areas throughout the CNS. For example, Sobel and Ahmed (2001) showed that when a CSPG GAG disaccharide breakdown product was administered to experimental autoimmune encephalomyelitis afflicted mice, they exhibited a reduction in clinical disease scores; however, the exact mechanism for this finding remains to be elucidated (Sobel and Ahmed 2001; Haylock-Jacobs et al. 2011).

In relation to spinal cord injury, an upregulation of CSPGs at various sites of injury were identified as disadvantageous for the promotion of axonal regeneration (McKeon et al. 1991; Davies et al.

1997; Jones et al. 2003; Yick et al. 2003; Galtrey et al. 2007; Haylock-Jacobs et al. 2011). Its non-permissive nature was explored further by Yick et al. (2003) who reported the effects of ChABC on the axonal regrowth of Clarke's nucleus, the intermediate zone of the spinal cord. They found that in neonatal and adult rats, ChABC digestion at sites of induced injury promoted the regeneration of neurons by 8.3% and 12.3%, respectively (Yick et al. 2003). Their follow up study was meant to elaborate on their 2003 findings and determine if ChABC injected into sites of injury along the rubrospinal tract could yield similar regenerative properties. Consequently, they observed similar axon regeneration which was enhanced by 20%; furthermore, when treatment was combined with lithium chloride, regeneration could be significantly improved to 42% (Yick et al. 2004).

Plasticity in the Visual System

A well-studied example of CSPG involvement in therapeutic application with respect to the visual system was done by Pizzorusso and colleagues. This was done in the form of rehabilitating shifts in ocular dominance as a result of sensory deprivation, aiming to rebalance dominance after over-representation of the normal eye in the visual cortex was induced (Pizzorusso et al. 2002). This study considered that removal of CSPG side chains allowed for more freely flowing neural circuity (Fox and Caterson 2002), inferring that CSPGs, therefore must play a role in plasticity. Therefore, treatment with ChABC was conducted and showed that ocular dominance shifts could be evoked by the absence of CSPGs (Pizzorusso et al. 2002). This was substantiated by Berardi et al. (2003) who found that CSPGs have a role in limiting cortical plasticity (Berardi et al. 2003). Furthermore, Pizzorusso went on to combine ChABC treatment with reverse lid suturing resulting in complete recovery of ocular dominance, dendritic spine density and visual acuity in adult rats following monocular deprivation during the critical period (Pizzorusso et al. 2006).

Osteoarthritis

Current regenerative approaches in the treatment of joint disfunction by arthroplasty, like that applied for osteoarthritis have been achievable primarily through surgical implantation of artificial joints (Kurtz et al. 2005; Hollander et al. 2010); however, even with this intervention, there still remains a risk of long-term residual pain (Wylde et al. 2007; Hollander et al. 2010). As cartilage is inherently a difficult tissue to repair, the challenge of determining alternative strategies to those already employed in clinical practice represents a taxing one.

Nevertheless, many promising results have also been seen in the form of pharmacokinetics; one such study which highlights this was done by Omata et al. (2000) which found that oral

administration of CS (1000 mg/kg) to mice with collagen-induced arthritis could reduce synovitis, fibrosis, and importantly destruction of the articular cartilage (Omata et al. 2000). Parallel to oral treatments, there have also been advances in biotechnology, with the production of CS bioscaffolds taking the front seat in the field of alternative therapeutics. A diverse range of biomatrices have been developed, however, the most successful cases have been with the use of bone marrow stromal mesenchymal stem cells as a source to fuel cell proliferation into chondrogenic phenotypes (Melrose et al. 2008; Hayes et al. 2018). Potential applications in repair are currently looking into the most effective way of administering engineered tissue with injectable hydrogel scaffolds being the most promising (Hayes et al. 2018).

1.3 Corneal Development in the Chicken

The white leghorn chicken *(Gallus gallus domesticus)* has steadily become a robust paradigm linked to high-throughput translational studies investigating more effective prevention and treatment options against sight-threatening ocular surface diseases (Hamburger and Hamilton 1951; Quantock et al. 2003). Pioneering work by Hay and Revel (1969) was the first detailed study to evaluate corneal development in the chicken *(from embryogenesis to maturation)*, illustrating individual stages leading to the formation of a multi-layered transparent tissue. They categorised the precisely controlled sequence of corneal development into four main stages: preliminary events prompting the formation of the primary stroma, development of the primary stroma, development of the secondary stroma, and dehydration leading to the compaction of the stroma (Hay and Revel 1969). From this study, many parallels in the anatomical and cellular composition between the chicken and human cornea were drawn giving impetus for future experimental application (Wisely et al. 2018).

1.3.1 Preliminary Events

To set the stage for the initial formation of the primary stroma, an optical vesicle is formed at the forebrain from the complete closure of the neural tube. Not until stage nine *(30 hours of incubation)* was the primary optical vesicle first observed, showing clear signs of anatomical separation from the overlying ectoderm by the basement membranes of the ectoderm and neuroectoderm, respectively (Hamilton 1953; Weiss and Jackson 1961; Hay and Revel 1969). During stage 13 *(day two)*, the overlying ectoderm was seen to progressively thicken to form the lens placode. The initial succession of morphological events (Figure *1.9*) involves the invagination of the optic vesicle followed closely by the lens placode in the changing contour of the rudimentary eye (Byers and Porter 1964; Hay and Revel 1969).

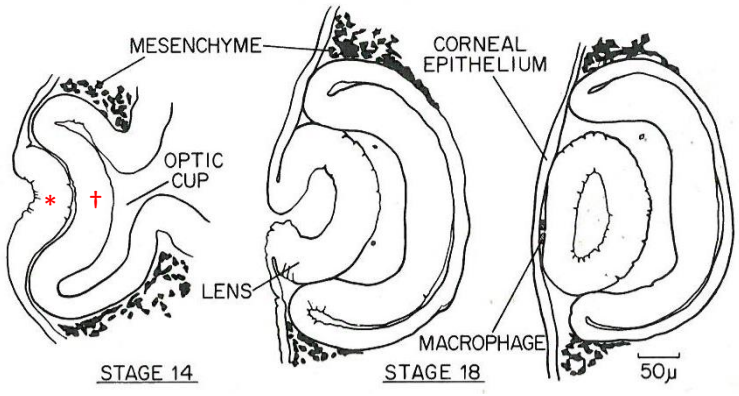

Figure 1.9: Depiction of the formation of the lens placode during stage 14 to stage 18 in a developing chicken cornea. Lens placode (*) and optical vesicle (†). *Taken from:* Hay and Revel (1969).

1.3.2 Development of the Primary Stroma

By stage 18 *(day three)*, complete invagination and detachment of the lens structure from the overlying ectoderm *(now the presumptive two cell-thick corneal epithelium)* was observed (Hay and Revel 1969). Towards the end of stage 18, the initial presentation of the primary corneal stroma could be seen characterised by the presence of interstitial collagen fibrils between the newly formed corneal epithelium and the basal surface of the anterior lens epithelium (Hay and Revel 1969). In subsequent stages 23-25 *(day four)*, the corneal endothelium[20] migrated to its position between the newly formed primary stroma and lens structure (Salzmann 1912; Hay and Revel 1969). The amalgamation of the corneal epithelium, stroma, and endothelium at this stage was eventually coined, the corneal "Brille" (Hay and Revel 1969). Between stages 25-27 *(day five)* a visible swelling of the stroma was seen, representing the increased hydration and surge of newly formed collagen fibrils (Hay and Revel 1969).

1.3.3 Development of the Secondary Stroma

Consequent to the formation of the corneal Brille *(at the end of stage 27;* Figure *1.10*) a preliminary invasion of mesenchymal cells along the peripheral cornea was reported. Once the stroma had reached its maximum swelling and thickness, a rush of additional mesenchymal cells proceeded to populate the complete domain of the stroma *(stage 28)*. By stage 30 *(day 6.5-7)*, mesenchymal cells had differentiated into corneal fibroblast cells which thereafter contributed to the deposition and

[20] Originating from the developing blood vessels in the mesenchyme at the optic cup.

organisation of the collagenous matrix (Meyer and O'Rahilly 1959; Hay and Revel 1969; Garret and Conrad 1979).

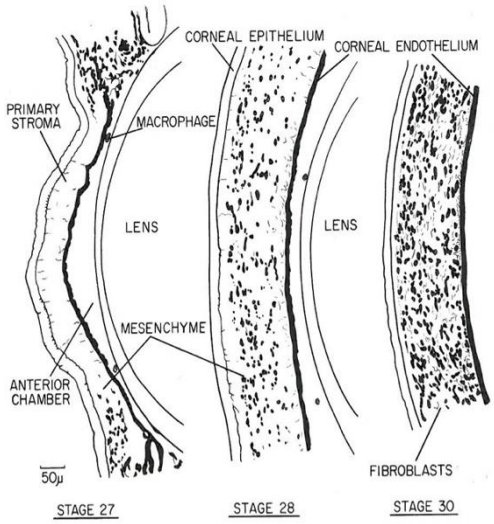

Figure 1.10: Diagram representing the initial invasion of mesenchymal cells into the primary stroma at stage 27 and differentiating into fibroblasts by stage 30. *Taken from:* Hay and Revel (1969).

It is important to note there was a measured difference between the number of collagen lamellae in the anterior and posterior stroma, prior to the first invasion of mesenchymal cells. The anterior stroma was reported to contain approximately 20 lamellae, whereas the posterior stroma contained only half as many, resulting in the anterior stroma remaining virtually uninvaded by cells (Hay and Revel 1969). This thin layer devoid of cells would later go on to form the Bowman's layer (Figure *1.11*). In other respects, the continued proliferation of newly differentiated fibroblasts was observed between stages 30 and 36 *(day ten)*. Additional to reaching approximately 20 layers of cells by the latter end of stage 36, the visible condensing of the anterior stroma could also be seen (Hay and Revel 1969). Similarly, during stage 25, an early indication of the Descemet's membrane was reported. However, just like the Bowman's layer, it continued to develop up to and after hatching (Jakus 1956; Hay and Revel 1969).

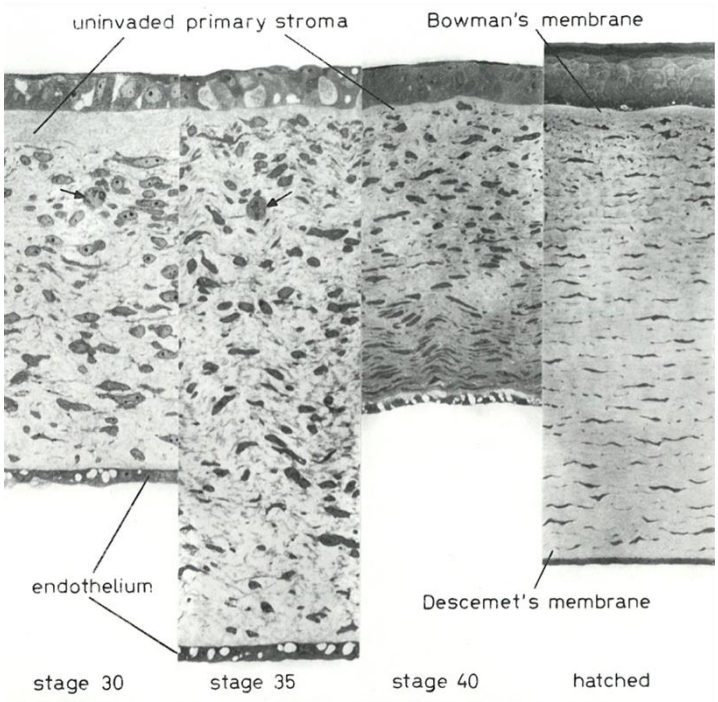

Figure 1.11: Depiction of the formation of the Bowman's layer from uninvaded anterior primary stroma in stage 30 up until hatching. *Taken from:* Hay and Revel (1969).

1.3.4 Post-Hatching

In brief, corneal development persisted well past the hatching stage, with structures such as Bowman's layer and Descemet's membrane continuing to become more defined and condensed. Similarly, the stroma became a more tightly packed structure of lamellae and ECM components (Hay and Revel 1969).

1.4 Stem Cells

1.4.1 Background

Stem cells display two defining characteristics: perpetual, unlimited self-renewal, and the ability to differentiate into a specialised adult cell type; the combination of these two attributes work to maintain homeostasis and repair tissues throughout the human body (Biehl and Russell 2009; Nadig 2009). Following injury, the self-renewal cascade of a stem cell results in cell division leading to the production of one daughter stem cell and one progenitor cell[21] (Nadig 2009).

Stem cells originate from two main sources: embryonic, which exist only at the earliest stages of development, and adult stem cells, that appear during fetal development but continue postnatally (Nadig 2009). They can be further categorised into five types based on their potential to differentiate into other cell types: (1) totipotent, which generate all the cell types found in the embryo in addition to germ cells; (2) pluripotent, which generate almost all cell types excluding those found in the embryonic membrane; (3) multipotent, which differentiate into one or mature cells in a closely related family; (4) oligopotent, which differentiate into a few different cells types; and (5) unipotent which only produce one cell type (Nadig 2009).

1.4.1.1 Stem Cell Fates

Based on the defining characteristics of stem cells, four possible outcomes or fates exist. Firstly, stem cells can remain quiescent, thus maintaining their location in the stem cell pool. Secondly, they can undergo symmetrical self-renewal, in which two daughter cells are produced as a result of cell division, which can later develop into specialised cells in subsequent divisions (Biehl and Russell 2009). Conversely, stem cells can also undergo asymmetrical self-renewal, where two daughter cells are produced, but only one remains a copy of the parent cell and the other goes on to become a progenitor cell. The fourth and final fate is where a stem cell produces two daughter cells both of which are specialised and different from the parent cell (Biehl and Russell 2009).

1.4.2 Stem Cell Niche

Stem cells are found to reside in specialised microenvironments throughout the human body where they receive stimuli that ultimately determine their fate; yet the classic notion that the niche is simply an anatomical location is misleading, rather it is now thought of as a place where extrinsic

[21] Progenitor cells are an intermediate cell type on a committed path to full differentiation along a particular pathway of stem cells.

signals *(i.e., cell-to-cell and cell-matrix signals that activate and/or repress genes and transcription)* interact and integrate to influence stem cell behaviour (Ferraro et al. 2010). Components of the niche include: (1) ECM proteins that act as a mechanical scaffold for the transmittance of stem cell signals, (2) stromal support cells which are found in close proximity to stem cells, (3) blood vessels that supply nutrition and systemic signalling to the niche from other organs, and (4) neural inputs that mobilise stem cells out of the niche to areas of damage to restore tissue function and integrity (Ferraro et al. 2010).

1.4.2.1 Stem Cell Niche in the Cornea

In the cornea, the stem cell niche is located in the transitional zone between the cornea and conjunctiva, otherwise known as the limbus. Within its specialised microenvironment, a framework of distinct stromal undulations or invaginations *(PoV)*, are apparent and used to characterise regions populated with stem cells (Daniels et al. 2009). These papillae-like projections are advantageous in their morphology as they provide protection to stem cells from external environmental factors, as well as increasing the surface area to fashion a concentrated and narrow annulus that circumscribes the periphery of the adult cornea (Davies et al. 2009). Furthermore, this structure conveniently overlays a rich vascular network that allows for efficient diffusion of chemical signals, in response to internal and external stimulation, to influence stem cell behaviour and fate (Davies et al. 2009).

1.4.2.1.1 Corneal Epithelial Homeostasis

As the anterior-most layer of the cornea, the epithelium is subject to an onslaught of external and mechanical traumas leading to the periodic exfoliation of cells throughout the day. To counterbalance these losses, the cornea possesses an internal mechanism that facilitates the renewal[22] and replenishment of cells (Sharma and Coles 1989; Wagoner 1997). Without the retention of cell volume, corneal transparency and consequently visual clarity would be hampered. The internal mechanism is best understood by the model proposed by Thoft and Friend (1983), commonly referred to as the "XYZ hypothesis." The theory suggests epithelial homeostasis is achieved by a reservoir of ocular surface stem cells residing within the basal layer of the epithelium (Figure *1.12*). These resident LECs undergo asymmetrical division to produce one daughter cell that remains in the limbal niche and one highly proliferative TAC, that progressively differentiates[23]

[22] The renewal rate of the whole epithelial surface is thought to take between nine and twelve months.
[23] Basal TACs progress to become intermediary suprabasal wing cells *(post-mitotic)* before terminally differentiated into superficial squamous epithelial cells.

as it migrates centripetally towards the central cornea (Thoft and Friend 1983). For this reason, the resultant desquamation experienced by superficial epithelial cells, "Z", in response to external and mechanical forces is restored from the proliferation and migration of basal epithelial stem cells, "X", and centripetal migration from the limbus, "Y" (Wagoner 1997; Yoon et al. 2014).

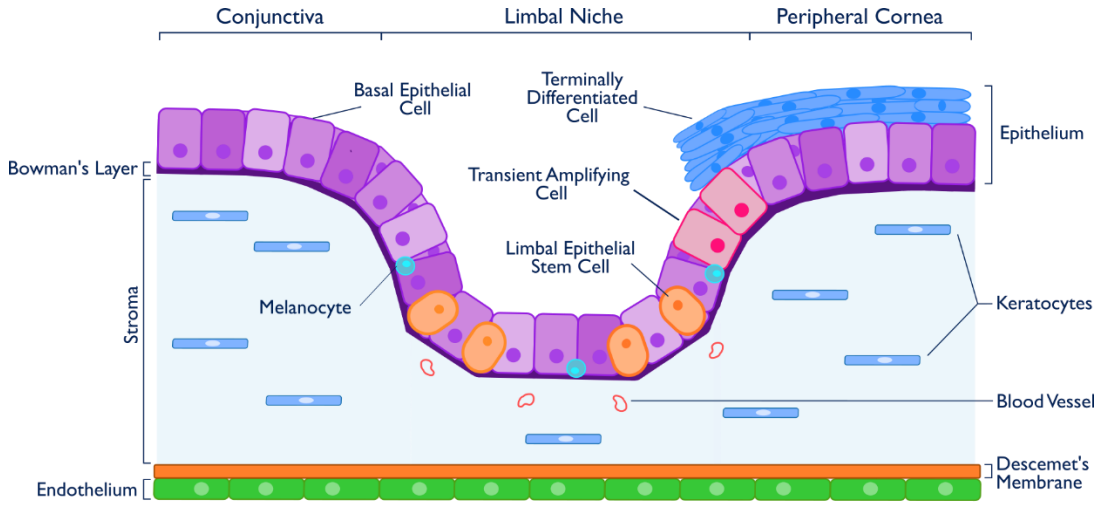

Figure 1.12: The human limbal stem cell niche. Schematic representation of the corneal limbal stem cell niche and some of its constituent elements.

1.4.2.1.2 Anatomical Features of the Human Limbal Epithelial Stem Cell Niche

In the last decade, substantial progress has been made in characterising the putative stem cell niche located within the corneal limbus. Multiple anatomically unique features have been proposed in an effort to better identify the exact location of stem cells for research and therapeutic purposes (Sherwin 2016). Features like the PoVs, limbal crypts *(LC)*, and focal stromal projections *(FSP)* are some of the widely recognised attributes native to the human limbus and will be considered in greater detail below.

Palisades of Vogt

The PoV are a series of radially oriented striae located peripheral to the terminal capillary loops (Figure 1.13) and centrally to the Schlemm's canal at both the upper and lower aspect of the limbal arc (Goldberg and Bron 1982). The close proximity of the niche to a complex vascular plexus suggests it is a necessary interface to supply essential nutrients and convey signalling directives to influence LESC behaviour (Shortt et a. 2007a). The appearance of the palisades can vary markedly between individuals with respect to length *(0.5-0.9 mm)* and pigmentation, making visualisation in some individuals unremarkable *(*Graves 1934; Goldberg and Bron 1982; Townsend 1991).

However, some degree of symmetrical distribution of palisades is reported to exist between eyes in the same individual (Goldberg and Bron 1982).

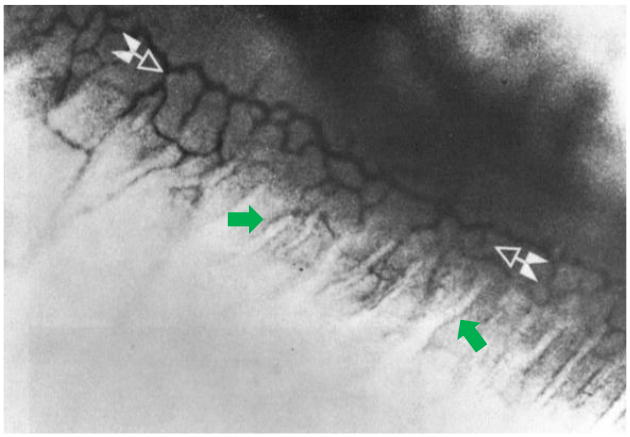

Figure 1.13: Limbal palisades of Vogt *(green arrows)* located peripheral to terminal capillary loops *(white arrows).* *Taken from:* Goldberg and Bron (1982).

Limbal Epithelial Crypts

Novel work by Dua et al. (2005) identified distinct anatomical extensions, referred to by the author as "limbal epithelial crypts" (LECs), spreading from the peripheral aspect of the limbal palisades in human corneas. Unlike the PoV above, LECs were not taken to be restricted to the superior and inferior arc of the limbus, rather they were uniformly distributed around the limbal circumference (Dua et al 2005; Shanmuganathan et al. 2007). From their analysis of five donor corneas, LECs were determined to extend radially into the conjunctival stroma *(parallel to the palisade)* or circumferentially along the limbus *(perpendicular to the palisades)*; both originating from the peripheral aspect of the supporting surface of the interpalisade ridge (Dua et al. 2005; Shanmuganathan et al. 2007; Dziasko and Daniels 2016). Further characterisation of LECs was performed by Shanmuganathan et al. (2007) using 74 LECs isolated from eight human corneoscleral rims. The cells contained within the crypts demonstrated negative phenotypic expression of CK3 and CD43 and positive expression of CK19, Vimentin, p63 and Connexin 43 *(CX43)* (Shanmuganathan et al. 2007). Morphologically, LECs comprise three distinct cell types: epithelial *(primarily basal)*, suprabasal and central cells (Shanmuganathan et al. 2007).

Limbal Crypts

LCs, similar to LECs, are another anatomical structure found in the proposed human limbal stem cell niche. They were first observed by Goldberg and Bron (1982), yet only later formally characterised by Shortt et al. (2007a), who described them as "distinct invaginations of epithelial cells extending from the peripheral corneal epithelium into the corneal limbal stroma." They also

noted the downward projections were enclosed laterally by PoV and a highly cellularised surrounding stroma, inclusive of a distinct vascular supply (Shortt et al. 2007a). They also noted that suprabasal cells contained with the LCs were larger and with a lower nucleus to cytoplasm ratio than suprabasal cells lining the base and edges of LCs (Shortt et al. 2007a). Moreover, the distribution of LCs was predominantly in the inferior and superior corneal limbal quadrants yet absent along the horizontal meridian of the limbus (Shortt et al. 2007a).

Focal Stromal Projections

Focal stromal projections are described by Shortt et al. (2007a) as being finger-like projections that extend upwards into the limbal epithelium from the stroma. In addition to encasing a central blood vessel, focal stromal projections are surrounded by tightly adherent basal cells that are discerningly smaller in diameter with a higher nucleus to cytoplasm ratio than neighbouring basal cells lining the base and edges of the focal stromal projections. And like resident LCs, focal stromal projections have a comparable distribution along the corneal limbus (Shortt et al. 2007a).

1.4.3 Limbal Stem Cell Deficiency and Stem Cell Therapy

1.4.3.1 Limbal Stem Cell Deficiency

The characteristics of stem cells are what give them the capacity to play an integral role in maintaining the transparency of the cornea. However, in the absence of an adequate reservoir of stem cells owing to external *(chemical or thermal burns, contact lens wear, iatrogenic trauma, etc.)* and internal *(i.e., Steven-Johnson syndrome, mucous membrane pemphigoid, aniridia, etc.)* factors, limbal stem cell deficiency can arise, manifesting as corneal neovascularisation, conjunctivalisation, chronic inflammation, and/or persistent epithelial defects leading to loss of cornel transparency and subsequent corneal blindness (Bains et al. 2019).

1.4.3.2 Therapies for Limbal Stem Cell Deficiency

Over the course of the past two decades there has been a rising demand for donor corneas to treat varying degrees of ocular surface disease. However, the reservoir of viable, transplantable corneas has been on a steady decline (Funderburgh et al. 2016). Consequently, through the pioneering work of Pellegrini, Tsai, Kinoshita and others, the dependency on donor corneas has successfully been combatted, in some cases effectively replacing the need for them altogether, by advancing avenues into alternative tissue-based bioengineering therapeutic applications, which will be briefly

overviewed in subsequent sections (Pellegrini et al. 1997, Tsai et al. 2000, Inatomi et al. 2005; Funderburgh et al. 2016; Bains et al. 2019).

1.4.3.2.1 Ocular Surface Reconstruction: Tissue Engineering

Researchers have established innovative transplantation techniques that use allogeneic *(donor-derived)* or autologous *(patient-derived)* tissue sources to generate functionally stratified corneal epithelial cell sheets (Bains et al. 2019). The underlying concept for these tissue engineering strategies is that an *ex vivo* expanded multi-layered sheet has the capacity to regenerate and repair the stem cell deficient ocular surface to promote renewed epithelial healing, which in turn leads to regression of neovascularisation and cessation of recurrent epithelial erosion (Koizumi et al. 2000, Burman and Sangwan 2008, Bains et al. 2019).

Earlier strategies *(i.e., explant culture system)* involved placing a healthy limbal biopsy onto a substrate *(i.e., human amniotic membrane*) for *ex vivo* cell expansion. Epithelial cells would migrate from the corneal biopsy and adhere to the substrate surface, which also acted as a physical carrier to support the expanded sheet as it was transplanted onto the corneal surface *(following removal of fibrous scar tissue from the transplant area)* (Bains et al. 2019). It is important to note that early expansion strategies involved a co-culture system that integrated a growth-arrested 3T3 cell feeder layer beneath the amniotic membrane to encourage epithelial differentiation (Grueterich et al. 2003; Bains et al. 2019). However, there was a growing concern regarding the use of xenobiotic material[24] in the production of transplants in this way and the potential it had for immunological complications to recipients. As a result, a modified explant approach *(suspension culture system)* was introduced which used human- and/or non-animal-derived digestive enzymes to isolate epithelial cells from limbal biopsies to form a cell suspension that, after an incubation period, formed confluent, transplantable cell sheets (Daya et al. 2005; Nakamura et al. 2006; Shortt et al. 2007b; Kolli et al. 2014; Sangwan et al. 2011; Bains et al. 2019). Published literature alludes to both culture systems *(explant and cell suspension)* as being effective reconstructive strategies, although, current surgical bodies employ the cell suspension method more routinely (Bains et al. 2019).

Moreover, an alternative method, not requiring a substrate and carrier, was introduced by Nishida and colleagues which used a temperature-responsive polymeric culture surface on which multi-layered epithelial cell sheets could be cultured (Nishida et al. 2004a; 2004b: Bains et al. 2019). The

[24] Xenobiotic materials typically refer to any chemical or compound foreign to an organism, specifically, in that it does not occur normally within the metabolic pathway of an organism's biological system.

chemical property of the polymer was such that when exposed to reduced temperatures *(below the critical solution temperature),* cell sheets would lose adherence to surface and readily detach allowing for a carrier-free transplantable tissue; this approach provides a direct adhesion interface to the recipient's exposed ocular surface (Nishida et al. 2004a; 2004b; Bains et al. 2019). As such, these advances have represented a key insight into the direction alternative therapeutic strategies are headed to replace box standard keratoplasty transplantations to treat various aetiologies of ocular surface disease (Bains et al. 2019).

1.4.3.2.2 Cell Sources for Corneal Reconstruction Using Ex Vivo Expanded Cell Constructions

There are two widely accepted methods of ocular surface reconstruction, at this time, to produce multi-layers of expanded epithelial sheets: Cultured limbal epithelial transplantation *(CLET)* and cultured oral mucosal epithelial transplantation *(COMET)*. With respect to CLET, both autologous and allogeneic cell sources *(in the form of a biopsy)* are utilised, whereas, in the case of COMET, only autologous cells *(from the patient's inner cheek)* are harvested for cell culture (Bains et al. 2019). Although published literature provides favourable clinical outcomes for both, it is still widely speculated which is manifestly superior to the other.

1.4.3.2.2.1 Cultured Limbal Epithelial Transplantation

In relation to allogeneic CLET, a 2 mm limbal stem cell biopsy *(evenly extending across the corneoscleral junction)* is obtained from either a living relative or donor eye (Fasolo et al. 2017). The drawback to this method is the long-term, post-operative care *(i.e., immunosuppressants)* that is fundamental to avoid graft rejection (Kinoshita et al. 2004). An alternative is to use autologous limbal stem cells, which are derived from, and contingent on the availability of, an unaffected, healthy limbus, from which a biopsy can be obtained – an option only possible in unilateral ocular surface disease (Bains et al. 2019). Numerous studies have reported the successful use of both allogeneic and autologous expanded *ex vivo* limbal epithelial cells to repair the corneal surface and both represent a viable method of treating limbal stem cell deficient eyes (Shortt et al. 2007b; Zhao and Ma 2015, Holland 2015, Sasamoto et al. 2018; Bains et al. 2019).

1.4.3.2.2.2 Cultured Oral Mucosal Epithelial Transplantation

First reported by Nakamura and colleagues in 2004, oral mucosal epithelial transplants were derived from autologous, interior buccal mucosal epithelial stem cells (Nishida 2004a; Nakamura et al. 2004). This procedure involved the surgical extraction of an inner cheek biopsy containing

buccal cells that were subsequently enzyme-treated with dispase or trypsin to form a single cell suspension, prior to being seeded onto a temperature-responsive cell-culture insert, as previously described (Nishida 2004a). As an alternative to limbal epithelial stem cells, this method is advantageous in cases of both unilateral and bilateral injury or disease and does not expose a healthy unaffected cornea, like in autologous CLET, to the possibility of contracting limbal epithelial stem cell deficiency as a direct result of surgical intervention (Bains et al. 2019).

1.5 Summary

This chapter gives an overview of the substantial literature surrounding the corneal ultrastructure and its cellular constituents, in addition to describing the key research undertaken to provide the basis for modern translational studies investigating alternative therapeutic strategies for the treatment of stem cell related ocular surface disease.

In brief, the literature characterises:

i. **The corneal architecture:** highlighting the unique structural layers and cellular components which assemble together to form a robust optical surface.
ii. **The stromal ultrastructure:** describing the configuration and distribution of extracellular constituents *(collagen, GAGs, stem cells, and keratocytes)* vital to the maintenance of corneal integrity and transparency. Furthermore, the topic of CS PGs and its potential as a prospective therapeutic agent is exemplified by numerous studies that have manipulated CS PG expression across different organ system to elicit a spectrum of both positive and negative responses. In addition, its potential influence on limbal stem cells, as was surmised in association within the articular cartilage stem cell niche, is presented.
iii. **The chicken animal model:** classically used for studying developmental events of the corneal structure, also appears to be an excellent model for understanding more about corneal repair by virtue of the similarities it shares anatomically and cellularly to the human cornea. Further investigations using this model have the ability to generate vital information with translatable, longer-term potential for new therapies to treat ocular surface disease.
iv. **The limbal stem cell niche:** a specialised microenvironment which regulates internal mechanisms that facilitate the renewal and replenishment of cell populations across the cornea. Innovative transplantation techniques have established a viable replacement for donor corneas using stem cells as a source for engineering transplantable grafts for the treatment of a broad spectrum of ocular surface morbidities affecting the global population.

1.5.1 Project Overview and Aims

The overriding hypothesis for this thesis is that the limbal stem cell niche can be identified by GAG sulphation epitopes and variably sulphated CS GAGs play an essential role in modulating the pluripotency of cells. Subsequent chapters use the developing avian cornea as a model to perform a series of *in vitro* and *in vivo* experiments *(i.e., cell culture, immunolocalisation, and advanced imaging)* to illustrate key structural associations and cellular properties within the presumptive limbal stem cell along with elucidating the effect of variably sulphated GAGs on "stemness." Specifically, in the context of combined 'differentiation' and 'self-renewal' capabilities. Results obtained from these investigations have led to novel characterisations that foster the present intrigue surrounding stem cells and their potential application in regenerative therapies.

Outlined in Chapter two are the adaptations made to standardised protocols which in turn were applied to successive experimental Chapters three-six. In Chapter three, the immunolocalisation of selected putative stromal stem cell and matrix markers was evaluated *ex vivo* at specific developmental time points and *in vitro* using standardised culture conditions. The collection of qualitative and quantitative data was a logical first step towards establishing a baseline of results for use as a comparison to assess changes in phenotypic expression associated with increased pluripotency, presented in Chapter six. In Chapter four, the immunolabelling of variably sulphated CSPGs using sulphation-specific antibodies: 4C3, 6C3, 7D4, and 3B3 were mapped in the developing avian limbus for the first time. The hypothesis of this study is that specific GAG sulphation motifs define the stem cell niche in the cornea, just as they have been shown to do in the stem cell niche of articular cartilage.

Chapter five describes the application of scanning electron microscopy *(SEM)*, transmission electron microscopy *(TEM)*, and serial block face scanning electron microscopy *(SBF-SEM)* to evaluate the limbal microstructure in greater detail in order to determine whether anatomical features and cell-cell interactions that characterise the human limbal stem cell niche are also present in the presumptive niche of the avian cornea. The study described in Chapter six was focused on investigating the resultant phenotypic expression of corneal progenitor cells grown using novel, modified culture conditions, where cells were expanded on petri dishes coated with either crude or purified CSPGs. Comparative analysis was performed with baseline controls, obtained from Chapter three, to show evidence of enhanced expression promoting "stemness" in otherwise differentiated cells. Finally, Chapter seven outlines the general conclusions and addresses ideas for

future work using adapted cell culture techniques and other forms of high-resolution imaging *(e.g., in vivo micro-optical coherence tomography).*

To summarise there are three main aims of the research presented in this thesis:

- To determine immunolocalisation of putative stromal stem cell and matrix markers *ex vivo* at key corneal developmental stages in addition to standardised *in vitro* culturing.
- To characterise limbal stem cell niche microstructures, recognised in the human cornea, within the avian cornea.
- To further understand the relationship between CSPGs and corneal progenitor cells within the ECM in relation to non-sulphated and minimally sulphated CSPGs being linked to the maintenance of the stem cell niche in multiple organ systems.

Chapter 2: Materials and Methods

2.1 Introduction

In this chapter, the basic protocols and principles of the methods used in later experimental chapters will be introduced. Details of the materials used, and specific modifications made to the described methods here will be expanded on further in each individual chapter as needed.

2.2 Cell Extraction and Culture

2.2.1 Basic Protocol

2.2.1.1 Sample Processing

Fertilised, white leghorn chicken eggs (Henry Stewart & Co. Ltd., Fakenham, UK) were incubated at 37°C in a humidified incubator until embryonic *(E)* day 18 – E_{18}. At that point, chicken embryos were terminated via cervical decapitation and whole eyes were dissected out. Corneas *(approximately 9 mm in diameter and 400 μm in thickness)* were removed from whole eyes and placed in culture media containing Dulbecco's Modified Eagle Medium (*DMEM,* ThermoFisher Scientific, UK, Cat. # 61965-026), 1% Penicillin/Streptomycin (ThermoFisher Scientific, UK, Cat. # 15140-122), and 0.25 μg/mL Amphotericin B/Fungizone (ThermoFisher Scientific, UK, Cat. # 15290-026). All corneas were then transferred into a 0.04% solution of Ethylenediaminetetraacetic acid (*EDTA*, Sigma Aldrich, UK, Cat. # ED2SS) in phosphate buffered saline (*PBS,* Fisher Scientific, UK, Cat. # 12821680) and incubated at 37°C for 45 minutes. Following incubation, corneas were transferred into 0.15% collagenase type I (Sigma Aldrich, UK, Cat. # SCR103) solution and incubated at 37°C for a further two hours. Resulting supernatant *(containing cells)* was transferred into a new test tube and centrifuged for five minutes at 1450 revolutions per minute *(RPM)*. The supernatant was discarded, and the resultant pellet was resuspended in culture media *(as described above)* with the addition of 5% *(w/v)* of fetal bovine serum (*FBS,* Gibco, ThermoFisher, UK, Cat. # 10270-098) to the media.

2.2.1.2 Cell Seeding

Prior to seeding at an initial density of $3.0x10^5$ cells/mL, a cell-count was performed by transferring 10 μl of suspension onto a haemocytometer (Hausser Scientific Bright-Line™, Thermos Fisher Scientific, Cat. # 02-671-51B). Cells were suspended in the appropriate amount of culture medium

containing 5% FBS and seeded into 35 mm petri dishes (Fisher Scientific, UK, Cat. # 10654161) to be incubated at 37°C until 80-100% confluency.

2.2.1.3 Cell Maintenance/Passage

After two days of incubation at 37°C, initial attachment of keratocytes to the petri dish was observed. Prior to changing the medium, following the initial isolation of keratocytes, a wash with Dulbecco's phosphate-buffered saline (*D-PBS*, Fisher Scientific, UK, Cat. # 10388739) was performed to remove resultant dead cells and debris from the samples. From there, fresh media *(DMEM)* containing 5% FBS was placed in each dish and cultures were then incubated at 37°C to allow for further cell growth.

Samples requiring serial passage *(P)* had old media removed and replaced with 1 mL of PBS *(per dish)* to remove dead cells and debris. Then 1 mL of 0.05% Trypsin-EDTA (Gibco, ThermoFisher, UK, Cat. # 25300-054) was added to each dish to loosen cells from the base of the dish followed by 1 mL of new media containing 5% FBS to neutralise the action of Trypsin-EDTA. The samples from each petri dish were then transferred into a single test tube that was centrifuged at 1450 RPM for five minutes. The resultant pellet was resuspended in the appropriate amount of new media and seeded into petri dishes again at a cell density of $3.0x10^5$ cells/mL. Dishes were incubated at 37°C to allow for cellular re-attachment and subsequent growth.

2.2.1.4 Fixing

Culture media were removed and 1 mL of 90% ethanol (Fisher Scientific, UK, Cat. # 4450-17) was instilled for five minutes before being removed; cultures were air dried before being stored in a -80°C freezer until required.

2.2.1.5 Imaging and Analysis

Phase contrast microscopy was carried out using an Olympus IX71 Inverted Fluorescence & Phase Contrast Tissue Culture Microscope (Olympus, UK). Live image acquisition was performed using SPOT Basic™ image capture software (SPOT Imaging, USA) which supported the adjustment of brightness and contrast of samples.

2.3 Cryo-Sectioning

2.3.1 Basic Protocol

2.3.1.1 Specimen Processing

Fertilised, white leghorn chicken eggs (Henry Stewart & Co. Ltd, Fakenham, UK) were incubated 37.8°C and ~60% humidity until E_{10}, E_{14}, and E_{18}. Whole eyes were extracted after cervical decapitation. Eyes were transferred into vials of 1% PFA in D-PBS for 30 minutes before being washed in a solution of D-PBS for 20 seconds. Eyes were then transferred into a solution of equal parts D-PBS and optimal cutting temperature compound *(OCT, cryo-embedding compound)* (Scigen, Fisher Scientific, UK, Cat. # 23-730-573) overnight at 4°C. Eyes were removed from solution and corneas were excised from E_{14} and E_{18} eyes, whereas E_{10} eyes were kept intact. Moulds were filled with OCT compound and corneas/whole eyes were positioned in the centre of the moulds with the epithelium oriented downwards *(towards the base of the mould)* before being placed in a -80°C freezer to set. Once set, embedded corneas were removed from moulds, and wrapped in aluminium foil and returned to -80°C for storage.

2.3.1.2 Cryo-Sectioning

Embedded corneas/whole eyes in OCT compound were oriented to be cut along the sagittal plane and freeze mounted to a cryostat chuck using additional OCT compound. Mounted samples were then positioned within the cryostat (OTF5000, Bright Instruments, UK), sectioned at 14 μm, and transferred onto glass slides (Fisherbrand™ Superfrost™ Plus, Fisher Scientific, UK, Cat. # 12-550-15) before being labelled accordingly and stored at -80°C.

2.4 Immunohistochemistry

2.4.1 Basic Protocol

2.4.1.1 Staining

Specimens were brought back to room temperature before a hydrophobic ring (ImmEdge Pen, Vector Labs, UK, Cat. # H-4000) was made around each sample. Samples were rehydrated using a mixture of PBS in Tween®20 (Sigma Aldrich, UK, Cat. # P9416-50ML) for five minutes. Following rehydration, blocking serum *(300 μl per dish/150 μl tissue section)* was applied for 30 minutes. Afterward, primary antibodies were instilled overnight at 4°C. Samples were washed three times using PBS/Tween®20 for five minutes before conjugated secondary antibodies were applied

for three hours and left to sit in complete darkness. Samples were then washed three more times using PBS in Tween®20 before one drop of DAPI, cell nuclear counterstain (Vectashield, Vector Laboratories, Cat. # H-1200) was applied followed by mounting using coverslips (Sigma Aldrich, UK, Cat. # BR470819 and BR470055).

2.4.1.2 Imaging and Analysis

Observations and image acquisition were carried out using an Olympus BX61 fluorescence microscope (Olympus, UK). Image analysis was performed using ImageJ Software (National Institute of Health, USA).

2.4.2 Basic Principle

2.4.2.1 Antibodies

Unlike in innate immunity, the adaptive immune response is integral in recognising, reacting to, and remembering foreign substances invading the body. Antibodies[25] play a functional role in adaptive immunity by detecting and binding specific foreign molecules to trigger responses such as activation of complement and phagocytosis (Onley 2007; Chui et al. 2019). The basic structure of an antibody is composed of two identical heavy chains and light chains. The pairing of one heavy chain with one light chain associates with an identical heterodimer to form an immunoglobulin. Moreover, the linkage between the heavy chain and light chain of the heterodimer is stabilised by disulphide bonds, whereas the two heavy chains of the heterotetramer are linked by disulphide bridges (Onley 2007; Chui et al. 2019). The hypervariable region within the light chains is responsible for mediating the binding of the antibody to specific antigen or target molecules. Whereas the constant domain of the heavy chain is what determines the isotype of the antibody (Onley 2007; Chui et al. 2019).

2.4.2.2 Immunoglobulin Isotype G

Antibodies are members of an immunoglobulin family (Ig) of proteins that comprise five distinct isotypes: IgA, IgD, IgE, IgG, and IgM which differ in the amino acid sequence of their heavy chain's constant regions (Chui et al. 2019). All members of a species inherit the same set of isotype gene whereas differing species will instead have different constant region genes leading to expression of different isotypes (Onley 2007; Chui et al. 2019). Of the different types of isotypes, IgG is found to comprise 75% of the total immunoglobulins in circulation and in most tissue types,

[25] Antibodies are blood plasma proteins produced by plasma cells *(effector B cells).*

therefore, making up most of the antibody reagents used in research (Chui et al. 2019). There are four subclasses of IgG *(IgG1-IgG4)* which differ in their heavy chain C-terminus, hinge region length, and number and position of inter-chain disulphide bonds (Chui et al. 2019). As seen in Figure *2.1*, IgG is classified as a monomer due to its singular Y-shaped antibody subunit and its heavy chain is comprised of three constant domains and one variable domain that enables a characteristically high degree of flexibility and affinity to antigen binding (Onley 2007; Chui et al. 2019).

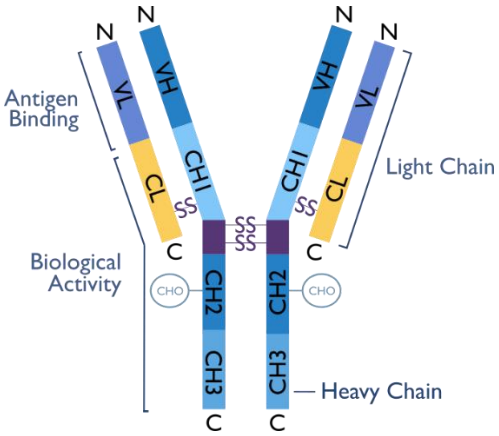

Figure 2.1: Schematic of IgG structure. VL = variable domain of light chain, CL = constant domain of light chain, VH = variable domain of heavy chain, CH = constant domain of heavy chain. SS = disulphide bonds, "N" = N-terminus, "C" = C-terminus.

2.4.2.3 Epitope and Antibody Specificity

As mentioned above, the activation of an immune response is primarily achieved by the presence of antigens within the body. Antigens possess active segments called epitopes to which B and T cell lymphocyte antigen receptors bind via their variable regions to initiate the immune systems defence mechanisms (Onley 2007). For any given antigen there are several unique antibodies able to recognise it, but these will only bind to a specific epitope on the protein. It is important to note that a specific epitope can appear on multiple antigens, allowing for a single antibody to recognise various proteins if they are highly homologous and possess the same epitopes. Moreover, multiple antibodies can be generated against an antigen, leading to the possibility of cross-reaction with other proteins that possess the same epitopes. This provides the basis for techniques which have been developed to produce antibodies by way of direct collection from serum or by isolation via B cell*(s)* producing said antibody; these two production techniques will be discussed in more detail below (Onley 2007).

2.4.2.4 Antibody Production

Antibodies used for experimental purposes are usually purified from the sera of an immunised animal. Initial exposure of an animal to an antigen will stimulate a primary immune response with a characteristic lag phase, where proliferation of predominantly IgM-producing plasma cells occurs before antibodies can be detectable in serum (Cooper and Luumas 2007). The lag phase stems from naïve lymphocytes encountering the antigen for the first time and many events needing to be activated; subsequent exposure to the same antigen activates a secondary immune response that is faster, more intense and occurs for a longer duration than the primary immune response, because memory cells induced in the primary response are more rapidly stimulated (Cooper and Luumas 2007). However, there is a significant shift from IgM to IgG production with antibodies possessing a higher affinity as a result (Onley 2007).

Antibody affinity relates to the measure of strength between the interaction of an epitope and an antibody's paratope, that is, its antigen-binding site. Therefore, higher affinity antibodies will bind antigens quicker as well as permitting greater sensitivity in assays, compared to low affinity antibodies (Cooper and Luumas 2007). Protein antigens generally contain many distinct epitopes, so when injected into an organism, they will result in the stimulation of many B cell clones, with each clone being specific for a particular epitope to proliferate and differentiate into antibody-secreting plasma cells (Chui et al. 2019). Polyclonal antibodies can recognise multiple epitopes on the same antigen as they are made up of an assortment of antibodies from different B cells, whereas mAbs can recognise only a single, unique epitope because they are generated from a single B cell clone (Cooper and Luumas 2007). Monoclonal antibodies have many important applications in research with several advantages over polyclonal antibodies, mainly for their high specificity to single epitopes, which reduces the probability of cross reactivity, and that they provide more reliable results when performing assays to quantify protein levels (Onley 2007, Chui et al. 2019).

2.5 Scanning Electron Microscopy

2.5.1 Basic Protocol

2.5.1.1 Fixation and Post-Fixation Processing Using Hexamethyl-Disilazane (HMDS)

Whole embryonic eyes and adult corneas *(maintaining the cartilaginous ossicles at the corneo-scleral junction)* were transferred into primary, half-strength Karnovsky fixative ((2.5% glutaraldehyde, Sigma Aldrich, UK, Cat. # G6257) and 2% paraformaldehyde *(PFA*, Sigma Aldrich, UK, Cat. # 158127) in 0.1M sodium cacodylate buffer to a pH of 7.4 – *hereby afterwards referred to as Karnovsky fixative))*. Samples were left overnight at 4°C. The next day, samples were washed with 0.1 M cacodylate buffer before tissue maceration was carried out using 10% NaOH over a course of several days. Samples were post-fixed in 2% tannic acid (Mallinckrodt Inc., Kentucky, USA, Cat. # 8835) for five hours before being washed with distilled water and treated with a secondary, post-fixative solution of 1% osmium tetroxide (Agar Scientific, Essex, UK, Cat. # ARG1015). Following post-fixation, samples were washed three more times with distilled water before undergoing a stepwise dehydration using ascending concentration of ethanol.

Dehydration:

70 %	30 minutes each
90 %	
100%	
100% ethanol: HMDS	
HMDS x2	1 hour each

Next, samples were infiltrated with HMDS, a low-surface tension solvent, using a 1:1 mixture of 100% ethanol: HMDS followed by two consecutive, one-hour treatments of 100% HMDS. These samples were then transferred to a desiccator in a fume hood and the HMDS was allowed to evaporate. Once dried, samples were mounted onto aluminum stubs using carbon cement and sputter coated with gold, before being placed in the scanning electron microscope for imaging.

2.5.1.2 Imaging and Analysis

Samples were observed using a Zeiss Sigma HD Field Emission Gun Analytical scanning electron microscope (Carl Zeiss Ltd, Cambridge, UK) and imaged with SmartSEM Software (Zeiss, UK).

2.5.2 Basic Principles

Scanning electron microscopy is a technique commonly used to study the surface, or near the surface, structures of bulk specimens (Goodhew et al. 2017). It provides bioimaging capabilities to reveal, on a microscopic-scale, information regarding a specimen's microtextures, that is, its size, shape, composition, and physical properties that would not normally be visible to the naked eye (Goldstein et al. 2018). The basic operating principle behind SEM involves creating a thin, focused beam of energised electrons (*emitted from an electron source*) that is then scanned across a sample, resulting in various interactions leading to scattered signals being emitted from the incident plane on which the sample's excitation source emanates (Figure *2.2*) and are captured and transformed by the SEM into analyzable information *(i.e., magnified images and graphics)* (de Assumpcao Pereira-da-Silva and Ferri 2017).

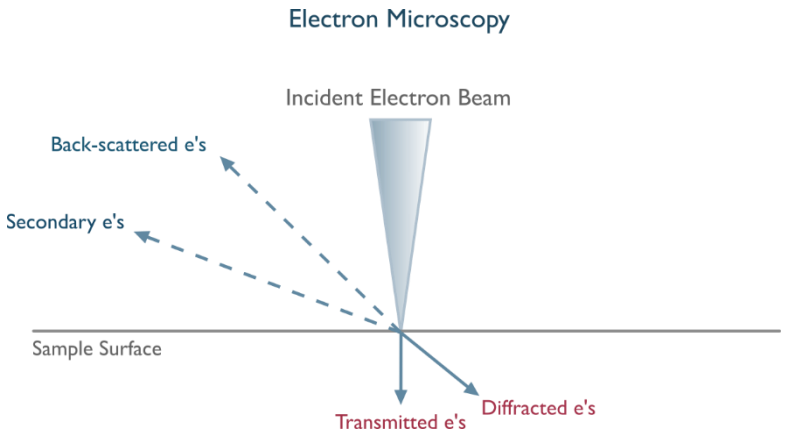

Figure 2.2: The position of the captured signal defines the electron microscope.

When accelerated electrons enter the specimen, they scatter from the specimen surface both elastically (*by electrostatic interactions with atomic nuclei*) and inelastically (*by interactions with atomic electrons*) (Egerton, 2008). The main interactions detected by SEM are the emission of secondary electrons *(SE)* by inelastic scattering and of backscattered electrons *(BSE)* generated by elastic scattering (Yoshida et al. 2016). The SEs are produced from the emission of the valence electrons of the constituent atoms and have a low energy emission, meaning that signals generated internally are absorbed by the specimen, whereas the ones generated closer to the specimen surface can reach the outside of the specimen to be captured for processing (Yoshida et al. 2016). On the other hand, BSEs produce high-energy electron emissions that are multidirectional and provide information associated with deeper composition of the specimen; their high kinetic energy provides a higher probability of electrons being able to leave the specimen and re-enter the surrounding vacuum to be captured for processing (Egerton 2008; Yoshida et al. 2016).

2.5.2.1 Scanning Electron Microscope Components

The scanning electron microscope consists of two main components: a column and a cabinet. The column is the site where electrons transverse from the emission source to interact with the specimen (Figure *2.3*), resulting in scattered signals being captured by detectors before being sent to the cabinet where the generated electrical signals are quantified and turned into magnified images and graphics for viewing (de Assumpcao Pereira-da-Silva and Ferri 2017).

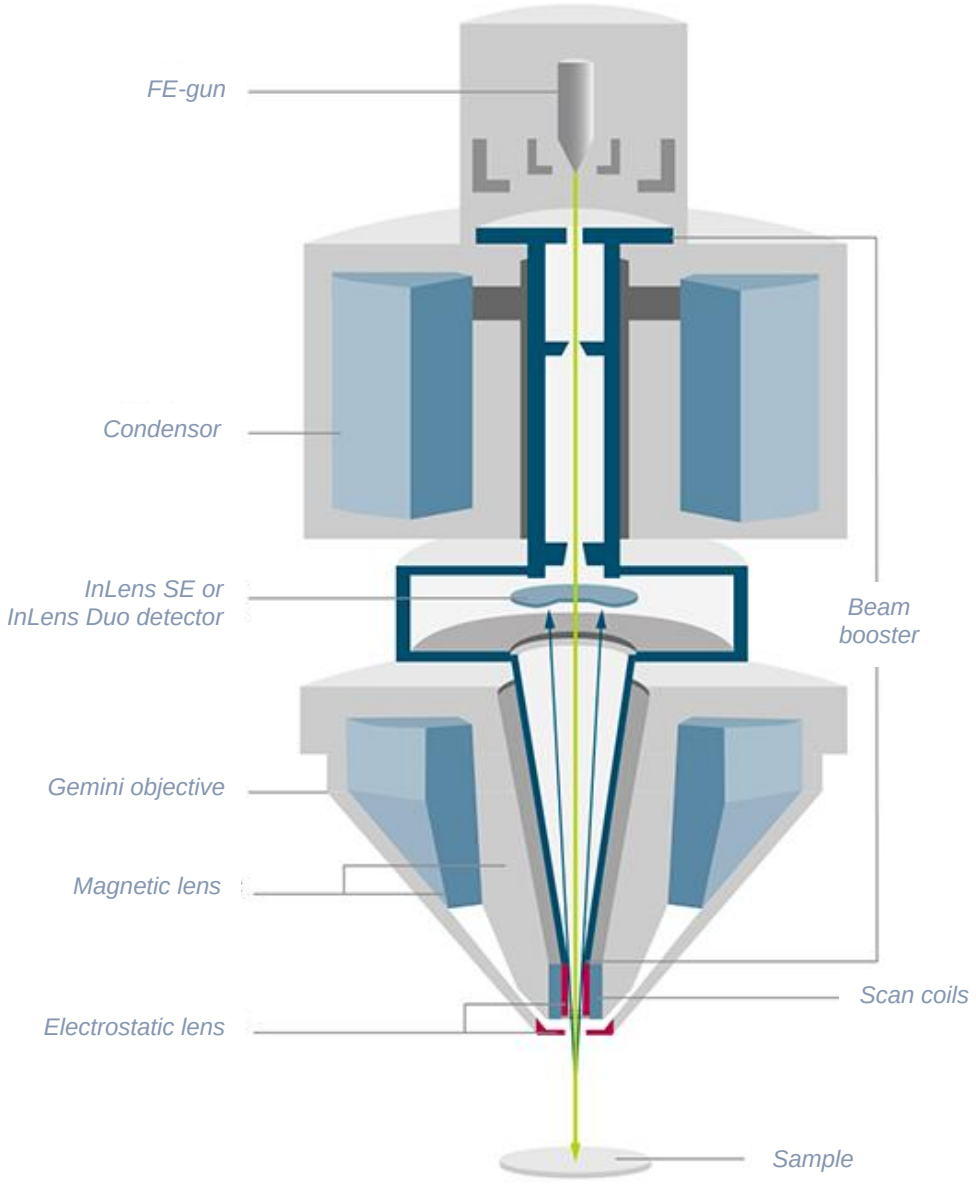

Figure 2.3: Schematic diagram showing the main components of a scanning electron microscope. Field Emission (FE), Secondary Electrons (SE). *Taken from:* Ziess.com (2019).

2.5.2.1.1 Vacuum

In a SEM, a vacuum is produced through a turbomolecular pump that pre-evacuates the chamber of air before the processes of SEM can begin. As electrons are only able to travel a small distance through air before dissemination occurs, the vacuum aids in stabilising the electrons to maintain a focused trajectory (de Assumpcao Pereira-da-Silva and Ferri 2017).

2.5.2.1.2 Electron Gun

The electron gun, positioned at the top of the column, acts as the electron source through which electron microscopy is possible. Electrons are emitted from a sharp tip, filament (*i.e., metallic tungsten crystal coated with zirconium*) after being heated (~1500 K) causing electrons to be accelerated down the column into the specimen (de Assumpcao Pereira-da-Silva and Ferri 2017). There are three electrically isolated parts contained within the gun: (1) a filament that acts as a cathode, emitting electrons that create a cloud around it; (2) a metal cylinder *(Wehnelt)* with an aperture that controls the diameter of the electron cloud using field lines formed by applying a negative potential around both the cylinder and enclosed aperture; and (3) a disc with an aperture that acts as an anode to accelerate electrons at a voltage between 0.1 and 30 kV by forming an electrical field with the cylinder to propel electrons along the gun (de Assumpcao Pereira-da-Silva and Ferri 2017).

2.5.2.1.3 Electron column

Located just below the disc aperture is the electron column which houses condenser lenses, objective lenses, and scanning lenses. The electron beam which enters the column is cylindrical in shape and is reduced by a condenser lens into a cone with a vertex of a few nanometers and a cross section of 5-50 nm in diameter – a reduction upwards of 1000 times less than the original diameter (de Assumpcao Pereira-da-Silva and Ferri 2017). Next, the objective lenses, one of which is positioned closest to the specimen, functions to focus the image by altering the vertical position of the vertex of the beam up and down at different vertical positions across the surface of the specimen. Finally, a platinum disc located just before the sample chamber functions to reduce the effects of spherical aberrations by limiting the angular width of the beam to enhance the depth of field in the image (de Assumpcao Pereira-da-Silva and Ferri 2017). Functional scanning of the specimen is achieved by a secondary lens system within the column that contains scanning coils which deflect the electron beam across the specimen surface in sync with the imaging monitor (de Assumpcao Pereira-da-Silva and Ferri 2017).

2.5.2.1.4 Sample Chamber

Contained within the sample chamber is a moveable sample stage and an electron and X-ray signal detector. The detectors capture signals that are emitted by the sample and transduce them into electrical signals, which are then sent to the control cabinet to be quantified by an electronic system to produce viewable images and graphs (de Assumpcao Pereira-da-Silva and Ferri 2017).

2.6 Serial Block Face Scanning Electron Microscopy

2.6.1 Basic Protocol

2.6.1.1 Specimen Preparation

Whole embryonic and adult chicken eyes were harvested and immediately stored in a Karnovsky fixative. Corneas were excised, maintaining the corneo-scleral junction for both, with the addition of the cartilaginous ossicles in adult corneas. Corneas were subsequently cut along either the sagittal or transverse plane to obtain orientation-specific wedged sections *(inferior, superior, nasal, or temporal in nature which encompassed portions of the peripheral cornea, limbus, and scleral ossicles)* that were then fixed overnight in the same solution.

The following treatment protocol was modified from the method of Deerinck et al. 2010 for 3View SBF-SEM:

Tissue samples, in vials on a Rotator, underwent treatment in the following sequence of freshly made solutions: 1.5% potassium ferricyanide (Sigma-Aldrich, UK, Cat. # 455989)/1% osmium tetroxide at room temperature for one hour, 1% aqueous thiocarbohydrazide (Sigma-Aldrich, UK, Cat. # 223220-25G) for 30 minutes, 1% osmium tetroxide for one hour, 1% uranyl acetate (Agar Scientific, UK, Cat. # AGR1260A) for one hour, and lead aspartate for 1 hour (at 60°C; lead nitrate, Agar Scientific, UK, Cat. # AGR1217 and 0.03 M aspartic acid (Acros Organics, Thermo Fisher Scientific, UK, Cat. # 10341614) which was made immediately before use by dissolving 66 mg lead nitrate (Agar Scientific, UK, Cat. # R1217) in 10 mL L-aspartic acid (0.4 g/100 mL; Sigma-Aldrich, UK, Cat. # A9256) and adjusting pH to 5.5 with 1 N KOH (Sigma-Aldrich, UK, cat. #P5958). Between each treatment, all samples were washed in several changes of double distilled water (ddH_2O) over a course of 30 minutes. Moreover, all fresh solutions and ddH_2O were filtered through a 0.22 μm Millipore syringe filter (Merck, Massachusetts, USA, Cat. # SLGP033RS) prior to instillation.

Following the above sequence of treatments, tissue samples underwent a stepwise dehydration using ascending concentrations of ethanol:

Dehydration:

70 % 90 % 100 % x2	15 minutes for each concentration of ethanol

Following dehydration, tissue samples were submerged in two consecutive treatments of propylene oxide (Agar Scientific, UK, cat. # AGR1080) lasting for 15 minutes each before being transferred into a 1:1 mixture of propylene oxide and Araldite resin (*without benzyl dimethylamine*) overnight. The following morning, tissue samples underwent five, one-hour treatments in Araldite (*without benzyl dimethylamine)* before being sequentially transferred into a new batch of Araldite *(with benzyl dimethylamine)* for one hour, two hours, one hour, and then overnight with vial lids off exposing samples to the air. Finally, samples underwent three more treatments in fresh Araldite *(with benzyl dimethylamine*), with each treatment lasting two hours each before being oriented and embedded into moulds that were then transferred to a 60°C oven for 48 hours.

2.6.1.2 Serial Block-Face Image Acquisition

Specimen Mounting

Small pieces of resin embedded tissue samples were mounted on aluminum pins (Leica, Vienna, Cat. #16701950) using Loctite® Super Glue (Henkel, UK). The blocks were faced and trimmed with a glass knife to a 1.0 mm x 1.0 mm square for 360-degree sample exposure. Leit-C conducting carbon cement (Agar Scientific Ltd., Cat. # AGG3300) was applied to the exposed edges to electrically ground the sample to the aluminum pin, caution was taken to not coat the block face or edges of embedded tissue that would ultimately be sectioned; the sample was then coated with an 8 nm thick layer of gold in an EM ACE 200 sputtercoater (Leica Microsystems, Vienna). The block was inserted into the SEM chamber and surfaced using the internal mini-ultramicrotome to remove the superficial layer of gold from the block face; datasets were collected–automatedly imaging the block surface over periods up to 36 hours using the backscatter electron detector.

Image Acquisition

Serial block-face imaging was accomplished using a Sigma VP FEG Scanning Electron Microscope (Carl Zeiss Ltd, Cambridge, UK) with integral 3View®2 system (Thermo Fisher Scientific-Gatan Inc, Pleasanton, CA). For this work, cells and tissues were typically imaged at 3.5 kV accelerating

voltage, 25 Pa nitrogen gas pressure and beam dwell time of 8 msec. With a scan resolution of 4096 x 4096 pixels; pixel size was 9.3 nm at 4.5 Kx magnification. Sequences of up to 1000 serial images were acquired using a 100 nm cutting interval.

2.6.1.3 Image Processing and Analysis

Once a stack of images was recorded, the stack underwent multiple processing manipulations so that the 2D images could be reconstructed into a 3D volume image. This was done using the 3D Viewer plug-in in ImageJ/Fiji, and Amira-Avizo 6.2 image analysis software with both manual and automated segmentation techniques to render 3D visualisation of a partial volume of the specimen.

2.6.2 Basic Principle

Serial block face scanning electron microscopy is a modern technique that utilises the key principles outlined in Section 2.5.2 regarding SEM and applies them for the acquisition of serial images of a specimen to provide digitally aligned ultrastructural data in three spatial dimensions *(x-y-z)* (Cocks et al. 2018). The major difference between an SEM and SBF-SEM is that SBF-SEM houses a mini-ultramicrotome equipped with a knife inside the SEM chamber (Cocks et al. 2018; Smith and Starborg, 2019). The process of removal of an ultrathin slice *(20-200 nm)* from the surface of a sample embedded in a resin block (Figure *2.4*) takes a matter of seconds and is followed by the top of the block face being scanned by an electron beam; backscattered electrons are detected and recorded to produce a digital image and the process of cutting and subsequent imaging is repeated many times (Smith and Starborg 2019). The digitized stack of images can be analyzed in a multitude of ways to follow cellular arrangements and intracellular structures; moreover, image analysis software can be employed to create 3D reconstructions of the stack (Cocks et al. 2018).

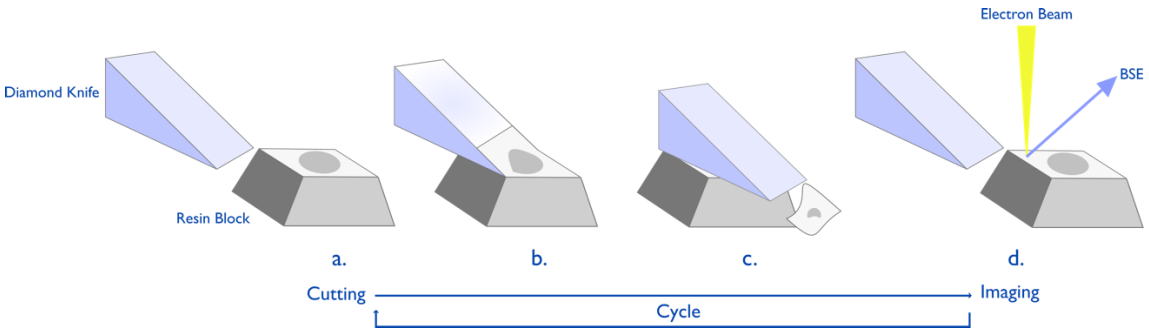

Figure 2.4: Illustration of the steps in SBF-SEM. (a.) Stage raises up bringing the resin block *(containing a fixed sample)* into position (b. and c.) the diamond knife cuts away an ultrathin surface slice *(20-200 nm)* to expose a new surface and retracts (d.) the knife retracts to expose a new face and the block face is scanned and imaged. This process can be repeated multiple times to produce a digitized set of serial images. Backscattered electrons (BSE).

2.7 Transmission Electron Microscopy

2.7.1 Basic Protocol

2.7.1.1 Specimen Preparation

See Section 2.6.1.1

2.7.1.2 Specimen Sectioning

See Section 5.2.3.1.

2.7.1.3 Imaging

Electrons were transmitted through ultrathin sections using a JEM 1010 transmission electron microscope operating at 80 kV (Jeol (UK) Ltd, UK) and images acquired using an Orius SC1000 CCD camera (Gatan, CA, USA).

2.7.2 Basic Principles

Transmission electron microscopy is a powerful technique used to characterise nanomaterials by providing high-resolution, two-dimensional information of its fine ultrastructure *(cellular composition, morphology, density, etc.)* which exceeds the imaging capabilities of even conventional SEM and SBF-SEM (Kumar et al. 2019). The working principle of TEM (Figure *2.2*) uses a focused beam of highly energised electrons that are transmitted through an ultrathin section *(<100 nm)* of the sample. TEM is primarily interested in detecting those electrons that do not deviate far from the incident-electron direction *(as forward scattered electrons)* as they provide key information about internal structures. The amount of transmitted electrons is dependent on the electron density of the specimen and therefore darker regions of the contrast image correspond to regions in the specimen where electrons are not transmitted but absorbed or backscattered (Le Marchand and Dalva 2020).

2.7.2.1 Transmission Electron Microscope Components

Like a scanning electron microscope, a transmission electron microscope consists of three main components: an electron gun, an image producing system, and an image-recording system (Bradbury et al. 2019). The electron gun (Figure *2.5*), which generates an electron beam, is focused onto the specimen using an internal condenser system. Within the image-producing system, a moveable specimen stage, an objective lens, and both intermediate and projector lenses can be

adjusted to focus electrons transmitting through the specimen to produce a highly magnified image; permanent acquisition of these transmitted electrons are converted using the image-recording system via a fluorescent screen for observation of the image and a digital camera for acquisition (Bradbury et al. 2019).

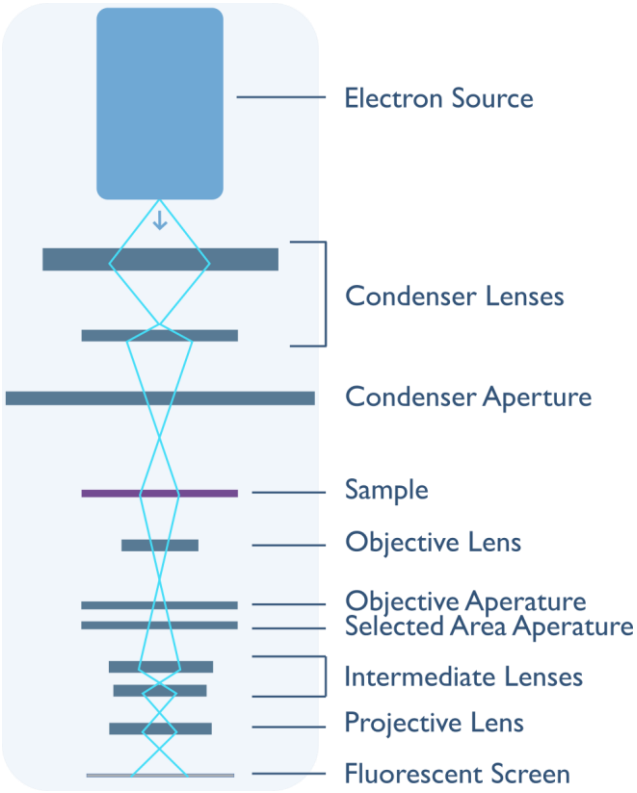

Figure 2.5: Schematic diagram showing the main components of a transmission electron microscope.

2.7.2.1.1 Electron Gun

The electron gun consists of a cathode electron source, generated from heating a tungsten filament, which is surrounded by a column-shaped control grid known as a Wehnelt cylinder. Both the cathode and the control grid are negatively charged[26] with the end of a disk-shaped anode featuring an axial hole (Bradbury et al. 2019). Electrons are accelerated from the cathode to the anode at a high voltage and focused onto the specimen using a condenser-lens system that controls the column hole and the energy intensity of the electron gun (Bradbury et al. 2019).

[26] Negative potential is equal to the accelerating voltage, by increasing the negative voltage it narrows the emission area whereby reducing the source size and increasing image resolution.

2.7.2.1.2 Image-Producing System

The function of this system is to produce a highly magnified image by focusing incident electrons transmitted through the specimen using both mechanical and electrical adjustments to the movable specimen stage, objective and projector lenses, and illumination system (Bradbury et al. 2019). The objective lens within this system is positioned at a short focal length *(1-5 mm)* to generate a real, intermediate image of the transmitted electrons from the condenser lens that passes through two projector lenses *(one being an intermediate lens)* allowing for the transmitted image to be progressively magnified to a range of 1000x – 250,000x on the screen (Bradbury et al. 2019).

2.7.2.1.3 Image-Recording System

To make the monochromatic electron image visible to the human eye the transmitted electrons are caught by the microscopes fluorescent screen and are digitally displayed on the computer screen prior to image acquisition using electronic software (Bradbury et al. 2019).

2.8 Flow Cytometry

2.8.1 Basic Protocol

2.8.1.1 Staining

Live cells in suspensions ($1x10^6$ cells/mL) were centrifuged in Eppendorf tubes (Star Lab, UK, Cat. # E1415-2600) for five minutes to form a pellet and remaining supernatant was discarded. Cells were resuspended in ice-cold D-PBS containing 0.1% *(w/v)* bovine serum albumin (*BSA*, Sigma Aldrich, UK, Cat. # A9418-10G) and mixed thoroughly before being centrifuged for five minutes *(supernatant was discarded)*. Blocking serum was instilled and tubes were put on rotation for one hour before being centrifuged and resultant supernatant being discarded. Cells were again resuspended in fresh ice-cold D-PBS/0.1% BSA, mixed thoroughly and centrifuged with supernatant being discarded. Cells were resuspended in 10 μg/mL of primary antibodies and Eppendorf tubes were put on rotation for one hour at 4°C. A D-PBS/0.1% BSA wash was performed three times and cells were resuspended in 1 μg/mL of corresponding conjugated secondary antibody and placed on rotation for 45 minutes *(in the dark)* at 4°C. Cells were washed repeatedly three times with D-PBS/0.1% BSA before being analysed.

2.8.1.2 Data Analysis

Flow cytometry was performed using a BD LSRFortessa™ cell analyser (BD, UK). Acquisition and analysis of results was performed using BD FACSDiva™ and FlowJo (BD, UK) software.

2.8.2 Basic Principle

Flow cytometry is a method for sorting and quantifying heterogenous mixtures of living cells by both cellular and electronic means; it has a great advantage over traditional microscopy as it permits the analysis of a significantly greater number of cells in a fraction of the time (Nunez 2001). The basic operating principle behind flow cytometry (Figure *2.6*) involves passing a single-cellular suspension through a chamber, where a continuous flow of cells, in the form of a liquid stream, encounters a laser beam of light. Passage of cells through the laser light leads to a (1) scattering of light and (2) emittance of fluorescent light; both signals produced from these phenomena are then collected for analysis by the machine (Nunez 2001; Givan 2010).

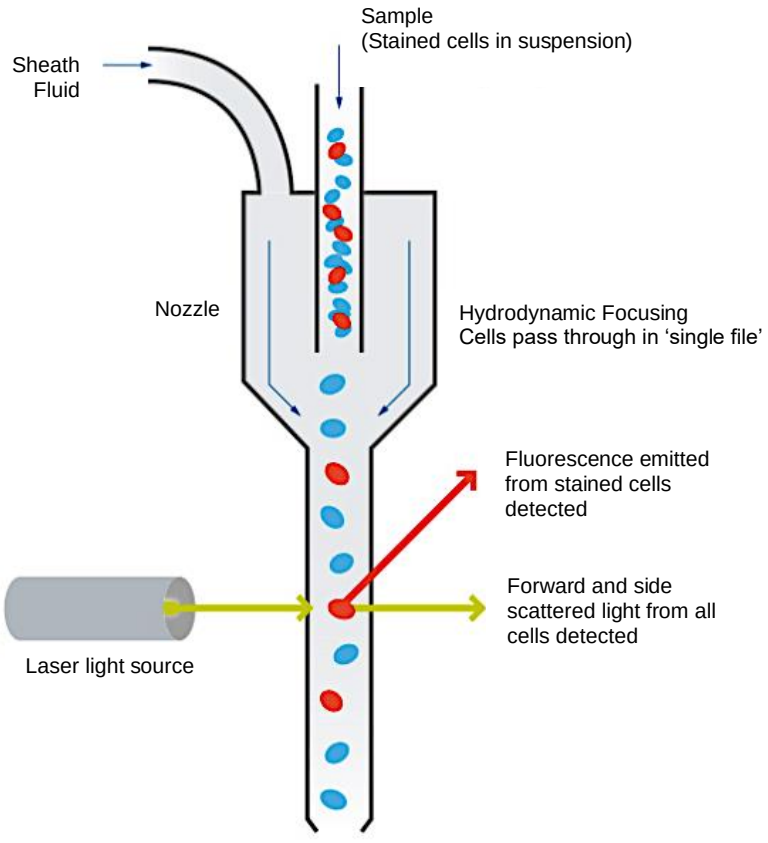

Figure 2.6: Schematic illustrating flow cytometry. *Adapted from:* Abcam.com (2019).

Components

Simultaneous measurement of several parameters can be achieved for each cell:

i) *Forward angle scatter intensity (FSC):* indicative of cell diameter.

ii) *Side angle scatter intensity (SSC):* indicative of granularity of the cell as higher granularity will result in greater light scatter leading to an increased SSC value.

iii) *Antigen fluorescence:* measured at multiple wavelengths, indicates subpopulations of cells that have fluorescent probes coupled to specific antibodies (Nunez 2001).

The electronics can quantitate the faint flashes of scattered and fluorescent light for each parameter, recording thousands of cells per sample to display it graphically for interpretation (Nunez 2001).

2.8.2.1 Fluorescence

Fluorescence is an optical phenomenon that is achieved by the unique property of fluorescent molecules *(fluorophores)*, whereby absorbed light from a photon trigger (*i.e., a laser beam)* is partially emitted at a different wavelength (Godbey 2014; Hegyi and Hegyi 2016). With respect to biotechnological application, fluorophores can be attached to antibodies to allow for simultaneous detection and quantification of cellular expression (Godbey 2014).

Absorption

Applying Newton's law on the conservation of energy, it is apparent that if a fluorophore absorbs energy from an incoming photon, the resulting emission of energy (*as a photon*) will be to a level that is less than or equal to the amount of energy that was initially held by the photon prior to absorption (Godbey 2014). Applied to the visible light spectrum, as seen in Figure *2.7*, this means that photons with a shorter wavelength *(in the violet region)* carry more energy than do photons with a longer wavelength *(in the red region);* therefore, fluorophore absorption at any given color leads to photon emittance at the same or a lower level or energy *(thus a longer wavelength)* which presents to the right of that color (Godbey 2014; Hegyi and Hegyi 2016).

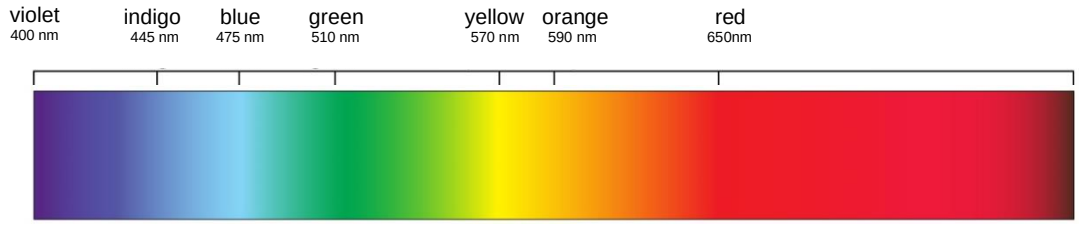

Figure 2.7: A rendering of the visible light spectrum.

Excitation and Emission

Fluorophore excitation and potentiality is most efficiently achieved by a particular wavelength – the emission maximum for that fluorophore. However, excited fluorophores can simultaneously emit light at a wavelength near the emission maximum but will do so at a lesser intensity; to understand how this occurs, it is important to consider the nature of the interactions occurring between energy and a material on a subatomic level (Hegyi and Hegyi 2016). Most molecules, at room temperature, exist in a relatively low-energy, stable configuration called a ground state with the potential of achieving multiple higher-energy states, called excited states (Godbey 2014). However, at higher-energy states, fluorophores are in a significantly less stable configuration and will, therefore, adopt a transient, semi-stable configuration in the lowest-energy excitable state (Godbey 2014; Hegyi and Hegyi 2016). Next, fluorophores will transition back to ground state from a semi-stable excited state and emit the excess energy which presents as a different colour *(of a longer wavelength)* to the light energy initially absorbed (Godbey 2014).

2.8.2.2 Flow Cytometer Components

The common elements that make up all flow cytometers are: (1) a light source, that emits a focused laser; (2) a fluidic system, that transports cells from the sample tube into the direct liquid stream that travels through the focused beam; (3) an optical system, that collects and orients light around the instrument to generate a photocurrent that is converted to numbers relating to light intensity; and (4) an electronic system, that digitizes the photocurrent for analysis (Givan 2010).

2.8.2.2.1 Laser

In a flow cytometer, spherical lenses are used to narrow an initial beam of 1-2 mm into a focused 60 μm wide beam, through which cells flow. Cells that pass peripherally through the beam will exhibit reduced resultant illumination, compared to cells travelling through centrally; therefore, cells need to be confined to a well-defined path, one by one, to receive identical illumination as they flow through the beam (Givan 2010).

2.8.2.2.2 Fluidics System

The fluidic system is responsible for centering cells in the illuminating beam by providing a supporting vehicle *(sheath fluid)* through which cells can travel. Cells within a tube are connected to an O-ring on a manifold that deposits air into the test tube, thus pushing the cell-suspension up the tube into the reservoir of pressurized sheath fluid, which transfers into tubing containing the illumination point (Givan 2010).

2.8.2.2.3 Optics System

The optical system provides a stable surface to maintain alignment of the light source and light detectors with the cells being illuminated. The point at which the stream of cells and light beam intersect is referred to as the "analysis point" and surrounding this point are lenses that collect light as it emerges after its intersection with the cells in the stream (Givan 2010). This emergent light constitutes the signal that focuses onto photodetectors *(FSC, SSC, and antigen fluorescence)* that convert the light signal into an electrical impulse, where intensity of the impulse is proportional to the intensity of light impinging on the detector (Givan 2010).

2.8.2.2.4 Electronic System

The electrical current generated from signal scatter and fluorescence enters an amplifier that is then converted to a voltage pulse, that is assigned a digital value and is displayed in an appropriate position on the relevant data plots – *refer to Figure 6.1* (Givan 2010).

2.9 Summary

This chapter outlines basic protocols and general principles for conducting *in vitro* and *ex vivo* analysis of avian corneal tissue.

To summarise, the main techniques to be used are:

- Primary cell culture
- Immunohistochemistry
- High resolution imaging *(TEM, SEM, and SBF-SEM)*
- Flow cytometry analysis

The following chapter describes the immunolocalization of putative stromal stem cell and matrix markers *ex vivo* at specific developmental time points and *in vitro* using standardised culture conditions, to establish a baseline dataset for comparisons with changes in phenotypic expression of cells associated with modifications made to culture conditions, which are presented in Chapter six. Furthermore, the techniques used for immunohistochemistry in Chapter three will also be applied in assessing the immunolocalization of CS antibodies in the developing avian limbus in Chapter four.

Chapter 3: Immunolabelling of Putative Stromal Stem Cell Markers in the Developing and Adult Avian Cornea

3.1 Introduction

In recent years, various animal models [27] have been used to examine corneal development and response to surgery and trauma (Wisley et al. 2018). Yet the once-overlooked domestic chicken (*Gallus gallus domesticus)* has since superseded them all to become one of the "most practicable" model for studying a broad range of ocular surface diseases and conditions (Hamburger and Hamilton 1951; Quantock et al. 2003). In addition to the several advantages afforded by this model *(reduced cost, availability, and ease in handling)*, corneal research in particular has benefited greatly from the shared homology between the chicken and human cornea with respect to anatomical, cellular, and extracellular matrix features (*i.e., keratocytes, proteoglycan and collagen profiles*) (Wisely et al. 2018). Notable, is the similarity of the proportionate thickness ratio of their corneal layers with the added advantage of the chicken cornea also possessing a true Bowman's layer[28] and a stable blood-aqueous barrier[29]. In a more recent investigation by Feneck et al. (2020), the homology between the human and avian models was further substantiated by demonstrating analogous developmental events using advanced imaging techniques. In particular, an acellular collagenous primary stroma was observed during week seven of human corneal development which also supported subsequent mesenchymal cell migration that mimicked the initial developmental events previously documented in the chicken cornea (Feneck et al. 2020). Collectively, these characteristics highlight the robustness of the avian model and how it is more reflective of the human corneal physiology than previously thought which has the potential to offer high-throughput and translational knowledge for future applications in vision research (Fowler et al. 2004; Ritchey et al. 2011; Wisely et al. 2018; Feneck et al. 2020).

Consequently, many investigations into corneal wound healing, refractive surgery, opacification, and transplantation have gone on to successfully exploit these shared commonalities for the advancement of corneal research (Quantock et al. 2003). Notably, a study by Fowler et al. (2004), was the first to compare and quantify post-mechanical debridement re-epithelialization rates in a

[27] Species include rodents, rabbits, felines, non-human primates, and certain avian species.
[28] Important for studies involving penetrating traumas or corneal refractive studies *(i.e., epithelial debridement where epithelial re-growth is examined).*
[29] Beneficial in excluding one possible cofounding factor in the analysis of wound healing rates following penetrating ocular surface traumas.

species *(other than human)* with a Bowman's layer. Analysis of corneas with laser-disrupted or preserved Bowman's layers revealed rapid re-epithelization in the presence of an intact Bowman's layer, compared to that of a laser-disrupted one. Histological irregularities between the Bowman's layer and stroma when the former was subject to laser-disruption were also observed. These findings were able to explain why development of corneal haze was a common side-effect of photorefractive keratectomy and aided in improving surgical techniques to reduce future incidence rates (Fowler et al. 2004; Wisely et al. 2017). Similarly, Ritchey and colleagues went on to study the mechanism of corneal wound healing by assessing the resultant cellular processes following incisions made to chicken corneas. The outcome revealed similarities in the mechanism for wound healing between the chicken and human cornea such that both epithelial and stromal cell changes were seen to cause, at the site of the wound, the migration of cells *(keratocytes and CD45-expressing monocytes)* and subsequent re-innervation by the ophthalmic division of the trigeminal nerve. (Ritchey et al. 2011; Wisely et al. 2017).

The potential of the avian model was further highlighted by Koudouna et al. (2020) who used the embryonic chicken cornea as a wound healing model and successfully showed it had the ability to fully recapitulate the three-dimensional collagen architecture following *in ovo* wounding. These findings coupled with a well-established morphological description of chicken corneal development serve as a primer for future works in understanding the mechanisms which control tissue regeneration versus repair. Moreover, the clinical and scientific implications that can be elucidated from the avian model can lead to development of novel therapeutics to combat sight-threatening diseases and disorders affecting the refractive properties and integrity of the corneal tissue as a whole (Koudouna et al. 2020).

3.1.1 Corneal Stroma: Cells and Matrix

The optical properties and physical strength of the cornea are derived mainly from the stroma, an architecture of tough connective tissue, combined with specialised ECM components (Funderburgh et al. 2016). The stromal framework consists of fibrils *(type I & V collagens combined in a heteropolymer with filaments of type VI collagen)* that are organised into stacked, orthogonally oriented lamellae (Maurice 1957). The nature of the fibrils higher order packing and interfibrillar spacing is a key characteristic that contributes to the promotion of corneal transparency and mechanical durability (Maurice 1957; Hart and Farrell 1969; Benedek 1971). In addition to collagen, the corneal stroma contains various types of proteoglycan molecules, mainly KS and CS/DS that interact with collagen fibrils to regulate their diameter and spacing (Iozzo 1997).

As discussed earlier, the structure of a corneal proteoglycan molecule is comprised of singular or multiple GAG side chains that are covalently bonded to a core protein. In the case of KS, the side chain is bound to a core protein, keratocan, lumican, or mimecan, whereas side chains of CS/DS are bound to core proteins, decorin or biglycan (Iozzo 1997). The net negative charge attributed to these PGs, as a result of their sulphated amino sugars, is what institutes interactions with other collagen fibrils as well as ECM components to promote the transparency of the corneal structure (Iozzo 1997). Moreover, another vital component of the corneal stroma are keratocytes; these neural crest-derived mesenchymal cells play an important role in the healing of the cornea throughout life in addition to supporting homeostasis *(i.e., renewal of proteoglycans and other matrix components)* (Lwigale et al. 2005). A key characteristic of keratocytes is that they are not terminally differentiated cells and are able to retain a level of plasticity and multipotency, which aids in the mechanisms of removing, replenishing, and reconstructing the stroma in response to damage.

3.1.2 Selected Matrix Markers for Investigation in the Avian Cornea

Keratocytes are well known for supporting the maintenance of stromal homeostasis through the synthesis of matrix elements that help to maintain the structural integrity and transparency of the cornea (Funderburgh et al. 2010). Extensive *in vitro* work by various authors found that keratocytes expressed an array of phenotype specific markers such as keratocan, KS, and pro-collagen type I (Hart 1976; Hay et al. 1979; Birk et al. 1981; Linsenmayer et al. 1983;1986; Birk and Trelstad 1984; Funderburgh et al.1986; Lwigale et al. 2005; Carlson et al. 2005; Funderburgh 2010; Scott et al. 2011). As such, they were included in this study for the purposes of substantiating that keratocytes had indeed been successfully isolated for primary cell culture.

Collagen type III was also included in the investigative phenotypic profile even though it still remains a point of contention amongst researchers in regard to it being synthesised by keratocytes (Hayes et al. 2015). Work by von der Mark et al. (1977) and Conrad et al. (1980) found type III collagen immunolabelling in the corneal epithelium of the developing chicken but absent from the stroma. However, Conrad and colleagues did find that keratocytes isolated for *in vitro* culturing did initiate the synthesis of type III collagen, but it was uncertain to them at the time if it was due to treatment with proteolytic enzymes used to expose keratocytes or due to stimulation by fetal bovine serum used to culture cells. More recent works have identified small quantities of collagen type III in the stroma, but its deposition has been associated with stromal fibrosis and alpha-smooth muscle actin which produce an activated myofibroblastic keratocyte phenotype (Schmut 1977; Newsome et al. 1982; Nakayasu et al. 1986; Michelacci 2003; Green et al. 2016; Kumar et al.

2016). Kumar et al. (2016) also found collagen type III synthesis following activation *in vitro*, and for that reason collagen type III was used in this study to discern myofibroblast differentiation.

3.1.3 Stem Cells in the Stroma

Functionally, stem cells have the unique capability of generating and propagating additional stem cells as well as differentiating into various progenitor cells that can mature into multiple cell lineages (Fuchs and Segre 2000; Du et al. 2005; Stemcells.nih.gov 2019). In recent years, characterization of various stem cell markers has been achieved by exploiting the biological uniqueness of stem cell receptors, allowing for the identification and isolation of stem cells within various tissues and cell populations (Stemcells.nih.gov 2019).

The progenitor potential of stromal cells first became apparent when early-passage stromal cells isolated from the limbus, the transitional zone between the cornea and sclera, maintained some potential to re-express differentiated keratocyte characteristics when expanded *in vitro*, that is, a dendritic morphology and an upregulated expression of matrix markers: keratocan, KS, and ALDH3A1 (Du et al. 2005; Ren et al. 2008; Funderburgh et al. 2016). However, the ability to differentiate to keratocytes was not equally distributed in the stromal cell population (Ren et al. 2008; Funderburgh et al. 2016). About 3% of stromal cells isolated from bovine corneas exhibited clonal growth and had elevated mRNA expression of several genes linked to stem cells[30] (Funderburgh et al. 2005). These small populations of cells, later referred to as corneal stromal stem cells *(CSSC)*, did not exhibit keratocyte morphology or gene expression, rather expressed a number of genes associated with mesenchymal stem cells.

3.1.4 Selected Stem Cell Markers for Investigation in the Avian Cornea

A review by Funderburgh et al. (2016) outlined an array of stem cell genes/markers found to be expressed by human neural crest-derived mesenchymal CSSCs. Gene expression of these markers was categorised into groups based on expression origin *(i.e., mesenchymal stem cells – Bmi-1 and CXCR4, and ocular precursors in embryonic development – PAX6)* (Funderburgh et al. 2016). The genes mentioned are not a representation of all the stem cell genes discussed in the paper but were the ones selected for the purposes of this thesis as an initial starting point for the investigation of stem cell marker expression in the chicken cornea *in situ* and *in vitro* cultures of expanded corneal stromal, mesenchymal-derived keratocytes. Similarly, Chen et al. (2006) found CX43 to be a reliable

[30] Markers include: PAX6, Notch1, FHL1, CD90, CD166, Bmi-1, ABCG2, SCF, CD73 (Funderburgh et al. 2005).

negative marker for stem cell containing populations in the human limbal stem cell niche and as such was included alongside positive markers PAX6, Bmi-1, and CXCR4. Moreover, the markers selected for this study were chosen over their counterparts as not all markers referenced in the Funderburgh et al. (2016) review had antibodies developed for dual reactivity in both the chicken and mouse *(which was used as a positive epitope, tissue control to validate the immunolabelling of each putative stromal stem cell (PSSC) marker).*

CX43

CX43 is a primary component of gap junctions that reside at the cell plasma membrane, neoplasm, and vesicles and participate in intercellular communication for the purposes of regulating cell proliferation, differentiation, and migration (Laird and Lampe 2018; Sorgen et al. 2018; Kotini et al. 2018). The expression of CX43 in normal corneas has previously been noted in the basal cell layer of the human corneal epithelium but absent from the limbal epithelium, suggesting that expression of CX43 denotes differentiation of stem cells into corneal TACs (Grueterich and Tseng 2002). Wolosin et al. (2000) went on to suggest the incongruity in CX43 expression across the cornea was so that limbal epithelial stem cells in the niche would remain segregated from further differentiated TACs by restricting communications that had the potential to influence cells to proliferate and differentiate (Wolosin et al. 2000; Grueterich and Tseng 2002).

Gap junctions are formed of two interacting hemichannels, with each channel being composed of six protein subunits *(connexins and pannexins)* that form a tetraspan transmembrane complex: an intracellular N- and C-terminal; two extracellular loops; and one cytoplasmic loop (Ribeiro-Rodrigues et al. 2017; Laird and Lampe 2018; Xu et al. 2019). In order to form the gap junction channel, the hemichannels are transported to the plasma membrane where they dock with similar structures present along neighbouring cell membranes (Ribeiro-Rodrigues et al. 2017). In order to mediate communication between non-opposed cells, CX43 uses tunnelling nanotubes, and extracellular vesicles (Wang et al. 2010; Soares et al. 2015; Ribeiro-Rodrigues et al. 2017).

PAX6

PAX6 is a transcriptional factor chiefly involved in eye development and maintaining normal function of certain tissues after birth[31]. In order to carry out these key functions its distinct protein domains bind specific areas on a DNA promoter region to activate expression (Sasamoto et al. 2016). PAX6 has two DNA-binding domains: a paired-domain and a homeodomain; the paired-

[31] PAX6 expression has been found in the remodeling and maintenance of adult tissues in the eye, pancreas, and cerebellum (Ton et al. 1991; Turque et al. 1994; Stoykova et al. 1994; Daniels et al. 2010).

domain contains both an N-terminal and a C-terminal sub-domain. Variations in the N-terminal sub-domain defines two PAX6 isoforms (*PAX6-a and PAX6-b)* which have previously been linked to development and maintenance of the posterior segment of the eye (Epstein et al. 1994; Azuma et al. 1996; Kozmik et al. 1997; Davis et al. 2003; Collinson et al. 2003; Ramaesh et al. 2003; Kiselev et al. 2012; Walther and Gruss 1991; Sasamoto et al. 2016). However, recent work by Sasamoto et al. (2016) determined that both isoforms were also differentially and cooperatively involved in regulating the expression of genes *(e.g., keratin 3/12)* relating to the structure and functional maintenance of the anterior segment of the eye including the corneal epithelium (Sasamoto et al. 2016). However, in many adult tissues, PAX6 is found to be downregulated, but in the case of the corneal epithelium it is sustained for the purposes of corneal maintenance and wound healing (Chao et al. 2000; Sivak et al. 2002; Baulmann et al. 2002; Davis et al. 2003; Sivak et al. 2004; Leiper et al. 2006; Ramaesh et al. 2006; Dora et al. 2008).

Bmi-1

Bmi-1 is a core component of the polycomb repressive complex that is a protein coding gene responsible for maintaining the transcriptionally repressive state of many genes linked to epigenetic inheritance, stem cell development, tumorigenesis, and fibroblast senescence (van der Lugt et al. 1994: 1996; Kiyono et al. 1998; Lessard et al. 1999; Park et al. 2003; Wang et al. 2004; Cao et al. 2005; Li et al. 2006; Gray et al. 2016). The Bmi-1 complex is composed of three regions: An N-terminal RING domain, a central domain and a C-terminal domain involved in stabilising the protein regulation. The N-terminal RING domain of Bmi-1 forms a complex with RING1A/B proteins, which constitutes the ubiquitin ligate subunit of the PRC1 complex; this direct, stabilising interaction is what leads to activities involved in promoting embryonic development and self-renewal of stem cells (Buchwald et al. 2006; Li et al. 2006; Sanchez-Pulido et al. 2008; Yadav et al. 2010; Gray et al. 2016).

CXCR4

CXCR4 is a complex member of the chemokine receptor subfamily of seven-transmembrane domain, G-protein coupled receptors with its natural ligand being CXCR4/SDF-1 (Murdoch and Finn 2000; Jacobson and Weiss 2013; He et al. 2018). The specific effects of CXCR4 on its target cells are mediated by several of its structural features: an extracellular N-terminus, which is responsible for ligand binding specificity; an intracellular C-terminus, which allows for intracellular signalling and receptor activation; seven helical transmembrane domains *(three intracellular and three extracellular),* which are oriented perpendicular to the plasma membrane: and a G-protein coupled through the C-terminus segment (Murdoch and Finn 2000). Cell signalling following ligand

binding causes subsequent activation of signalling cascades, leading to a broad repertoire of responses that regulate proliferation, differentiation, survival, and apoptosis (Cheng et al. 2017; He et al. 2018; Murdoch and Finn 2000).

The CXCR4/SDF-1 axis plays an important role in regulating the bone marrow microenvironment, homing of hematopoietic stem cells, retention, and proliferation of mesenchymal stem cells (Ratajczak et al. 2012; Boulais et al 2015; Chao et al. 2015; He et al. 2018). Moreover, the CXCL12/CXCR4 axis is also involved in homing of neural progenitor cells to the vascular niche, migration of embryonic neural crest cells to the dorsal root ganglia from the dorsal neural tube, recruitment of osteoblast progenitor cells to bone-development sites, and adhesion of mesenchymal stem cells to target tissues (Pellegrini et al. 2001; Belmadani et al. 2005; Kokovay et al. 2010; Ratliff et al. 2010; Xie et al. 2011; Ratajczak et al. 2013; He et al. 2018). With respect to the eye, the CXCR4/SDF-1 axis has been linked to human retinal pigmental epithelial cells, choroidal retinal endothelial cells, limbal epithelial stem cells, and corneal fibroblasts (Crane et al. 2000; Bourcier et al. 2003; Xie et al. 2011; Albert et al. 2012; Feng et al. 2015; Lopez et al. 2018). With respect to the limbal stem cell niche, the CXCR4/SDF-1 receptor ligand axis has been shown to modulate limbal stem/progenitor cells and maintain an undifferentiated state (Chen et al. 2011; Xie et al. 2011; 2012; Li et al. 2014).

3.1.5 Aims

In the present study, a protocol for the isolation of embryonic keratocytes was outlined in addition to specifying the modifications made to the protocol for the isolation of adult keratocytes. The aims were to:

- Assess the immunolabelling of selected PSSC markers CX43, PAX6, Bmi-1, and CXCR4 and matrix markers *(pro-collagen type I, collagen type III, keratocan, and KS)* following successful *in vitro* culturing of E_{18} and adult keratocytes
- Assess the immunolabelling of selected PSSC markers *in situ* at various developmental stages.

These assessments were carried out for the purpose of (1) establishing that keratocyte and native tissues did indeed label for both stem cell and matrix markers, as supported by positive murine controls for corneal staining and (2) establishing a baseline of qualitative dates prior to the investigation, as outlined in Chapter six, where quantification of expressional changes in PSSC markers by keratocytes could be assessed across multiple passages and coating conditions.

3.2 Material and Methods

All animals and procedures involved in this study were used in accordance with the Association for Research in Vision and Ophthalmology statement for the Use of Animals in Ophthalmic and Vision Research, as were local rules. Moreover, adult Hubbard JA87 chicken heads were obtained within hours of slaughter from a local abattoir (Capestone Organic Poultry Ltd., Haverfordwest, UK) and were transported on ice to the laboratory, adhering to the guidelines of the Animal and Plant Health Agency Regulation (EC) 1069/2009 and Regulation (EC) 142/2011 for the transport, storage, use and disposal of category 3 animal by-products.

3.2.1 Primary Cell Culture

Protocol modified from the unpublished method from Dr Elena Koudouna *(Cardiff University, UK)* and Dr Jim Ralphs *(Cardiff University, UK)*.

3.2.1.1 In Vitro Expansion (Cell Culture)

Collection and Initial Preparations

For the isolation of embryonic keratocytes, twelve fertilised white leghorn chicken eggs were obtained from a commercial hatchery and placed in an incubator *(37°C and ~60% humidity)* at 9:00 am to develop. With respect to the isolation of adult keratocytes, twelve Hubbard JA87 chickens *(matured 73-80 days)* were obtained from a local farm/abattoir and subsequently treated *(see below)* within three to four hours after collection.

Developing eggs were incubated to E_{18} as this was the point in time where active proliferation of fibroblasts occurred leading to the highest number of fibroblast layers *(~25)*, therefore a higher yield of keratocytes could be obtained initially (Hay and Revel 1969); moreover, E_{18} is the latest developmental stage at which embryos can be sacrificed under Schedule 1, of the UK Government's Animals *(Scientific Procedures)* Act 1986. As for the use of adult chicken corneas, it provided a novel opportunity to assess any variability that may have existed in activity between embryonic and matured keratocytes, specifically in response to being cultured where signalling and growth could be monitored.

Embryonic corneas were dissected from the eye at the limbus, requiring only an incision at the top of the crown to stabilise the head with forceps; corneas were simply removed by piercing the eye at the limbus with a fine-point forceps, grasping the cornea at the limbus and pulling it away. Once

removed, corneas were submerged in culture media on ice (Table *3.1*) to slow down the degradation of corneas until all were extracted before moving onto the next step. Adult corneas required a more intricate removal strategy involving detachment of the whole eyeball from the eye socket by severing the extraocular muscles using surgical scissors. Once whole eyeballs were removed and briefly placed in sterile D-PBS over ice to remove residual matter from the extraction before being transferred into a 1% *(v/v)* solution of Poly(vinylpyrrolidone)-Iodine Complex (Betadine, Sigma-Aldrich, Cat. # PVP1-100G) in distilled water *(over ice)* for two and half minutes, acting as an antiseptic to cleanse the ocular surface prior to corneal removal. Following treatment with 1% *(v/v)* betadine, eyeballs were washed with sterile D-PBS. Finally, corneas were removed in a similar fashion to embryonic corneas, but after first removing an intact ring of scleral ossicles to fully expose the limbal region.

Digestion

Extracted corneas were transferred into a 0.04% solution of EDTA in D-PBS and subsequently incubated at 37°C for 45 minutes on a rotator to loosen the epithelial and endothelial layers; adult corneas required additional preparation before EDTA treatment by removing the cartilaginous ossicles at the limbal junction. Following incubation, corneas were subjected to gentle scraping to further remove both the epithelium and endothelium to expose the stroma. In order to fully digest the stromal collagen matrix, samples were transferred into 5 mL solution of 0.15% collagenase type I and incubated at 37°C for two hours on a rotator; adult corneal tissue had to be lysed prior to treatment as initial attempts produced low yields of keratocytes. Resultant supernatant was isolated and transferred into a new test tube and centrifuged at 1450 RPM for five minutes. The resultant supernatant was discarded leaving behind a keratocyte-concentrated pellet. The pellet was re-suspended in 1-2 mL of culture media containing 5% *(v/v)* FBS.

Seeding

In order to seed at an initial density of 3.0 x 10^5 cells/mL in 35 mm petri dishes (Nunclon™ Delta, ThermoFisher Scientific, 150218), 10 µl of suspension was transferred onto a haemocytometer and a cell count was performed. Cells were re-suspended in the appropriate amount of culture media containing 5% *(v/v)* FBS and 2 mL of suspension was seeded into petri dishes for incubation at 37°C to allow for keratocyte attachment and growth. At a confluency of ~90% cells were dissociated from the culture surface by first removing old media and replacing it with pre-warmed dispase II solution (1 U/mL, ThermoFisher Scientific, Cat # 17105041) followed by incubation at 37°C for 30 minutes to dissociate cells very gently from cell culture surfaces. Adherent cells were

gently pipetted to supplement dispase treatment using pressurised force to further dissociate cells from cell culture surfaces before being transferred into a sterile tube to be centrifuged. The resultant pellet was washed using culture media before being resuspended in fresh media and seeded onto a new culture dish at the appropriate seeding density of the selected vessel. At passage 2 *(P_2)*, the seeding density of embryonic keratocytes was reduced to 1.50 x 10^5 cells/mL in 35 mm petri dishes to allow for individual keratocytes to be imaged. However, adult keratocytes were seeded at 3.0 x 10^5 cells/mL through P_2 as the reduced seeding density of 1.50 x 10^5 cells/mL led to insufficient connections being made between keratocytes resulting in stunted growth.

Fixing

Culture media was removed from dishes and 1 mL of 90% ethanol (Ethanol 99%$^+$, Absolute, Extra Pure, ThermoFisher Scientific, Cat. # E/0600DF/C17) was instilled for five minutes and then discarded – samples were allowed to air dry and were stored in a -80°C freezer.

Table 3.1: Standard cell culture media

	Components	**[Working]**	**Source: (Catalog No.)**
Culture Media	Dulbecco's Modified Eagle Medium	N/A	ThermoFisher: 61965-026
	Penicillin/Streptomycin Antibiotic	1% *(v/v)*	ThermoFisher: 15140-122
	Amphotericin *(Fungizone)*	0.25 µg/mL	ThermoFisher: 1529-029

3.2.2 Cryo-Sectioning

Dissection

Twelve fertilised white leghorn chicken eggs) were placed in an incubator *(at 9:00am)* to develop; at E_{10}, E_{14}, and E_{18} whole eyes were extracted after decapitation. Whole eyes from twelve adult Hubbard JA87 chicken heads were extracted as discussed in Section 3.2.1 eyes were submerged in a solution of 1% *(v/v)* PFA and PBS and rotated for 30 minutes before being transferred into a wash solution of PBS/Tween®20 (Sigma-Aldrich, Cat. # P9416-100ML) for 20 seconds. Eyes were then transferred into a solution of equal parts PBS/Tween®20 and OCT compound to be rotated overnight in a 4°C fridge. The overnight treatment was to allow for more effective penetration of OCT compound through the tissue to preserve structural integrity in addition to improving sectioning quality.

Eyes were removed from solution and E_{14} and E_{18} corneas were excised, maintaining the scleral-limbal junction; for adult corneas, the cartilaginous ossicles at the limbal junction were not removed as they were found to stabilise the shape of the cornea in OCT compound. With respect

to E_{10} and E_{12} corneas, whole eyes were kept intact as they were more fragile and found to be prone to damage. Moulds were filled with OCT compound and corneas/whole eyes were positioned in the centre of the moulds with the epithelium oriented downwards *(towards the base of mould)*. Moulds were then placed in a freezer at -80°C to set. Once set, embedded corneas were removed from moulds and placed in aluminium foil with their orientation clearly marked and returned to storage in the freezer.

Cryo-Sectioning

Corneas embedded in an OCT compound were oriented to mimic a sagittal plane view and freeze mounted to a cryostat chuck using OCT compound. Corneas were positioned within the cryostat *(at -20 °C internal temperature)* and sectioned at a 14 μm thickness before being transferred onto glass slides and stored in a freezer at -80°C.

3.2.3 Immunofluorescent Labelling of Putative Stromal Stem Cell Markers *In Situ* and *In Vitro*

Samples were brought to room temperature and a water repellent ring was made around the centre of cultured dishes using a PAP pen (ImmEdge®, Vector Laboratories, Cat. # H-4000) and around cryo-sectioned corneas to minimise the antibody volume used. Samples were rehydrated using PBS/Tween®20 for five minutes. The volume of solution used for *in situ* and *in vitro* immunostaining was 300 μl/dish and 150 μl/section.

Indirect immunoassay *(using conjugated secondary antibodies)* was performed by first treating samples with either normal horse (5% *(v/v)*, Vector Laboratories, Cat. # S-2000) or goat (5% *(v/v)*, Vector Laboratories, Cat. # S-1000) blocking serum in PBS with 0.1% *(w/v)* BSA for 30 minutes. Blocking serum combined with BSA was used to exclude experimental artefacts caused by non-specific antibody binding to endogenous Fc receptors in tissues and cells (Buchwalow et al. 2011). Once blocking serum was removed, primary antibodies (Table *3.2*) were instilled and placed in a fridge at 4°C overnight.

Validation of immunohistochemical assays was done using both positive and negative controls. Negative controls were also used to identify non-specific staining *(with primary antibodies omitted)* and isotype-specific naïve immunoglobulin *(IgG)* staining for each sample. Whereas positive controls were used to support antibody efficacy by affirming expression in another specimen *(in this case, wild-type mice corneal cross-sections)* known to contain the target molecules in a known location (Hewitt

et al. 2014). Conjugated secondary antibodies at a 1:200 dilution were instilled after multiple PBS/Tween®20 washes *(3x5 minutes)* and left for three hours in the dark at room temperature before an additional PBS washing *(3x5 minutes)*. Samples were mounted using one drop of DAPI (Vectashield, Vector Laboratories, Cat. # H-1200) under glass coverslips.

Table 3.2: Reagents used in immunofluorescence investigation

		Antibodies	[Working]	Source (Catalog No.)
Primary Antibodies	*In vitro*	Pro-Collagen Type I *(COL1A1)*	5 µg/mL	DSHB Hybridoma (M-38)
		Collagen Type III *(COL3A1)*	5 µg/mL	DSHB Hybridoma (3B2)
		Keratocan	1:5	Courtesy of Professor Clare Hughes *(Cardiff University: School of Biosciences)*
		Keratan Sulphate	5 µg/mL	DSHB Hybridoma (I22)
		Anti-Alpha Smooth Muscle Actin	5 µg/mL	Abcam (ab5694)
	In vitro & In situ	Anti-Connexin 43/GJA1	2.5 µg/mL	Abcam (ab117843)
		PAX6 Monoclonal *(AD2.38)*	2.5 µg/mL	Fisher Scientific (12-9914-82)
		Rabbit ∝ BMI-1		Sigma-Aldrich (PLA0208)
		CXCR4	2.5 µg/mL	Aviva Systems Biology (OALA00163)
Secondary Antibodies	*In vitro & In situ*	DyLight 488 Horse ∝ Mouse Ig_G	1:200	Vector Laboratories (DI-2488)
		DyLight 594 Horse ∝ Goat Ig_G	1:200	Vector Laboratories (DI-3094)
	In situ	DyLight 594 Goat ∝ Rabbit Ig_G	1:200	Vector Laboratories (DI-1594)

3.2.3.1 Phase Contrast Microscopy

In vitro image acquisition was performed using an Olympus IX71 Inverted Fluorescence & Phase Contrast Tissue Culture Microscope (Olympus, UK) to monitor morphological features and changes in keratocyte growth throughout P_0–P_2 at x10 and x20 magnification. Images were captured using SPOT 5.2 *(Basic)* Software (SPOT Imaging Solutions, Diagnostic Instruments Inc., USA) to adjust brightness and focus.

3.2.3.2 Immunofluorescence Microscopy of Samples

Image Acquisition

Epifluorescence imaging at different magnifications was performed using a BX61 fluorescence microscope (Olympus, UK) and Olympus CellSens software (Olympus, UK). Imaging of a single sample required acquisition across relevant channels dependant on the conjugated antibody dye. Individual fluorescence channels *(i.e., DAPI – blue, FITC – green, TRITC – red)* are linked to specific filters that excite a particular dye within a specimen and detect only the wavelength of interest emitted by the fluorophore. Within individual channels, camera setting such as exposure time were adjusted to mimic what was seen down the microscope, in addition to minimising saturation of

the resultant image, prior to being saved as a ".tiff" file. Exposure values for each channel within a sample at a specific magnification were recorded and applied to corresponding control samples *(isotype and without secondary antibody)*. All images presented in this chapter are representative of findings from three individual experiments.

Colour Processing

Images were individually exported into ImageJ software where the mean intensity of the area was subsequently subtracted to remove background "noise;" adjustments to both brightness and contrast were also made to mimic the appearance of immunolabeling seen down the microscope's objective lens. Images were also allocated a colour *(i.e., DAPI – blue, Alexa Fluor 488 – green, Alexa Fluor 594 – red),* prior to all relevant channels being overlaid to create a merged image that too was saved as a ".tiff" file. Note that any adjustment made to a raw image was also applied to its corresponding controls.

3.3 Results

3.3.1 Immunolabelling of Matrix and Putative Stromal Stem Cell Markers *In Vitro* by E_{18} and Adult Keratocytes

3.3.1.1 In Vitro Phase Contrast Imaging of Keratocyte Morphology

Primary chicken keratocytes were isolated from fresh E_{18} and adult stromas by collagenase digestion and cultured in the presence of 5% *(v/v)* FBS. Cultured cells retained elongated fusiform morphology typical of keratocytes *in vivo* across multiple passage (Figure *3.1*). Cells had the capacity to be cultured to 100% confluency within four days.

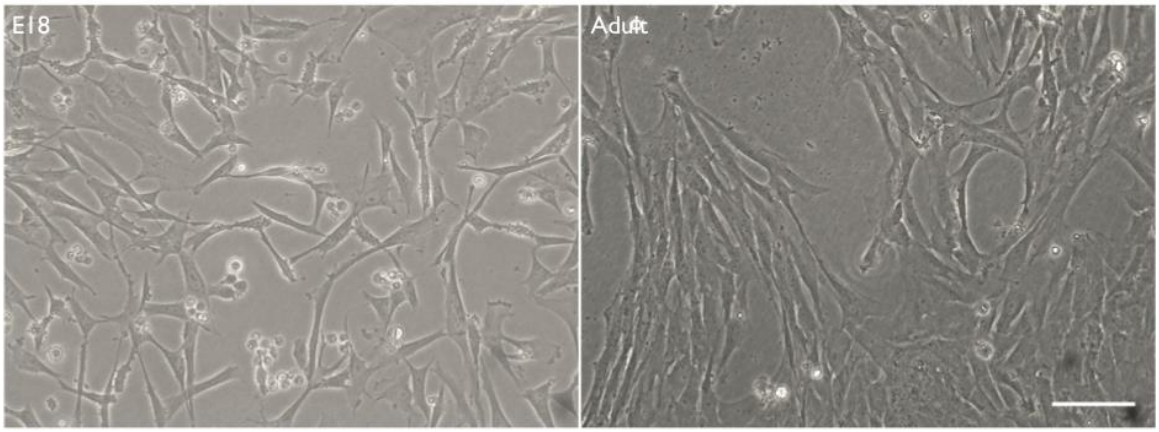

Figure 3.1: Keratocytes isolated and expanded in vitro from the corneal stroma of E_{18} and adult chickens. Phase contrast imaging shows P_2 expanded keratocytes from E_{18} and adult corneas using DMEM + 5% *(v/v)* FBS + 1% *(v/v)* P/S + 0.25 μg/mL fungizone. The scale bar represents 100 μm.

3.3.1.2 Phenotypic Labelling of Keratocyte Matrix Markers In Vitro

Immunofluorescence labelling of primary cultured keratocytes from E_{18} corneas (Figure *3.2*) showed strong signalling of matrix marker pro-collagen type I, moderate signalling of KS, and keratocan, and no observable signalling of collagen type III. It was also observed that the keratocan signalling pattern was that of a punctate nature, whereas KS adopted a clustered *(clumpy)* appearance. Comparatively, the results obtained from cultured adult chicken corneal keratocytes (Figure *3.3*) showed some parallels in matrix marker labelling to that of embryonic keratocytes, specifically, with respect to positive labelling of pro-collagen type I, KS, and keratocan. Incidentally, weak positive labelling of collagen type III was also observed in adult keratocytes. To supplement positive findings of collagen type III labelling by mature keratocytes, labelling of alpha smooth muscle actin was also investigated. Like collagen type III, weak staining of alpha smooth muscle actin was observed.

Moreover, the labelling of pro-collagen type I and collagen type III was only sparingly seen in some, but not all, adult cultured keratocytes, whereas, in embryonic keratocytes collagen type I was seen intracellularly within a majority of cells. Moreover, the pattern of KS and keratocan immunolabelling was comparatively different in adult cultured keratocytes with no clustered or punctate labelling being detected, respectively; rather, labelling was observed purely intracellularly and diffuse through the cytoplasm and dendritic processes of positively labelled cells. Negative controls confirmed a lack of non-specific binding of the secondary antibodies.

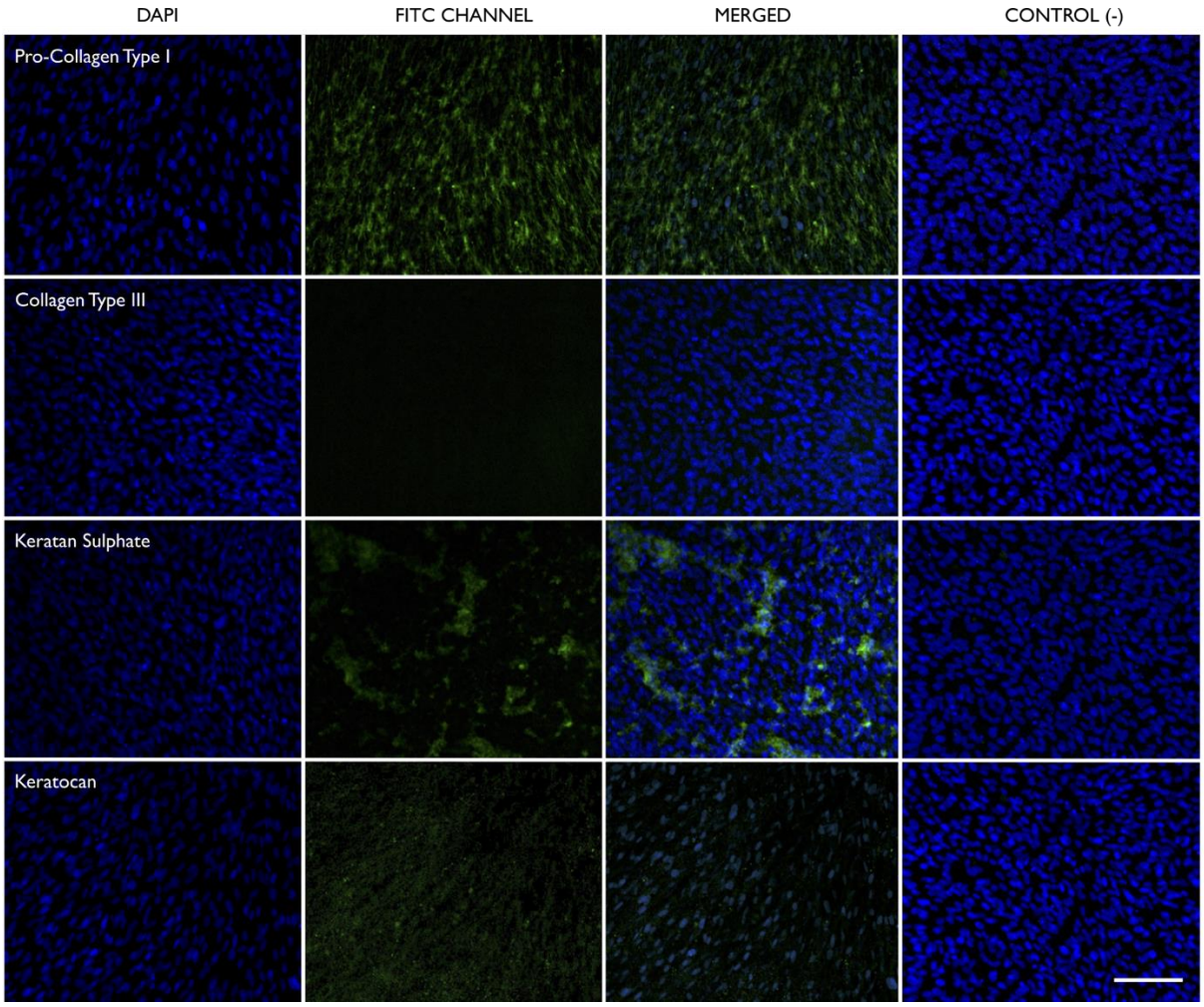

Figure 3.2: Immunolabeling of matrix markers in cultured E_{18} chicken corneal keratocytes. The horizontal panels show positive labeling *(green)* of pro-collagen type I, keratan sulphate, and keratocan; no observable labelling of collagen type III. Nuclei counterstained with DAPI *(blue)*. The scale bar represents 100 μm.

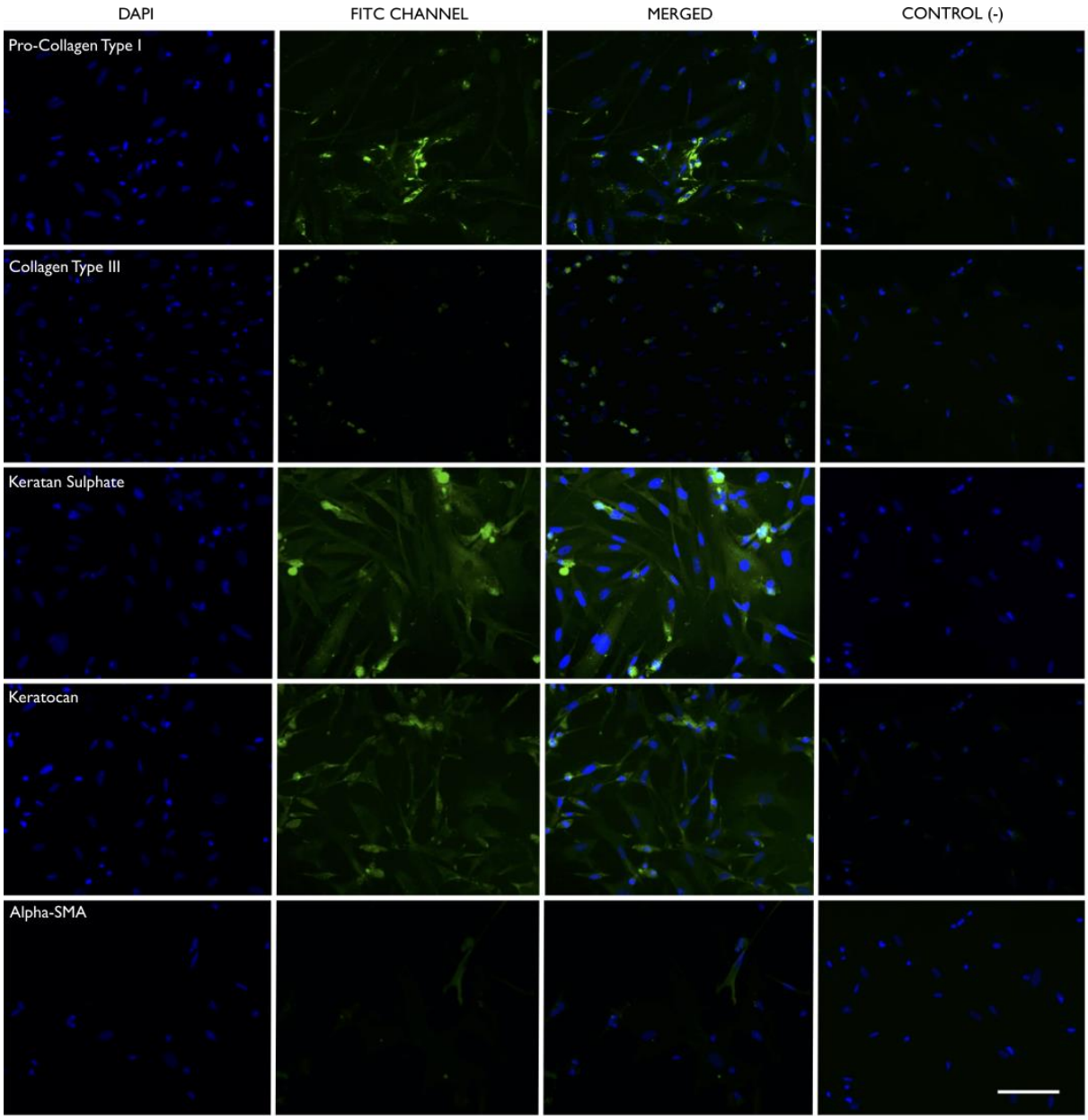

Figure 3.3: Immunolabeling of matrix markers in cultured adult chicken corneal keratocytes. The horizontal panels show strong labeling *(green)* of pro-collagen type I, keratan sulphate, and keratocan in addition to weak labelling of collagen type III and alpha smooth muscle actin (SMA) *(no visible intracellular microfilament stress fibres)*. Nuclei counterstained with DAPI *(blue)*. The scale bar represents 100 μm.

3.3.1.3 Immunolabelling of Putative Stromal Stem Cell Markers In Vitro

To further investigate the results obtained from immunofluorescence staining (*in situ)* in embryonic and adult chicken corneas, putative corneal stromal stem cell markers CX43, PAX6, BMI-1, and CXCR4 were investigated *in vitro*. As shown in Figure *3.4* and Figure *3.5*, strong signalling of CX43 (*green*), BMI-1 (*red*), and CXCR4 (r*ed*) was observed, however, no notable signalling of PAX6 *(green)* was observed. Moreover, negative controls showed a lack of non-specific binding of secondary antibodies. These results were consistent with findings to be further discussed in Section 3.3.1.4.

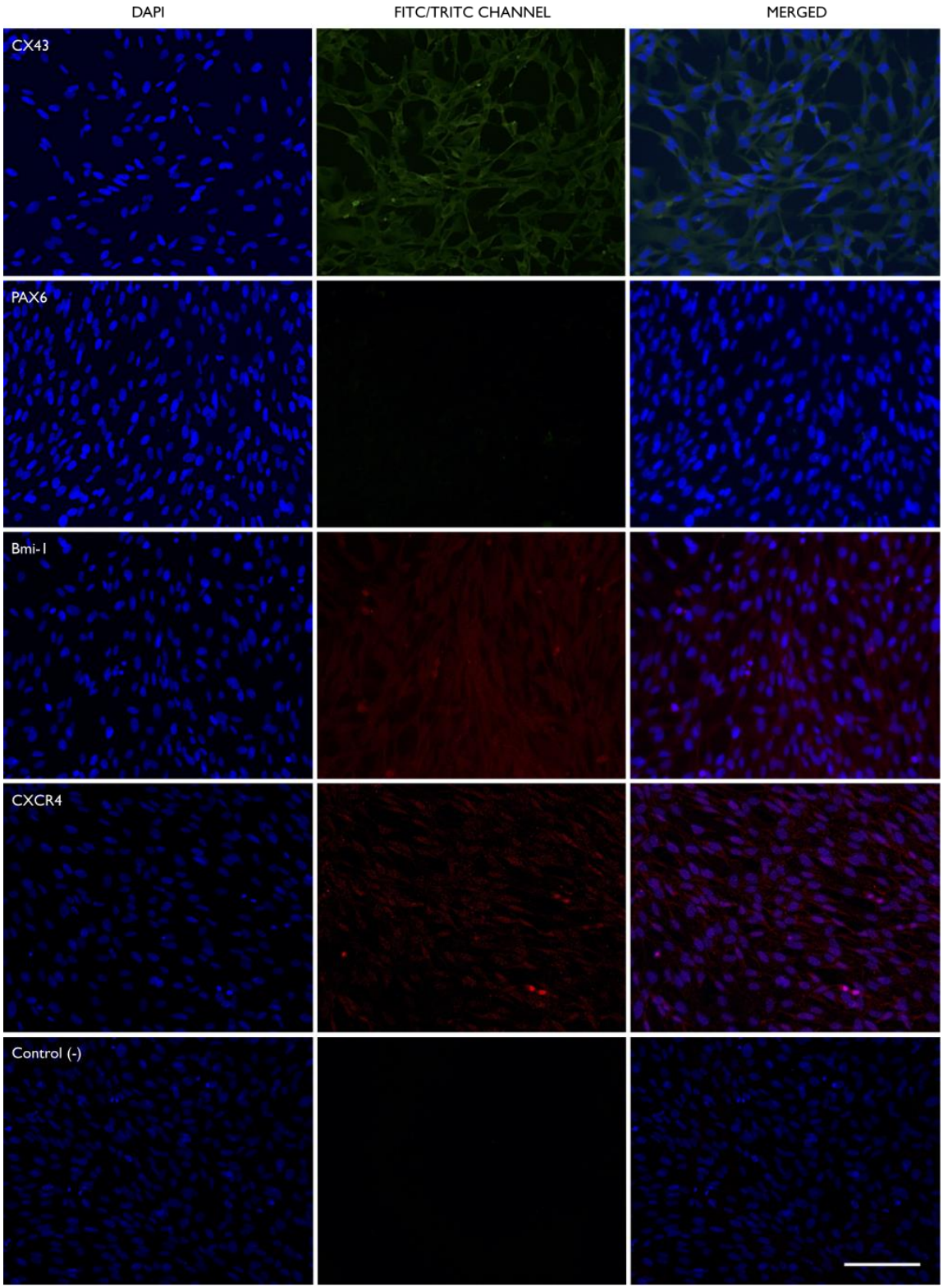

Figure 3.4: Immunolabeling of putative stromal cell markers in cultures E_{18} chicken corneal stromal keratocytes. The horizontal panels show positive labelling of CX43 *(green)*, Bmi-1 *(red)*, and CXCR4 *(red),* but no labelling of PAX6 *(green)*. Nuclei counterstained with DAPI *(blue)*. The scale bar represents 100 μm.

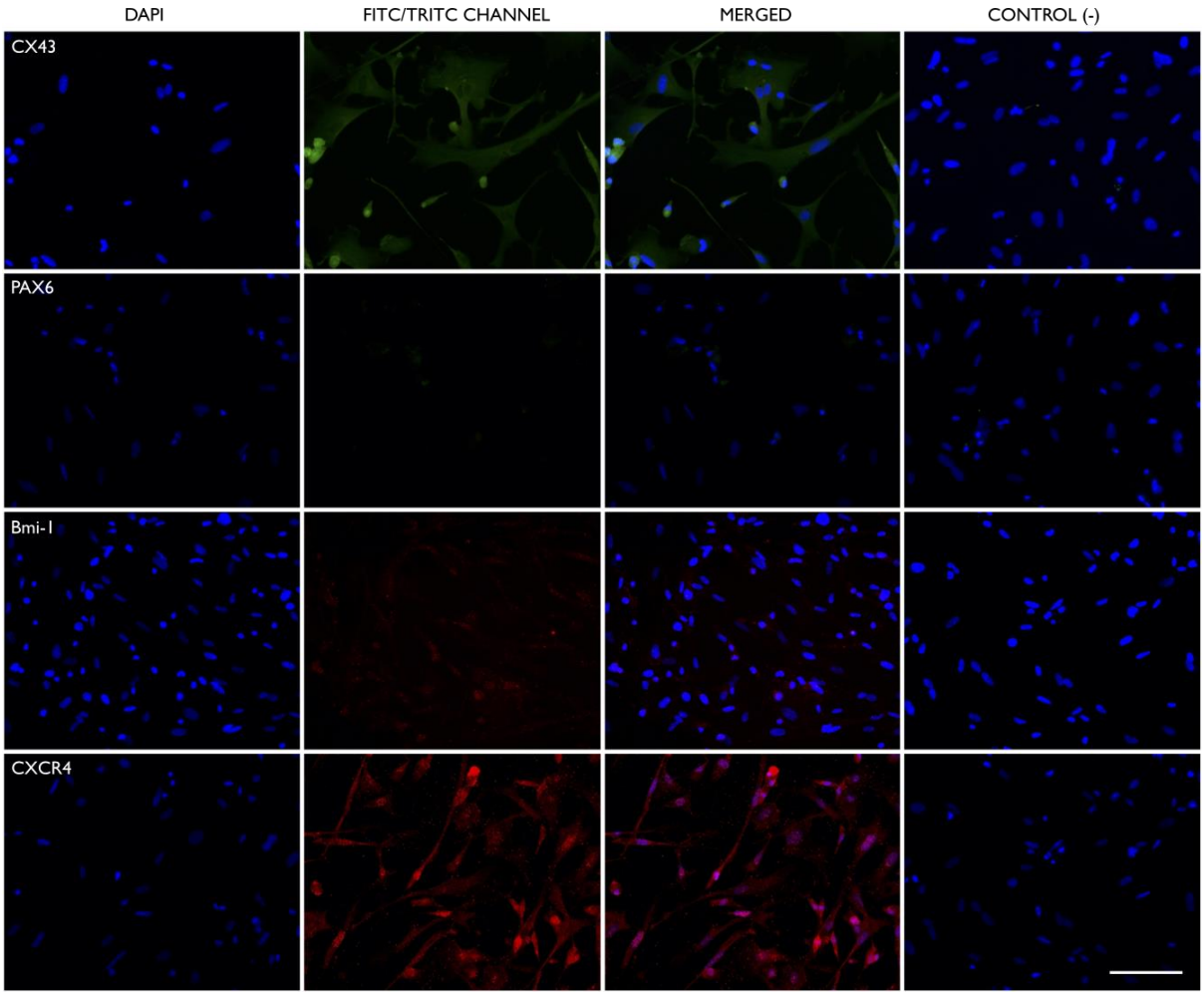

Figure 3.5: Immunolabeling of putative stromal stem cell markers in adult chicken corneal stromal keratocytes. The horizontal panels show strong positive labeling of CX43 *(green)*, Bmi-1 *(red)*, and CXCR4 *(red)* but no labelling of PAX6 *(green)*. Nuclei counterstained with DAPI *(blue)*. The scale bar represents 100 μm.

3.3.1.4 Immunolabelling of Putative Stromal Stem Cell Markers through Avian Morphogenesis

Following the *in vitro* assessment of putative corneal stromal stem cell markers, *in situ* expression of CX43, PAX6, Bmi-1, and CXCR4 was assessed along three different corneal regions *(limbus, mid-periphery, and central cornea)* at developmental stages: adult, E_{18}, E_{14}, and E_{10}. As seen in Figure 3.6, corneal signalling of CX43 in adult and E_{14} were strongly observed in the suprabasal epithelium and diffusely throughout the stroma and endothelium; furthermore, these signalling patterns were mimicked throughout the limbus, mid-periphery, and central cornea at these developmental stages as well. Similarly, in E_{18} corneas, strong signalling of CX43 was also observed in the suprabasal epithelium and endothelium at each of the corneal regions, however, unlike E_{14}, stromal expression in the mid-peripheral and central cornea was seen to be mainly localised in the anterior 1/3 of the stromal layer. As for E_{10}, moderate signalling was seen in the suprabasal epithelium and diffusely

throughout the stroma and endothelium with no difference in signalling patterns across the three corneal regions. It is also important to note the expression at E_{10} was less than that of later developmental stages. Negative controls did not indicate any non-specific secondary antibody binding.

Like CX43, PAX6 expression was subsequently investigated at the same developmental stages. As seen in Figure 3.7, diffuse epithelial signalling of PAX6 was observed throughout the limbus, mid-peripheral and central cornea with no notable signalling in the stroma and endothelium; this was a consistent finding throughout the three corneal regions and no difference in signalling strength was noted throughout the developmental stages. With respect to Bmi-1 and CXCR4, as seen in Figure 3.8 and Figure 3.9, respectively, strong signalling was seen in the epithelium and suprabasal epithelium as well as diffuse signalling throughout the stroma and endothelium in adult, E_{18}, and E_{14} but only moderate signalling was observed at E_{10}; no notable differences between corneal regions were observed at each of the developmental stages. Negative controls for PAX6, Bmi-1, and CXCR4 confirmed a lack of non-specific binding of their respective secondary antibodies.

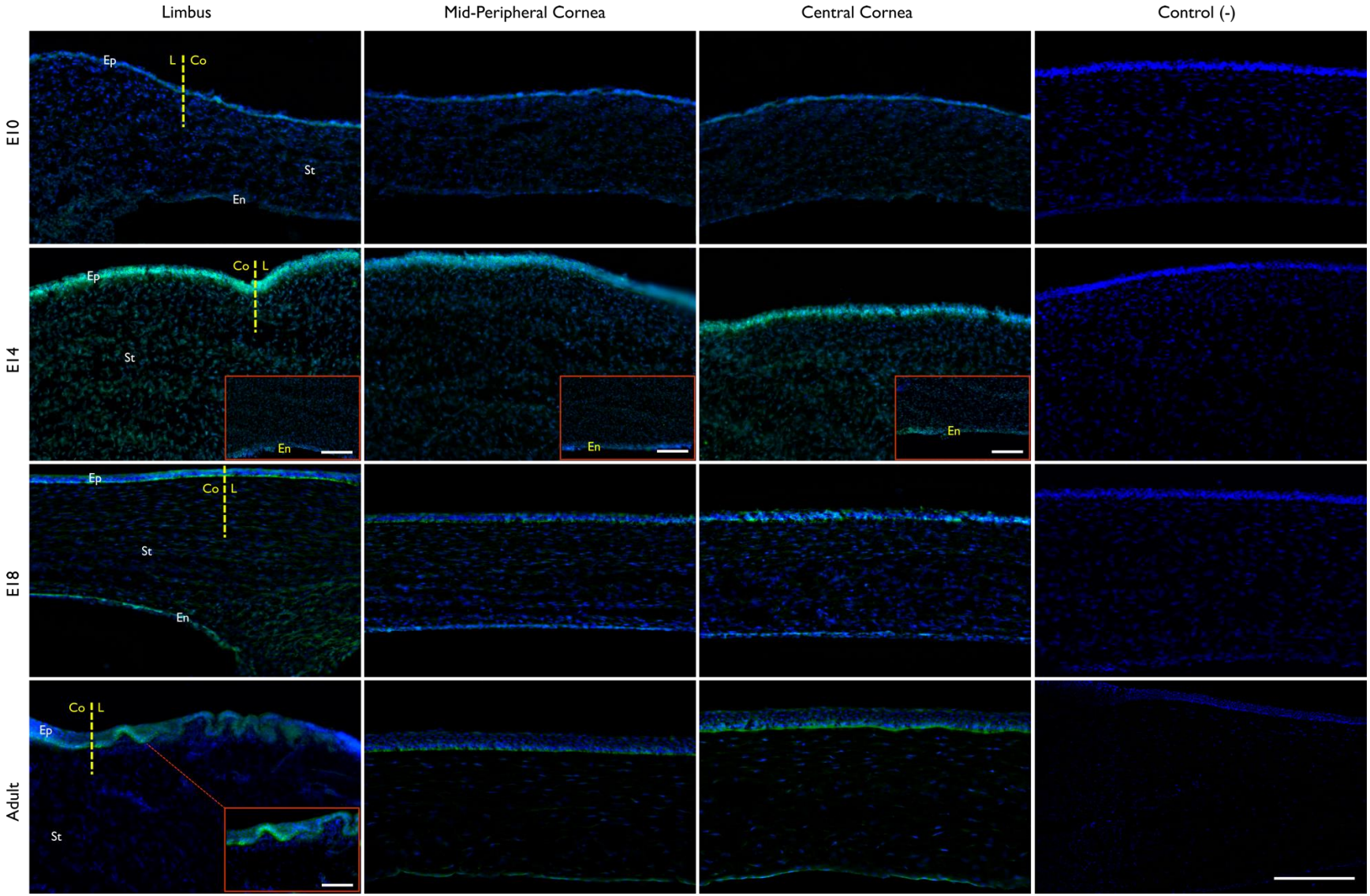

Figure 3.6: Immunolabelling of CX43 in the embryonic chicken limbus, mid-peripheral, and central cornea. Horizontal panels show positive labelling *(green)* throughout the corneal layers at developmental stages E_{10}, E_{14}, E_{18}, and Adult. Insets, where applicable, show immunolabelling of the endothelial layer. L = limbus, Co = cornea, Ep = epithelium, St = stroma, En = endothelium. Dashed vertical yellow lines represent the corneolimbal junction. Nuclei counterstained with DAPI *(blue)*. The scale bars represent 100 μm.

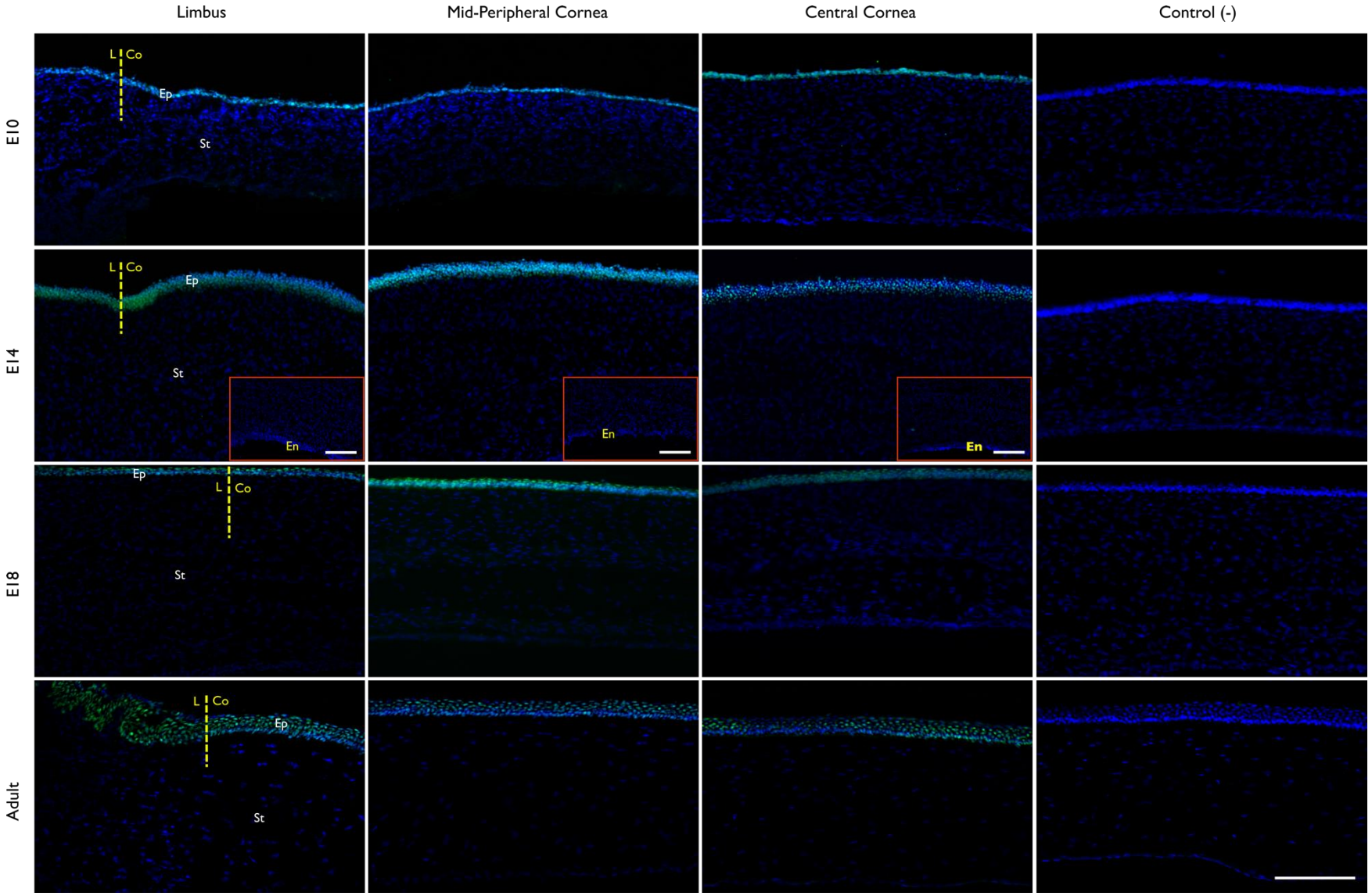

Figure 3.7: Immunolabelling of PAX6 in the embryonic chicken limbus, mid-peripheral, and central cornea. Horizontal panels show positive labelling *(green)* limited to the epithelial layer at developmental stages E_{10}, E_{14}, E_{18}, and Adult. Insets show immunolabelling of the endothelial layer. L = limbus, Co = cornea, Ep = epithelium, St = stroma, En = endothelium. Dashed vertical yellow lines represent the corneolimbal junction. Nuclei counterstained with DAPI *(blue)*. The scale bars represent 100 μm.

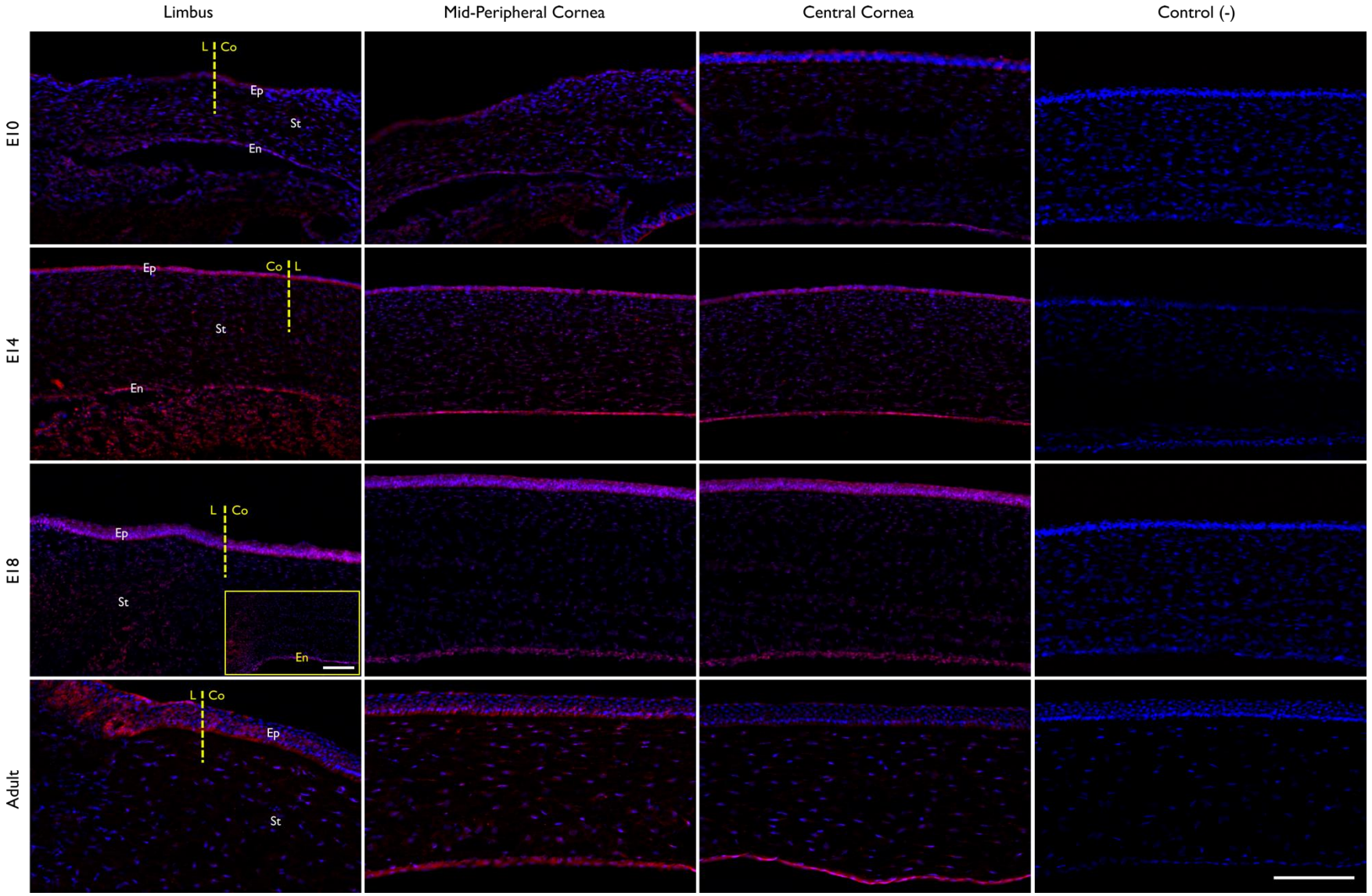

Figure 3.8: Immunolabelling of Bmi-1 in the embryonic chicken limbus, mid-peripheral, and central cornea. Horizontal panels show positive labelling *(red)* throughout the corneal layers at developmental stages E_{10}, E_{14}, E_{18}, and Adult. Inset shows immunolabelling of the endothelial layer. L= limbus, Co = cornea, Ep = epithelium, St = stroma, En = endothelium. Dashed vertical yellow lines represent the corneolimbal junction. Nuclei counterstained with DAPI *(blue)*. The scale bars represent 100 μm.

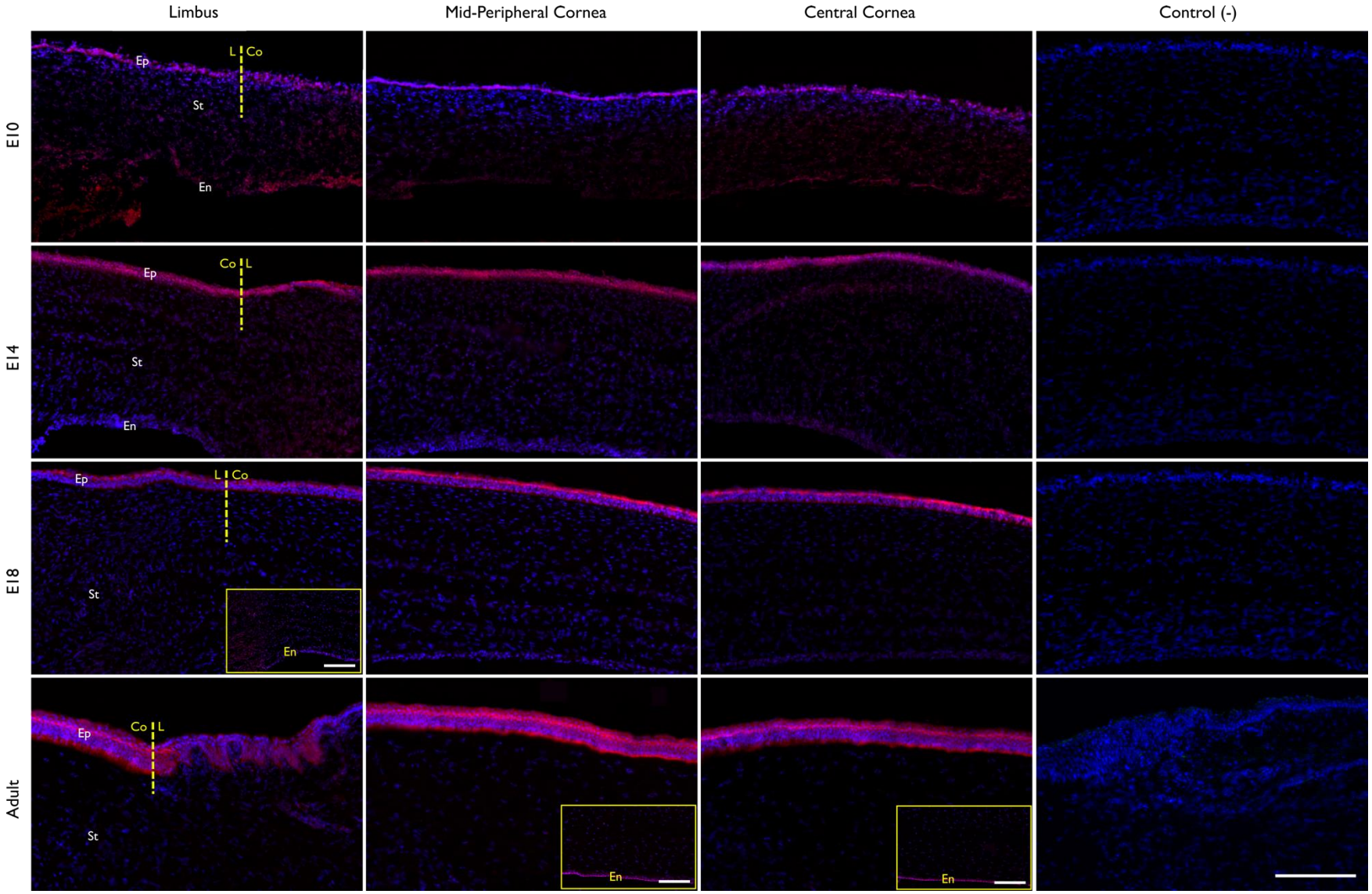

Figure 3.9: Immunolabelling of CXCR4 in the embryonic chicken limbus, mid-peripheral, and central cornea. Horizontal panels show positive labelling *(red)* throughout the corneal layers at developmental stages E_{10}, E_{14}, E_{18}, and Adult. Insets show immunolabelling of the endothelial layer. L = limbus, Co = cornea, Ep = epithelium, St = stroma, En = endothelium. Dashed vertical yellow lines represent the corneolimbal junction. Nuclei counterstained with DAPI *(blue)*. The scale bars represent 100 μm.

3.4 Discussion

3.4.1 *In Vitro* Labelling of Keratocyte Matrix Markers

The embryonic origins of the corneal stroma and its cellular constituents were foremost detailed in a 1969 study by Hay and Revel. They outlined that in the developing chicken cornea, periocular neural crest-derived mesenchymal cells were first seen to infiltrate the primary stroma from E_6 onwards. These biosynthetically active cells gradually mature into keratocytes which produce fibrillar collagens and SLRPs that contributed to the observed increase in stromal thickness until E_{12}. Thereafter, the systematic assembly of the ECM into a highly organised tissue with uniform interfibrillar spacing and diameter resulted in the reduction of stromal thickness and progressive increase in corneal transparency (Maurice 1957; Chakravarti et al. 1998; Quantock et al. 2001; Scott et al. 2011).

In situ findings reported a functional cell syncytium reactive to homeostatic changes in the cornea generated by a network of keratocyte interactions and communications via cellular extensions and gap junctions, respectively (Nishida et al. 1987; 1988; Pot et al. 2010). In response to corneal injury, keratocytes would dedifferentiate into one of two repair phenotypes: fibroblasts or myofibroblasts to aid in the repopulation and remodelling of corneal tissue in addition to wound contraction if damage was extensive (Pot et al. 2010). In the present chapter, it was shown that stromal cells isolated and cultured from both $E_{18,}$ and adult chicken corneas were indeed keratocytes. Moreover, that they retained some multipotentiality as observed in the positive immunofluorescence staining of selected PSSC markers. Supplementary *in situ* staining at key developmental stages substantiated the *in vitro* findings in addition to illustrating their pattern of immunolocalization throughout the various tissue layers and regions of the cornea.

Corneal Keratocyte Phenotype

Recent studies have shown that the dedifferentiation of mature, quiescent keratocytes is controlled and markedly changed by specific environmental cues when actively cultured *in vitro*. This in part is in accordance with their broader capability of supporting normal corneal function and repair, thus maintaining corneal transparency, as fibroblasts repopulating and remodelling the corneal tissue, and myofibroblasts contracting corneal wounds. As such, each phenotype has a defined difference in its biosynthetic output that facilitates these processes. For example, keratocyte isolates cultured in serum-free conditions maintained a quiescent keratocyte phenotype, characterised by an elevation in KS and keratocan production, in addition to a flattened and stellate

morphology with multiple extended processes interconnecting each individual cell (Kirschner et al. 1990; Beales et al. 1999; Funderburgh et al. 2003; Jester and Ho-Chang 2003). Yet in one study, where adult bovine keratocytes were cultured in a serum-free environment, gene expression data from semi-quantitative reverse-transcription polymerase chain reaction *(RT-PCR)* showed that keratocan was positively expressed in both low passage bovine fibroblasts and keratocytes, whereas it was only found to be positively expressed in the keratocyte phenotype in human cells (Scott et al. 2011). Exposure to serum has been found to promote a divergence from a quiescent phenotype to a fibroblastic phenotype; downregulation of KS and keratocan and an increase in metalloproteinase expression was observed, in addition to cells becoming morphologically larger and flatter with a reduction in cellular extensions (West-Mays et al. 1995; Beales et al. 1999; Funderburgh et al. 2003, Jester and Ho-Chang 2003). Similarly, cells cultured with transforming growth factor beta resulted in myofibroblast dedifferentiation, expressing higher levels of alpha smooth muscle actin *(presenting as intracellular microfilament stress fibres),* and marked decrease in KS expression with morphologically larger and polygonal cellular bodies (Jester et al. 1995; Beales et al. 1999; Wilson 2012; Jester and Ho-Chang 2003).

In this study, the results show that collagenase-isolated chicken keratocytes cultured *in vitro* from either embryonic or adult corneas retain the potential to express a fibroblastic phenotype. In relation to comments above, a considerable reduction in KS and keratocan immunolabelling in addition to morphological changes was expected in cultured cells grown with FBS leading to a transition to a myofibroblast phenotype. However, both embryonic and adult keratocytes were observed to maintain a fibroblastic morphology affirmed by the presence of cylindrical bodies with thick pseudopodia processes across multiple passages with marked immunolabelling of KS and keratocan– both of which complemented current literature findings in favour of an active phenotype. However, these studies only examined *in vitro* effects towards adult keratocytes cultured in serum from an array of animal models. Typically, a downregulation of KS biosynthesis was seen in culture *(and by implication in wound healing),* in response to KS-specific glycosyl- and/or sulfotransferases modifying PGs to produce shorter oligolactosamine chains with minimal sulphation (Funderburgh et al. 1990; Rodrigues et al. 1992; Funderburgh et al. 1996). As a result, keratocytes would mimic corneal fibroblasts *(as if responding to injury and inflammation),* leading to dedifferentiation into a fibroblastic phenotype signalling the activation of cell division (Nakazawa et al. 1998; Funderburgh et al. 2002). That being said, literature has yet to explore the impact on the phenotypical characteristics of embryonic keratocytes cultured *in vitro*, however, from the

current findings, it is reasonable to consider that embryonic keratocytes dedifferentiate to a fibroblastic phenotype when cultured *in vitro* in the presence of FBS.

In addition to the above findings, strong immunolabelling of pro-collagen type I was also observed. These results were consistent with the accepted notion that the general assembly of stromal architecture begins with procollagen type I – a precursor for collagen type I synthesis by keratocytes (Funderburgh et al. 2003; Hassell et al. 2008). Moreover, it also substantiated the claims made by the author that cultured keratocytes in this study favoured a fibroblastic phenotype *in vitro*. Work by Stearns (1940) was the first to provide evidence of fibroblast activity in the secretion and assembly of collagen fibrils. This observation was further supported years later by Birk and Trelstad (1984), who also acknowledged the involvement of activated fibroblasts in matrix morphogenesis specific to the cornea. The corneal architecture, which is largely composed of collagen type I fibrils, is synthesised from its precursor: procollagen type I through the cleavage of N- and C-terminal globular procollagen domains, prior to matrix assembly (Bard and Higginson 1977). Gealy et al. (2009) also found the extracellular distribution of type I pro-collagen was manifest in the stroma throughout the entirety of embryonic corneal development (Gealy et al. 2009).

The existence of collagen type III in unwounded and healthy corneal stroma is still a contentious topic to date (Hayes et al. 2015). Many studies have been conducted over the years yielding inconsistent findings in support of one position over the other. In an early study by Newsome et al. (1981), human corneas were cryo-sectioned and immunolabelled using anti-collagen type III antibody, which resulted in inconclusive presentation of type III collagen in the stromal region. While in contrast, an *in vitro* study where human corneal fibroblasts *(and corneal fibroblasts isolated from other species)* were cultured did not indicate the presence of type III collagen (Stoesser et al. 1978; Freeman 1978; Church 1980). The belief here was that the coexistence of type I and type III collagen could only occur in tissues that supported an epithelium or endothelium; however, the corneal stroma, which was supportive of both tissue layers, appeared to contradict this consensus by having an absence of type III collagen labelling (Church 1980). Despite these findings, other studies have favourably reported the presence of type III collagen *in situ* in bovine and rabbit corneas (Schmut 1977; Cintron et al. 1988; Etheredge et al. 2009). Moreover, it was present in fetal and wounded corneas, but to a lesser degree in adult corneal stromas (Chen et al. 2000; Funderburgh et al. 2003). Earlier work by Funderburgh et al. (2003) has generated positive evidence of type III collagen using RT-PCR analysis on primary keratocytes obtained from bovine

corneal stromas. Furthermore, the study showed that all three collagen phenotypes were implicated, with myofibroblast expression being the highest and quiescent keratocytes being the least. Interestingly, in this study in *vitro* cultures of embryonic keratocytes were not observed to label for type III collagen, whereas adult keratocytes demonstrated weak labelling. According to results obtained by Funderburgh et al. (2003) the weak labelling of collagen type III in adult keratocytes would be supportive of either a fibroblastic or myofibroblastic phenotype, however, there is limitation in discerning the specific phenotype without an established qualitative/quantitative threshold immunofluorescence between the two. Individually, the signalling outcomes of these molecular markers cannot distinguish between transdifferentiated states of fibroblast and myofibroblast phenotypes but when present together provide a discernible difference. Thus, it could be argued that both embryonic and adult keratocytes cultures were reflective of fibroblastic phenotype.

3.4.2 *In Vitro* and *In Situ* Signalling of Putative Stromal Stem Cell Markers

The derivation of stromal keratocytes from mesenchymal-derived cells has led many researchers to postulate that their regenerative properties, in cases of corneal injury, could be attributed to the retention of stem cell-like properties from embryogenesis (West-May and Dwivedi 2006). A study by Lwigale et al. (2005) used chicken and quail chimera grafts to show that late stage embryonic keratocytes could be introduced into neural crest populations of earlier embryos where they proceeded to proliferate, migrate, and dedifferentiate to contribute to a diversity of neutral crest-derived populations (Lwigale et al. 2005; West-May and Dwivedi 2006). These findings in combination with keratocytes remaining in a G_0 phase suggests they may not in fact be terminally differentiated, but rather exist as partially restricted precursors, prepared to readily respond and reform their environment in order to maintain corneal transparency (West-May and Dwivedi 2006; Etheredge et al. 2009). Demonstrating the multipotency of quail keratocytes was the first study of its kind that was later explored in other animal models. Notably, in a study by Chao et al. (2013) human fetal keratocytes were isolated from corneas and injected along the cranial neural migratory pathway as well as in the periocular mesenchyme of chicken embryos. It was found that human fetal keratocytes retained the ability to differentiate into many but not all related tissues, a similar finding to that with quail keratocytes, in addition to being able to respond to environmental cues from chicken embryos to generate corneal endothelium and stromal keratocytes. Most studies in the past have focused on the ability of keratocytes to retain their phenotype when cultured *in vitro*; however, a recent shift in the investigation of stromal keratocytes as a source for regenerative therapies has resulted in findings supporting their plasticity. In the present study, it was shown that

keratocytes retained multipotency as seen from the labelling of selected PSSC markers in embryonic and adult cultures, and throughout the corneal layers throughout development.

CX43

Gap junction proteins, which appear at the cell plasma membrane, have an essential role in intercellular communications by way of transferring cytosolic components between neighbouring networks of cells (Xu et al. 2019). CX43 is resolved as an important participant in the proliferation and differentiation of corneal cells, both of which are integral functions for the maintenance of corneal homeostasis (Yuan et al. 2009; Zhai et al. 2014; Xu et al. 2019). Coincidently, CX43 has been identified as the most common gap junction protein expressed in the epithelium and corneal stroma (Dong et al. 1994; Spanakis et al. 1998; Xu et al. 2019). Explorative work by Dong et al. (1994) was the first to describe the presence of CX43 in corneal stromal fibroblasts in addition to being predominantly expressed in the basal cells of the corneal epithelium in rats. Similarly, in a rabbit study by Ratkay-Traub et al. (2001), corneas that were subjected to excimer laser photorefractive keratectomy were reported to undergo an upregulation in CX43 levels with localisation occurring in the upper cellular layers of the corneal epithelium. Reproducible findings were also achieved by Grupcheva et al. (2012), in addition to the detection of smaller punctuate spots expressed between stromal keratocytes.

In this present study, *in situ* labelling of CX43 was demonstrated in the suprabasal epithelium at all investigated timepoints and transversely across the cornea, as well as diffuse stromal labelling extending across the full thickness of the cornea. These findings were partially in line with literature reports of CX43 expression within corneal tissue across multiple animal models, with localisation specifically, within the epithelium from central to limbal cornea, along with the anterior stromal localisation (Chen et al. 2004; King and Lampe 2005; Gatziousfas et al. 2007; Ebrahimi et al. 2009). However, Kubilus and colleagues, who had investigated the expression of CX43 at the corneoscleral junction at E_8 and E_{14} in chickens, only reported similar findings within the epithelium, making no mention of stromal labelling (Kubilus et al. 2017). That said, there are no other studies in chickens with which to compare these findings, but signalling patterns outlined here are similar to those seen in the human model and are further supported by the positive *in vitro* signalling seen in both embryonic and adult keratocytes (Gatziousfas et al. 2007; Zhai et al. 2014).

PAX6

The PAX6 gene is a transcriptional factor that is essential to early morphogenesis of the visual and CNS (Nishina et al. 1999). The localised labelling of PAX6 is well established in the nuclei of corneal epithelial cells, however, it is absent from the stroma and endothelium (Davis et al. 2003; Funderburgh et al. 2005; Li et al. 2008). These results confirm those previously published by Koroma et al. (1997); however, Davis et al. (2003) also discovered that labelling of PAX6 was reduced or absent from the anterior most layer of the stratified epithelium both centrally and peripherally in wild-type mice. Yet, analysis of freshly isolated stromal cells by flow cytometry has revealed a rare population of cells *(~4%)* which stained for PAX6 (Funderburgh et al. 2005). Furthermore, the expression of PAX6 was evident in the epithelium throughout development and in the adult epithelial tissue of bovine corneas. Collectively, these findings make sense as PAX6 is associated with neuroectodermal-derived lineages, like the corneal epithelium (Kawakami et al. 1997; Zhang et al. 2010a).

This present study reveals further evidence of *in situ* localisation of PAX6 in the epithelium using chicken corneas. What is more, the labelling remained consistent throughout development and in mature epithelial tissue. An absence of labelling was determined around stromal keratocytes, both *in situ* and *in vitro*. As there are no other studies that have investigated the expression of PAX6 in the chicken cornea, these findings are novel to this animal model, but they yield corresponding results to those previously reported in literature.

Bmi-1

Several groups have reported the expression of Bmi-1, a polycomb ring finger protein, in the stem cell population of a number of organs with functions ranging from cell cycle regulation to cell immortalization (Park et al. 2003; Molofsky et al. 2003; Iwama et al. 2004; Wang et al. 2012; Biehs et al. 2013; Kalha et al. 2018). In the human cornea, expression was identified within the limbal region and later confirmed *in vitro* using naive limbal epithelial cells (Barbaro et al. 2007; Levis and Daniels 2016). In other organs, Bmi-1 was found to function in stem cell self-renewal, and in its absence, severe defects were reported in intestinal development, haematopoiesis, and skeletal pattern (van Der Lugt 1994; Park et al. 2003; Molofsky et al. 2003; Iwama et al. 2004; Lopez-Arribillaga et al. 2014). A study by Kalha et al. (2018) using a murine model reported positive expression of Bmi-1 in the basal and suprabasal epithelial layers prior to stratification expanding to include all layers post-stratification; this pattern of expression was broader than that observed in the human cornea, which was restricted to the limbus (Barbaro et al. 2007). Due to the greater

than expected expression of Bmi-1, which at the time was regarded as a marker associated with stem cell populations, authors were led to perform genetic mapping. This determined a subset of Bmi-1^+ cells within the epithelium that were able to renew local epithelial cells but were not seen to be involved in wound healing, following induced superficial corneal injury. They, therefore, proposed that Bmi-1 could play a critical role in progenitor cell behaviour, opposed to the generally agreed role in stem cell self-renewal in the murine epithelium (Kalha et al. 2018).

In the present investigation, Bmi-1 labelling was identified in the chicken cornea during morphogenesis. As in the murine cornea, broader labelling was observed throughout the basal and suprabasal epithelium, centrally and peripherally, with evidence of strong labelling in the basal layer of the mature limbus. Surprisingly, labelling also appeared throughout the stroma and endothelium, the former not previously reported as being a layer expressing Bmi-1 in either the human or murine cornea. This was an interesting finding and taken together with Kalha et al.'s (2018) hypothesis that Bmi-1 is involved more with progenitor cells, it could presumably explain the labelling associated with the partially-restricted progenitor cells *(keratocytes)* seen in the chicken cornea and *in vitro*. However, additional work needs to be performed in order to enhance our current understanding of Bmi-1's distinct role throughout each corneal layer. Incidentally, Wang et al. (2012) had previously reported a significant down-regulation of Bmi-1 in the ageing endothelium of the human cornea, which led them to posit Bmi-1's link to endothelial cell senescence. On this basis, it would, therefore, have been expected that endothelial labelling might progressively weaken throughout chicken morphogenesis as well, but the opposite was true, as strong labelling was detected. Nevertheless, future work will have to be done to better understand the differences between these findings and the ones reported in other animal models.

CXCR4

Historically, chemokine proteins have been described as potent chemoattractants for various subpopulations of leucocytes, but in recent years this view has extended to include non-hematopoietic cells like fibroblasts, epithelial and endothelial cells, where chemokine receptors are also expressed (Bourcier et al. 2003). Yet the role and expression of chemokines and their receptors with respect to the cornea is limited and requires more in-depth investigation. Former studies have loosely suggested that stromal keratocytes may release chemokines and as a result could possibly be implicated to a degree in the inflammatory cascade, associated with acute infections and corneal allograft rejection (Yamagami et al. 1999; Kumagai et al. 2000; Abu El-Asrar et al 2001; Fukagawa et al. 2002; Bourcier et al. 2003). However, focus has shifted to specifically exploring chemokine CXCR4, due to increasing evidence implicating it alongside its unique ligand, SDF-1, in the process

of angiogenesis, leading to ocular neovascularisation (Mirshahi et al. 2000). Nevertheless, the wider biological role at the time of these publications was still unexplored and could not be regarded with confidence as being the true extent of CXCR4's function in relation to the cornea (Mirshahi et al. 2000; Crane et al. 2000).

Innovative work by Bourcier et al. (2003) was the first to demonstrate the presence of CXCR4 in human corneal tissue, as well as in cultured corneal fibroblasts, suggesting the CXCR4 chemokine receptor as being an integral player in corneal fibroblast function. Even more significant were the findings by Xie et al. (2011), who demonstrated that limbal stem cell function relied on the close physical association with native niche cells via CXCR4/SDF-1 signalling. Disruption to the CXCR4 receptor was reported to affect holoclone formation leading to increased differentiation of stem/progenitor cells. These findings were comparable to other discoveries that found CXCR4/SDF-1 signalling to be involved in: homing of neural progenitor cells to the identified vascular niche in the subventricular zone (Kokovay et al. 2010); recruitment of osteoblast progenitor cells to the site of bone formation (Otsuru et al. 2008); adhesion of mesenchymal stem cells to a target tissue (Ratliff et al. 2010); and the survival and migration of immature pancreatic epithelial progenitor cells (Kayali et al. 2003; Bourcier et al. 2003). In the investigation of the chicken limbus, CXCR4 labelling was detected in the suprabasal epithelium and diffuse in the stoma throughout the depth and width of the cornea at each developmental time point. Strong labelling was also observed *in vitro* in both embryonic and mature keratocyte cultures. These results were similar to a prior study reporting weak staining of CXCR4 at the human limbus, within the corneal epithelium and stromal cells, whereas strong staining was detected in limbal stromal cells (Xie et al. 2011). These findings provide a novel insight into the presentation of CXCR4 in the chicken cornea that can be used for future investigations into the broader extent of CXCR4 role in the cornea.

The findings described in this chapter demonstrate that primary cells isolated and cultured *in vitro* from both embryonic and adult chicken corneas positively label for key matrix markers associated with fibroblastic keratocytes. This is an important precedent to set as Chapter 6: will describe the results of manipulation of culture conditions to observe the impact on the immunophenotypic profile of keratocytes, with respect to the labelling of PSSC markers for the purpose of establishing if CS-based substrates can promote cellular expression towards a less-differentiated state. This has the potential to enhance current therapeutic strategies aimed at engineering corneal tissue for direct transplantation in cases of limbal epithelial stem cell deficiency and stromal scarring. Moreover,

the analysis of CX43, PAX6, Bmi-1, and CXCR4 during chicken morphogenesis illustrates a novel pattern of immunolocalization that has the potential of opening up future avenues of study to better understand the broader mechanisms at play in relation to corneal homeostasis and pathology.

3.5 Summary

The results of the present study establish a qualitative benchmark of: (1) *in vitro* immunolabelling that supports isolated cells for primary cell culture are indeed keratocytes; and (2) *in situ* labelling that suggests embryonic keratocytes retain a level of multipotentiality as supported by the labelling of selected PSSC markers. These findings will serve as a baseline for investigations, presented in Chapter six, into the changes in PSSC marker expression and morphology of keratocytes cultured on different CS-containing substrates towards their progenitor-like state *(prior to differentiation)*. Results from the immunohistochemical analysis, showed two major findings:

- E_{18} and adult corneal keratocytes were successfully isolated and optimised for *in vitro* culturing. Positive immunolabelling of widely recognised matrix markers: pro-collagen type I, KS, and keratocan were seen in both embryonic and adult keratocyte cultures with the addition of weak alpha smooth muscle actin labelling in adult keratocytes. Collectively, these results suggested cultured keratocytes were expressive of the fibroblastic repair phenotype.
- Positive, diffuse stromal labelling of PSSC markers CX43, CXCR4, and Bmi-1 was evident *in situ* at developmental time points: E_{10}, E_{14}, E_{18}, and adult. These results were further supported by *in vitro* cultures of embryonic and adult keratocytes, which also showed positive labelling for each marker. No stromal labelling of PSSC marker PAX6 was observed, which was also corroborated by embryonic and adult keratocyte cultures. Furthermore, no qualitative difference in PSSC labelling was observed across the three main regions of the cornea *(limbus, mid-periphery, central cornea)*.

The chapter that follows investigates the immunolabelling of variably sulphated CSPGs using sulphation-specific mAbs 4C3, 6C3, 7D4, and 3B3 in the developing chicken cornea. These epitope-specific antibodies have previously been employed to characterise the stem cell niche located in articular cartilage and will provide insight into the relationship of CSPGs, a component of the stromal ECM, to the presumptive stem cell niche in the chicken cornea.

Chapter 4: Chondroitin Sulphate Sulphation Motif Labelling in the Developing and Adult Avian Cornea

4.1 Introduction

CS PGs are naturally occurring extracellular matrix components that can be found in many connective tissues, like the cornea, cartilage, heart, tendon, and the CNS (Mourao 1988; Mantovani et al. 2016). The primary component of CS is a repeating disaccharide sequence of glucuronic acid and N-acetyl-galactosamine residues that can be non-sulphated or differentially sulphated on the carbon-2 position of the glucuronosyl residue, or the C-4 or C-6 positions of the galactosamine residue (Caterson et al. 1990b; Lauder et al. 2000; Lamari and Karamanos 2006; Sugahara and Mikami 2007; Mantovani et al. 2016). These possibilities, therefore, allow for the formation of different isotypes of CS which in turn have a determinant effect on the physical and chemical properties, as well as the biological and pharmacological activity of the CS molecules within their respective environments (Sugahara and Mikami, 2007; Mikami and Kitagawa 2013; Mantovani et al. 2016). The highly specific manner in which the CS sulphation motifs *(SM)* interact with other matrix molecules *(e.g., growth factors, cytokines, chemokines, etc.)* directly influences various cascades of events involved in cellular proliferation, differentiation, migration, and matrix secretion (Hayes et al. 2008).

In the early 1980's, Caterson and colleagues were the first to successfully generate and characterise mAb that could specifically recognise different "native" SMs/epitopes present along CS/DS GAG chains (Caterson et al. 1985; 1990; 2012; Hayes et al. 2008; 2011). Consequently, these mAbs have underpinned decades of research into identifying specific CS spatio-temporal motifs naturally occurring in tissue and organ development, as well as determining the importance and necessary roles of CSPGs (Hayes et al. 2011: Caterson 2012). More recently, they have been used to investigate the role of CSPGs with respect to the stem/progenitor niche in various organ systems (Caterson et al. 2012; Hayes et al. 2008; 2016).

4.1.1 Structural Domains Identified by Monoclonal Antibodies

Several anti-CS mAbs, as alluded to above, have been generated to characterise undigested chains, that is, without pre-treatment with enzyme ChABC to expose native epitopes in CS/DS chains *(some of which are shown in Table 4.1)* (Jenkins et al. 1981; Anvur and Geiger 1984; Yamagata et al. 1987; Mark et al. 1989; Sorrell et al. 1990;1993). In two studies conducted by Anvur and Geiger (1984) and Sorrell et al. (1990), CS chains were digested with ChABC, prior to antibody treatment,

resulting in the removal of most, if not all, of the epitope recognition by these mAbs. It was inferred by Sorrell et al. (1993) that mAbs *(4C3, 6C4, 7D4, 4D3, and CS-56)* did not recognise standard, linear 0-,4-, or 6-sulphated units. Rather, they recognised atypical subunits, non-randomly distributed across the CS chain, indicating that native CS epitopes were more structurally complex. As a result, these generated mAbs were able to recognise specific sequences of disaccharide/oligosaccharide SM epitope domains within the framework of the CS chains (Hayes et al. 2008).

Table 4.1: Antibodies generated to recognise various native chondroitin sulphate sulphation motif epitopes and keratan sulphate epitopes. *Adapted from:* Hayes et al. (2011).

Antibody *(dilution)*		**Species/clone *(isotype)***	**Specificity**	**References**
Native	6C3 (1:20)	Mouse/mono (IgM, κ)	Unidentified sulphation motif occurring towards non-reducing terminus	Caterson et al. 1990a
	4C3 (1:20)	Mouse/mono (IgM, κ)	Antibodies recognise distinct, yet undefined, native CS sulphation motif epitopes occurring towards linkage region	
	7D4 (1:20)	Mouse/mono (IgM, κ)		
	3B3 [-]* (1:20)	Mouse/mono (IgM, κ)	Antibody recognises the terminal disaccharide of CS chains *(6-sulphated galactose adjacent to a terminal glucoronate)*	Sorrell et al. 1988a;1990b;1996; Hardingham et al. 1994 Caterson et al. 1983

* [-] denotes the use of an antibody without pre-treatment with Chondroitinase ABC

A subsequent investigation was undertaken to map out the local distribution of these mAb epitopes across a typical CS chain (Table *4.1*). Three domains were established where: domain one *(containing epitopes for antibodies 4C3, 7D4, and partially 4D3)* was determined to reside directly adjacent to the proteoglycan linkage region, domain two *(containing epitopes for antibodies 6C3, CS-56, and partially 4D3)* was found to lie internally in the CS chain, and domain three *(containing epitope 3B3 in limited numbers)* was determined to reside near the non-reducing termini of some CS chains (Bourin et al. 1990; Caterson et al. 1990a, Sorrell et al. 1993). The subtle but non-random distribution of these detected epitopes along the CS chain further supports the supposed view that the antigenic domains contain specific, atypical disaccharide/oligosaccharide sequences. Moreover, the application of mAbs to detect these specific epitopes along the CS chain can provide an avenue to better understand the various roles CSPGs may play throughout the body (Sorrell et al. 1993).

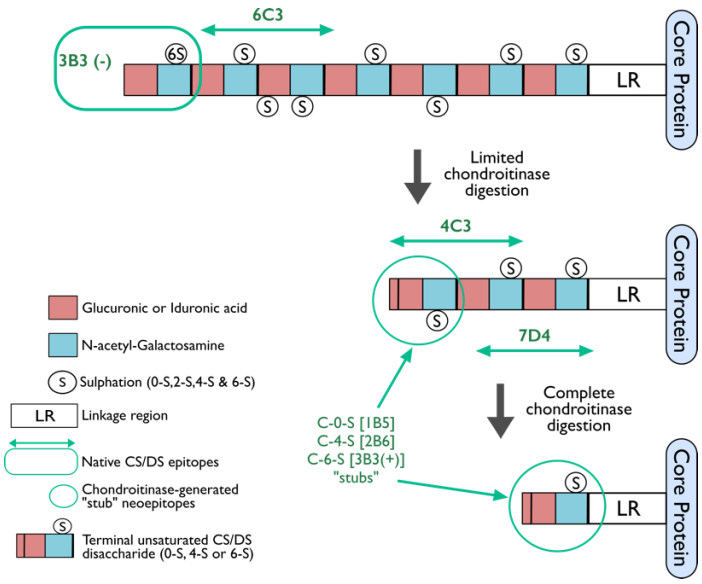

Figure 4.1: Schematic of the epitope locations recognised by anti-CS/DS monoclonal antibodies. *Adapted from:* Caterson (2012).

4.1.2 Localisation of Chondroitin Sulphate Sulphation Motifs/Epitopes in the Stem/Progenitor Cell Niche

The rising incidence of chronic osteoarthritis, a joint disease characterised by the progressive degradation of articular cartilage, has generated interest into the study of cartilage morphogenesis and consequently, the investigation into the existence of a stem cell niche within articular cartilage (Hayes et al. 2008). Various studies have alluded to the surface zone within the complex joint architecture as a key location for regulation of tissue development and growth, as a result of synthesis of differential matrix components (Ward et al. 1999), expression of numerous growth factors, and localisation of receptors along the articular surface (Archer et al. 1994; Hayes et al. 2001; Dowthwaite et al. 2004).

Dowthwaite et al. (2004) hypothesised that the superficial zone of knee articular cartilage was a site containing stem/progenitor cell populations that contributed to the appositional growth of the tissue and proceeded to isolate and partially characterise a sub-population of presumptive cartilage progenitor cells from that zone. Subsequent studies by William et al. (2010), Candela et al. (2014), and Grogan et al. (2009) further substantiated the presence of stem/progenitor cell sub-populations within the superficial region of the articular cartilage. However, it wasn't until the study of Hayes et al. (2016) that definitive biomarkers of the cells residing in the diarthrodial joint stem cell niche were recognised.

Using mAbs *(7D4, 4C3, and 3B3[-])*, immunolocalization of distinct SM epitopes showed clear labelling within the microenvironment of the superficial zone previously reported to house the stem/progenitor cell niche (Hayes et al. 2008). Previous studies have indicated that these mAbs recognise non and low-sulphated isoforms of CS (Couchman et al. 1984; Caterson et al. 1995; Ong-Chai 1999; Hayes et al. 2008), with Hayes et al. (2008) reporting an abundance of both non sulphated and minimally sulphated CSPGs within the stem/progenitor cell niche of articular cartilage. A hypothetical model was therefore suggested by Hayes and colleagues proposing that CSPGs carrying lesser-sulphated GAGs acted as a physical and biochemical barrier around stem cells. Moreover, as their chains lack negatively charged sulphated epitopes to inherently attract opposingly charged matrix molecules *(e.g., cytokines, growth factors, etc.),* it was inferred that CSPGs were directly involved in maintenance of the stem/progenitor cell niche. They also suggested that when cells translocated out of the niche, as in the case of cellular division or repair/regenerative responses, daughter cells would then become exposed to signalling molecules leading to differentiation (*Hayes et al. 2008*).

4.1.3 Aims

As was done in the stem cell niche of articular cartilage, the labelling of CS SM epitopes that recognise variable degrees of CS sulphation will be investigated in the avian limbus, a recognised location of a stem cell niche in other animal models (Cotsarelis et al. 1989; Dua et al. 2005; Shortt et al. 2007a; Grieve et al. 2015). To do this, corneal tissue sections were taken from the developing and adult avian cornea to assess the immunolabelling of mAb specific epitopes: 4C3, 6C3, 7D4, and 3B3.

4.2 Methods and Materials

4.2.1 Sample Collection *(Extraction and Cryo-Sectioning)*

Whole eyes were extracted *(at developmental time points: E_{14}, E_{18}, and adult)* and prepared for cryo-sectioning as previously described in Section 2.3.1.

4.2.2 Fluorescent labelling of Chondroitin Sulphate Sulphation Motif Epitopes

Antibodies (Table *4.2*) that recognise native CS SM epitopes 4C3, 6C3, 7D4, and 3B3 were assessed in the avian limbus, mid-peripheral, and central cornea. Samples were treated as described in Section 2.4.1.

Table 4.2: Immunofluorescent reagents

Blocking Serum		[Working]	Source (Catalogue No.)
Normal Goat Serum		1:20	Vector Laboratories (S-2000)
Antibodies		**[Working]**	**Source (Catalogue No.)**
Primary	4C3 6C3 7D4 3B3	1:20	Courtesy of Professor Clare Hughes *(Cardiff University School of Biosciences)*
Secondary	Alexa Fluor™ 488 Goat anti-mouse	1:200	Vector Laboratories (A-10680)

4.2.3 Epifluorescence Image Analysis

Immunolabelling of native CS SM epitopes *in situ* and *in vitro* was imaged and processed as described in Section 3.2.3.2. All images presented in this chapter are representative of findings from three individual experiments.

4.3 Results

4.3.1 Monoclonal Antibody Validation in E_{14} Chicken Ankle

Prior to the assessment of mAbs 4C3, 6C3, 7D4, and 3B3 in the avian cornea, positive validation of each antibody was performed in E_{14} sections of the tibiotarsal/tarsometatarsal joint. A clear gradient of positive labelling was evident for all four antibodies, such that stronger labelling was localised in articular cartilage at the boundaries of bone and around chondrocyte lacunae *(where evident)*. Negative controls for 4C3, 6C3, 7D4, and 3B3 confirmed a lack of non-specific binding of secondary antibody.

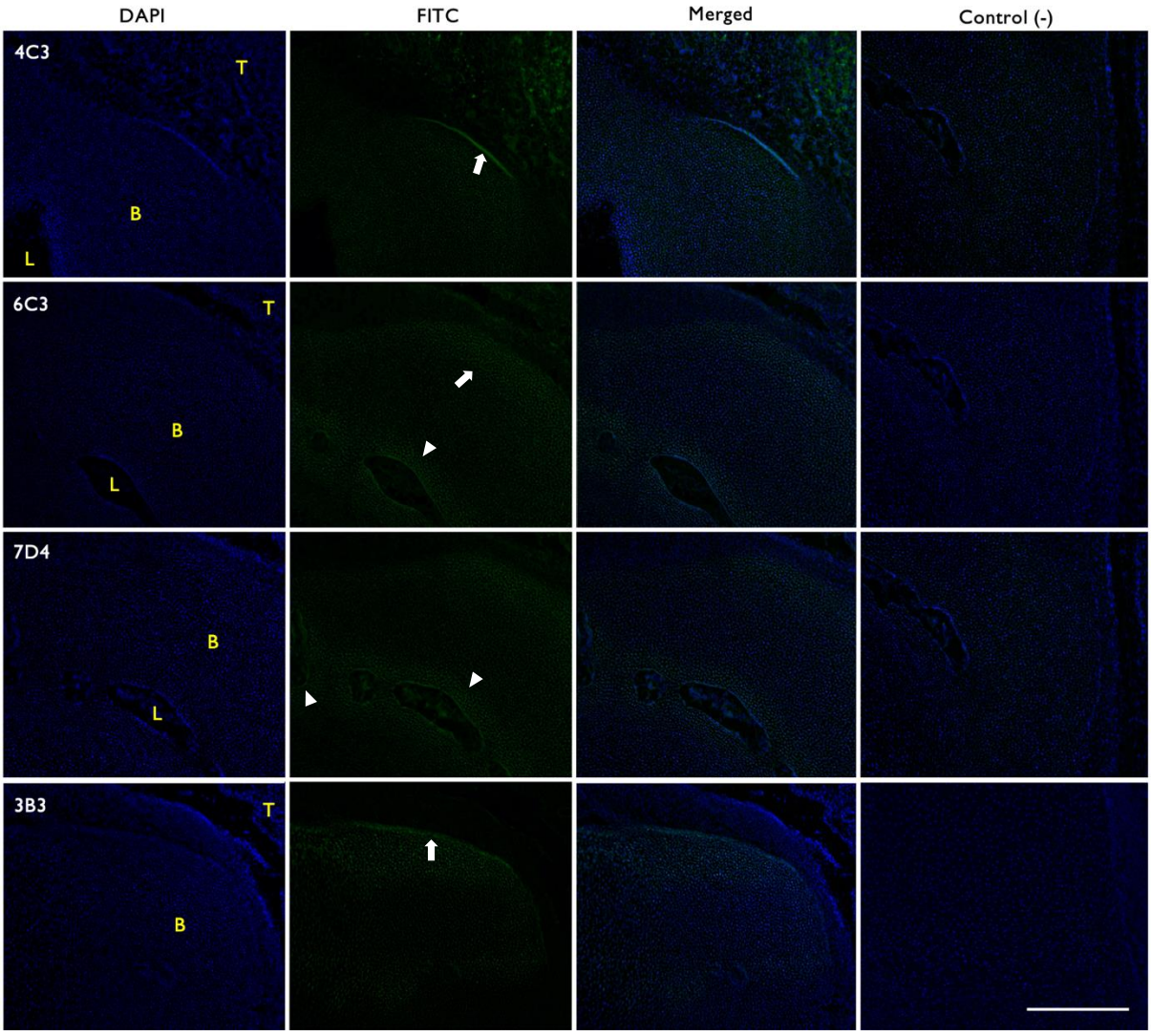

Figure 4.2: Localisation of sulphation-specific epitopes recognised by 4C3, 6C3, 7D4, and 3B3 in E14 chicken hindlimb. Fluorescence labelling of sulphation motif-specific monoclonal antibodies in transverse section of embryonic tibiotarsal/tarsometatarsal joint. Positive localisation of antibodies 4C3, 6C3, 7D4, and 3B3 is evident around chondrocyte lacunae *(*L*, arrowheads)* and in articular cartilage at boundaries of bone *(*B*, arrows)*. T = tendons. Scale bar represents 100 μm.

4.3.2 Localisation of 4C3, 6C3, 7D4, and 3B3 in the Adult Avian Limbus

Immunolocalisation of mAbs associated with sulphation-specific motifs along CS/DS PG chains were investigated in the adult avian limbus *(mAb specificity is outlined in Figure 4.1)*. Tissue specific labelling of native *(4C3, 6C3, and 7D4)* epitopes in the limbal region (Figure *4.3*) of the avian cornea was of particular interest in view of data supporting their association with a stem cell niche at this location in multiple other animal models *(i.e., human, mice, and rabbits)* (Nowell and Radtke 2017). Localised labelling of CS epitopes recognised by mAb 4C3 and 6C3 was seen only in the limbus, primarily in the stromal matrix, whereas labelling of mAb 7D4 did not localise strictly in the corneal limbus but was rather seen to label the stromal matrix across the corneolimbal

junction diffusely. Moreover, 7D4 also exhibited a distinctive punctate staining pattern in histological sections. In the absence of ChABC enzyme digestion pre-treatment, no labelling of 3B3 was observed throughout the limbus. Negative controls for 4C3, 6C3, 7D4, and 3B3 confirmed a lack of non-specific binding of secondary antibody.

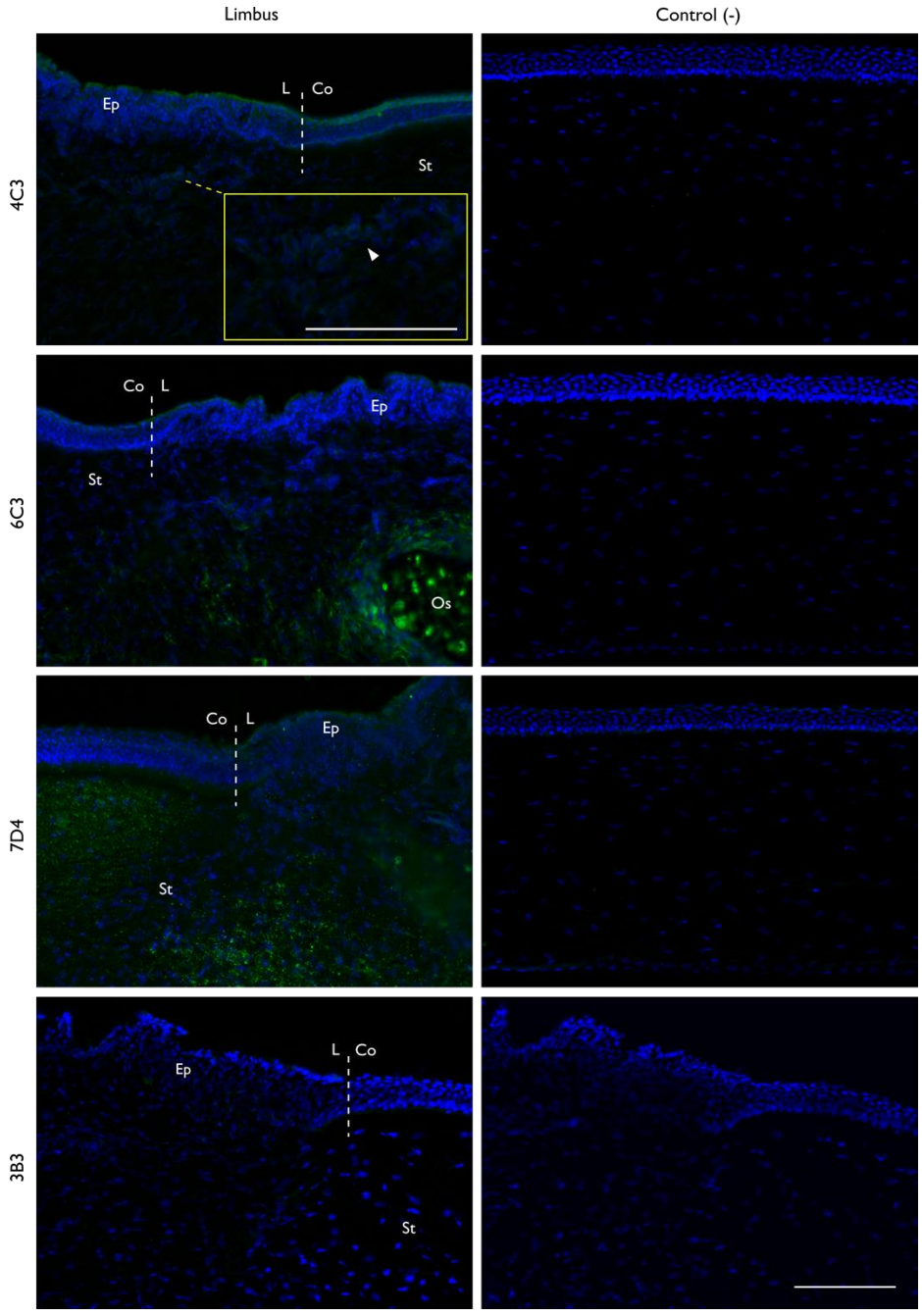

Figure 4.3: Immunolabelling of chondroitin sulphate proteoglycans in the adult avian limbus. The left-hand panel shows chondroitin sulphate specific epitopes recognised by monoclonal antibodies 4C3, 6C3, 7D4, and 3B3. Positive labelling *(green)* of 4C3 *(arrowhead)* and 6C3 was localise in the stroma subjacent to the epithelial basement membrane, whereas 7D4 was ubiquitous across the corneolimbal region. Nuclei counterstained with DAPI *(blue)*. Dashed vertical white lines represent the corneolimbal junction. Ep = epithelium, St = stroma, L = limbus, Co = cornea. Os = scleral ossicle. Scale bar represents 100 μm.

4.3.3 Localisation of 4C3, 6C3, 7D4 3B3 in the Developing and Adult Avian Cornea

To supplement the investigation into the immunolabelling of 4C3, 6C3, 7D4, and 3B3 in the adult avian limbus, the mid-peripheral and central cornea were also examined in addition to earlier developmental time points: E_{14}, E_{18}, and adult to ascertain if regional distribution of labelling changed with maturation. For antibody 4C3 (Figure *4.4*), diffuse stromal labelling was observed in all three regions of E_{14} sections but was seen to progressively localise in only the limbal and mid-peripheral cornea; similar findings were also observed in E_{12} and E_{10} sections *(not shown)*. Following maturation, more distinct localisation was seen in the anterior limbal stroma only and absent from the mid-peripheral and central cornea. Negative controls for 4C3 also confirmed a lack of non-specific binding of secondary antibody.

Similar to antibody 4C3, antibody 6C3 (Figure *4.5*) labelled diffusely all regions of the E_{14} corneas and in E_{12} and E_{10} sections *(not shown)*, whereas labelling was seen to localise primarily in the limbus and mid-periphery of the E_{18} cornea. However, subjacent to the basal epithelium, labelling was observed in the anterior matrix of the central cornea. In the mature cornea, labelling was localised only in the limbal stroma and absent from the mid-peripheral and central cornea. Moreover, positive labelling was seen inside and around a peripheral scleral ossicle that was present in the adult section. Negative controls for 6C3 also confirmed a lack of non-specific binding of secondary antibody

Interestingly, the immunolabelling pattern of mAb 7D4 (Figure *4.6*) was distinct from that of 4C3 and 6C3 and more widespread. In the E_{14} corneal section, strong, diffuse labelling was primarily observed in the limbus, however, was also evident in the mid-peripheral and central cornea. E_{18} labelling profile was the same as in E_{14}, however, in the central cornea, labelling was present more in the inferior stroma. Following maturation, diffuse labelling could be seen in the stromal of all three regions. Negative controls for 7D4 also confirmed a lack of non-specific binding of secondary antibody.

For 3B3, the absence of positive labelling (Figure 4.7) in the adult avian limbus was also uniform across the mid-peripheral and central cornea; and similar findings were observed with respect to E_{18} and E_{14} sections, in addition to E_{12} and E_{10} sections *(not shown)*. Negative controls for 3B3 also confirmed a lack of non-specific binding of secondary antibody.

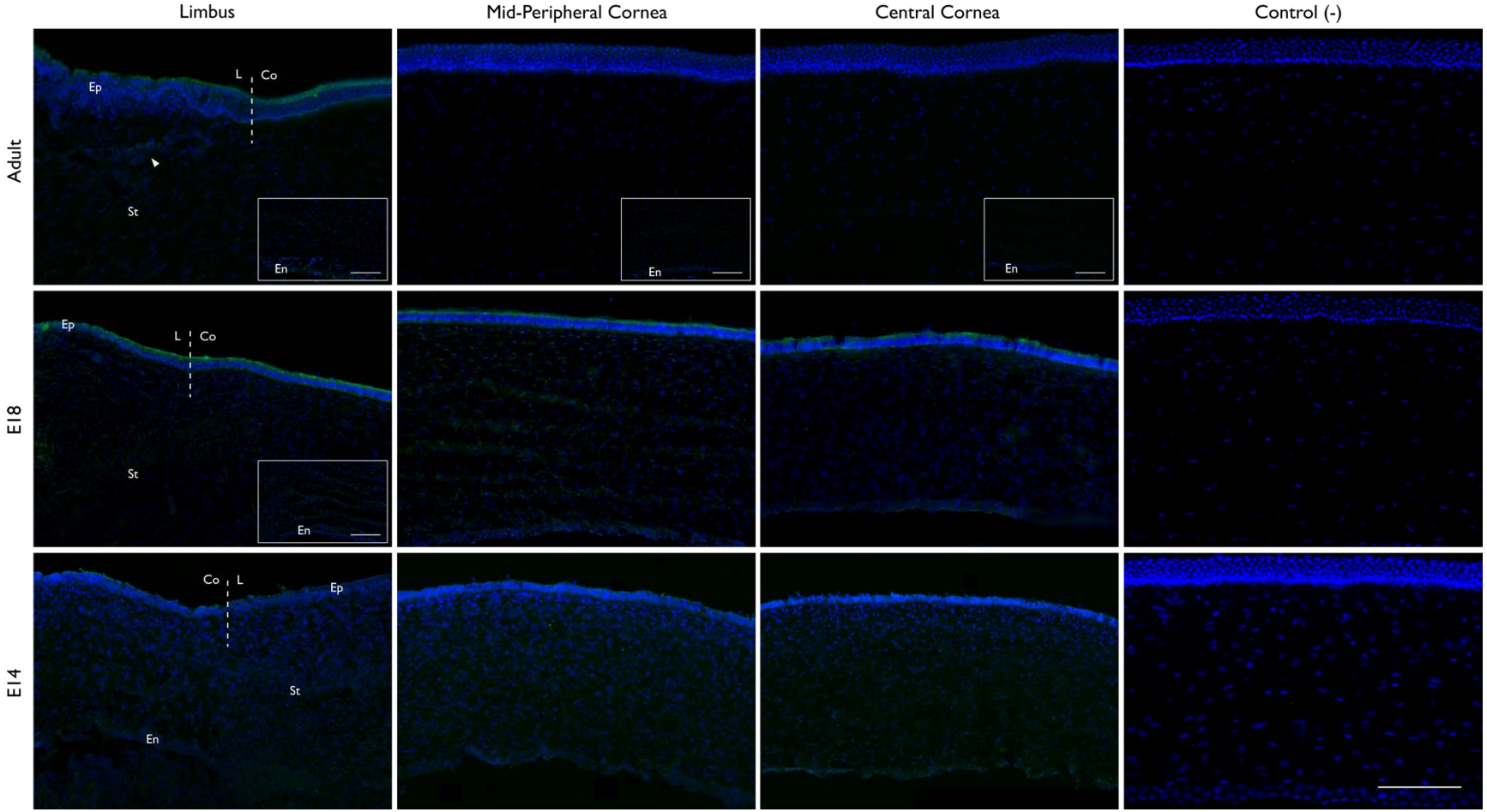

Figure 4.4: Immunolabelling of 4C3 in the developing avian cornea. Labelling of sulphation motif-specific antibody 4C3 was assessed in corneal cross-section for developmental time points E_{14}, E_{18} and Adult. Positive, diffuse labelling *(green)* was detected in all regions of the stroma (St) in E_{14} sections. By E_{18}, diffuse stromal labelling *(green)* persisted only in the limbus (L) and mid-peripheral cornea, however, minimal labelling by anterior matrix cells was also seen in the central cornea. In the adult cornea, labelling *(green)* was localised in the limbus only. Nuclei counterstained with DAPI *(blue)*. Dashed vertical white lines represent the corneolimbal junction. Insets show immunolabelling of the endothelial layer**.** Ep = epithelium, En = endothelium, Co = cornea. Scale bar represents 100 μm. *Adult limbal image also used in Figure 4.3.*

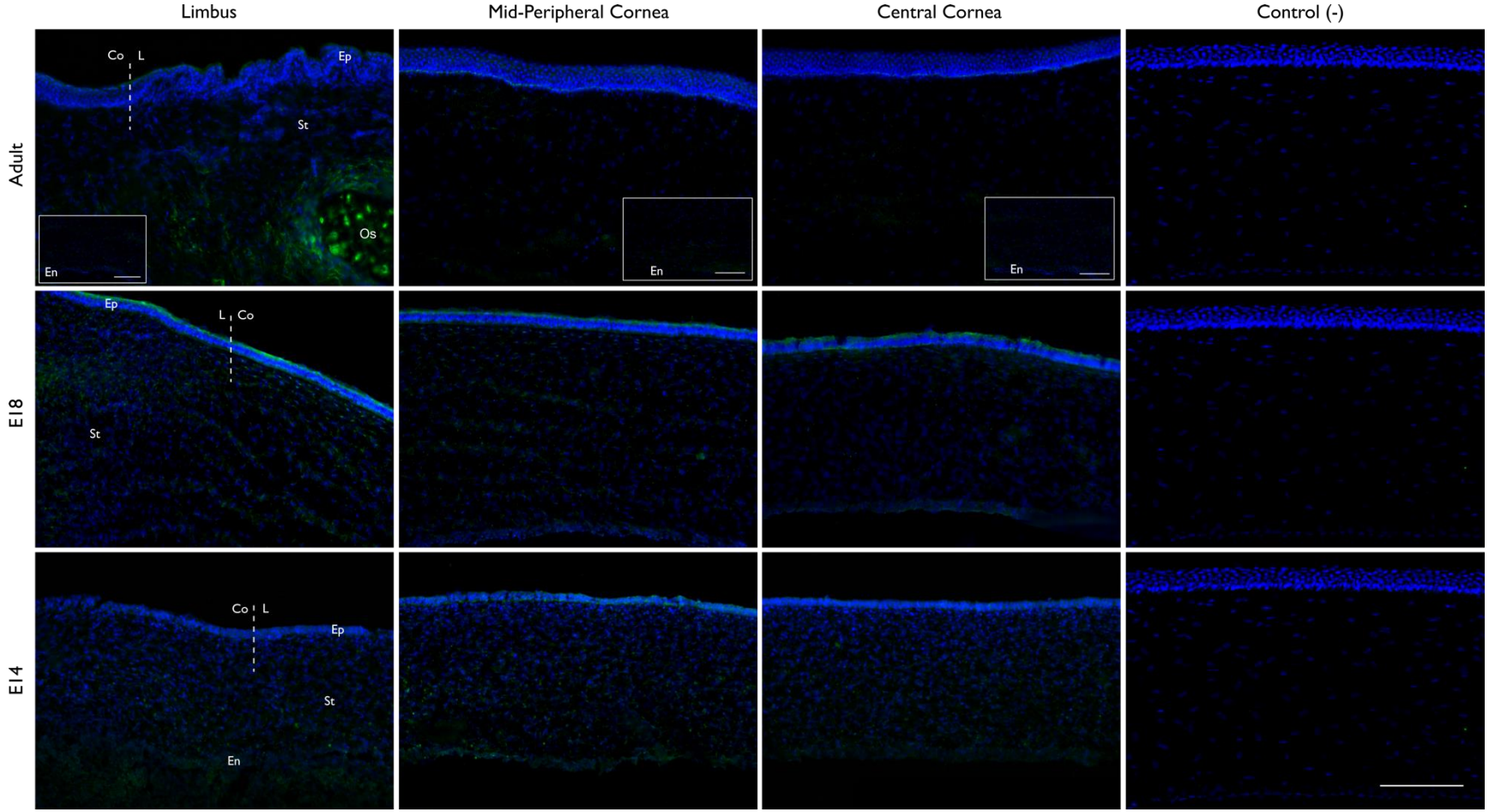

Figure 4.5: Immunolabelling of 6C3 in the developing avian cornea. Labelling of sulphation motif-specific antibody 4C3 was assessed in corneal cross-section for developmental time points E_{14}, E_{18} and Adult. Positive, diffuse labelling *(green)* was detected in all regions of the stroma (St) in E_{14} sections. By E_{18}, diffuse stromal labelling *(green)* was seen in the limbal and mid-peripheral cornea, however, minimal labelling by anterior matrix cells was also seen in the central cornea. In the adult cornea, labelling *(green)* was localised in the limbus only. Strong labelling was also seen around a scleral ossicle (Os). Dashed vertical white lines represent the corneolimbal junction. Insets show immunolabelling of the endothelial layer. Ep = epithelium, En = endothelium, Co = cornea, L = Limbus. Nuclei counterstained with DAPI *(blue)*. Scale bar represents 100 μm. *Adult limbal image also used in Figure 4.3.*

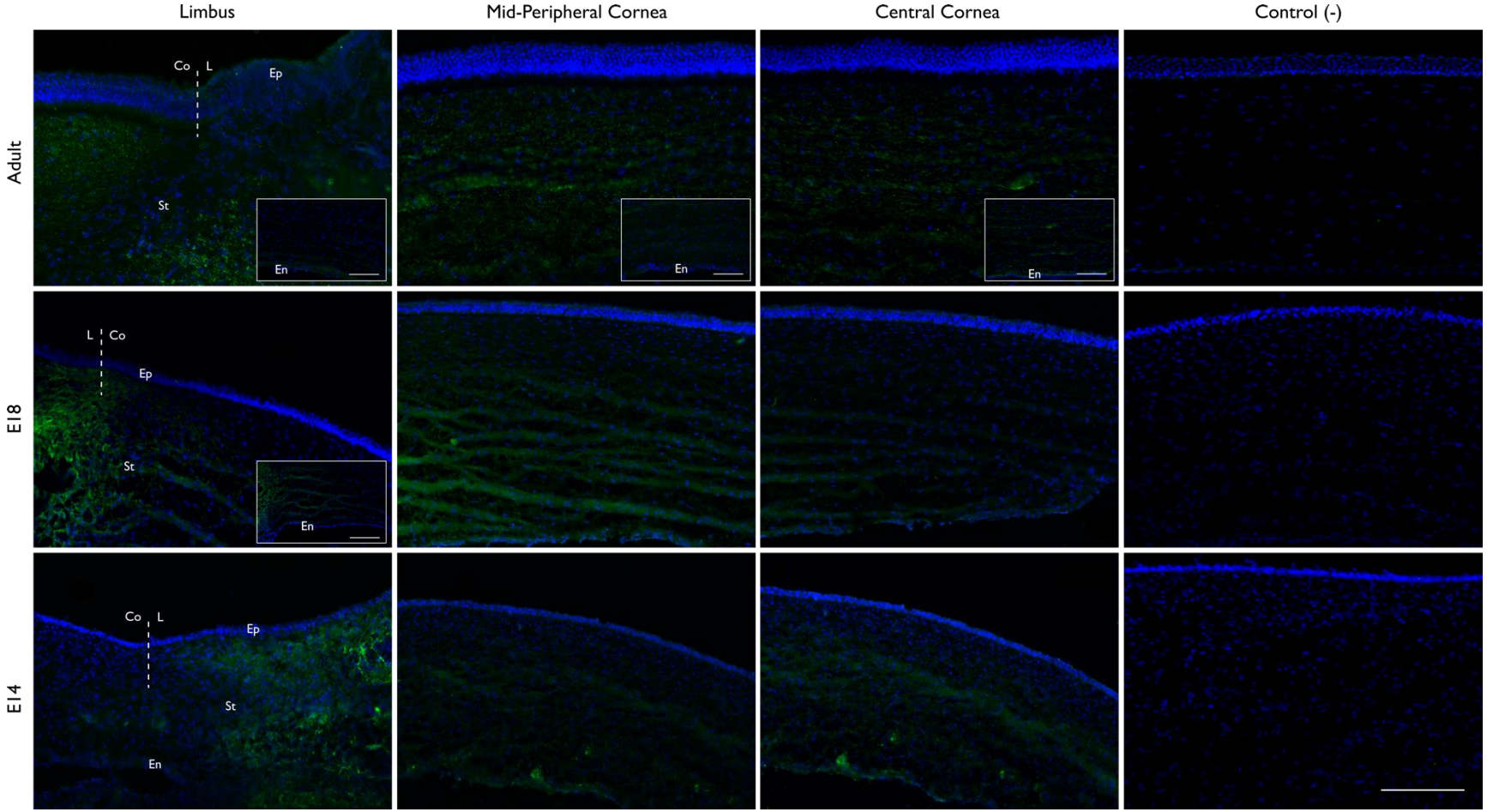

Figure 4.6: Immunolabelling of 7D4 in the developing avian cornea. Labelling of sulphation motif-specific antibody 7D4 was assessed in corneal cross-section for developmental time points E_{14}, E_{18} and Adult. Positive, diffuse stromal (St) labelling *(green)* was detected in all regions of the E_{14} section. In E_{18} sections, diffuse stromal labelling *(green)* persisted in the limbal and mid-peripheral cornea but was also evident in the inferior portion of the stroma in the central cornea. In the adult cornea, diffuse stromal labelling was seen in all three corneal regions. Dashed vertical white lines represent the corneolimbal junction. Ep = epithelium, En = endothelium, Co = cornea, L = limbus. Insets show immunolabelling of the endothelial layer. Nuclei counterstained with DAPI *(blue)*. Scale bar represents 100 µm. *Adult limbal image also used in Figure 4.3.*

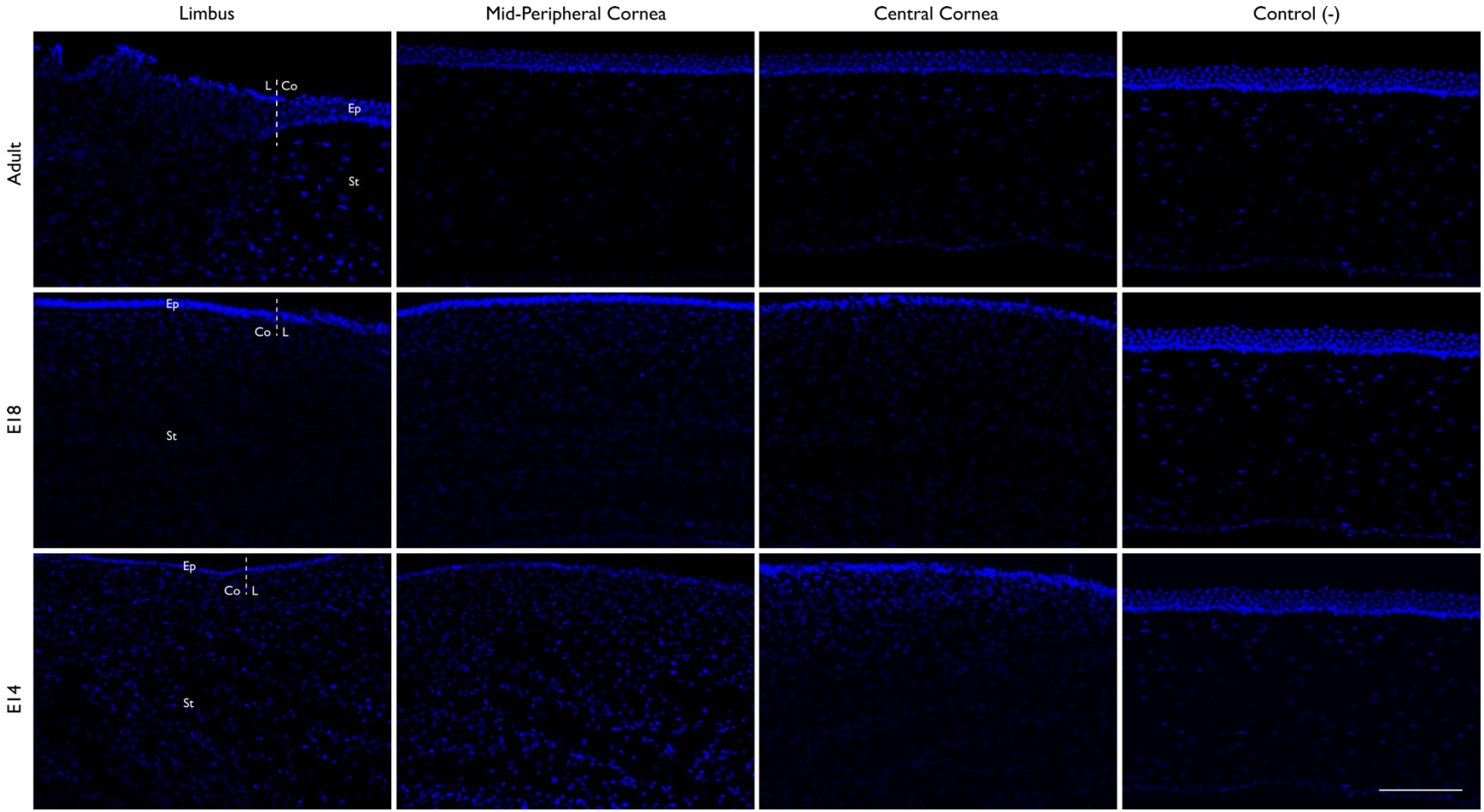

Figure 4.7: Immunolabelling of 3B3 in the developing avian cornea. Labelling of sulphation motif-specific antibody 3B3 was assessed in corneal cross-section for developmental time points E_{14}, E_{18} and Adult. No observable labelling was detected in any of the corneal layers of points E_{14}, E_{18} and adult corneal sections. Dashed vertical white lines represent the corneolimbal junction. Ep = epithelium, En = endothelium, Co = cornea, L = limbus. Nuclei counterstained with DAPI *(blue)*. Scale bar represents 100 μm.

4.3.4 Localisation of 4C3, 6C3, and 7D4 *In Situ*

A supplementary investigation was done to support *in situ* stromal labelling of native epitopes recognised by mAbs 4C3, 6C3, and 7D4 antibodies by assessing for positive labelling in cultures of E_{18} corneal keratocytes cultured to P_2 (Figure 4.8). As a result, weak labelling of all three antibodies was observed in a majority of the cultured cells. Moreover, negative controls for 4C3, 6C3, 7D4, and 3B3 confirmed a lack of non-specific binding of secondary antibody.

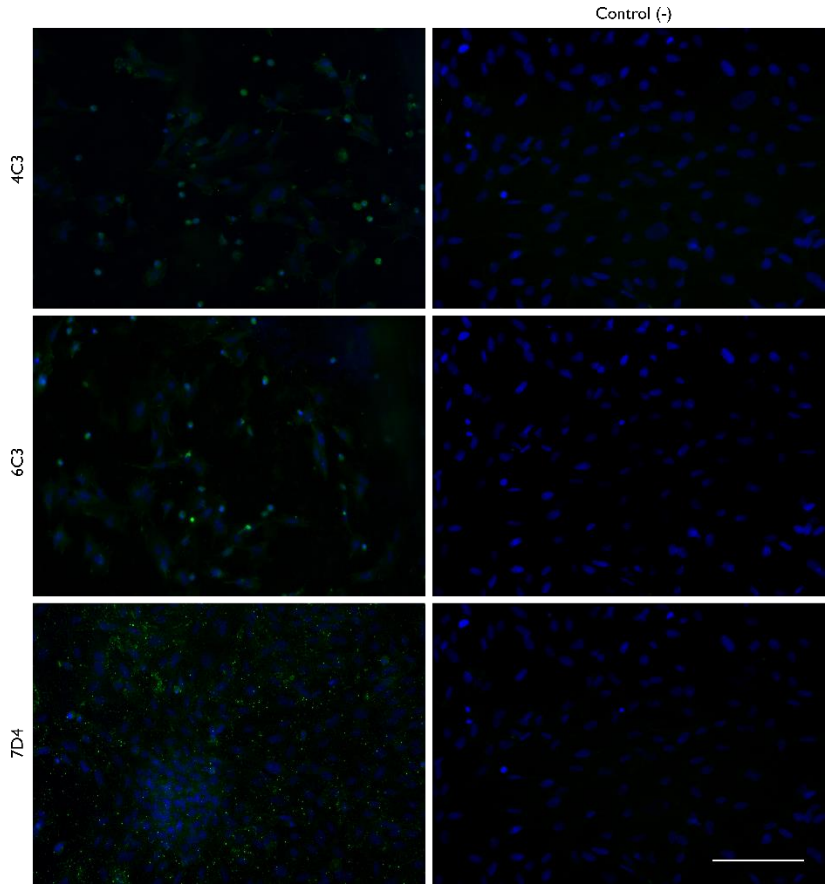

Figure 4.8: Immunolabelling 4C3, 6C3, and 7D4 *in vitro*. Labelling of sulphation motif-specific antibodies 4C3, 6C3, and 7D4 were assessed in cultures of E_{18} avian corneal keratocytes cultured to P_2. The left-hand panel shows native epitopes of chondroitin sulphate proteoglycans positively labelled *(green)* cells. The right-hand panel shows corresponding negative antibody controls. Nuclei counterstained with DAPI *(blue)*. Scale bar represents 100 μm

4.4 Discussion

4.4.1 Monoclonal Antibody Validation in E_{14} Chicken Ankle

Prior to assessing staining of 4C3, 6C3, 7D4, and 3B3 in the avian cornea, labelling of the mAbs was validated using E_{14} white Leghorn chicken sections of the tibiotarsal/tarsometatarsal joint. The results of this preliminary investigation showed positive staining in specific areas of the developing joint cartilage for all four antibodies. Moreover, the staining pattern for CS/DS sulphation motifs observed in these positive controls corresponded to what was observed by Caterson et al. (2012) for 3B3 [-] and 6C3 in embryonic joint tissue of chickens and 4C3 and 7D4 in 12-week-old human foetal knee joint. Hayes and colleagues also performed similar examinations in immature bovine articular cartilage and rat intervertebral discs and found positive staining of 3B3 [-], 7D4, and 4C3 in the bovine cartilage and positive staining of 4C3, 6C3, 7D4, and 3B3 [-] in rat intervertebral discs (Hayes et al. 2008; 2011).

4.4.2 Immunolabelling of 4C3, 6C3, 7D4, and 3B3 in the Avian Cornea

In this study, the differential distribution of mAbs [4C3, 6C3, 7D4, and 3B3], which recognise distinct SM epitopes in CS/DS GAG chains, were examined in the developing and mature avian cornea. Differences in the immunohistochemical labelling patterns of each mAb were subtle yet distinct. In the past, anti-CS antibody 3B3 has been linked to the detection of neoepitopes *(CS stubs)* exposed through ChABC digestion but subsequent investigations determined 3B3 recognised native epitopes as well (Sorrell et al. 1998; 1990a). Work by Yamada et al. (2015) and Hammond (2021) investigated the CS SM distribution in the rabbit and porcine cornea, respectively, and found positive labelling of 3B3 neoepitopes exposed by ChABC treatment only, in the absence of enzyme digestion, 3B3 labelling was ubiquitously negative across the cornea. In the current investigation, no observable labelling of 3B3 was detected in the developing avian limbus, mid-peripheral and central cornea. In sections of the adult limbus, where limbal undulations were evident, 3B3 labelling was also absent.

Staining of mAb 4C3 was also detected in the avian cornea, however, the labelling pattern was such that once the cornea reached maturation, 4C3 localised in anterior stoma of the limbus. *In vitro* assessment of E_{18} stromal keratocytes also revealed weak by positive labelling of 4C3. Incidentally, positive 4C3 labelling in the current investigation differed from the findings reported by Yamada et al. (2015) and Hammond (2021) who both found no specific labelling of 4C3 within the limbal region of the rabbit and pig, respectively, but did report positive labelling of 4C3 in

other regions of the corneal stroma. Conversely, mAb 7D4 was seen to label more prominently in the limbus, but was nevertheless ubiquitous across all corneal regions. Moreover, *in vitro* assessment of E_{18} stromal keratocytes also showed positive labelling of 7D4 which further supported *in situ* observations. Labelling of 7D4 in the avian cornea was similar to findings reported by Hammond (2021) with respect to the porcine cornea, however, Yamada et al. (2015) observed positive staining in the mid-stroma of the peripheral rabbit cornea which was absent along the basement membrane of the putative limbal stem cell zone.

Studies by Hayes et al. (2016) and Melrose et al. (2016) found overlapping distribution of 4C3, 7D4, and 3B3 [-] CS SMs in particular zones of joint tissue linked to bone morphogenesis during human foetal development. Previous studies have indicated that mAbs 3B3 [-] and 7D4 recognise epitopes on non- and low-sulphated isoforms of CS, respectively which adds support to the already mounting evidence in favour of Hayes et al's (2008) theory of non- and minimally-sulphated isoforms of CS being involved in the maintenance and regulation of a stem/progenitor cell niche in articular cartilage. However, the ubiquitous labelling of 7D4 and absence of 3B3 in the avian limbus does not align with Hayes' hypothesis. With respect to mAb 7D4, anterior stromal labelling was evident along the corneal aspect of the corneolimbal junction. As this is the migratory path taken by TACs towards the central cornea, it was fair to expect instead a population consisting of higher sulphation to promote differentiation, as was observed in a study by Schlötzer-Schrehardt et al. (2007), who noted the association of CS with the anterior portion of the limbal stem cell niche. The absence of mAb labelling of 3B3 in the avian cornea is also inconsistent with Hayes' proposed theory and findings with respect to stem/progenitor stem cell niche in articular cartilage, however, they aligned with the findings observed in the presumptive stem cell niche of the rabbit and porcine cornea. Interestingly, labelling of 4C3 in the avian cornea aligned with Hayes' theory but deviated from that labelling observed in the rabbit and porcine cornea.

Similar to mAb 4C3, the staining pattern of 6C3 in the developing and adult avian cornea was seen to localise in the limbus, specifically within the mid- to anterior stroma in close proximity to the undulating epithelial basement membrane. Positive labelling of stromal cells was further substantiated from the *in vitro* results of cultured E_{18} keratocytes. In the rabbit, labelling of 6C3 was detected along the limbal basement membrane and around limbal capillaries at the site of epithelial-mesenchymal associations – an area regarded to have a putative stem cell niche (Yamada et al. 2015). In a subsequent preliminary investigation by Yamada and colleagues, the aforementioned mAbs were also investigated in the human corneal limbus as well, where only 6C3

was seen to positively label the limbal matrix – another site known to house a stem cell niche. Moreover, within intervertebral discs of rats, Hayes et al. (2011) reported restricted labelling of 6C3 in the cambial layer of the perichondrium – an area associated with proliferating chondrocytes (Kronenberg 2007; Hayes et al. 2011). Whereas preliminary work by Ashworth et al. (2021) found localised labelling of 6C3 in close proximity to putative limbal epithelial stem cells in the porcine cornea which led them to speculate upon 6C3's involvement with the stem cell milieu. Based on the hypothetical model by Hayes et al. (2008), low- and minimally-sulphated CS have been suggested to protect stem cells in their respective environments by preventing the influence of growth factors through the lack of cell surface receptors. Although the exact structure of the 6C3 epitope has yet to be elucidated, it is known to occur towards the non-reducing terminus of the CS chain. Moreover, Sorrell et al. (1993) have shown it to contain both 4- and 6- sulphated CS, however, the degree of sulphation *(minimal or highly sulphated)* remains unknown for the time being. The results of 6C3 labelling in this study, with respect to the avian limbus, and the current literature lends further support to its association with a putative limbal stem cell niche.

The observed labelling pattern of mAbs 4C3, 6C3, and 7D4 in the adult avian limbus is a novel finding, but what was more telling was the structured process through which this was achieved across key developmental timepoints. Much like in the study by Hayes et al. (2011), where the distribution of antibodies 4C3, 6C3, and 7D4 throughout the ontogeny of the intervertebral disc in rats was found to coincide with major morphological events pertaining to disc differentiation, the mapping of these antibodies in the developing avian limbus, also appeared to coincide with important developmental stages. Previous work by Nuttall (1976) found that during earlier stages of corneal development, keratocyte proliferation remained relatively uniform across the thickness of the stroma but from E_{11}, cell proliferation rates were determined to be higher in the anterior stroma opposed to the posterior stroma (Nuttall 1976). Accordingly, it was observed that at E_{14}, antibodies 4C3, 6C3, and 7D4 labelled the stroma diffusely followed by an anterior shift in positive signalling at later stages with an initial concentration occurring towards the limbus, directly subjacent to the epithelial basement membrane, that continued to localise well into maturation.

CS has been well-documented in the avian corneal stroma prior to and during the migration of presumptive keratocytes (Doane et al. 1996; Quantock and Young 2008). In an investigation by Zhang et al. (2005), electrospray ionization tandem mass spectrometry was used to track and quantify changes in differentially sulphated CS/DS molecules in the chicken cornea between E_8 to post-hatching. They found roughly equal concentrations of differentially sulphated CS PGs

(chondroitin-4-sulfate and chondroitin-6-sulfate) by E_{14}, which corresponded with the initiation of transparency within the cornea. However, prior to this cross-over point, chondroitin-4-sulfate was reported as expressed in lower concentration and chondroitin-6-sulfate in higher concentrations, but as the cornea matured there was a progressive reversal in concentration levels with chondroitin-4-sulfate increasing and chondroitin-6-sulfate decreasing when assessed. The authors as a result hypothesised chondroitin-6-sulfate was more significant in early development for stromal morphogenesis, whereas chondroitin-4-sulfate was necessary for the promotion of a stable and compact stroma that would increase in transparency well into maturity (Zhang et al. 2005; Quantock and Young 2008). Moreover, it was by E_{18} that the avian cornea possessed a CS/DS PG with a single GAG chain, as suggested by the authors, to provide mechanical aid for collagen fibrils to slide over during the restructuring and stabilization late in corneal development (Midura and Hascall 1989: Quantock and Young 2008). Zhang's characterisation of the changing expression of chondroitin-4-sulfate and chondroitin-6-sulfate in the developing cornea is an interesting one. In the current study, the labelling pattern of epitope specific mAbs 4C3, 6C3, and 7D4 overlapped in some arears throughout development and in some respects was subtle but distinct. Unfortunately, the specificity of the antibodies used in this study cannot directly be compared to the expressional profile observed by Zhang and colleagues as the precise specificities of all antibodies involved between both studies are not known. That said, it provides an avenue for more robust investigations into the specific spatio-temporal expression patterns of CS /DS GAG sulphation motifs in cornea and its involvement in stromal morphogenesis and corneal transparency.

It is also important to acknowledge that the investigation into characterising and the function of the human limbal stem cell niche is further along and more extensively understood in comparison to any other animal model also currently under investigation. Similarly, the investigation of mAb labelling and its association with stem cell niches outside of articular cartilage is only just emerging. As a result, more explorative work will need to be done to further elucidate the involvement of CS as a potential modulated of the corneal limbal stem cell niche.

4.5 Summary

The results presented in this chapter provide the first evidence of immunolabelling of native epitopes, recognised by antibodies 4C3, 6C3, and 7D4 in the developing and adult avian cornea and limbus. During immunohistochemical analysis, observations of SM-specific mAbs 4C3 and 6C3 showed a gradual localisation in the anterior limbal matrix of the mature avian cornea,

whereas, 7D4 was observed to ubiquitously label the corneal stroma, but with more intense labelling along the peripheral-cornea at the corneolimbal junction of the mature avian cornea. Positive labelling of mAbs 4C3, 6C3, and 7D4 in the avian stroma was also confirmed in cultures of E_{18} keratocytes. Furthermore, the native CS SM epitopes identified by the mAbs appeared to coincide to an extent with findings reported in literature relating to the stem cell niche in the rabbit, human, and porcine cornea.

The chapter that follows will use SEM, TEM, and SBF-SEM to investigate anatomical features and cell-cell interactions in the avian limbus which are analogous to those seen in the human limbal stem cell niche. The formation of key anatomical cellular features, suggestive of a presumptive stem cell niche, will be evaluated in late-stage embryonic eyes *(E_{16} and E_{18})* in addition to the mature avian cornea.

Chapter 5: High Resolution and 3D Imaging of the Presumptive Limbal Stem Cell Niche in the Avian Cornea Using Light and Electron Microscopy

5.1 Introduction

The corneal limbus, the transition zone between the cornea and sclera, has been a region of intense interest with investigations encompassing the mechanisms and cells involved in the renewal and regeneration of the ocular surface (Boulton and Albon 2004). General opinion now supports the idea that limbal stem cells *(epithelial and mesenchymal stem cell populations)* have the capability of restoring damaged or lost epithelial cells and keratocytes, respectively, during corneal wound healing and normal homeostasis (Dua et al. 2005; Yamada et al 2015; Funderburgh et al. 2016). Despite the recent literature being inundated with articles confirming the presence of stem cells within a range of different tissues, our understanding remains limited with respect to the stem cell biology of the eye (Boulton and Albon 2004). For instance, it is only now being elucidated that the limbal microenvironment plays a critical role in the pathways involved in stem cell regulation and differentiation and despite several literary claims being made, no definitive corneal stem cell markers have been fully accredited to date (Boulton and Albon 2004).

5.1.1 Limbal Stem Cells

5.1.1.1 Corneal Epithelial Stem Cells

As alluded to above, it is commonly regarded that the continued maintenance and replenishment of the corneal epithelial mass is achieved by a distinct population of slow-cycling stem cells located in the basal epithelium at the limbal junction. (Kinoshita et al. 1981; Tseng 1989, Boulton and Albon 2004; Schiotzer-Schrehardt and Kruse 2005). It is these stem cells that give rise to TACs which are fast-dividing progenitor cells that in turn contribute to much of the proliferative cell potential (Lehrer et al. 1998; Schiotzer-Schrehardt and Kruse 2005). Furthermore, it is believed that TACs have a limited proliferative capacity before they become terminally differentiated and slough off the epithelial surface as flattened superficial cells (Thoft and Friend 1983; Tseng 1989; 1996 Lavker et al. 2004; Schiotzer-Schrehardt and Kruse 2005).

Characterisation of Limbal Basal Epithelium

The evolution of this complex and generally-accepted corneal limbal stem cell hypothesis emerged from several key investigative break-throughs starting in the mid-1980's, when Sun and colleagues

were examining the growth and differentiation potential of epithelial cells in the rabbit cornea; they fortuitously discovered that epithelial cells synthesised tissue-restrictive keratin proteins – K3 and K12 (Sun 1984; Tseng et al. 1982; Sun and Lavker 2004). Supplementary examination of the in-culture and *in vivo* expression of K3 by Schermer et al. (1986) revealed positive labelling within the anterior portion of the stratified epithelial layer in the limbal zone, a consistent finding, as K3 expression was associated with advanced stages of epithelial cell differentiation. Surprisingly, they also found uniform expression of K3 in the central cornea throughout the stratified epithelium, including the basal cells, which until then were thought to be undifferentiated. This demonstrated, with respect to K3 marker expression, the existence of biochemical heterogeneity between epithelial basal cells located at both the central and limbal cornea. More specifically, it contended that central basal epithelial cells were more differentiated than basal cells localised in the limbus. Following this discovery, Shermer and colleagues went on to propose that corneal epithelial stem cells *(CESC)* were not uniformly distributed throughout the corneal basal layer, rather they were localised only within the limbal basal epithelium (Schermer et al. 1986).

More compelling evidence in support of this hypothesis came from Cotsarelis et al. (1989) who used the slow cycling potential of stem cells as a way of distinguishing between stem cells, progeny TACs, and terminally differentiated cells. Here, they continuously perfused corneal tissue with 3H-thymidine before shifting to a chase period. They found that the *in vivo* label retention was preferentially observed in a subpopulation of limbal corneal epithelial basal cells and not in the central corneal epithelium, whereas diluted label retaining cells *(dividing TACs)* were observed to be located uniformly within the corneal epithelium (Cotsarelis et al. 1989; Sun and Lavker 2004). Contemporary *in vitro* studies, like the ones done by Pellegrini et al. (1997) and Daniels et al. (2001; 2007) provided compelling support to the belief that stem cells were localised within the corneal limbus. From the human limbus, small biopsies were surgically excised and used to generate long-term proliferative clones that in turn could be used to construct transplantable cell sheets; post-clinical assessments showed that tissue-engineered sheets were able to reconstitute successfully the damaged corneal surface upon grafting (Pellegrini et al. 1997; Daniels et al. 2001; 2007; Sun and Lavker 2004; Nowell and Radtke 2017).

Rousing as all these findings may be, there are still some contentious aspects of the Schermer hypothesis that require deeper investigation. For instance, the ambivalence of some researchers as to whether or not CESCs exclusively reside within the limbus. In a study by Majo et al. (2008), the stem cell activity in various mammalian ocular surfaces *(rabbits, mice, and pigs)* were investigated.

Here, they found that stem cell isolates could be obtained from multiple regions across the cornea in addition to the limbal region, however, the limbal epithelium and peripheral corneal regions contributed to the highest number of possible isolates (Majo et al. 2008; Nowell and Radtke 2017). Moreover, by using lineage-tracing, they were able to demonstrate that stem cells isolated from the limbus contributed solely to reparative cascades involved in corneal wound healing and remained dormant throughout normal homeostatic processes (Majo et al. 2008; Nowell and Radtke 2017). It has therefore been postulated that multiple stem cell populations exist within the cornea which would, therefore, explain the distinction in roles where a dormant population of limbal stem cells participate in only extreme reparative cascades and another stem or progenitor cell population, distributed throughout the cornea, participates in the specific maintenance of normal ocular homeostasis (Nowell and Radtke 2017).

Nevertheless, all these intriguing findings were arguably the impetus that led to the emerging hypothesis that in most animal species the LESCs belonging to the ocular surface reside enveloped within the basal layer at the interface of the limbus (Davanger and Evensen 1971; Sun 1984; Schermer et al. 1986, Cotsarelis et al. 1989; Dziasko et al. 2015). Moreover, it is within the superior and inferior limbal regions where an abundance of LESCs can be observed in the human eye, along radial ridges of the underlying stroma (Dziasko et al. 2015). Here, LESCs are characterised as being smaller than neighbouring basal cells and possess a high nucleus-cytoplasm ratio (Romano et al. 2003; Dziasko et al. 2015).

5.1.1.2 Corneal Stromal Stem Cells

Subjacent to the limbal basement membrane within the corneal stroma is a subpopulation of cells that, when isolated in culture, exhibit the typical phenotype of mesenchymal stem cells *(MSC)* (Funderburgh et al. 2016). In an earlier study done by Funderburgh et al. (2005), three percent of all isolated adult bovine corneal stromal cells were found to have the capacity for colony formation. The gene expression and morphology of these cells was determined to be distinct from keratocytes and they had the capacity to maintain a stable progenitor phenotype through more than 50 population doublings, with replicative senescence occurring after 70-80 population doublings (Funderburgh et al. 2016). Future works have since built on Funderburgh's findings to implicate these 'niche cells' as important contributors to limbal epithelial cell support, suppression of inflammation, rehabilitation of damaged stromal tissue, and restoration of corneal transparency (Funderburgh et al. 2016).

Mesenchymal Stem Cells in the Human Corneal Stroma

In many non-epithelial tissues, discernible subpopulations of adult stem cells were identified and generically termed MSCs. These subpopulations were typically non-participatory in the normal local homeostatic regulation of the tissues in which they resided; moreover, they were accredited with the shared capacity to undertake multipotent differentiation, self-renewal, and clonal growth (Funderburgh et al. 2016). Interestingly, these cells were found to efflux fluorescent dyes, and using techniques like flow cytometry, cells presenting with reduced fluorescent output appeared as isolated 'side populations' in post-data analysis. Using the dye Hoechst 33342, stem cells isolated in the human corneal stroma as a side population were later termed CSSCs, which presented at a frequency of <1% in early passages (Funderburgh et al. 2016). FACS-isolated, these cells could be expanded clonally, achieving upwards of 100 cumulative population doublings, all of which expressed properties of MSCs (Funderburgh et al. 2016). To date, CSSCs in both mice and rabbits have successfully been expanded clonally (Yoshida et al. 2005; Amano et al. 2006; Yoshida et al. 2006; Funderburgh et al. 2016).

Localisation of Stromal Stem Cells in Tissue

The first observations of CSSCs in the corneoscleral transition zone were made by immunostaining of notable MSC markers ABCG2 and PAX6 – both of which were determined to be highly expressed by CSSCs in a gene array analysis (Du et al. 2007; Funderburgh et al. 2016). Positively stained cells were found to be localised in the anterior stroma, specifically, in regions where the basement membrane exhibited anatomical ripples and folds, resembling PoV, a known morphological characteristic associated with the LESC niche.

Supplementary investigation into the associative relationship between LESCs and stromal cells was explored further by Higa et al. (2013). The direct, shared cell-to-cell interactions were demonstrated using SEM which revealed aquaporin-1-positive stromal cells penetrating through the epithelial basement membrane to interface with N-cadherin positive limbal basal epithelial cells, forming cellular adhesions in the process. Further work by Dziasko et al. (2015) substantiated these findings in their study using SBF-SEM to produce three-dimensional reconstructions of the LESC niche, which showed the extension of stromal processes through fenestrations in the epithelial basement membrane to interface with basal epithelial cells. Earlier work by Basu et al. (2014) identified these anterior stromal cells as CSSCs by isolating aggregates of epithelial-mesenchymal cells from biopsies and comparing them to CSSCs. They were able to show that anterior stromal 'niche' cells were indistinguishable *in vitro* from previously characterised CSSCs,

in terms of their clonal growth, formation of spheroids, expression of stem cell gene markers, and capacity for differentiation into functional keratocytes (Basu et al. 2014; Funderburgh et al 2016.)

5.1.2 Specialised Corneal Stem Cell Niche

The corneal surface is a highly active tissue which uses a combination of homeostatic and reparative processes to maintain its characteristic transparency, a vital attribute for functional visual acuity (Norwell and Radtke 2017). As in other self-renewing tissues, CESCs are regulated by a microenvironment commonly referred to as a 'niche', which is perceived to comprise unique matrix composition and/or microstructure to provide a range of cues and subsistence to the resident stem cell population, in order to meet the regenerative demands of the cornea at any given time (Nowell and Radtke 2017). Though the molecular mechanisms that regulate stem cell behaviour are only now being elucidated, the components of this anatomically distinct region have long been recognised as having a combined influence on the determination of stem cell fate.

In the human cornea, there are several features of the limbus that reinforce the concept of a physical niche. Perhaps the most notable structures that can be found, which characterise the limbal stroma are the PoV, which are described as papillae-like invaginations in between which are contained limbal epithelial crypts (Nowell and Radtke 2017). Expression of putative stem cell markers N-cadherin, ABCG2, and Fzd-7 are some of the commonly cited markers that have been positively associated with the high proportion of basal cells residing within the epithelial crypts (Dziasko and Daniels, 2016; Nowell and Radtke 2017). In addition, the location of the limbal stem cell niche is advantageous as it is supported by a heavily vascularised network of capillaries, which facilitates the appropriate metabolic conditions for stem cell maintenance, specifically, by providing a means for the transfer of nutrients and maintaining oxygen tension. In fact, they also contain distinct extracellular matrix components like β2 laminin, α1 and α2 collagen IV, and vitronectin which are believed to be critical to the maintenance of CESCs (Dziasko and Daniels, 2016; Nowell and Radtke 2017). There is also evidence of physical cell-to-cell interactions that occur between epithelial cells within the limbal crypts and mesenchymal cells in the limbal stroma which are essential for maintaining the CESC population (Dziasko and Daniels, 2016; Nowell and Radtke 2017). Melanocytes are also niche-associated cells distributed throughout the PoV, specifically, within the basal layer of the epithelium (Li et al. 2007). They are known to synthesise and transport melanin pigments into the epithelium, presumably to minimise damage caused by ultraviolet irradiation (Narisawa et al. 1997; Lie et al. 2007).

5.1.3 Aims

In this study, the primary aim was to determine whether anatomical structures and cell-to-cell interactions strongly associated with the human limbal stem cell niche are also a characteristic/defining feature of the developing and mature avian cornea. For this purpose, a detailed examination of the avian limbus was carried out using high-resolution imaging techniques: SEM, TEM, and SBF-SEM.

5.2 Material and Methods

5.2.1 Scanning Electron Microscopy

5.2.1.1 Sample Collection

Six fertilised, white leghorn chicken eggs were placed in an incubator *(at 10:00 am on day one of the experiment, E_0)* to develop to E_{16} and E_{18}; whole eyes were harvested after decapitation. Whole eyes were obtained from six adult Hubbard JA87 chicken heads *(as discussed in Section 3.2.1.1)*. Whole embryonic eyes were maintained throughout preparation for SEM; however, adult eyes were dissected at the cartilaginous ossicles, maintaining the anterior-segment of the corneolimbal junction, so that samples could fit onto the 12.5 mm aluminium stubs *(used as specimen supports for the SEM)*.

5.2.1.2 Sample Preparation

Protocol modified from published methods in (Komai and Ushiki 1991) and (Thale and Tillmann 1993).

Primary Fixation

Once whole embryonic and adult chicken eyes were isolated, they were placed in individual vials containing half strength primary Karnovsky fixative for 24 hours at room temperature on a rotator. Samples were washed in cold cacodylate buffer twice for 30 minutes and stored in 4°C fresh buffer overnight.

Tissue Maceration

Maceration of glutaraldehyde/PFA-fixed samples was achieved by immersion in 10% NaOH over a course of five days to remove all cells and to effectively expose the three-dimensional arrangement of the collagen fibre network (Ohtani 1992). Embryonic eyes were treated only for three days in 10% NaOH due to fragility of the eyes, whereas adult corneas were treated for the

full, five-day course. Daily changes of 10% NaOH was performed, and samples were placed on a rotator at room temperature. At the end of each treatment course *(three and five days)*, samples were washed five times with distilled water before being stored in fresh distilled water for 24 hours.

Post-Fixation

Samples underwent a two-step post-fixative treatment; they were initially incubated in an aqueous fixative solution of 2% tannic acid (Mallinckrodt Inc., UK, Cat. # 8835) for five hours at room temperature on a rotator-before being washed with distilled water three times for 30 minutes and were stored in fresh distilled water overnight. The use of tannic acid in SEM is to aid in preserving and reinforcing the structural surface of the anterior segment and acts as a mordant for osmium tetroxide (Persi and Burnham 1981; Levanon and Stein 1993). Samples were subsequently treated with aqueous 1% osmium tetroxide for two hours again with rotation at room temperature. Osmium tetroxide is a cross-linking reagent that reacts by oxidizing unsaturated lipid moieties to form double bonds, whereby increasing density and contrast (Bozzola and Russell 1998; Fischer et al. 2013).

Dehydration

Following post-fixation, samples were dehydrated using ascendant concentrations of ethanol of 70%, 90%, 100%, and 100% for 30 minutes each. Immediately after, samples underwent final dehydration in 100% ethanol: HMDS (Alfa Aesar, UK, A15139), 100% HMDS, 100% HMDS for one hour each. Samples were then transferred into vials of fresh HMDS *(just submerging the sample)* and placed in the fume hood until liquid fully evaporated.

Mounting/ Gold Sputter Treatment

Samples were attached to 12.5 mm aluminum stubs *(cornea facing upwards)* with carbon cement. Embryonic whole eyes had to be fortified with carbon cement midway up the eye, filling the gap between the eye and the aluminum stub, whereas adult corneas were close enough to the stub surface that they required no additional fortification. Samples were then coated with ~15 nm of gold-palladium using a BioRad SC 500 sputter coater (BioRad Laboratories, Inc., UK) with argon as the sputtering gas for 30s at ~70 mTorr pressure and subsequently removed for final SEM analysis. Coating specimens with a conductive layer of metal was for the purpose of preventing/limiting electrical charging effects which can lead to blurred images (Suzuki 2002). Samples were finally placed into the sample chamber of the electron microscope for subsequent image acquisition.

5.2.1.3 SEM Image Acquisition

Areas of interest on the sample were centred and focused in the Zeiss Sigma HD Field Emission Gun Analytical scanning electron microscope which was equipped with detectors for both secondary electron and back scatter electron signals. Under high vacuum conditions, in-lens backscattered secondary electron images were observed using SmartSEM Software. For this work, specimens were typically imaged with a beam energy between 5–10 kV, a 30 µm final aperture, and a nominal beam current of ~150 pA. Working distances ranged between 5.1–48.5 mm and images were acquired between 21–40,000x magnification.

5.2.2 Serial Block Face Scanning Electron Microscopy

5.2.2.1 Sample Collection

See Section 5.2.1.1.

Prior to removal of whole embryonic *(E_{16} and E_{18})* and adult eyes from the orbital socket, a reference incision of 1 cm in length was made to the superior sclera (Figure *5.1*) to allow for the correct orientation of eyes during corneal dissection. Prior to being placed in primary Karnovsky fixative, eyes were sorted into vials based on whether they were right eyes or left eyes. Following overnight suspension in primary fixative at 4°C, the anterior portions of the eyes were cleaved away followed by either a gross sagittal or transverse incision to isolate multiple 5 mm long by 2 mm wide sections (Figure *5.1*), retaining portions of the corneo-scleral junction at the limbus *(with the addition of the ossicles in adult corneal sections)*. Dissected sections were then separated in vials based on developmental timepoint *(E_{16}, E_{18}, and adult)* and location *(inferior, superior, nasal, and temporal)*.

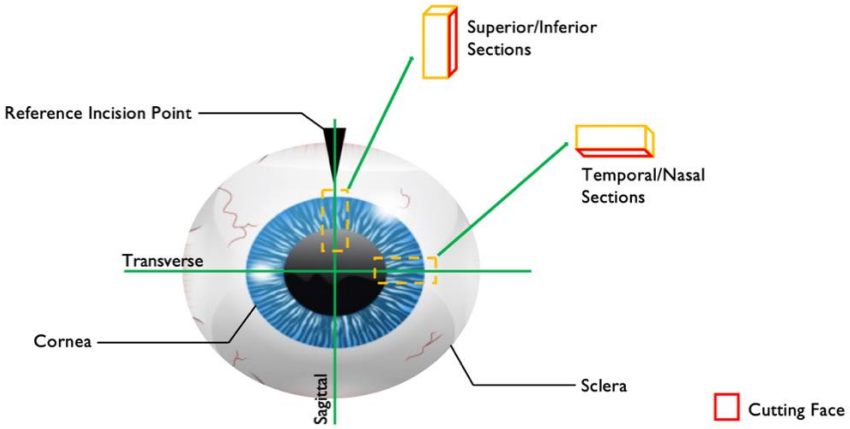

Figure 5.1: Schematic representing the dissection method of embryonic chicken corneas for SBF-SEM analysis. A reference incision point was made with a scalpel blade while the eye was *in situ* to aid in the correct orientation of the eye post removal. Corneal sections 2 mm wide were excised along the sagittal and transverse plane to produce superior/inferior or nasal/temporally oriented sections containing the corneolimbal junction.

5.2.2.2 Sample Preparation

Post-Fixative, Heavy Metal Staining

Modified from the (Deerinck et al. 2010) treatment protocol for the purposes of 3View SBF-SEM.

Following overnight fixation in Karnovsky fixative, tissue samples were cut down to 1 mm cubes to ensure that adequate penetration of stains and resin occurred. After that, samples were subjected to a sequence of three heavy metal staining treatments in aqueous osmium tetroxide (Agar Scientific, UK, Cat. # AGR1022), uranyl acetate (Agar Scientific, UK, Cat. # AGR1260A), and Walton's lead aspartate (Lead nitrate, Agar Scientific, UK, Cat. # AGR1217 and 0.03 M aspartic acid (Acros Organics, Thermo Fisher Scientific, UK, Cat. # 10341614) with the aim of increasing the concentration metal within the tissue to enhance membranous contrast and the respective surrounding structures (Aguas 1982; Willingham and Rutherford 1983, Smith and Starborg 2019).

The first of two reduced-osmium treatments (1.5% potassium ferricyanide/1% osmium tetroxide for 1 hour) was used to generate strong lipid membrane staining by exploiting osmium's affinity for binding C=C bonds in unsaturated fats (Khan et al. 1961; Smith and Starborg 2019). Further enhancement of the stain was achieved by subsequent treatment with 1% aqueous thiocarbohydrazide for 30 minutes, which acted as a mordant between residually remaining osmium from the previous treatment and the addition of osmium from a further treatment with 1% osmium tetroxide for one hour (Seligman et al. 1966; Smith and Starborg 2019). Successive treatment with uranyl acetate for one hour and lead aspartate for one hour at 60°C was done to compliment previous membrane enhancing steps, as uranyl acetate actively bound proteins and lipid molecules, as well as nucleic acid phosphate groups of DNA and RNA located in the inner matrix of the cellular membrane (Höög et al. 2010; Odriozola et al. 2017).

Dehydration

Tissue samples were then subjected to a stepwise dehydration using ascendant concentrations of ethanol (70%, 90%, 100%, 100% - 15 minutes each). This was performed to gradually replace the water present within the tissue with ethanol, so as to preserve the tissue structures from damage through shrinkage (Murtey and Ramasamy 2016).

Resin Embedding

Following the sequence of electron contrasting stages and dehydration, multiple treatments with epoxy resin were performed to ensure adequate penetration throughout the sample. This was done

by first submerging samples in two consecutive, 15-minute treatments in propylene oxide. Propylene oxide was used as an intermediate between ethanol and resin because otherwise, they would not have been miscible with one another. Soon after, samples were transferred into a 1:1 mixture of propylene oxide and Araldite *(without benzyl dimethyamine)* overnight; Araldite is an epoxy resin made up of three components: a resin monomer CY212, dodecenyl succinic anhydride *(a hardener)*, and benzyl dimethylamine *(an accelerant)*.

The following morning, tissue samples underwent five, one-hour treatments in Araldite *(without the accelerant)*; this permitted an extended infiltration time whilst preventing the premature polymerisation of the resin. Afterwards, tissue samples were sequentially transferred into Araldite containing accelerant for one hour, two hours, one hour, and then overnight *(exposed to air)* before an additional three, two-hour treatments the following day. Finally, samples were oriented and embedded into moulds with the remaining resin before being transferred into a 60°C oven for 48 hours to set. Multiple resin changes were carried out to dilute out any residual propylene oxide, as any remaining amount would lead to poor resin quality, which in turn would hinder the ability to cut even and intact sections.

5.2.2.3 SBF-SEM Imaging, Data Acquisition, and 3D Analysis

Resin blocks were glued to aluminium specimen pins before being polished using ultramicrotomy and sputter-coated with gold (10 nm thick gold layer deposited by diffuse sputtering in an ACE 200 sputter coater, Leica Microsystems, Milton Keynes, UK). Samples were transferred into the SEM chamber of a Zeiss Sigma VP Field Emission Gun scanning electron microscope (Carl Zeiss Ltd., Cambridge, UK). The block face of the specimen was then imaged by the microscope at 3.5 KV at a pixel resolution of 4 nm and a dwell time of 8 µs.

A series of approximately 550-1000 images of the block face were acquired, each alternating with removal of a 100 nm slice from the block surface by the in-chamber ultramicrotome. All SBF-SEM data sets were recorded at 4096 x 4096 (4K) in Gatan format dm4 files then batch converted to ".tiff" format. Converted data was then exported into Amira-Avizo software (version 2020.2, ThermoFisher Scientific, UK) to generate 3D reconstructions of each SBF-SEM data set.

The limbal ultrastructure was reconstructed and 3D rendered with the Amira-Avizo software using a combination of surface generation *(isosurface)* and semi-automated 3D volume generations *(Volren)*. Due to grey scale values of each data set, manual segmentation was used to segment out

specific ultrastructural elements from the 3D data set as the contrast was not great enough for an automated approach to be taken to accurately identify structures of interest from the surrounding matrix. Where applicable, videos of 3D reconstructions were produced using the "Animation" feature in the Amira-Avizo software to show a 360° view of the reconstruction and were saved as ".mpg" movies.

5.2.3 Light and Transmission Electron Microscopy

5.2.3.1 Sample Collection and Preparation

Sample acquisition and preparations are the same as described in Section 5.2.1.1 and Section 5.2.2.2. Resin blocks were transferred to a specimen chuck, trimmed around the sample into trapezoidal shaped pyramid using a single-edge razor blade before being mounted onto the arm of a UC6 ultramicrotome (Leica Microsystems, Milton Keynes, UK).

Sectioning for Light Microscopy

Using glass knives, made on a KMR2 glass knife-maker (Leica Microsystems, Milton Keynes, UK) semithin sections (0.2 μm to 0.3 μm) were cut from the resin embedded samples to identify regions of interest; once identified, sections were collected onto Superfrost Plus microscope slides (Thermo Fisher Scientific, UK, Cat. 12-550-15) and bonded using a hot plate. Subsequently, slides were stained with 1% aqueous Toluidine blue in 1% sodium borate on the hot plate at 90°C for 30 seconds, before being gently rinsed with distilled water and dried again on the hot plate. Coverslips were mounted on slides using paraffin oil and sealed with nail varnish (Rimmel, '60 Seconds Supershine', Superdrug, UK).

Sectioning for TEM

After identification of an area of interest, a diamond knife was used to cut ribbons of ultrathin sections (90 to 100 nm thickness). These were stretched using chloroform vapour and collected onto uncoated G300 copper grids for TEM (Gilder Grids Ltd, Grantham, UK).

5.2.3.2 Image Acquisition (Light and Electron Microscopy)

Light Microscopy

Mounted slides were viewed using a Zeiss Axio Scope A1 microscope (Carl Zeiss Ltd., Cambridge, UK) and imaged with GX Capture-T Software (GT Vision Ltd., UK).

TEM

Sections *(on grids)* were examined in a JEM 1010 transmission electron microscope operating at 80 kV. Images of anatomical structures, along the epithelial basement membrane, resembling a putative limbal stem cell niche *(i.e., limbal crypts)* were acquired with a 11-megapxel 14-bit Orius SC1000 CCD camera.

5.2.4 Epifluorescence Image Analysis

Immunolabelling of PSSC markers in adult chicken tissue sections exhibiting undulating limbal folds were imaged and processed as described in Section 3.2.3.2. Relevant images presented in this chapter are representative of findings from three individual experiments.

5.3 Results

5.3.1 Scanning Electron Microscopy

5.3.1.1 Adult Cornea

In the scanning electron microscopy images obtained from an adult avian cornea, a distinct margin illustrating the limbal transition zone between the peripheral cornea and sclera was evident circumferentially around the cornea (Figure *5.2*a.). The peripheral cornea was observed to be flat and smooth in appearance, whereas, on the scleral side of the limbal zone, non-uniform, concentric ridge, and furrow projections parallel to the marginal line were seen. Increased magnification of the concentric projections (Figure *5.2*b.) showed two apparent belts differing in their underlying framework. The inner belt *(closest to the limbal zone)* was similar in appearance to the human anterior limbal cribriform layer, presenting as a highly porous and irregular network of thin fibres interspersed between and around contorted ridge projections (Figure *5.2*b., *yellow box*). However, the outer belt *(furthest from the limbal zone)* showed a more compact network of fibres (Figure *5.2*b., *red box*), evident more so at the furrows of the concentric projections; ridges also appeared to be more continuous and aligned with the bend of the margin.

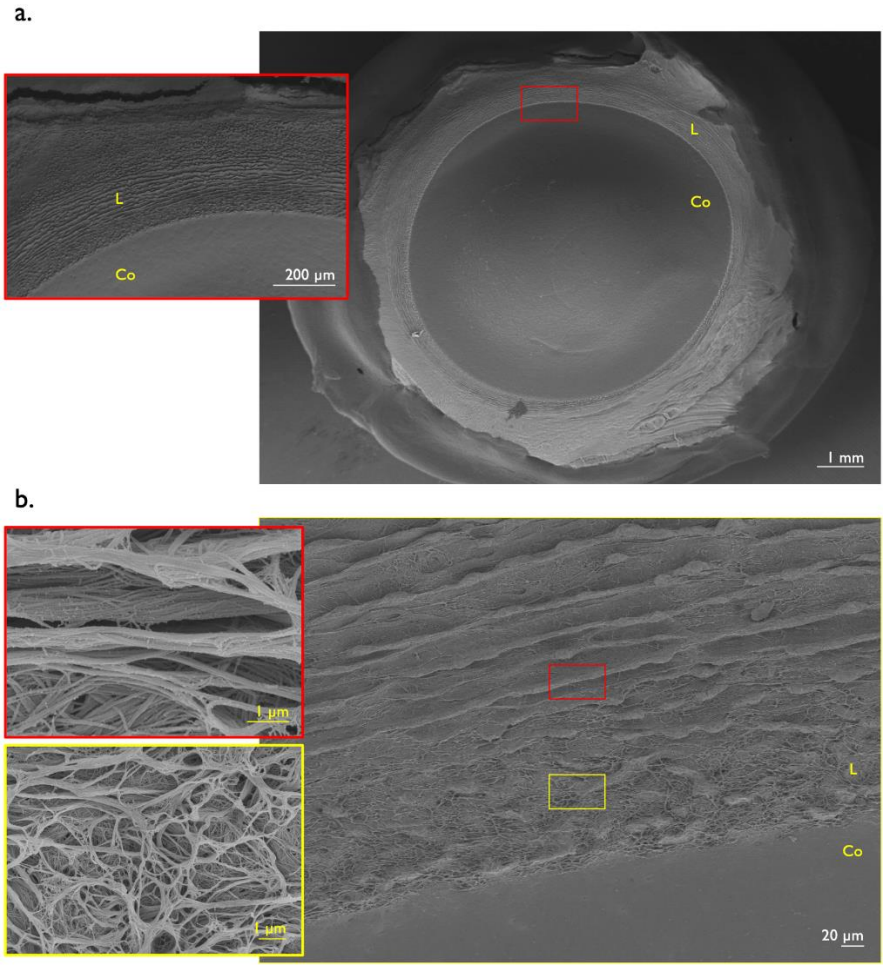

Figure 5.2: Scanning electron microscopy images of the limbal zone of the adult chicken cornea. (a.) *En face* view of the adult cornea showing the distinct demarcation *(red box)* between the limbal zone which can be seen extending circumferentially around the cornea. (b.) Further magnification of the *en face* view of the corneoscleral margin shows a porous texture *(yellow box)* with distinct but non-uniform, concentric ridge and furrow projections *(red box)* running parallel to the limbal boundary. L = limbus, Co = cornea.

5.3.1.2 Developing E_{18} and E_{16} Cornea

High resolution imaging of the developing E_{18} and E_{16} avian corneas was also performed. At the E_{18} limbal zone, long striae were seen to extend radial from the limbus towards the peripheral cornea (Figure *5.3*a.ii, *white arrowheads*). In addition to evidence of micropores (Figure *5.3*a.ii, *yellow arrowheads*) dispersed irregularly on the limbal side of the transition zone only and absent on the corneal side. Micropores were also seen to be juxtaposed along the E_{16} limbal zone (Figure *5.3*b.ii, *yellow arrowheads*), however, no radially extending projections were observed along the E_{18} limbal zone. Evidence of a developing ossicle ring around the corneal structure was visible at E_{16} (Figure *5.3*b.i, *white arrowheads*) and persisted until maturation; however, this was fully formed and therefore, indiscernible in the *en face* view of the E_{18} eye (Figure *5.3*a.i).

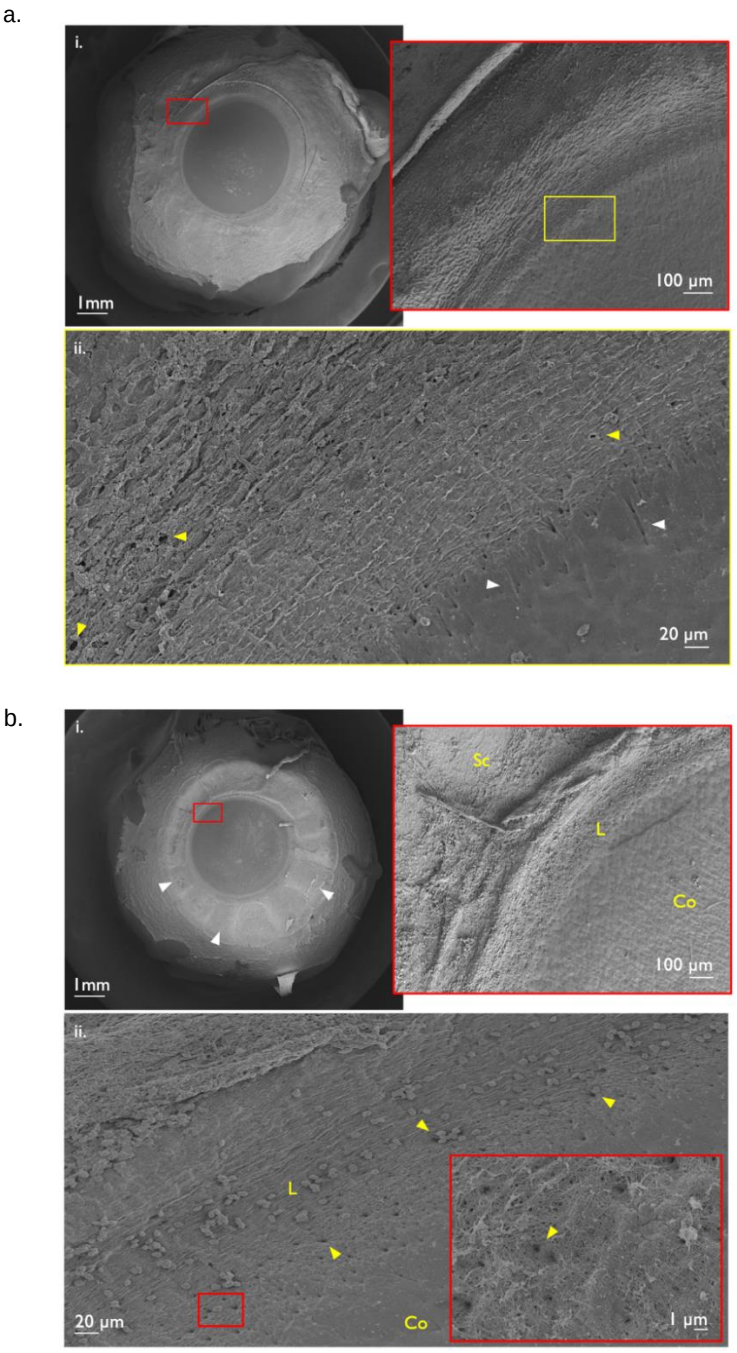

Figure 5.3: Scanning electron microscopy images of the limbal zone in the developing E_{18} and E_{16} cornea. An en face view of the E_{18} cornea (a.i) with the superior limbal zone magnified *(red box)*. The superior limbal zone *(*a.i., *yellow box*) is further magnified in (a.ii) showing micropores *(yellow arrowheads)* and radially extending projections *(white arrowheads)* from the limbus towards the peripheral cornea. An *en face* view of the E_{16} cornea (b.i) with the superior limbal zone magnified *(red box)*. The magnified limbal zone (b.ii) shows an array of micropores *(arrowheads)*. L = limbus, Co = cornea, Sc = sclera.

5.3.2 Serial Block Face Scanning Electron Microscopy

5.3.2.1 Adult Limbus

A number of adult corneal cross-sections, originally processed for immunohistochemical analysis, were observed to have a limbal transition zone consisting of distinct undulating folds with upward *(stromal)* and downward *(epithelial)* projections (Figure *5.4*a.). Contained within the upward stromal projections were vessel-like structures, however, they were difficult to discern based on the imaging modality used. Subsequent SBF-SEM of the limbal region was performed to generate large data sets of serial images of the adult cornea. In a 3D reconstruction using Amira software, the undulations can more clearly be seen traversing the corneolimbal junction (Figure *5.4*b.). From the same data set, vessel-like structures were also apparent throughout the serial images, presenting as circular cross sections of lumina (Supplementary video 1).

The orientation plane of the adult cornea *(superior and inferior vs. nasal and temporal)* was not known prior to processing specimens for SBF-SEM. However, the cornea was subdivided into four quadrants *(one-four)* from which 5 mm long by 2 mm wide sections (Figure *5.1*) were taken and labelled accordingly before treatment. This was done to allow for assessment of different limbal areas in a single cornea. As seen in Supplementary video 2 and 3, limbal folds were evident in opposing quadrants one and four, respectively.

On closer examination of SBF-SEM generated micrographs of the adult limbus, evidence of a blood vessel was observed in the upward projections of the stroma (Figure *5.5*). A magnified view showed the vessel surrounded by capillary endothelial cells in addition to a vessel lumen containing a nucleated red blood corpuscle. Using the quadrant four data set, the vasculature within the stromal projections was reconstructed (Figure *5.6*). The complex network was interconnected (Supplementary video 4) and have several branches extending perpendicular to the sectional plane. Using the Amira software, red blood corpuscles were reconstructed (Figure *5.7*) from the same data file to show them occupying the lumen of individual vessels within the 3D vascular network.

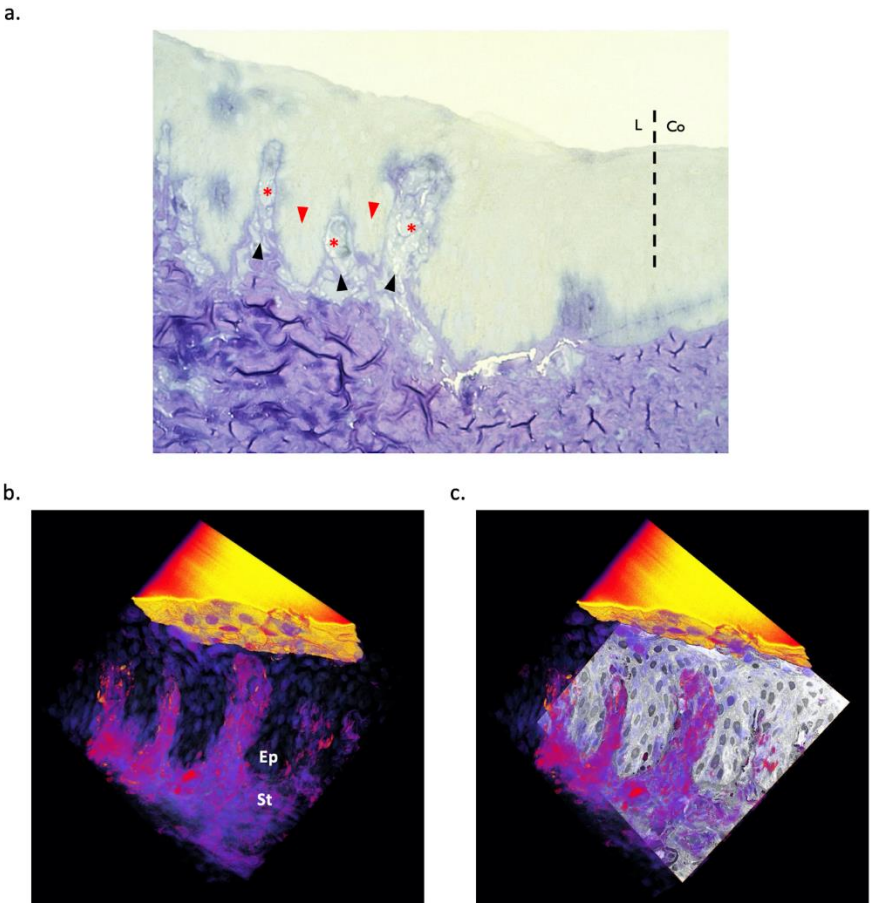

Figure 5.4: Anatomical features of the adult corneal limbal zone. (a.) Toluidine blue stained tissue cross- section of the adult corneal limbus shows upward stromal projections *(black arrowheads)* containing blood vessels *(asterisks)* and downward epithelial projections into the stroma *(red arrowheads)*. (b.) 3D undulating folds of epithelium (Ep) and superficial stroma (St) reconstructed from 941 serial images obtained using serial block face electron microscopy and rendered using the automated segmentation function within the Amira software. (c.) Montage of the 3D reconstruction with a back-scatter electron generated cross sectional image to orient along the sagittal plane. L= limbus, Co = cornea.

Supplementary video 1: A 2D flythrough of the adult avian limbus generated from images obtained using serial block-face scanning electron microscopy. Cross-sections of the cornea show downward projections of the epithelium *(dark grey)* into the stroma and conversely, upward stromal projections *(light grey)* into the epithelium to form distinct undulating folds. Vessel-like structures are also seen in most of the upward stromal projections. https://figshare.com/s/d9cf1b22e0ba9c27ad96.

Supplementary video 2: 3D reconstruction of limbal quadrant one in the adult avian cornea from serial block-face scanning electron microscopy images. Cross-sectioning of the adult cornea shows distinct undulating limbal folds of epithelium and stroma. Blood vessel can be seen *(00:08 seconds)* with a dark grey lumen. https://figshare.com/s/39878b5c7cd1995ad6bd.

Supplementary video 3: 3D reconstruction of limbal quadrant four in the adult avian cornea from serial block-face scanning electron microscopy images. Cross-sectioning of the adult cornea shows distinct undulating limbal folds of epithelium *(light grey)* and stroma *(dark grey)*. Blood vessels *(00:01 seconds)* can be seen within the upward stromal projections (circular white lumen). Reverse contrast was applied to the reconstruction for better visualisation**.** https://figshare.com/s/42f869949f6e06754b80.

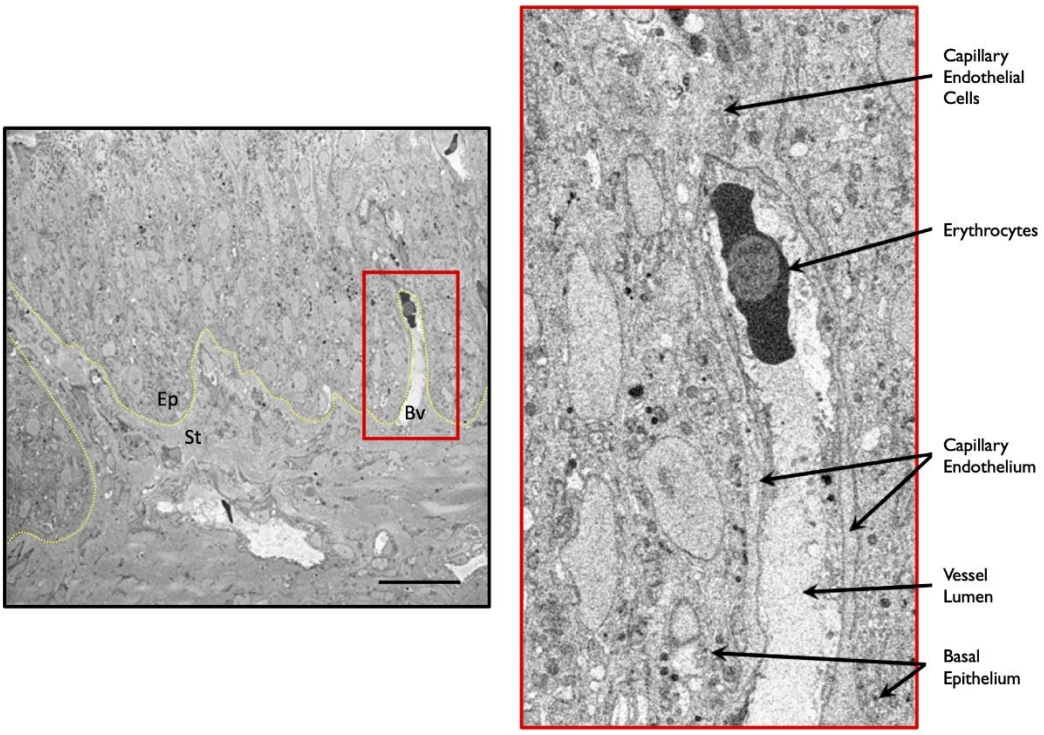

Figure 5.5: Micrographs of a blood vessel in the adult avian limbus acquired using serial block-face scanning electron microscopy. A cross-section of the limbus showed evidence of a blood vessel *(Bv, red box)* in the upward stromal projection. A magnified view of the blood vessel was seen to be surrounded by capillary endothelial cells and was also observed to possess a vessel lumen containing a nucleated red blood corpuscle cell. The basement membrane *(yellow line)* was outlined the distinguish between the epithelium *(Ep)* and stroma *(St)*. Scale bar = 20 μm.

On closer examination of the adult limbus (Figure *5.8*), particularly within the downward projections of epithelium, evidence of cells morphologically different to neighbouring basal cells were identified. These cells appeared comparably smaller and rounder with a higher nucleus to cytoplasm ratio in addition to a barely detectable nucleolus and a lightly packed euchromatin.

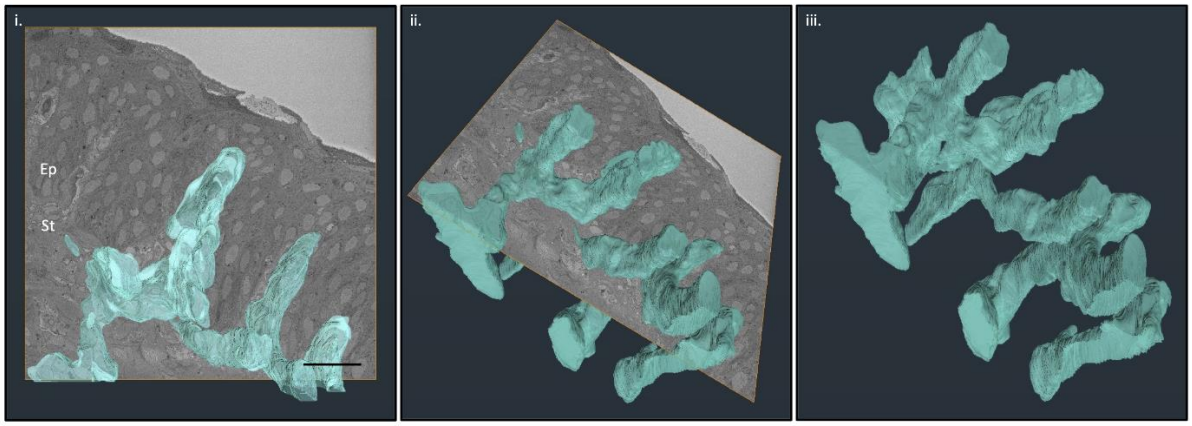

Figure 5.6: A 3D reconstruction of a complex network of blood vessels located within the upward stromal projections of the adult corneal limbus. (i.) A 3D network of blood vessels *(blue volume),* generated from 614 serial images using serial block face scanning electron microscopy, superimposed on a back-scatter electron generated micrograph to orient along the sectional plane and at a rotated view (ii.). (iii.) An isolated view of the network of blood vessel. Ep = epithelium, St = stroma. Scale bar = 20 μm.

Supplementary video 4: A 3D reconstruction, made using Amira software, of stromal blood vessels and red blood corpuscles in the adult avian cornea. The initial flythrough of the adult limbal zone was generated from 941 serial images obtained using serial block face scanning electron microscopy. The blue volume *(appearing at 00:11 seconds)* represents an intricate network of blood vessels within the upward projections of the stroma and the red volume *(appearing at 00:31 seconds)* represents red blood corpuscles within the lumen. https://figshare.com/s/337848602f28435bb529.

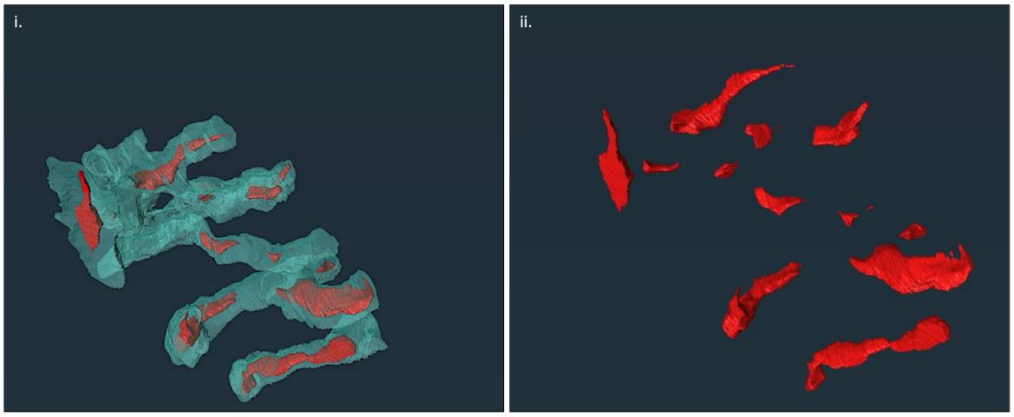

Figure 5.7: **A 3D reconstruction of blood vessels and internal red blood corpuscles within the adult avian limbal zone.** (i.) Rotated view of blood vessel network *(blue volume)* with red blood corpuscles *(red volume)* within the lumen of the vessels. (ii.) Isolated view of red blood corpuscles *(red volume)* from the blood vessels. Both volume renderings were reconstructed using Amira software from 614 serial images obtained from serial block face scanning electron microscopy.

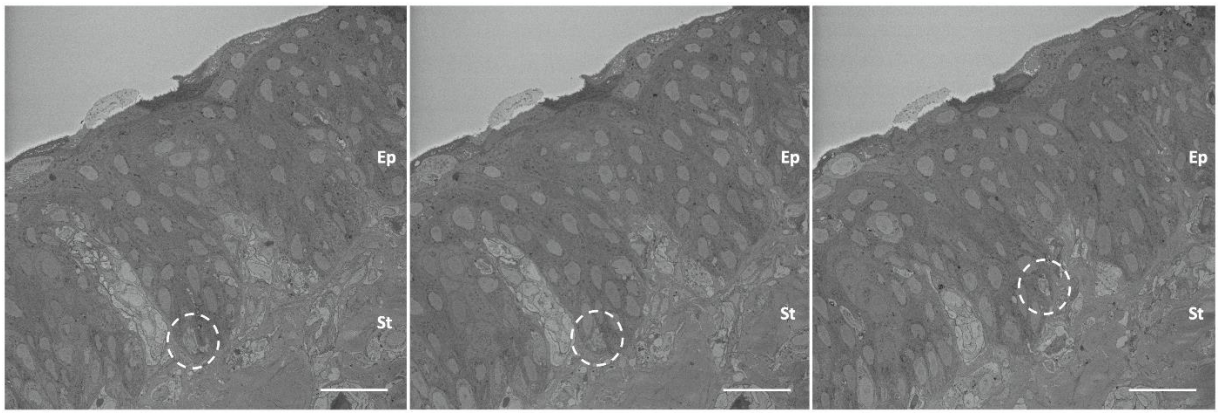

Figure 5.8: Cells with high nucleus to cytoplasm ratio within the presumptive limbal crypts of the adult avian cornea. Micrographs of the block face taken from three different locations within the same SBF-SEM generated dataset show limbal epithelial cells *(dashed circles)* morphologically smaller than neighbouring basal cells with a high nucleus to cytoplasm ratio, a barely detectable nucleolus, and euchromatin as open DNA. Ep = epithelium, St = stroma. Scale bars represent 20 μm.

5.3.2.2 E_{18} Limbus

Using SBF-SEM, a dataset of 941 images was acquired from the superior quadrant of the developing E_{18} limbal zone. As seen in Figure *5.9*i-iv and Supplementary video 5, a distinct nerve bundle can be seen to penetrate distally through the Bowman's layer and enter the epithelium from the anterior stroma before continuing parallel to the corneal surface with a gradual shift distally towards the superficial epithelium before joining with a second nerve bundle, already in the corneal epithelium, and subsequently moving out of the visible plane.

A 3D reconstruction of the limbal area (Figure *5.10*b., Supplementary video 6), also found that anterior stromal cells *(red and purple volumes)* formed focal contact points (*white arrowheads*) with the epithelial basement membrane. Moreover, the reconstruction also demonstrated the irregularity of the basement membrane profile in comparison to the adult basement membrane profile. Specifically, that the profile of the adult limbal area presented with large but less frequent undulating folds, whereas the E_{18} basement membrane profile exhibited notably smaller and more frequent undulations.

In addition to the nerve bundles observed in the SBF-SEM micrographs of the superior quadrant, thin matrix "cord" projections were seen to emerge from protrusions in the epithelial basal lamina (Figure **5.11**a., Supplementary video 3). A 3D reconstruction of a single matrix "cord" (Figure **5.11**b., Supplementary video 7, *blue volume*) can be seen to extend proximally from the basal lamina of the epithelial into the stroma where it was also seen to interface with two stromal cells *(red and green volumes).*

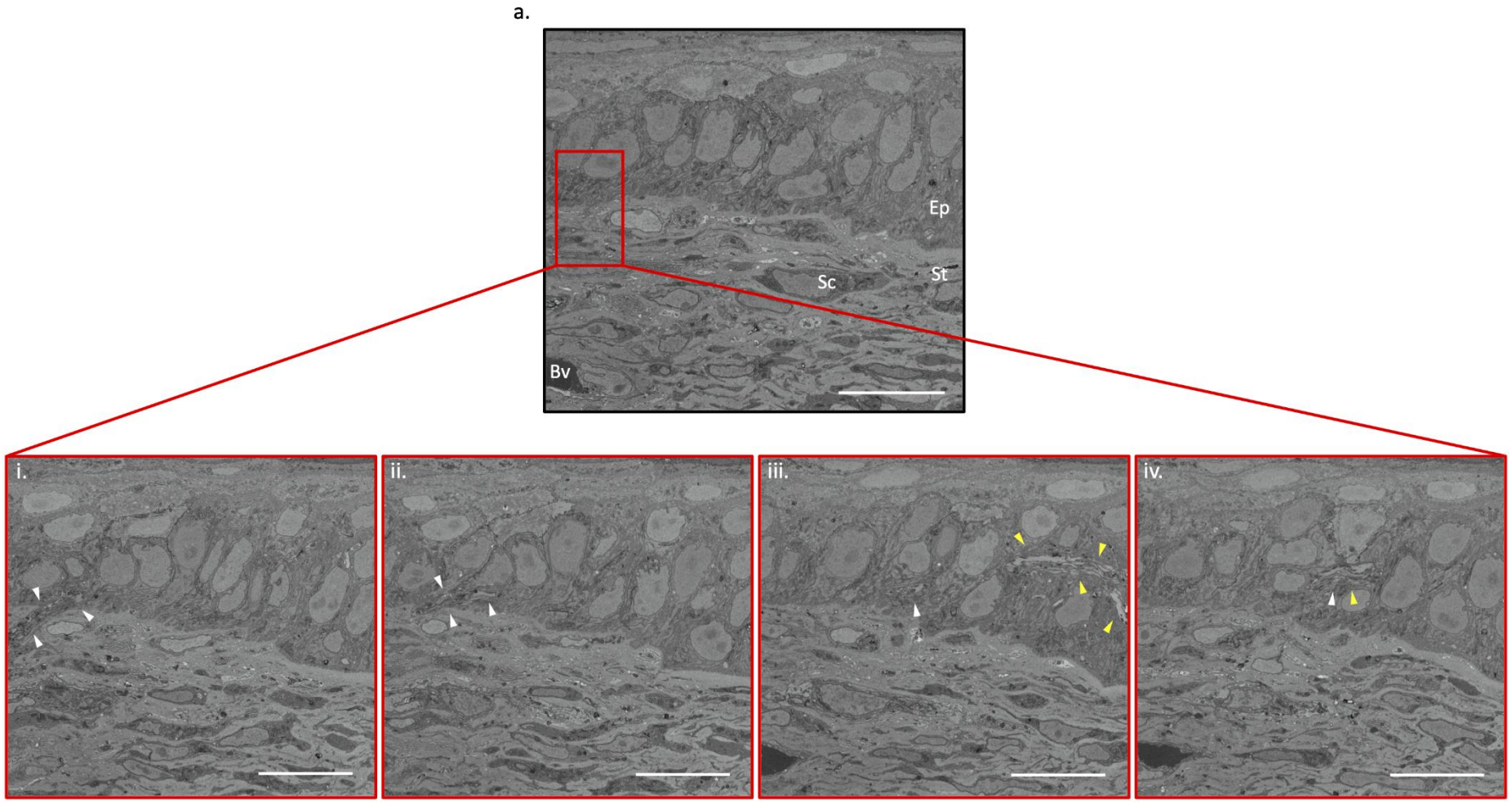

Figure 5.9: Nerve fibres within the developing E_{18} corneal limbus. Micrographs obtained along the sagittal plane using serial block face scanning electron microscopy demonstrate the region of interest (a. *red box*) where nerve one (i, *white arrowheads*) enters the basal epithelium from the stroma. Nerve one is seen to move parallel to the basement membrane (ii.) and continues distally to the surface while nerve two *(yellow arrowheads)* enter the frame from the left (iii.). Nerve one and two come into close proximity of one another and change plane (iv.). Bv = blood vessel, Ep = epithelium, Sc = stromal cell, St = stroma. Scale bars = 10 μm.

Supplementary video 5: Nerve fibre entering the corneal epithelium in a 2D flythrough of the limbal zone using serial block-face scanning electron microscopy in a developing E_{18} cornea. A nerve fibre located in the stroma is seen to penetrate the basement membrane of the epithelium *(left-hand side of frame, 00:11 seconds)* move upwards towards the surface. A secondary nerve, already in the epithelium, comes into frame *(right-hand side of frame, 00:21 seconds)* and moves parallel to the basement membrane before changing direction and moving out of viewing plane. At 01:11 minutes, a central protrusion of the epithelial basal lamina can be seen to extend a matrix "cord" into the stroma.

https://figshare.com/s/91c2a7b4c2f59cb4347f.

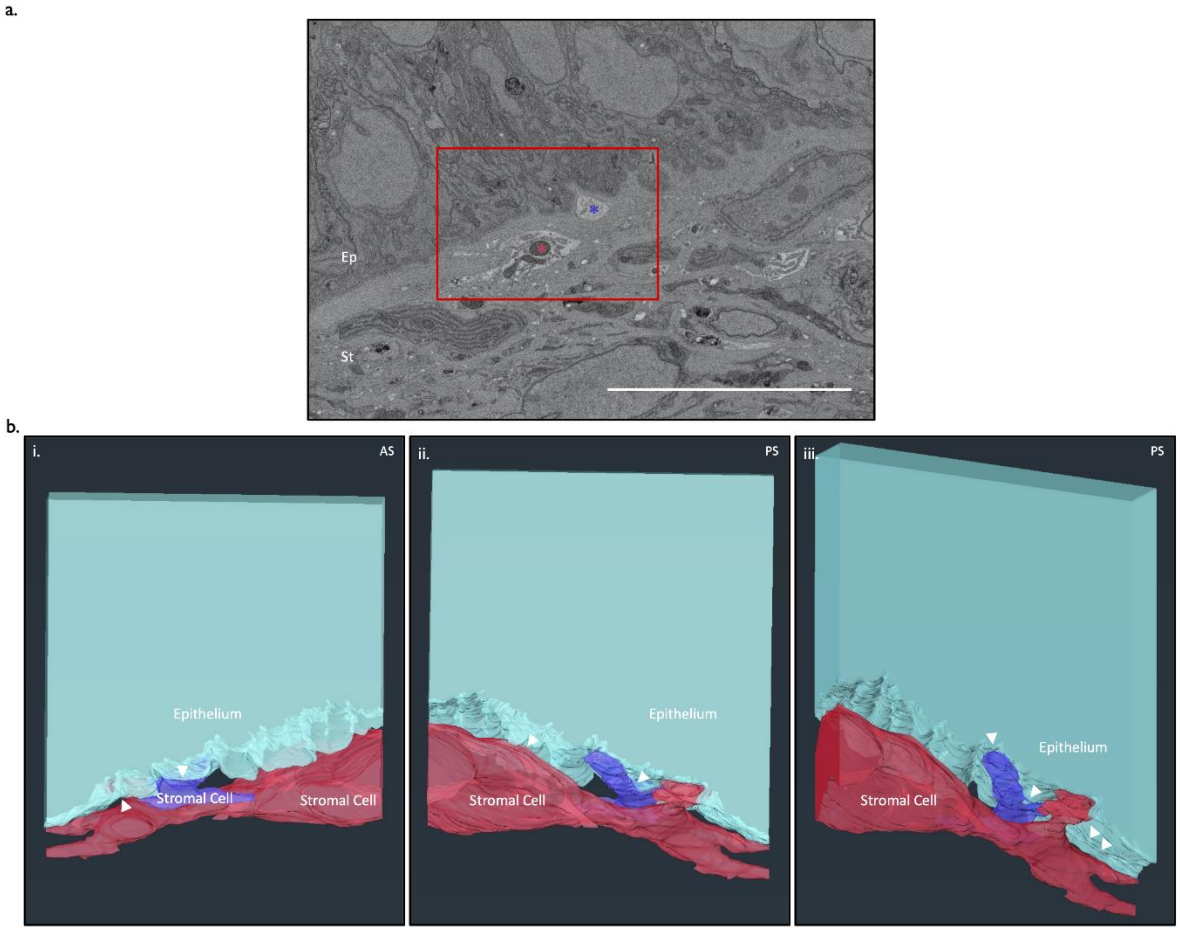

Figure 5.10: Direct contact between E_{18} limbal stromal cells and the basal epithelium. (a.) The limbal area *(red box)* and stromal cells *(coloured asterisks)* correspond to the 3D reconstruction in (b.) generated from 61 serial images obtained from serial block face scanning electron microscopy. The red and purple volumes represent individual stromal cells interfacing with the basal epithelium *(white arrowheads)*. (b.i.) = anterior surface (AS), (b.ii.) = posterior surface (PS), (b.iii.) = rotated view of PS. Ep = epithelium, St = stroma. Scale bar = 10 μm.

Supplementary video 6: A serial block face scanning electron microscopy 3D reconstruction of the stromal-epithelial interface in the developing E_{18} avian limbus. The red and purple volumes represent individual stromal cells interfacing with the epithelium *(blue volume)*.
https://figshare.com/s/aab93a01088d898b251d.

Supplementary video 7: A serial block face scanning electron microscopy 3D reconstruction of a matrix "cord" projection in the developing E_{18} Cornea. The blue volume represents the epithelium with a matrix "cord" extending from the basal lamina of surface epithelium into the stroma and in the vicinity of stromal cells, represented as red, green, and purple volumes.
https://figshare.com/s/93e80a702d32fc3af410.

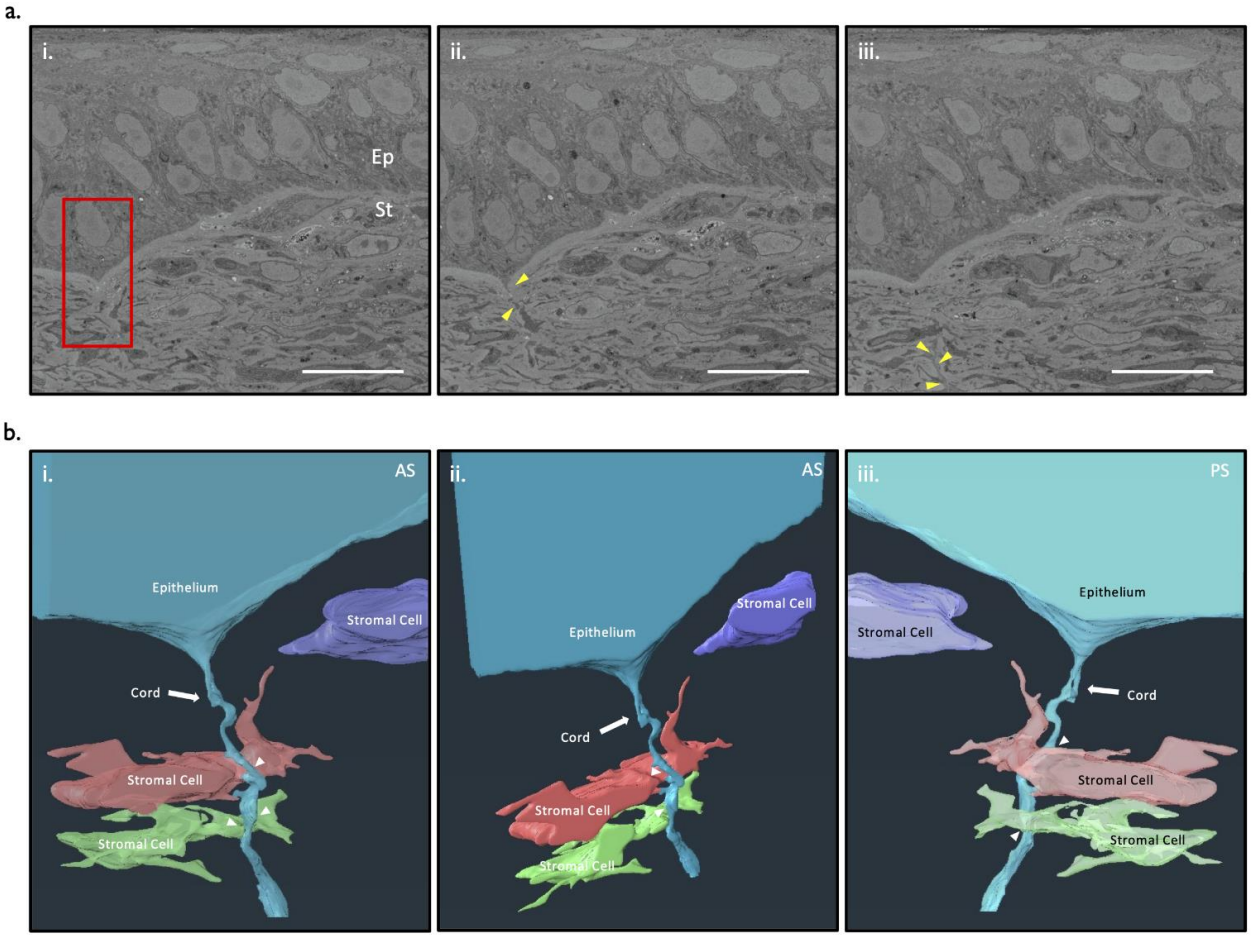

Figure 5.11: Matrix "cord" projection in the developing E_{18} chicken cornea. (a.) a sequence of three serial images at 600 nm intervals obtained using serial block face scanning electron microscopy. A single matrix cord, emerging from a protrusion (a.i., *red box*) in the epithelial basal lamina and is seen to extend proximally into the matrix (a.ii and a.iii., *yellow arrowheads*). (b.) A 3D reconstruction generated from 39 serial images depicts the epithelium *(blue volume)* extending a matrix "cord" proximally from the basal lamina into the stroma. The 100 nm resolution in z-plane, determined by the slice thickness can, as here, lose some information in structures of smaller dimensions than 100 nm; thus, complete continuity along the whole length of the cord is sometimes lost, hence at the position shown by the white arrow, missing information has been added, to show to the continuity of the matrix cord projection into the stroma. The green, red, and purple volumes represent individual stromal cells. The matrix cord is seen to interface with stromal cells *(white arrowheads)*. (b.i.) = anterior surface (AS) of reconstruction, (b.ii.) = rotated view of AS, (b.iii.) = posterior surface (PS) of reconstruction. Ep= epithelium, St = stroma. Scale bar represents Scale bar = 10 μm.

5.3.2.3 E_{16} Limbus

SBF-SEM was also performed on E_{16} specimens where a dataset of 580 micrographs were acquired from the limbal zone of the superior quadrant. A 3D reconstruction (Figure *5.12*b., Supplementary video 8) of a single stromal cell *(green volume)* was seen to form a point of contact with the epithelial basement membrane *(yellow arrowheads)*. The epithelial basement membrane profile was also similar to that of the profile observed in the E_{18} cornea. Moreover, in the superior quadrant, similar matrix "cords" were seen to emerge from protrusions in the epithelial basal lamina (Figure *5.13*a., Supplementary video 9). A 3D reconstruction (Figure *5.13*b., Supplementary video 10) showed a singular matrix "cord" *(blue volume)* interfacing with two anterior stromal cells *(orange and red volumes)*.

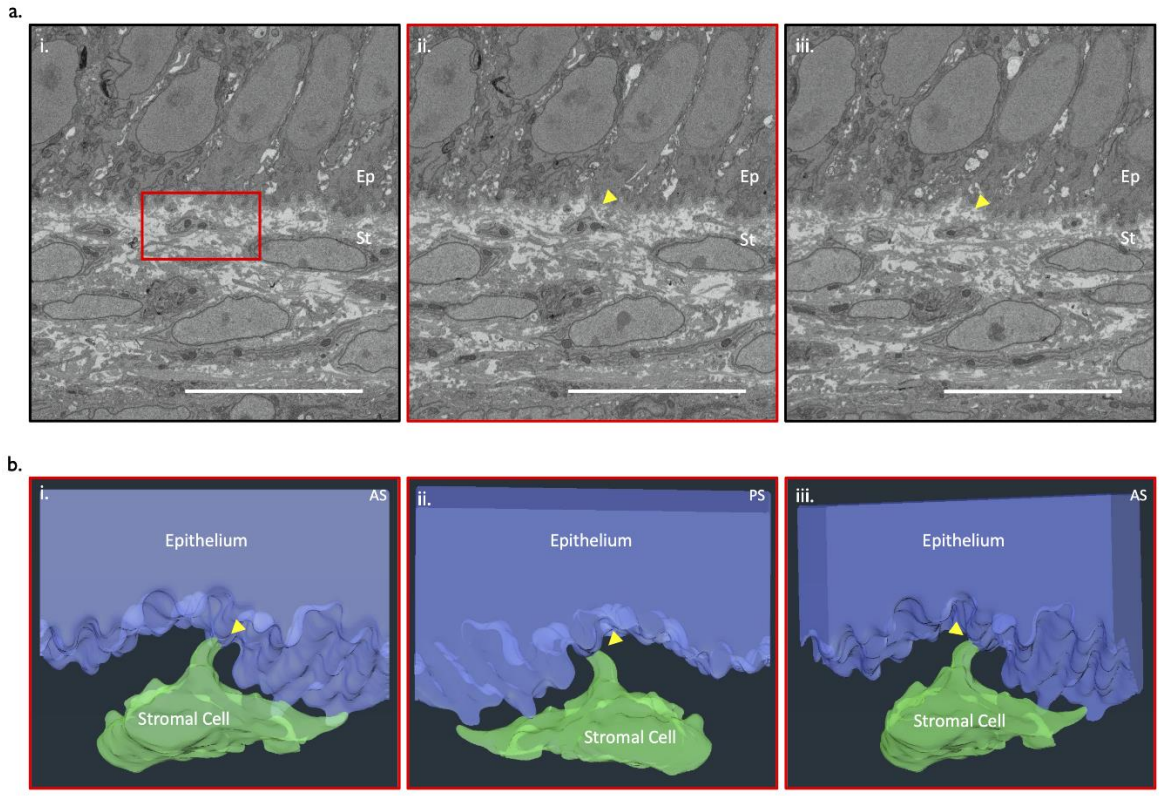

Figure 5.12: Direct contact between an E_{16} limbal stromal cell and a basal epithelial cell. (a.) A sequence of three serial images at 300 nm intervals obtained using serial block face scanning electron microscopy showing a stromal cell (a.i. *red box*) in close proximity to the basal limbal epithelium (a.ii and a.iii, *yellow arrowheads*). (b.) 3D reconstruction, made using Amira software, from 23 serial images. A stromal cell *(green volume)* is seen to extend a process that makes direct contact *(yellow arrowheads)* with the epithelium *(blue volume)*. (b.i.) = anterior surface (AS) of reconstruction, (b.ii.) = posterior surface (PS) of reconstruction. (b.iii.) = rotated view of AS. Ep = epithelium, St = stroma. Scale bar = 10 μm.

Supplementary video 8: A serial block face scanning electron microscopy 3D reconstruction of the stromal-epithelial interface in the developing E_{16} avian limbus. An individual stromal cell *(green volume)* interfacing with the epithelium *(blue volume)*.

https://figshare.com/s/f62be6f1900e05ac30b3.

Supplementary video 9: A 2D flythrough of the limbal zone using serial block-face scanning electron microscopy in the developing E_{16} cornea. Matrix "cord" can be seen extending from the basal epithelium down into the stroma *(01:05 and 01:10 minutes)* where it interfaces with multiple stromal cells. https://figshare.com/s/3e0fb489c26e169720e3.

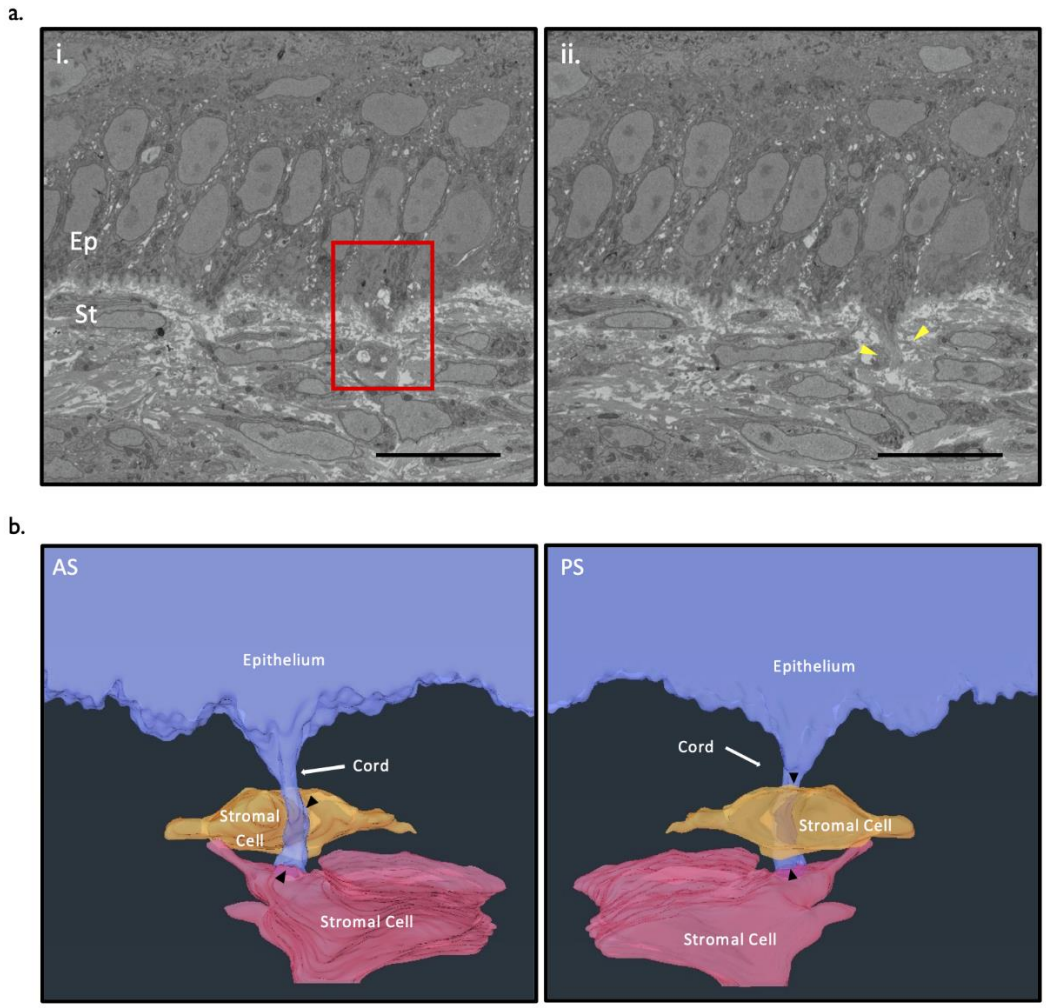

Figure 5.13: Matrix "cord" projection in the developing E_{16} chicken cornea. (a.) a sequence of two serial images at 500 nm intervals obtained using serial block face scanning electron microscopy. A single matrix cord, emerging from a protrusion (a.i., *red box*) in the epithelial basal lamina and is seen to extend proximally into the matrix *(*a.ii, *yellow arrowheads*). (b.) 3D reconstruction, made using Amira software, from 71 serial images. The purple volume represents the epithelium with the matrix cord extending proximally into the stroma. The matrix cord is seen to interface *(black arrowheads)* with stromal cells *(orange and red volumes)*. (b.i.) = anterior surface *(AS)* of reconstruction, (b.ii.) = posterior surface *(PS)* of reconstruction. Ep= epithelium, St = stroma. Scale bar = 10 μm.

Supplementary video 10: A serial block face scanning electron microscopy 3D reconstruction of a matrix "cord" projection in the developing E_{16} Cornea. The blue volume represents the epithelium with a matrix "cord" extending from the basal lamina of surface epithelium into the stroma and in the vicinity of stromal cells *(orange and pink volumes)*. https://figshare.com/s/38cd4f4a764593c6c139.

5.3.3 Transmission Electron Microscopy

5.3.3.1 Adult Limbus

Using TEM, micrographs of the adult corneolimbal region showed a distinct and regular profile to the basement membrane between the epithelium and underlying stroma along the peripheral cornea (Figure *5.14*a.). However, once in the limbal zone an abrupt change in direction and regularity of the basement membrane could be observed (Figure *5.14*b., *arrowhead*). Looking closely at the cell-to-cell interactions within the upward projections of the stroma, a small cell (Figure *5.14*c., *asterisk*) with a high nucleus to cytoplasm ratio was observed between basal epithelial cells. Basal cells were also seen to form bulbous lobed protrusions into the underlying stroma (Figure *5.14*c., *arrowheads*), with the basal lamina remaining intact and true along the irregular contour of the limbal zone. Superficial upward stomal projections bordering basal cells (Figure *5.14*d., *arrowheads*) were found to be highly cellularised.

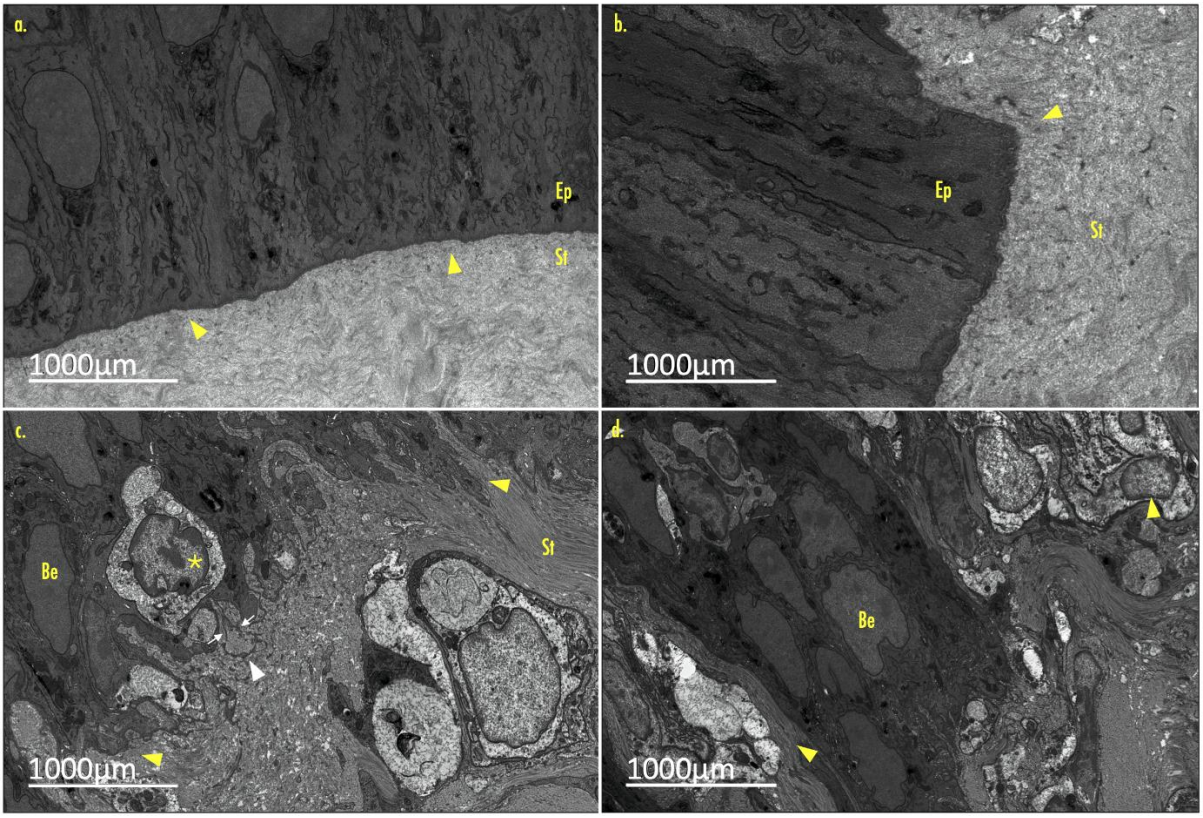

Figure 5.14: Transmission electron microscopy of the epithelium basement membrane zone in the adult avian corneal limbus. (a.) Peripheral cornea with distinct and smooth margins *(arrowheads)* separating the epithelium (Ep) from the stroma (St), (b.) abrupt change in basement membrane orientation at limbal junction *(arrowhead)*, (c.) limbal basal epithelial cells surround a smaller and rounder basal cell *(*Be*, asterisk)* exhibiting a high nuclear to cytoplasm ratio. Lobed basal processes *(yellow arrowheads)* with associated basal lamina are also seen to project downwards into the underlying superficial stroma. Cytoplasmic extensions *(white arrows)* can be seen extending from a mesenchymal cell *(white arrowhead)* to contact the basal lamina and insert between basal cell processes. (d.) Highly cellular areas adjacent to a basal cell where an upward projection of the superficial stroma is evident *(arrowheads)*.

5.3.3.2 E_{16} Limbus

Comparatively, in the inferior limbus of the E_{16} cornea, similar to the adult limbus, a regular profile of the basement membrane was observed along the peripheral cornea (Figure *5.15*a.). However, at the limbal junction a less pronounced but noticeable change in the direction and regularity was seen (Figure *5.15*b., *arrowheads*). Closer examination along the limbal zone (Figure *5.15*c., *arrowheads*) shows an intact basement membrane adopting multiple and frequent undulations. No cells with a high nucleus to cytoplasmic ratio were observed to be interspersed between basal cells in the epithelial layer.

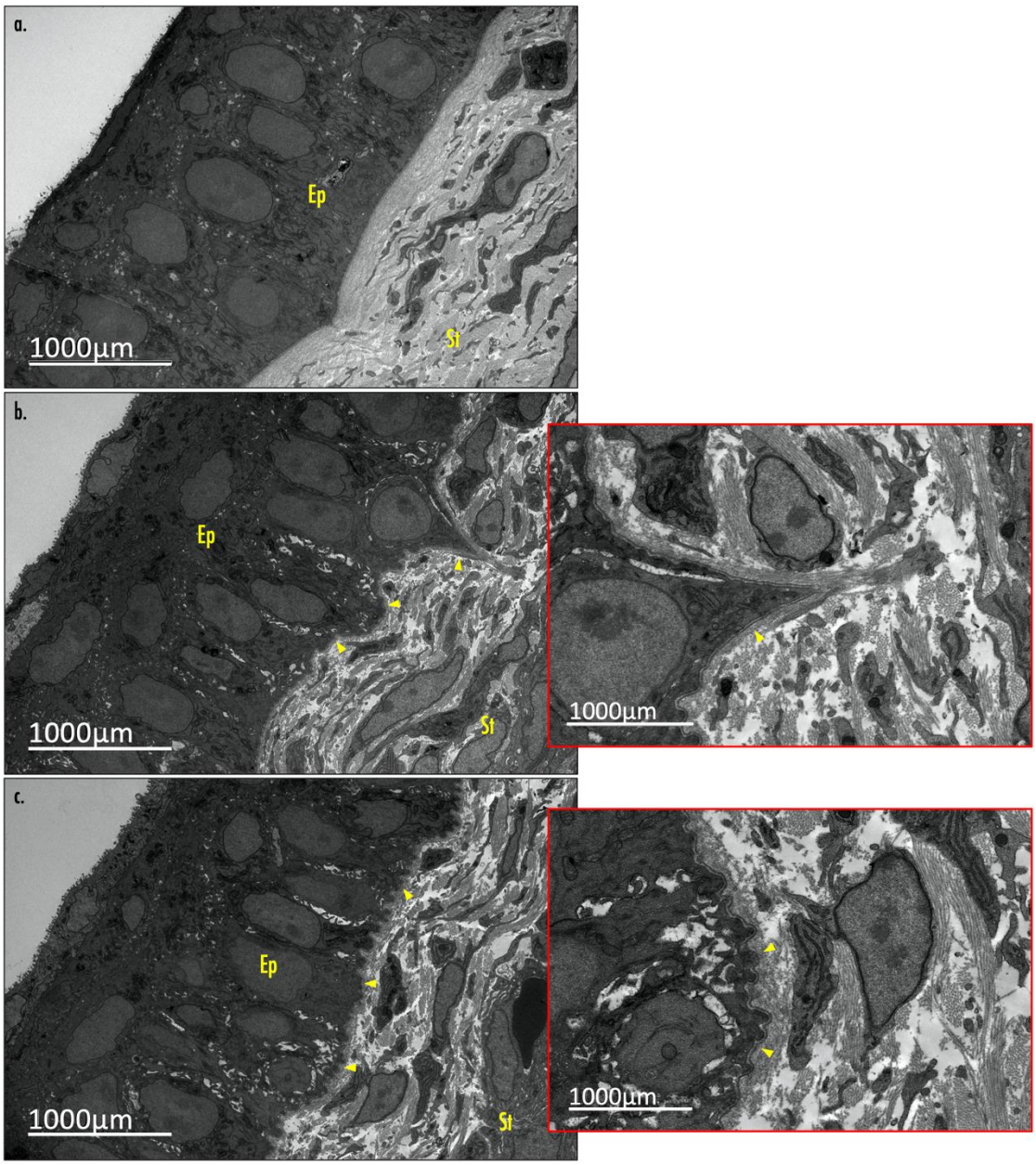

Figure 5.15: Transmission electron microscopy of the epithelial basement membrane zone in the inferior quadrant of E_{16} avian corneal limbus. (a.) peripheral cornea with distinct and smooth margins separating the corneal epithelium (Ep) from the stroma (St), (b.) initial presentation of irregularity in basement membrane orientation at corneoscleral junction *(arrowheads)*, (c.) initial presentation of developing undulating folds *(arrowheads)* showing a consistent lamina densa spanning the entire basement membrane *(arrowheads)*.

5.3.3.3 Putative Stromal Stem Cell Marker Immunolabelling in Adult Limbal Folds

As discussed earlier, a select number of adult limbal cross-sections were observed to have an irregular limbal profile. Specifically, these sections exhibited undulating folds with upward projections of stroma and downward projections of epithelium along the limbal zone. Subsequent immunolabelling of the adult limbal zone were performed to supplement the findings obtained

from high resolution microscopy. Specifically, PSSC markers CX43, PAX6, Bmi-1, and CXCR4 were evaluated in avian tissue sections exhibiting undulating limbal folds (Figure *5.16*) to assess for any differences in immunolabelling compared to previously observed *in situ* findings reported in Chapter 3. Similar immunolabelling of CX43 was observed towards the peripheral cornea and within the suprabasal epithelium and anterior stroma. However, in tissue sections presenting undulating folds, CX43 negative cells were also observed in the downward projections of the epithelial basement membrane *(arrowheads)*. Immunolabelling of PAX6, Bmi-1, and CXCR4 in limbal sections containing undulating folds was similar to sections exhibiting a uniform limbal profile, however, for CXCR4, additional labelling in the anterior stroma, directly subjacent to the more peripheral limit of the limbal junction was observed. Negative controls for CX43, PAX6, Bmi-1, and CXCR4 confirmed a lack of non-specific binding of secondary antibody.

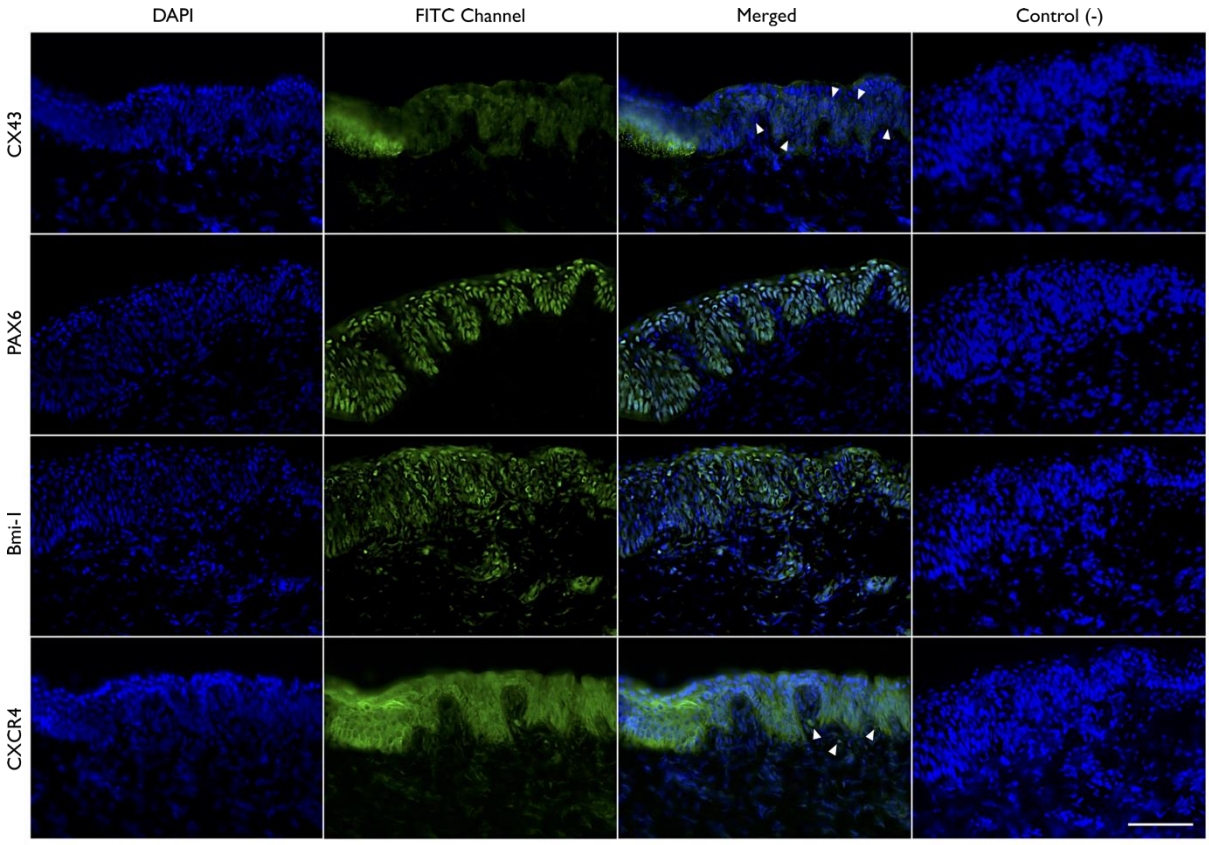

Figure 5.16: Immunolabelling of putative stromal stem cell markers in the adult corneal limbus as the site of distinct undulations. Panels show positive labelling *(green)* at the site of limbal undulations for CX43, PAX6, Bmi-1, and CXCR4. CX43-negative cells *(arrowheads)* and CXCR4-positive stromal cells *(arrowheads)*. Nuclei counterstained with DAPI *(blue)*. The scale bar represents 100 μm. *Adult limbal image for CXCR4 also used in Figure 3.6*.

5.4 Discussion

In recent years, a substantial amount of investigative research has been directed towards combating sight threatening sequelae associated with ocular surface diseases resulting from limbal stem cell deficiency. The affiliation of the limbus as a supportive microenvironment to both epithelial and mesenchymal stem cell populations is widely acknowledged, however the full extent of its functional role has yet to be ascertained in addition to the processes leading to the renewal of epithelial and keratocyte cells contained within the anterior most layers of the cornea (Boulton and Albon 2004; Schlotzer-Schrehardt and Kruse 2005; Mort et al. 2012; Pinnamaneni and Funderburgh 2012; Yamada et al. 2015). Nevertheless, accumulated data has provided a framework of reliable, though not definitive, markers and morphological features for the identification of stem/progenitor cells and their niche, respectively (Yamada et al. 2015).

In this study, imaging of the developing and adult avian limbal zones were carried out using different forms of electron microscopy that resulted in new details of the corneal limbus being discovered. Anatomical features, cell-cell interactions, and supportive structures, similar to those previously identified within the human limbal stem cell niche, were observed which suggest a presumptive limbal stem cell niche may be present in the avian cornea.

5.4.1 Ultrastructure of the Presumptive Avian Limbal Stem Cell Niche

SEM was initially applied to assess the *en face* profile of the developing and adult avian cornea for the detection of limbal stem cell niche microstructures *(PoV, LCs, and FSPs)* previously identified in the human limbus by Shortt et al. (2007a). Clinically, human limbal crypts and PoV can be viewed using a slitlamp microscope, however focal stromal projections are concealed by the overlaying stratified epithelium. In this study, imprints of what appeared to be radial striae, similar in presentation to the LCs and PoV reported by Dziasko et al. (2016), were seen to extend towards the peripheral cornea from the limbus of the E_{18} cornea *(en face view)* but were indiscernible in the E_{16} and adult limbus. It was initially thought that the harsh NaOH treatment may have obscured these structures, preventing their visualisation *en face*. However, using gross light microscopy, intact eyes from each developmental stage *(E_{16}, E_{18}, and Adult)* were assessed and no evidence of radially extending structures akin to the LCs and PoV reported by Dziasko and colleagues were seen in any of the specimens. In a study by Goldberg and Bron (1982), they observed that lighter pigmented individuals had a lower concentration of melanin-containing cells and limbal melanocytes lining interpalisade ridges which obscured the visualisation of them by light microscopy, this may have been the case for their apparent absence in the avian cornea. However,

Short and colleagues found that even with the decellularization of the corneal surface, as a result of SEM processing, the aforementioned structures remained visible. These reports taken together with the SEM findings of the present study, would favour an absence of said structures in the limbus, however, a number of adult corneal cross-sections of adult avian tissue exhibited distinct invaginations of epithelium and underlying stroma to form undulating folds at the limbal zone. On account of this, SBF-SEM was performed to visualise a cross-sectional view of the limbus to determine more clearly if comparable microstructures characteristic of the human limbal stem cell niche existed in the avian cornea but presented differently to equivalent structures in the human limbal stem cell niche. As a result, large datasets were obtained and mined to generate 3D reconstructions of the limbal zone with the purpose of providing a detailed and comprehensive impression of whether a presumptive limbal stem cell niche ultrastructure existed.

As alluded to above, cross sections of the adult cornea presented a unique limbal architecture comprised of distinct invaginations of epithelial cells extending into the corneal limbal stroma. Higher resolution SBF-SEM of the adult limbal zone confirmed these findings which were anatomically similar to that of human LCs and PoV described in literature (Dua et al. 2005; Dziasko et al. 2015; Dziasko and Daniels 2016; Bizheva et al. 2017). In the human limbus, FSPs are distinct from limbal crypts and are described as fingerlike projections of limbal stroma containing an upward extending central blood vessel. Shortt and colleagues found that FSPs were surrounded by a compact arrangement of basal cells and when imaged using SEM, the decellularisation of the epithelium surrounding them left remnants of protruding blood vessels, visible along the limbal zone (Shortt et al. 2007a). In this study, no such structures were observed in the same orientation using SEM or SBF-SEM. However, serial images of the adult limbus showed blood vessels housed within the upward stromal projections along the cross-sectional plane rather than the *en face* orientation.

In the limbal niche structure of the human cornea, PoV also contain a vascular complex, however, unlike with FSPs, the blood vessels with the PoV have a radial orientation *(parallel to the PoV)* rather than upward *(anterior surface plane)* projecting blood vessels. The orientation of the blood vessels therefore suggests the vascularised stromal projections seen in the adult avian cornea are more akin to PoV rather than FSPs. Interestingly, the anatomical orientation of the presumptive LCs and PoV were seen to run circumferentially along the limbus in the avian cornea opposed to radially in the human cornea. The apparent difference is unsurprising as the presentation of the limbal stem niche structures in the human are not exact or universal across all mammalian species.

PoV, for example are reportedly absent in rabbit and rodent corneas but present in porcine corneas (Gipson 1989; Notara et al 2011, Yamada et al. 2015). Whereas more recent work by our research group has found that in the porcine cornea, multiple limbal "troughs" are seen in place of small, discrete LCs as found in the human limbus (Hammond 2021). Therefore, it can be speculated that the difference in orientation of the presumptive niche structures in the avian cornea also arise because of species differences. However, the reason for the aforementioned differences will require more investigative work before a robust hypothesis can be put forth to explain why this is the case.

In addition to imaging the adult limbus, the limbi of later developmental stages *(E_{16} and E_{18})* were also investigated. Unlike in the adult limbus, well-defined presumptive LCs and PoV were not observed in either of these developmental stages, rather miniature undulating folds were present in their place, similar to those observed in the rabbit (Yamada et al. 2015). In a study by Davies et al. (2009), fetal corneas from 8.5 to 22-week's-gestation were examined in a concerted effort to better understand the development of the human limbal niche. The authors found that papillae-like structures *(PoV)* were absent from fetal corneas but were evident in 3-week postnatal specimens. Other limbal stem cell structures also remained unidentifiable in both fetal neonatal specimens which suggests that niche structures do not form until after birth. Moreover, Yeung and colleagues also failed to identify LCs in the cornea of a 4-month-old infant which substantiated reports suggesting the development of human cornea continued until 6 months post-birth (Yeung et al. 2009). It is, therefore, plausible that the presumptive limbal niche structures identified in the adult avian cornea do not present until post-hatching. To test this, a more robust investigation of the limbus will be required at more frequent developmental time points pre/post-hatching.

In this study, immunolabelling of PSSC markers, previously assessed in Chapter three, was also investigated in adult corneal specimens that exhibited obvious limbal folds. Notable findings included evidence of CX43-negative cells distributed sparingly within the downward projections of limbal epithelium, specifically, along the epithelial basement membrane, in addition to CXCR4-positive stromal cells subjacent to the basement epithelium *(to be discussed in the subsequent section)*. Matic et al. (1997b) found that CX43 was expressed in the suprabasal epithelium but absent in basal epithelial cells of the limbus. Chen et al. (2010) also found similar basal epithelial staining in their investigation; however, they also noted a small subset of basal cells that did not express CX43. They also found that human limbal stem cells could be partially selected *(using fluorescence activated cell sorting)* based on their apparent lack of CX43 expression. For this reason, CX43 was proposed

as a negative marker for stem cells residing within the human limbal epithelium. Subsequent work by Matic et al. (2002) also found that using CX43 as a negative marker could identify and separate out keratinocyte stem cells in neonatal foreskin by FACS. Since cell-cell communication is essential for mediating development and differentiation, the apparent lack of CX43 expression by stem cells may be key in protecting them from intrinsic influence.

5.4.2 Cell-Cell Interactions in the Presumptive Avian Limbus

This investigation highlighted the changes to the limbal epithelial basement membrane profile in the developing avian cornea compared to the mature adult cornea. The avian profile observed in later stages of embryonic development revealed a highly irregular epithelial basement membrane that extended elaborate lobed processes of basal cells along the limbal zone that were distinct from the uniform interface present in the periphery of the cornea; this was a similar appearance and profile to what was reported in the rabbit by Yamada et al. (2015). In the absence of LCs in the rabbit cornea, an irregular profile was viewed to markedly increase the surface area towards the superficial mesenchyme and was suggested by the authors to represent small-scale palisades that broadly fulfilled the same role as those seen in the human limbus (Yamada et al. 2015). Unlike in the rabbit limbus, where only lobed processes were seen to extend from the basement membrane, the matured avian limbus was observed to also develop more pronounced and regular undulations to the basement membrane profile that followed along the folds of epithelium and stroma, similar to those seen in the human limbus by Dziasko et al. (2014) with respect to the limbal crypt region. In both the developing and adult avian limbus, it was clear that the basement membrane profile increased the surface area between the epithelium and underlying stroma, however, as the cornea matured more distinct and pronounced protrusions in the form of folds also became evident to allow for greater interaction between the superficial mesenchyme. As was suggested by Yamada and colleagues, the profile of the basement membrane in the developing avian cornea could also be comparable to miniature palisades but with the profile changing following maturation, it is more likely that they were in the process of developing into the pronounced structure seen in the adult cornea, with greater similarity to PoV and LCs observed in the human limbal stem cell niche.

This investigation also showed evidence of direct cell-cell interaction between stromal and epithelial cells in the developing avian limbus, a finding also reported by Dziasko et al. (2014) and Yamada et al. (2015) in relation to the putative limbal stem cell niche in the human and rabbit cornea, respectively. The contacts in the human limbus were seen form along the "walls" of limbal crypts, whereas the connections observed in the avian limbus were seen to form with the lobed

processes of basal cells in the developing limbus, similar to the connections observed in the rabbit limbus. A number of stromal cells were seen in close proximity to the epithelial basement membrane, however, only a few were seen to form direct contact with the epithelial cells. More stromal cells may have possibly formed connections with overlaying epithelial cells, but these features were removed within the 100 nm serial sections taken by the 3View system. A section thickness of 100 nm was used to allow for a large sample dataset to be generated, however, using a reduced section thickness of 50 nm may have allowed for greater resolution along the z-axis and imaging of the processes extending from stromal cells towards the epithelial basement membrane.

Within the undulating folds of the adult limbus, specifically, in the downward projections of epithelium, small circular basal epithelial cells with a high nucleus to cytoplasm ratio, a barely detectable nucleolus, and euchromatin presenting as open DNA were also identified. The location and distinct morphology of these cells, indicative of limbal epithelial stem cells, have also been reported in the putative stem cell niche by Dziasko et al. (2014) and Yamada et al. (2015). Smaller limbal epithelial cells were involved in direct contact with stromal cells in the human niche. However, unlike in the aforementioned studies, the resolution and contrast of the SBF-SEM images obtained in this study were lower which made it more challenging to rapidly discern the nucleus to cytoplasm ratio between basal cells and whether these cells were in contact with underlying stromal cell processes. That said, cells with a high nucleus to cytoplasm ratio were sparingly seen in the presumptive LCs of the adult cornea. TEM of the adult limbus further substantiated these findings with higher resolution and contrast micrographs of a small epithelial basal cell that indeed exhibited a distinctly larger nucleus compared to its surrounding cytoplasm, in addition to lobed processes of basal cells projecting into the superficial stroma that had the potential to interact with neighbouring stromal cells.

As discussed previously, a combination of anatomical structures and different cell types that surround mature stem cell populations are what constitute a stem cell niche. The notion that limbal niche cells may regulate limbal epithelial stem cell quiescence, self-renewal, and fate has been explored extensively by researchers. Many studies have shown that stem cells can only be maintained when co-cultured with fibroblast feeder layer and 3T3 fibroblasts, however, work by Zhang et al. (2010b) found human limbal mesenchymal *(stromal)* cells were equally as capable and a viable alternative for culturing limbal epithelial stem cells. Subsequent work by Xie et al. (2012) found that limbal stromal niche cells expressive of stem cell markers supported the maintenance of limbal epithelial progenitor cells in culture, particularly through their close physical association

mediated via the SDF-1/CXCR4 axis. In the human cornea, they specifically observed CXCR4-positive labelling by limbal stromal cells in addition to weak labelling by limbal epithelium cells which was a similar observation of CXCR4 immunolabelling seen in the adult avian limbus, specifically with respect to the presumptive PoV. Findings from Xie and colleagues were further substantiated by González and Deng (2013) who found that limbal stromal cells helped to maintain the undifferentiated state of limbal stem cells via their intact cell-cell contact.

Melanocytes were another cell type implicated in modulating the human limbal stem cell niche. As demonstrated by Dziasko et al. (2014), melanocytes in the human limbus were preferentially located within limbal crypts and closely associated with small basal limbal epithelial cells proximal to limbal stromal cells. Further work by Dziasko and colleagues also suggested that melanocytes, like limbal stromal cells, could also play a supportive role in maintaining limbal epithelial stem cells in the limbal stem cell niche (Dziasko et al. 2015). They showed that co-culturing with a feeder layer comprised of human limbal melanocytes *(hLM)* was just as effective as using standard 3T3 feeder cells for the initial expansion of limbal epithelial stem cells. Moreover, when hLM were subsequently co-cultured on a collagen tissue equivalent *(i.e., RAFT - real architecture for 3d tissue)*, they promoted multi-layering of epithelial sheets in which basal cells remained in an undifferentiated state (Dziasko et al. 2015). The mechanism by which hLM and stromal cells support the limbal epithelial stem cells and the niche itself, however, still remains to be understood. In the adult avian limbus, cells similar to melanocytes were not ostensibly detected in the presumptive crypts or in close proximity to cells with high a nucleus to cytoplasm ratio. This in part could have been due to the low contrast and resolution of the micrographs which limited a robust visualisation of them. Further investigation of the limbal zone is required at higher magnification and reduced serial section thickness to provide clarity on this matter in addition to immunostaining the adult limbus, where presumptive crypts are present, with MelanA – a primary antibody specifically expressed by melanocytes.

Incidentally, while investigating the anatomical and cellular components of the presumptive cell niche in the developing avian cornea, evidence of matrix structures proximally extending from the epithelial basement membrane were observed in the limbi of late-stage embryonic corneas. These structures, similar to matrix cords, were first described as a consequence of the dissociation between the connected presumptive lens and the corneal epithelium during very early ocular development (Hay and Revel 1969; Bee et al. 1988). Later work by Young et al. (2020) also saw that these cords interfaced with underlying stromal cells; specifically, they showed that matrix cords

emerged from the epithelial basal lamina and persisted during early corneal development *(E_4 – E_6)* (Young et al. 2020). Other members of our research group *(unpublished studies by Dr Elena Koudouna and Dr James R. Ralphs)* also observed that these cords persisted throughout development, from E_4 – E_{18} in the avian cornea.

That said, there is still much yet to be understood about their primary function in relation to corneal development. It's generally regarded that matrix cords may have a mechanical function in regulating stromal hydration by preventing excessive swelling that precede the influx of neural crest cells destined to populate the mature stroma with keratocytes and form the endothelium (Young et al. 2020). This notion stems from the similarity between matrix cords and sutural fibres seen in the corneal ultrastructure of other vertebrate species. Both originate from the epithelial basal lamina and traverse the stroma along the same orientation. However, in the avian cornea, these cords were relatively fewer in number compared to sutural fibres seen in other vertebrate species and also did not persist into the mature avian cornea like suture fibres. Therefore, these observations seem to not be consistent with matrix cords possessing a functional role in preserving stromal thickness and hydration due to their scarcity, whereas, for sutural fibres it does.

Conversely, there has also been some speculation as to whether matrix cords have any function at all. Winkler et al. (2015) argued that sutural fibres *(matrix cords)* are merely vestiges of the separation between the epithelium and the presumptive lens which had their function potentially replaced by collagen lamellar branching. However, as these cords are seen to interact with other matrix components *(i.e., stromal cells)*, an argument can be made for their involvement and influence in corneal morphogenesis. A study by Petroll and Miron-Mendoza (2015) found that direct mechanical interactions between the extracellular matrix and corneal keratocytes enabled crosstalk to allow for influence on cell behaviour. From this perspective, Young and colleagues speculated that the developing avian cornea may derive mechanotransduction cues through these cell-matrix interactions to detect physical and compositional information about the surrounding corneal environment in order to regulate cell behaviour (Young et al. 2020). Three dimensional reconstructions presented in this chapter further support the presence of matrix cords structures in the developing avian cornea and absence from the adult avian cornea. However, these findings do not shed light on the role of matrix cords beyond speculation and will require more detailed investigations into both the mechanically and biochemical mechanisms that may be at play in the construction of a transparent corneal tissue.

5.4.3 Non-Limbal Niche-Associated Structures

While investigating the presence of limbal niche-associated structures in the developing and adult avian limbus, additional observations of structures unrelated to the limbal-niche were identified. For instance, clear bony trapezoidal plates were observed in the embryonic eye which formed a loosely connected annulus around the corneoscleral junction. Similar observations were also noted by Wang et al. (2020) using SEM and synchrotron x-ray interferometry. Following maturation, separate plates became indiscernible as they fused together to form a scleral ring. These findings aligned with reports made by previous researchers and although they are well documented in literature, experimental investigations have been limited to purely a descriptive nature and therefore the biological function of scleral ossicle rings as a whole are still poorly understood. One of the prevailing theories, however, claims the function of a scleral ring is primarily as a supporting structure to the eye. In relation to the bird, the size of the eye is relatively large but the orbit is small, the scleral ring is thought to be an extension of the orbit (Fischer and Schoenemann 2019). Franz-Odendaal (2011) has also suggested that the ossicles serve to alter the shape of the eye and assist with the accommodative mechanism; this theory is also supported by other researchers (Quieroz 1982; Lima et al. 2009; Yamashita et al. 2015). This study merely highlighted their presence using advanced, high-resolution SEM, however, did not provide context for their functional role in the avian eye and as a result more extensive work is still required to understand the interplay between ossicles and the orbit in addition to its potential role in avian accommodation.

En face SEM imaging also revealed along the adult corneoscleral junction a network of collagen exhibiting a porous architecture similar to the anterior limbal cribriform layer, first identified by Park et al. (2015) in the human limbus. Using advanced second harmonic generation *(SHG)* imaging, Park and colleagues were able to coalesce autofluorescence *(AF)* and SHG images along the limbus *(ranging a depth of 20-50 μm)* to effectively demonstrate an interplay of how the "honeycomb" collagen network was occupied by blood vessels *(AF-positive)*, circumferentially along the limbal epithelial niche (Park et al. 2015). Furthermore, they noted an absence of this unique collagen structure from both histologically- and immunologically stained limbal cross-sections - which was a corresponding finding seen here in similarly treated avian limbal cross-sections. On the basis of its location along the peripheral cornea, it can be speculated that the presumptive anterior limbal cribriform layer provides structural support to the limbus with a role in maintaining the surrounding microenvironment occupied by stem cells and vasculature. Much like in the human limbus, the function of this structure in the avian eye remains inconclusively

determined. One possible way to solve this shortcoming would be to obtain images of more periodic developmental stages *(as would be permittable by the Human Tissue Act 2004)* to gain a more comprehensive visualisation of the structural development in order to gain a better understanding of its function circumferentially along the limbus.

En face SEM imaging also revealed micropores along the developing limbal zone, which however, were concealed in the adult limbus due to the dense collagen network. Initially, they were thought to be vestiges of blood vessels removed in the processing of specimens, however, the pore size was significantly smaller than the diameter of blood vessels identified from SBF-SEM micrographs. As alluded to above, Shortt et al. (2007a) found that SEM treatment did not completely eliminate the presence of blood vessels and remained intact, presenting as erect prongs following decellularisation; this observation was different from the micropores observed in this study. During the re-mining of SBF-SEM micrographs, evidence of matrix-dense structures similar to nerves were seen to enter from the anterior stroma, to proceed distally through the Bowman's layer and into the stratified corneal epithelium. In the human cornea, nerves are also seen to penetrate the Bowman's layer throughout the peripheral and central cornea, whereas, in monkeys they only penetrated up into the epithelium from the periphery. Due to the small specimen size, limited by the method of microscopy used in this study, it could not be determined if avian corneal nerves entered through both the peripheral and central cornea like in the human or only from the periphery like in the monkey. Moreover, the diameter of the nerves in the avian cornea were measured from SBF-SEM micrographs and observed to have the same diameter as the micropores seen along the limbal zone in E_{16} and E_{18} corneas which supports their complex network throughout the corneal surface and apparent absence following processing for SEM.

5.5 Limitations

Multiple sections from all four limbal quadrants of each developmental stage were prepared for assessment using SBF-SEM and TEM. However, due to the Covid-19 pandemic and subsequent shutdowns in addition to equipment outages following a return to the lab, only two limbal quadrants from a single eye were imaged from each developmental timepoint using SBF-SEM. Similarly, TEM images of the E_{18} limbal region could not be obtained as a result of an extended and ongoing period of equipment outage. Thus, the sample size for each developmental stage was not ideal, yet evidence of direct epithelial cell-stromal cell interactions within the presumptive avian limbal stem cell niche were demonstrated, specifically within the superior quadrants of the developing limbal cornea. Future work will have to be done to image the remaining limbal

quadrants to determine whether direct cell-cell interactions are also present in the presumptive stem cell niche of both meridians of the avian limbus, specifically within the adult limbus as no evidence of interactions were observed in the specimen that was sectioned. Moreover, as the orientation of the adult cornea was not known, due to eyes being obtained from a collaborator without an orientation incision being included, future work would benefit from defining the orientation prior to investigating these undulating limbal folds so that any regional localisation can be determined.

Another limitation of this study was the antibodies that could be evaluated in the timeframe of this thesis. As discussed in Chapter 3 and Chapter 6, CX43, PAX6, Bmi-1, and CXCR4 were selected from a broad range of potential stem cell markers described in Funderburgh et al. (2016) review. However, limitations in the cross-reactivity of antibodies with the chicken and available funds prevented more robust analysis of other markers previously reported in literature like CD-90, CD-105, ABCG2, p63, N-cadherin, MelanA, and SDF-1 to name a few. That said, CX43-negative cells were found in the presumptive limbal crypts in addition to CXCR4-positive cells subjacent to the limbal crypts in the limbal stroma. These findings set a precedent which warrants additional characterisation using, but not limited to, the aforementioned markers.

5.6 Summary

The results of the present study show cellular interactions and anatomical features in the avian corneal limbus which are similar to those that have been observed in the human limbal stem cell niche. The novel acquisition of high-resolution images using three main techniques provided the first evidence that a presumptive limbal stem cell niche may exist in the avian cornea, in addition to highlighting some non-limbal niche-associated structures as well. A summary of key findings from each imaging modality are listed below.

- **SEM:** provided evidence of a porous network of collagen, speculated to be a presumptive anterior limbal cribriform layer, was observed circumferentially around the limbus and thought to provide structural support and maintenance of the cellular components in the surrounding microenvironment *(i.e., presumptive stem cells)*. Furthermore, evidence of micropores *(speculated to be remnants of nerves)* were seen along the limbal zone of the developing adult avian cornea. High resolution images of trapezoidal scleral ossicles were seen to form a loosely connected annulus around the corneoscleral margin in later stage avian eyes which matured into a fully fused, scleral ring in the adult eye. Most notable of observations was that an *en face* view of each of the developmental stages did not illustrate radial striae consisting of PoV and LCs along the limbal

margin *(as seen in the human)*, suggesting the presentation of the aforementioned structures may have species related differences.

- **SBF-SEM:** 3D reconstructions of the adult corneal limbus clearly illustrate distinct limbal invaginations of epithelial cells extending from the limbal cornea into the limbal stroma. Within the upward stromal projections, blood vessels were also seen to run parallel to the section plane. The anatomical appearance of these structures *(regarded by the author as presumptive PoV and LCs)* share similarities in appearance to their human limbal counterparts. In addition to the anatomical observations, cell-cell interactions were also seen at the limbus with respect to underlying stromal cells being evidenced in close proximity to the base of presumptive LCs in addition to matrix "cord" projections extending from the basal epithelial lamina down into the stroma to interface with deeper stromal cells. These interactions strengthen the suggestion of a presumptive stem cell niche existing in the avian cornea as it is widely accepted that limbal niche *(stromal)* cells may regulate limbal epithelial stem cell quiescence, self-renewal, and fate.
- **TEM:** micrographs corresponding to the limbal zone provided a higher contrast visualisation of the limbal basement membrane and the distinct undulations of epithelium and stroma. Micrographs of the E_{16} limbus showed miniature undulations in the basement membrane that would later become more distinct invaginations like the ones seen within the adult limbus. Within the presumptive crypt of the adult limbus, a small round basal cell was identified as a stem cell on the basis of it having morphological characteristic of a high nucleus/cytoplasm ratio.
- **Immunohistochemistry:** In addition to advanced microscopy, immunolabelling of PPSC markers CX43, PAX6, Bmi-1, and CXCR4 were also performed on adult sections where limbal folds were evident. Notably, CX43-negative cells were found within the presumptive LCs in addition to CXCR4-positive cells subjacent to the LCs in the limbal stroma. These findings add weight to the argument of a stem cell niche-like structure in the avian cornea as CX43 is regarded as a negative marker for epithelial stem cells, and the CXCR4 labelling is linked to limbal niche *(stromal)* cells that may maintain the undifferentiated state of limbal stem cells via their intact cell-cell contact.

The chapter that follows investigates the resultant expression of PSSC markers following modification to culture conditions, in addition to evaluating colony formation and growth kinetics of isolated limbal stem cells. Modifications include pre-treatment of culture plates with crude or purified CSPGs prior to cell seeding. Flow cytometry analysis was performed on PSSC markers over multiple passages to assess phenotypic changes in expression of cultured keratocytes and results are compared to corresponding controls.

Chapter 6: The Effect of Chondroitin Sulphate Based Substrates on Embryonic Keratocyte Phenotype *In Vitro*

6.1 Introduction

It is well documented that hybrid CS/DS GAGs within the cornea contribute to collagen fibrillogenesis and organisation, in addition to regulating a spectrum of signalling molecules during corneal development (Lewis et al. 2010; Chen and Birk 2011; Parfitt et al. 2011; Chen et al. 2015; Ashworth et al. 2021). It was through the pioneering work of Meyer et al. (1953) and Davison and Meyer (1954), who alluded to the presence of CS in the cornea, which provided the impetus for understanding its function within the extracellular milieu of the stroma. Such investigations led to the identification of CS preferentially within the peripheral cornea at the corneolimbal junction (Borcherding et al. 1975; Ho et al. 2014); in addition, an increased concentration of more highly sulphated CS/DS GAGS in the limbus was found to coincide with a decrease in ordered arrangement and increase in the diameter of collagen fibrils (Borcherding et al. 1975). More recently, Zhang et al. (2005) demonstrated, using electrospray ionization tandem mass spectrometry, that the expression levels of differentially sulphated CS/DS molecules chondroitin-4-sulphate and chondroitin-6-sulphate changed throughout development in the chicken cornea. From their results, they hypothesised that higher concentrations of chondroitin-6-sulphate, seen during early development, were critical for the initial stages of stromal morphogenesis, whereas higher concentrations of chondroitin-4-sulphate, during later developmental stages, were necessary for the promotion of a stable and compact stroma in order to support corneal transparency well into maturity (Zhang et al. 2005; Quantock and Young 2008).

6.1.1 Chondroitin Sulphate in the Corneal Limbal Stem Cell Niche

Even though there is substantial work outlining the role of CS in relation to defining the corneal stroma ultrastructure, there is little-known of its role towards supporting the corneal limbal stem cell niche. Recent developments in the study of osteoarthritis, however, have shed some light on the potential of CS/DS GAGs in the regulation and maintenance of the stem cell niche of articular cartilage (Hayes et al. 2008; 2016; Melrose et al. 2012; Caterson 2012). Specifically, that low, and minimally sulphated CS motifs may play a role in preserving the phenotype of stem and progenitor cells within the localised stem cell niche by forming a protective shield around stem cells to prevent binding of cell signalling molecules, which directly influence cascades involved in cellular proliferation, differentiation, migration, and matrix secretion (Hayes et al. 2008; Ashworth et al. 2021). Recent findings by Yamada et al. (2015) showed a distinct pattern of CS distribution within

the rabbit cornea with anti-CS/DS sulphation motif-specific antibodies, previously used in the examination of the stem cell niche in articular cartilage. Tissue-specific immunolocalisation was detected at the corneal limbus and was seen to be associated with deep limbal vasculature and the ECM along the basement membrane at the site of limbal epithelial and mesenchymal cell interactions. Furthermore, these interactions were reproduced using three-dimensional SBF-SEM reconstructions; cellular processes were seen to extend from the corneal epithelium to subjacent mesenchymal cells to make connections with the basal lamina in addition to distal connection between basal cells. However, further work is still underway to clarify the involvement of CS/DS in the limbal environment as a likely modulator of the stem cell niche.

6.1.1.1 Chondroitin Sulphate in Regenerative Medicine

As mentioned in Section 1.2.3.1.2.1, investigations into the functional role of CS have been skewed towards engineering a reduction of CS expression or degradation of existing CSPGs in various tissue structures. Consequently, these findings have served as a catalyst for application in therapeutics primarily with respect to CNS disorders, plasticity in the visual system, and osteoarthritis. In the context of developing strategies for the treatment of various pathological conditions, the potential of applying CS to bioengineered scaffolds has long been documented and used for several tissue engineering products (Yannas et al. 1980; Osborne et al. 1998; Liang et al. 2011). Moreover, they have been shown to possess several advantageous properties when compared to scaffolds made from other materials; for instance, they are made from naturally occurring materials, common to the ECM of most tissues; they have haemostatic properties, low antigenicity, mechanical durability and promote cell attachment and proliferation in a variety of tissue engineering applications (Kuberka et al. 2002; Ma et al. 2003; Buijtenhuijs et al. 2004; Liang et al. 2011). This is exemplified in the study by Corradetti et al. (2016), where a chondroitin sulphate-based biomimetic scaffold was used to recapitulate the physiochemical features of the chondrogenic niche in articular cartilage, to modulate the host immune response following implantation. The authors' integration of CS into a collagen-based scaffold was primarily for its immunomodulatory properties, in addition to being one of the most represented components of cartilage (Alberts et al. 2002; Akiyama et al. 2004; Corradetti et al. 2016). CS, crosslinked onto a collagen-based scaffold in this way preserved the protective and regenerative ability of mesenchymal stem cells when exposed to a proinflammatory environment by way of immunosuppression. In addition, chondrocyte proliferation *in vivo* was enhanced when transplanted (Corradetti et al. 2016).

Hayashi et al. (2016) were the first to show that a self-formed ectodermal autonomous multi-zone *(SEAM)* could be generated from human induced pluripotent stem cells when cultivated in differentiation media. These concentric zones mimicked whole eye development with each zone representing a different primordial cell lineage, ranging from the ocular surface ectoderm to the retinal pigment epithelium (Hayashi et al. 2016). In a study by Shibata et al. (2018) various isoforms of laminin, an ECM molecule found in the corneal limbus, were found to have varied effects on the differentiation pathway of corneal epithelial cells obtained from human induced pluripotent stem cells *in vitro* (Ashworth et al. 2021). Preliminary work by members of our research group has indicated that CS, similar to laminin, is also likely to be involved in modulating the differentiation of human induced pluripotent cells in a developing SEAM, as seen through the localisation of CS moiety *(using purified antibody 7D4)* and its increasing deposition from weeks 4-6 in SEAM zones 3 outwards to zone 4 *(correspond to cells within the ocular surface ectoderm)* (Ashworth et al. 2021). That said, there has been little exploration in relation to the application of CS in bioengineered scaffolds for the purposes of modulating cell differentiation in the stem cell niche of the corneal limbus (Ashworth et al. 2021). As a whole, the complexities of the interactions between biomaterials and host cellular environment have yet to be fully explored and clearly defined. Emerging knowledge will continue to provide a clearer understanding as to how CS modulates stem cell behaviour with the hope of contributing to more affordable and alternative ways of regenerative therapeutic interventions.

6.1.2 Mesenchymal Stem Cells in the Corneal Stroma

As previously described, the corneal stroma contains a sub-population of mesenchymal-derived cells characteristic of adult stem cells, termed CSSCs, that reside within the limbal stem cell niche and actively support multiple cell types within the cornea to maintain corneal transparency (Funderburgh et al. 2016). Much like CSSCs, stromal keratocytes are also derived from mesenchymal cells. However, even in the case of late-stage embryonic keratocytes, data has shown them to not be terminally differentiated, rather they are believed to exist as partially restricted precursors, equipped to respond promptly to reform their environment to maintain corneal transparency (Lwigale et al. 2005; West-May and Dwivedi 2006; Etheredge et al. 2009). Their retention of multipotentiality was demonstrated by Lwigale et al. (2005) through the introduction of later stage embryonic keratocytes into various neural crest-derived populations of earlier embryos. The authors found translocated keratocytes successfully proliferated, migrated, and dedifferentiated into many but not all the neural-crest populations; similar findings were also

reported by Chao et al. (2013) who used human fetal keratocytes in a similar investigation (Lwigale et al. 2005; West-May and Dwivedi 2006; Chao et al. 2013).

In a recent review by Funderburgh et al. (2016), CSSCs were digested from the limbal stromas of human corneas and expanded in culture to evaluate the expression of both stem cell markers and genes. Selected markers and genes were categorised based on the association with pluripotent cells, mesenchymal stem cells, neural stem and progenitor cells, or ocular precursors in embryonic development (Funderburgh et al. 2016). Using flow cytometry, the authors were able to isolate adult stem cell side-populations, in addition to quantifying the percentage of cells expressing selected cell surface, stem cell markers. Similar techniques and markers will be used in experiments described here to evaluate alterations in phenotypic expression of keratocytes cultured *in vitro* in two different CS-based substrates.

6.1.3 Aims

The present study aimed to test this hypothesis, in relation to corneal progenitor cells, by using flow cytometry to quantify the expression of putative stromal stem cell markers CX43, PAX6, Bmi-1, and CXCR4. Marker expression was compared between embryonic keratocytes cultured on two different CS-based substrates, derived from either a crude composition of proteoglycans containing KS and CS GAG chains with their core proteins, or a purified extract enhanced for CS GAG chains. The secondary aim was to investigate the relationship between marker expression and passage *(up to Passage 5)* for each coating condition. If a significant difference exists in putative stromal stem cell marker expression between coating conditions, all markers can be evaluated collectively for each coating condition to identify the coating which best supports a non-differentiated phenotype, similar to that of stem cells in their niche environment.

6.2 Materials and Methods

6.2.1.1 In Vitro Expansion (Cell Culture)

Collection and Initial Preparation

As described in Section 3.2.1.1, E_{18} keratocytes were isolated from a pooled sample of corneas extracted from twenty-four fertilised white leghorn chicken eggs *($n= 40 \pm 2$ corneas)* for the purposes of assessing the phenotypic expression profile of selected putative stromal stem cell markers: CX43, PAX6, Bmi-1, and CXCR4 using flow cytometry. A pooled sample of corneas was used because a single cornea could not provide a sufficient number of cells to successfully perform

flow cytometry and serial passage. Cells were analysed at initial extraction *(P_0)* and from P_2-P_5 following keratocyte growth on uncoated *(control)* and coated *(crude GAG or enhanced PG)* culture plates.

Cells Cultured on GAG Coated Plates

Two substrates were kindly provided by fellow PhD candidate Sean Ashworth, MSc *(Cardiff University School of Optometry and Vision Sciences, UK)*. The first was a crude proteoglycan substrate purified from porcine peripheral cornea, containing both KS and CS glycosaminoglycan chains *(CS-7D4/KS-5D4),* in addition to their protein cores[32] and the second was a 6C3 enhanced substrate purified from shark cartilage *($CS\text{-}6C3^{+++}/KS\text{-}5D4^{-}$)*. Both 6C3 and 7D4 are mAbs that recognise native CS epitopes, whereas 5D4 is a mAb that recognises sulphated KS epitopes.

Preparation of Substrate Solution

An 80% saturated solution of ammonium sulphate (4.1M, Sigma Aldrich, Cat. # A4418-500G) at 4°C was filter-sterilised prior to the addition of GAG-substrate to make a 1 μg/mL solution.

Coated Culture Plates

Substrate solution was coated at a density of 0.055 μg/cm^2 *(predetermined using indirect enzyme-linked immunoassay – See Appendix III)* onto 35 x 10 mm plates (Nunclon™ Delta, ThermoFisher Scientific, Cat. # 153066), or T-75cm^2 flasks (Nunc EasYFlask, ThermoFisher Scientific, Cat. # 156472). Coated plates and/or flasks were wrapped in clingfilm and placed in a 4ºC fridge on top of an open-air rocker overnight. Prior to seeding cells onto plates or flasks, surfaces were washed four times with D-PBS to remove any residual ammonium sulphate, used to immobilise GAGs onto the surfaces of culture plates, as this would hinder cell viability.

6.2.2 Flow Cytometry

6.2.2.1 Sample Preparation

A cell count was performed on harvested cells using a haemocytometer to determine the volume of single-cell suspension required for a final concentration of 1x10^6 cells/mL. All samples were centrifuged for five minutes at 1450 RPM to form a cell pellet. Supernatant *(media)* was discarded, and cells were subsequently washed with ice cold PBS.

[32] Protein cores for KS proteoglycans were a mixture of lumican and keratocan, whereas, for CS proteoglycans they were a mixture of biglycan and decorin.

Live/Dead Staining

The cells in each sample were resuspended in ice cold PBS with the addition of 4 µl of fixable live/dead stain (Live/Dead™ Fixable Far Red Dead Cell Stain Kit, Invitrogen, Cat. # L10120). Samples were incubated at 4°C in the dark for 30 minutes before being washed with ice cold PBS. This dye was used to differentiate between live and dead cell populations within the sample so that the relevant population could be isolated for analysis – as discussed in Section 6.2.2.3.2. In principle, the dye would enter necrotic cells with damaged membranes and react with free amines both inside and outside the cell, resulting in high fluorescence staining. In contrast, it would only interact with the cell-surface amines of viable cells resulting in dim fluorescence staining, to create a difference in intensity between the live and dead cell populations within the sample of greater than 50-fold. This stain also allowed for the differential in fluorescence between the two populations to be preserved following cellular fixation.

Fixation of Cells

All samples were then fixed with 4% *(w/v)* PFA in Sorensen's phosphate buffer *(pH 7.4)* for 15 minutes before being washed with PBS. Fixative was added gradually into the sample tube while it was gently vortexed to allow for the cell pellet to fully separate and prevent cell clumping that would impede adequate fixation. Cells were mildly fixed using PFA to help stabilise the cellular membrane via reversible methylene bridges; the reversible nature is advantageous as it enhances the signal for immunolabelling (Thavarajah et al. 2012).

Permeabilisation of Cell Membrane

For the detection of intracellular expression, as in the case of CX43, PAX6, and Bmi-1, Tween®20 (0.2%, Sigma Aldrich, Cat. # P1379-500ML), a mild nonionic detergent, was used for permeabilisation to allow antibodies into the cellular structure to bind relevant epitopes by breaking protein-lipid and lipid-lipid associations across the cell membrane. Samples were treated for 30 minutes in solution at 4°C before being washed with PBS.

Immunofluorescent Staining

Cells were re-suspended in normal horse serum (1:20, Vector Laboratories, Cat. # S-2000) and placed on gentle rotation for one-hour. Samples were washed with PBS before re-suspension in 500 µl of primary antibody and placed on slow rotation for one-hour at 4°C. Primary antibodies used were as follows: Anti-Connexin 43/GJA1 (10 µg/mL, Abcam, Cat. # ab11370), Anti-PAX6 [AD2.38] (10 µg/mL, ThermoFisher Scientific, Cat. # 14-9914-82), Bmi-1 (10 µg/mL, Sigma-

Aldrich, Cat. # PLA0208), CXCR4 (10 μg/mL, Aviva Systems Biology, Cat. # OALA00163), Rabbit IgG *(Isotype control antibody)* (10 μg/mL, Vector Laboratories, Cat. # I-1000), Mouse IgG *(Isotype control antibody)* (10 μg/mL, Vector Laboratories, Cat. # I-2000).

Following treatment with the primary antibody, cells were washed with PBS three times before resuspension in 500 μl of conjugated secondary antibody and placed on rotation for 45 minutes *(in the dark)* at 4°C. Secondary antibodies used were as follows: DyLight 488 Horse Anti-Rabbit (1:200, Vector Laboratories, Cat. # DI-1088) and DyLight 488 Horse Anti-Mouse (1:200, Vector Laboratories, Cat. # DI-2488). All solutions *(blocking serum, primary and secondary antibodies)* were made in PBS/0.1% BSA *(w/v)*. Samples were washed with PBS three times before final resuspension in 500 μl of PBS/0.1% BSA *(w/v)*. and transfer to labelled polystyrene test tubes (Falcon™, Fischer Scientific, Cat. # 352054).

Visual Validation

From the final cell suspension of each sample, 10 μl was pipetted onto individual glass slides and imaged using an Olympus IX71 Inverted Fluorescence & Phase Contrast Tissue Culture Microscope (Olympus, UK). Micrographs at x20 magnification were captured using SPOT 5.2 *(Basic)* Software (SPOT Imaging Solutions, Diagnostic Instruments Inc., USA).

6.2.2.2 Flow Cytometric Analysis

Prepared samples were kept in the dark until analysis by flow cytometry. Samples were analysed on a BD LSRFortessa™ cell analyser (BD, San Diego, CA, USA) equipped with 405/488/561/640 nm lasers. Fluorescein isothiocyanate *(FITC)* and Allophycocyanin *(APC)* were detected using the 530/30 and 670/40 filters, respectively. An unstained control was prepared *(fixed and untreated by blocking serum, primary and secondary antibody)* for instrument calibration. A total of 50,000 cells were acquired for each sample. Data were expressed as median fluorescence intensity *(MedFI)* and a normalised median fluorescence intensity *(nMedFI)* – the ratio between the MedFI of sample cells and that of the isotypic control cells. A repeat of *(n=5)* was performed to establish the consistency of the instrument analysis but only a single analysis for each marker, passage, and coating condition was performed.

6.2.2.3 Data Preparation Using FlowJo

6.2.2.3.1 Application of Compensation to Sample Sets

Two, single stained, compensation controls were prepared: Live/Dead™ only stained[33] and antibody *(Bmi-1)* only immunostained[34] *(see Section 6.2.2.1)*. A standard unstained *(fixed)* control was also prepared in addition to a sample immunostained with Bmi-1 and Live/Dead™ stain. It should be noted that Bmi-1 was arbitrarily selected to compensate multichannel spillover *(between* Fluorescein isothiocyanate area – *FITC-A and* Allophycocyanin area – *APC-A)* as all primary antibodies were conjugated with the same secondary fluorophore *(detected by the FITC-A channel)*.

Post-acquisition compensation was calculated manually using NovoExpress® Software (v. 1.30, ACEA, San Diego, USA). Manual compensation was performed instead of automated compensation as only two channels were used for this experimental design and more accurate compensatory values could be determined this way. The NovoExpress software facilitated real-time adjustment and comparison between gated single stained control samples before the application of compensation, a feature not available in the FlowJo software. A compensation matrix was generated with values corresponding to the spillover percentage between each channel *(FITC into APC and vice versa)* that was applied to each data set prior to gating.

6.2.2.3.2 Gating Cell Population

Following data acquisition on the BD LSRFortessa™ cell analyser, FC 3.0 files were exported from the BD FACSDiva™ software and imported into FlowJo v.10.6.1 (BD Biosciences, Oregon, USA). To the initial graph window of each sample (Figure *6.1*), which displayed the distribution of collected events along cytometric parameters: side scatter area *(SSC-A)* vs. forward side scatter area *(FSC-A)*, an ellipse gate was applied to encompass the major cell population *(higher-density regions of events)* and labelled as "Keratocytes." Using parameters FSC-A vs. forward scatter height (FSC-H), doublets were discriminated from the "Keratocytes" population to ensure only single cells were counted for data analysis. Doublets are characterised as having an increased area whilst maintaining a similar height to single cells which present as a subpopulation of cells dispersing

[33] To generate a distinct separation between positively and negatively stained populations, a small sample of cells was heat-treated at 65°C for one minute before being placed on ice for one minute; these heat-killed cells were combined 1:1 with live cells prior to adding the Live/Dead™ stain.

[34] A small sample of unstained cells *(fixed)* was incorporated into the antibody-stained sample prior to flow cytometric analysis for the purpose of generating a distinct separation between positively and negatively stained populations.

away from the main population. A polygonal gate was applied to exclude this subpopulation and labelled as "Singlets." A subsequent parameter change was then made to: APC vs. FSC-A to distinguish between living and necrotic cells. The APC channel was selected to excite *(at 650/665 nm)* the Live/Dead™ Fixable Far Red Dead Cell stain instilled prior to analysis. Gating was applied accordingly to exclude higher signalling positive events from the main population and labelled as "Live Cells". A final parameter change was made to "Histogram vs. FITC-A" to generate a log-distribution of the "Live Cells" population. Where applicable the isotype was overlayed onto the corresponding sample to visualise both distributions.

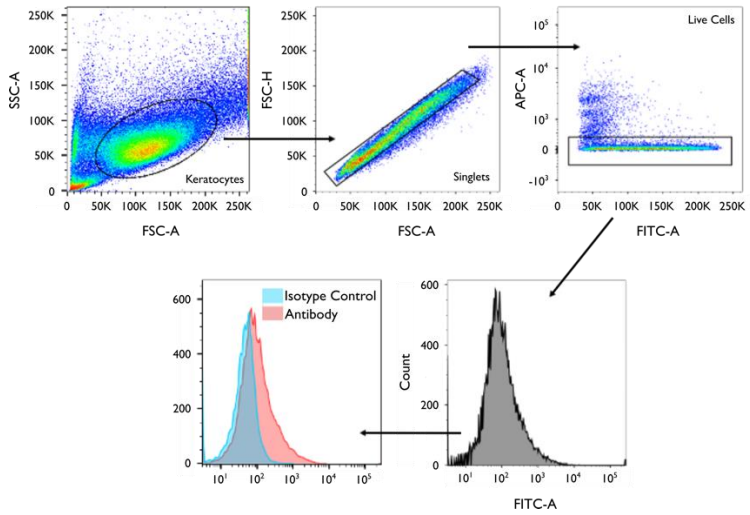

Figure 6.1: Schematic of sample plots demonstrating the gating strategy employed on raw data in FlowJo to generate graphs. Forward vs. side scatter area *(FSC-A vs. SSC-A)* gating was applied to identify cells of interest based on size and complexity *(granularity)*, whereas FSC-A vs. forward scatter height *(FSC-H)* gating strategy was applied for the purposes of doublet exclusion. To distinguish between live and dead cells, FSC-A was gated against allophycocyanin area *(APC-A)* to detect fluorescence emitted by the Live/Dead™ Fixable Far Red Dead Cell stain. Finally, a fluorescein isothiocyanate area *(FITC-A)* vs. histogram parameter change was applied to generate a log-distribution of gated events. The antibody histogram was overlayed on its isotype control to produce the final graph.

6.2.2.3.3 Adding Statistics and Generating Comparison Histograms

To each sample in the workspace window of the software, the MedFI was applied using the software's "Statistics" tool. Using the "Layout Editor" platform, a comparison histogram was generated to overlay the fluorescence of each antibody with its corresponding isotype control. Images were exported into Microsoft PowerPoint for Mac (Redmond, Washington, United States) v.16.35 to prepare the relevant figures.

6.2.2.3.4 Data analysis

Flow cytometry data was used to track expressional changes within the keratocyte population across multiple passages *(P_0, P_2-P_5)*, comparing expression of PPSC markers by keratocytes grown on uncoated *(control)* dishes to two different CS-substrate coated dishes. The nMedFI values were generated using the equation below, as it has been shown in literature to be a more sensitive measure of pluripotent and differentiation marker expression, in addition to being more accurate in comparing data of different experimental runs (Chen et al. 2012).

$$\mathrm{nMedFI} = \frac{\mathrm{MedFI_{sample}}}{\mathrm{MedFI_{negative}}}$$

Where:

nMedFI = the normalised median fluorescence intensity.

$MedFI_{sample}$ = the median fluorescence intensity of the sample.

$MedFI_{negative}$ = the median fluorescence intensity of the corresponding isotype control to the sample.

6.2.2.3.5 Statistical Analysis

Statistical analyses were performed using the open-source statistics program JASP (version 0.14.1, Amsterdam, Netherlands). To investigate whether PSSC marker expression of CX43, PAX6, Bmi-1, and CXCR4 across multiple passages was affected by coating condition, a repeated-measures ANOVA of nMedFI was performed (within subject factor of passage [P_0, P_2, P_3, P_4, P_5] and between subject factor of coating condition [uncoated, crude CS-7D4/KS-5D4 coated, enhanced CS-6C3^{+++}/KS-5D4^{-} coated]). Post-hoc comparisons with a Bonferroni correction were performed to investigate pair-wise comparisons between coating conditions. Throughout the analysis of the present study, p values less than 0.05 were considered significant. Standardised effect sizes and associated 95% confidence intervals are also reported throughout the analysis.

To investigate the relationship between nMedFI and passage number for each PSSC marker and coating condition, repeat measurements of nMedFI were taken using flow cytometry. Linear regression analyses (model II; 'lmodel2' package – R Core Team 2019) were then used to fit regression lines between measurements of nMedFI and passage number for each coating

condition. Figures showing linear regression were generated using the open-source software RStudio (version 1.2.5003 R Core Team 2019) with the ggplot2 package (Wickham, 2009).

6.3 Results

6.3.1 Optimisation of Experimental Design

There are numerous fixation and permeabilisation protocols that have been developed by researchers for the detection of intracellular and extracellular antigens by flow cytometry. However, most of these protocols have been used to define cell populations in immunology, haematology, and oncology *(e.g., T/B cells, NK cells, neutrophils, eosinophils, resident/inflammatory monocytes, resident/interstitial macrophages)* (Menon et al. 2014; Yu et al. 2016). As this study investigated the expression of PSSC markers in embryonic fibroblasts *(keratocytes)*, parameters such as cell fixative, permeabilising detergent, and antibody concentration were critical to obtaining high quality flow data and had to be optimised empirically by myself; each of these steps was essential for ensuring the retention of target proteins in the original cellular location, access of antibody to intracellular proteins, and minimising background fluorescence, respectively. Other relevant, but more minor, aspects of protocol optimisation, such as incubation time, suspension volume, cell concentration, and temperature were pre-determined from literature.

6.3.1.1 Effect of Fixative on Cell Membrane Preservation

For the detection of intracellular antigens by flow cytometry, cells are chemically preserved using either precipitating *(i.e., organic solvents such as methanol and ethanol)* or cross-linking *(i.e., aldehydes such as paraformaldehyde)* fixatives before cell membrane permeabilisation and antibody staining can be performed. Fixatives are beneficial in immobilising antigens and fortifying the cell membrane to retain its integrity and subcellular morphology. Aldehyde-based fixatives produce intermolecular bridges from crosslinked proteins, which prevent against cell lysis when subsequently treated with permeabilising detergents to permit antibody access for epitope binding by disrupting the cell membrane. Alcohol-based fixatives, by contrast, compete with water molecules throughout the cell for protein hydrogen bonds leading to a disruption in the cell membrane and cause precipitation and aggregation of large cellular proteins, with subsequent dehydration of the cell; these solvents are also advantageous as they simultaneously permeabilise the cellular membrane for antibody access. In this preliminary investigation, samples of E_{18} keratocytes were treated with (a) 4% PFA for 15 minutes prior to permeabilisation with Tween®20 for 30 minutes, and (b) ethanol (70%, Fischer Scientific, Cat. # 10680993) or (c) methanol (70%, Fischer Scientific, Cat.

#11347996) for 15 minutes. This study was performed to assess the retention of cellular morphology following fixation and in the case of PFA-treated cells, absence of cell lysis following subsequent treatment with a permeabilising detergent. The fixative concentration and protocol of each solvent used for this investigation was selected based on the recommendations by bio-tech companies: Bio-Rad, Cell Signaling Technology, and Biolegend® (Bio-Rad, 2021a; Cell Signaling Technology 2021; Biolegend 2021).

Comparison of Different Fixatives

Following fixation, and permeabilization, where appropriate, a small sample from each keratocyte cell population was extracted and imaged to assess the integrity of cellular membrane and morphology. To substantiate these findings, flow cytometric analysis was subsequently performed on each sample by evaluating the populations cellular profile to show cell lysis was not evident in the larger population of single-cell suspension. As seen in Figure *6.2*, all three fixatives preserved the integrity of the cells, as illustrated by the clear circular shape and halo around cells. Corresponding density plots for each sample also indicated cell lysis was not evident as the majority of the acquired data was not localised at the intersection of the x- and y-axis of the plot. However, compared to the unfixed controls density plot, the plots of both ethanol- and methanol-fixed cells showed a clear reduction in FSC-A, corresponding to the shrinkage of the cells from the solvents mode of action and an elevation of SSC-A, resulting from protein precipitates in solution causing cellular aggregate formation. These cellular aggregates were also observed in corresponding micrographs taken for visual validation of both samples. Despite my best efforts to limit aggregate formation by using a stepwise instillation of each organic solvent with simultaneous vortexing, cell clumps were not successfully eliminated. Based on the above findings, 4% PFA was selected as the most appropriate fixative in this protocol with which to treat keratocytes for flow cytometric analysis.

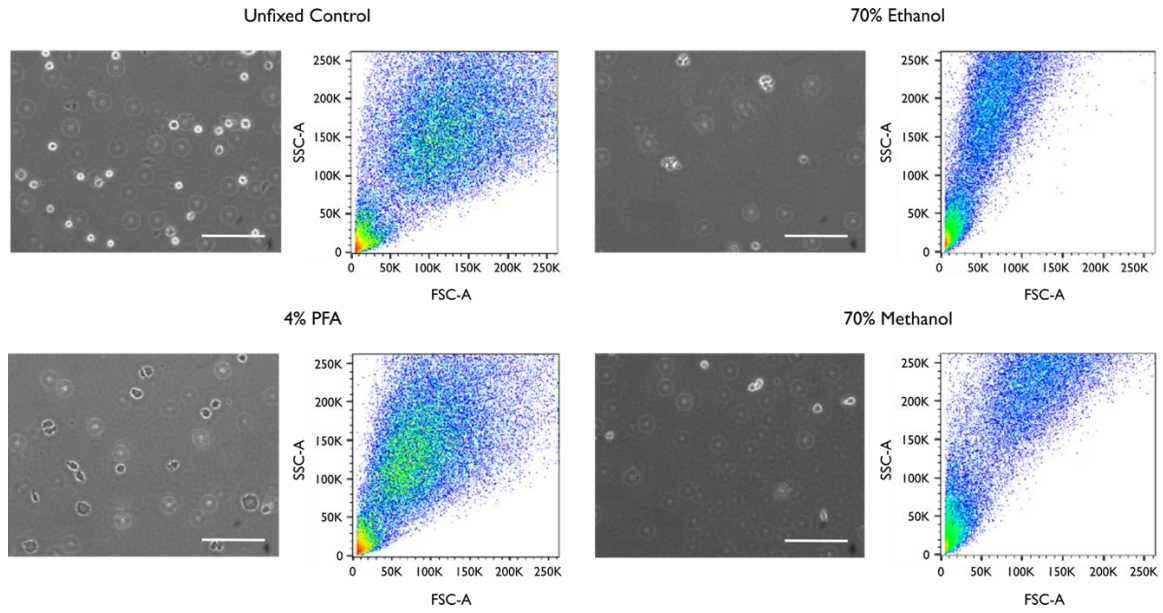

Figure 6.2: Comparison of fixative effect on cell integrity. Embryonic keratocytes were treated with 70% *(v/v)* ethanol, and 70% *(v/v)* methanol for 15 minutes, in addition to 4% *(v/v)* paraformaldehyde for 15 min prior to permeabilisation with Tween®20 for 30 min. Micrographs were acquired to visually verify that each sample contained visibly intact cells prior to flow cytometric analysis. Flow cytometry plots show gating strategy *(FSC-A vs. SSC-A*) to present all events acquired *(inclusive of debris)*. Scale bars represent 100 μm.

6.3.1.2 Effect of Detergent on MedFI

Subsequent to the fixation of cells, where the natural biological state of the cellular structure is preserved, a permeabilisation step is used for the access and binding of antibodies to intracellular antigens or nuclei *(DNA or RNA)* (Amidzadeh et al. 2014). Samples of E_{18} keratocytes were treated with either (a) Triton X-100 (Sigma Aldrich, Cat. # 10789704001), (b) Tween®20, or (c) Saponin (Sigma Aldrich, Cat. #47036-50G-F), prior to immunostaining with antibodies CX43, PAX6, and Bmi-1 to determine the non-ionic detergent that would produce the highest MedFI for each antibody, whilst retaining the integrity of the cellular structure. For application in flow cytometry, the recommended concentrations and incubation periods for each of these detergents ranges from 0.1–0.5% and 5–30 minutes, respectively (Novus Biologicals 2021). For that reason, several protocols were considered for each detergent prior to selecting a suitable combination of concentration and incubation time for this investigation.

Comparison of Different Permeabilisation Methods

All three detergents demonstrated the ability to permeabilise the keratocyte population in some way. However, Figure *6.3* clearly shows that 0.2% *(v/v)* Tween®20 generated the highest MedFI for CX43 *(MedFI= 18,720)*, PAX6 *(MedFI= 644)*, and Bmi-1*(MedFI= 20,666)*. Saponin, when compared to Tween®20, had a lower effect on the permeabilised cells as reflected in the MedFIs of CX43 *(MedFI= 10,364)*, PAX6 *(MedFI=534)*, and Bmi-1 *(MedFI=6133)*. The lowest MedFI was observed when Triton X-100 was used prior to treatment with CX43 *(MedFI=88.7)*, PAX6 *(MedFI=89.9)*, and Bmi-1 *(MedFI=556)*. Micrographs taken of each sample prior to flow cytometric analysis demonstrated that treatment with the lowest concentration and incubation time recommended for Triton X-100 resulted in round and intact cells with a propensity to form cellular aggregates. The forward and side scatter density plots for Triton X-100 reflected these aggregates with a cellular profile indicative of increased granularity for each tested antibody. Consequently, the number of cells included in the actual data analysis was nominal, as the majority of acquired cells were omitted following various gating strategies to eliminate debris and doublets from the final data set, making this detergent the least reliable for use across multiple trials in future studies. However, neither Tween®20 nor Saponin produced cellular aggregates, and cells were observed as singular and unattached in cell suspension. Based on the above results, Tween®20 was selected as the most appropriate detergent in this protocol as it generated the highest MedFI out of all three detergents for CX43, PAX6, and Bmi-1, in addition to not producing any cellular aggregates that would have affected flow cytometric analysis.

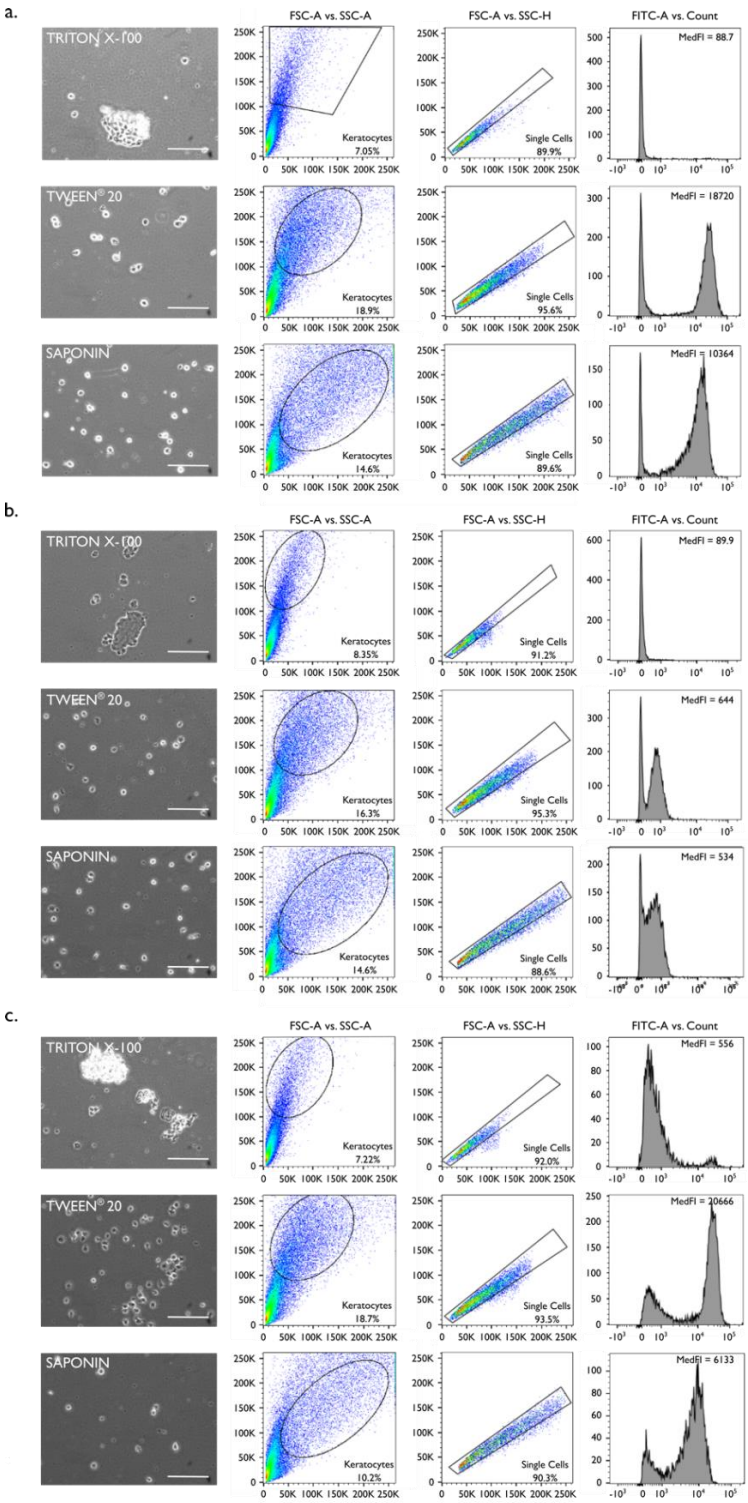

Figure 6.3: Comparison of median fluorescence intensity *(MedFI)* and micrographs of three different permeabilisation detergents to assess expression of antibodies CX43, PAX6, and Bmi-1. Embryonic keratocytes were treated with non-ionic detergents: 0.1% *(v/v)* Triton X-100 at 10 min incubation, 0.2% *(v/v)* Tween®20 at 30 min incubation, and 0.1% Saponin *(w/v)* at 15 min incubation prior to immunofluorescence staining with primary antibodies recognising, (a.) CX43, (b.) PAX6, and (c.) Bmi-1. Micrographs were acquired to visually verify samples contained visibly intact cells prior to flow cytometric analysis. Flow cytometry plots show gating strategies applied to isolate cells of interest from debris *(FSC-A vs. SSC-A)* and doublets *(FSC-A vs. SSC-H)* to generate histogram plots and corresponding MedFIs. Scale bars represent 50 μm.

6.3.1.3 Effect of Pre- and Post-Fixation on MedFI for Antibody CXCR4

In this experiment, embryonic keratocyte cell populations were immunostained with CXCR4 antibodies prior to and following fixation with 4% *(v/v)* PFA for the detection of cell surface antigens. Figure *6.4* shows the dramatic difference in MedFI following both treatment protocols with a greater MedFI for pre-fixation *(MedFI = 5404)* supported by a clear right-hand shift in FITC-A expression compared to post-fixation *(MedFI = 86.1)*. Prior to the application of the oval gate, as seen in the FSC-A vs. SSC-A plots, a number of other regions were considered and test-gated to determine the cell population most indicative of CXCR4 expression *(i.e., the population that provided the highest MedFI)* in each sample. Corresponding micrographs demonstrated both protocols produced visibly intact, single cells in suspension that increased the reliability of the data set as more cells were likely to be accepted in the final analysis. Based on the above results, fixation prior to antibody staining was appropriate in this protocol as it generated a higher MedFI than when fixation was applied after antibody staining.

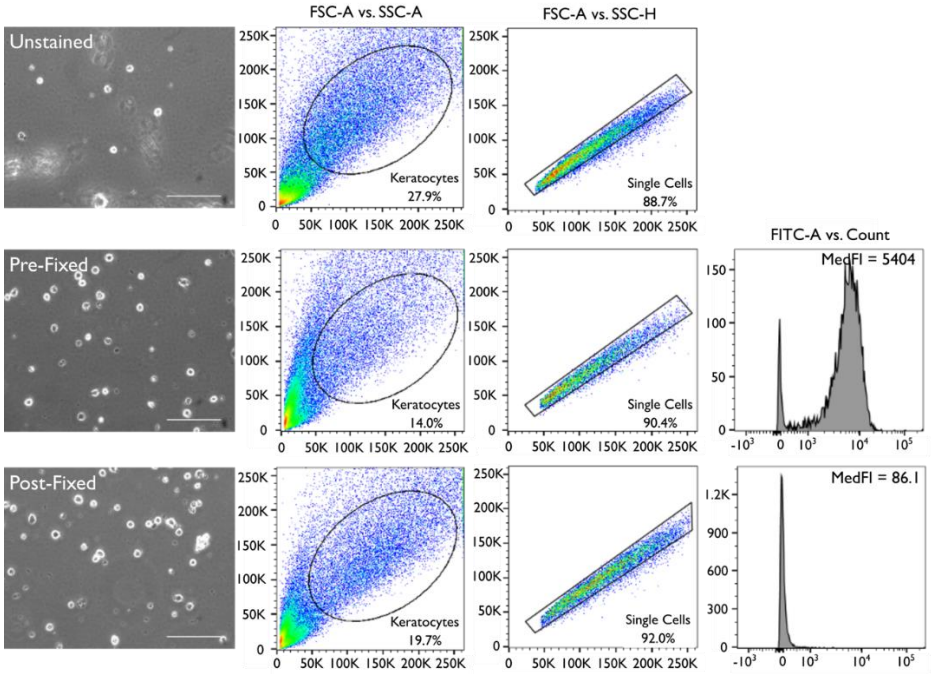

Figure 6.4: Comparison of median fluorescence intensity *(MedFI)* and micrographs for CXCR4 following pre- and post- fixation with paraformaldehyde. Embryonic keratocytes were immunostained with CXCR4 prior to and following fixation with 4% *(v/v)* PFA. Micrographs were acquired to verify samples contained visibly intact cells prior to flow cytometric analysis. Flow cytometry plots show gating strategies applied to isolate cells of interest from debris *(FSC-A vs. SSC-A)* and doublets *(FSC-A vs. SSC-H)* to generate histogram plots and corresponding MedFIs for pre- and post-fixed data sets. Scale bars represent 100 μm.

6.3.1.4 Effect of Antibody Concentration on Separation Index

Embryonic keratocytes were processed for flow cytometry *(as described in Section 6.2.2.1)* and immunostained with serially diluted primary antibodies *(CX43, PAX6, Bmi-1, and CXCR4)* at concentrations of 5, 10, 15, and 20 μg/mL. Each sample was analysed using the FlowJo software *(See Appendix II)* to generate a separation index *(SI)* value indicative of the separation between the positive *(antibody stained at varying concentrations)* and negative *(unstained control)* populations. As seen in Figure *6.5*a, the SI of each antibody, as determined by the antibody concentration, produced a characteristic titration curve where the optimal antibody concentration of anti-CX43 *(10 μg/mL)*, PAX6 *(10 μg/mL)*, Bmi-1 *(10 μg/mL)*, and CXCR4 *(10 μg/mL)* was clearly evident. Corresponding micrographs (Figure *6.5*b) demonstrated that cells sampled from each tube were single and intact cells in suspension.

During the process of optimizing the flow cytometry protocol for CXCR4, an antibody titration was also performed on unfixed cells at concentrations of 1.25, 2.5, 5, 10, and 20 μg/mL. The SI values (Table *6.5*) showed that as concentration was increased the SI notably decreased.

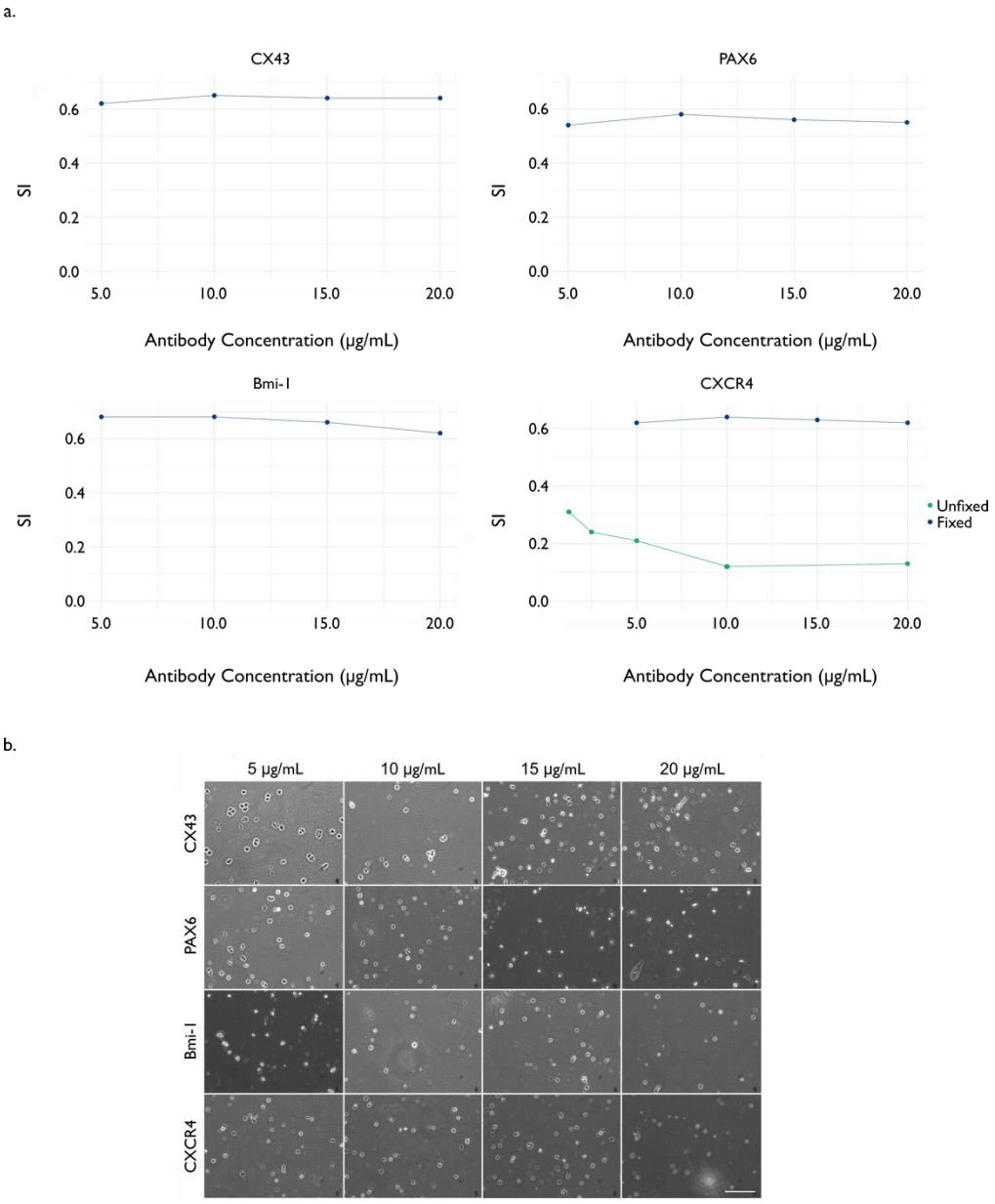

Figure 6.5: Antibody titration curves for primary antibodies CX43, PAX6, Bmi-1, and CXCR4 with corresponding micrographs. (a.) Embryonic keratocytes were pre-fixed with 4% *(v/v)* paraformaldehyde and permeabilised with 0.2% *(v/v)* Tween®20 *(where appropriate)* prior to immunostaining with primary antibodies to CX43, PAX6, Bmi-1 and CXCR4, serially diluted to concentrations of 5, 10, 15, and 20 µg/ml *(unfixed cells immunostained for CXCR4 at concentrations of 1.25, 2.5, 5, 10, and 20 µg/mL)*, (b.) Micrographs illustrate antibody-stained samples at varying concentrations showing round and intact cells following fixation and permeabilisation where appropriate. Scale bar represents 100 µm.

Table 6.1: SI values generated in FlowJo to determine optimal antibody concentration for CX43.

Concentration (µg/mL)	Median Positive	Median Negative	84th Percentile of Negative	SI
5	6836	93.8	10945	0.62
10 *	10318	93.8	15636	0.65
15	10602	93.8	16344	0.64
20	11639	93.8	17904	0.64

* The chosen antibody concentration is shown in bold font

Table 6.2: SI values generated in FlowJo to determine optimal antibody concentration for PAX6.

Concentration (µg/mL)	Median Positive	Median Negative	84th Percentile of Negative	SI
5	350	93.8	570	0.54
10 *	402	93.8	625	0.58
15	332	93.8	518	0.56
20	229	93.8	467	0.55

* The chosen antibody concentration is shown in bold font

Table 6.3: SI values generated in FlowJo to determine optimal antibody concentration for Bmi-1.

Concentration (µg/mL)	Median Positive	Median Negative	84th Percentile of Negative	SI
5	4692	93.8	6866	0.68
10 *	7546	93.8	11020	0.68
15	8318	93.8	12611	0.66
20	11222	93.8	18073	0.62

* The chosen antibody concentration is shown in bold font

Table 6.4: SI values generated in FlowJo to determine optimal antibody concentration for CXCR4 *(fixed cells)*.

Concentration (µg/mL)	Median Positive	Median Negative	84th Percentile of Negative	SI
5	1828	93.8	2877	0.62
10 *	3626	93.8	5568	0.64
15	3518	93.8	5486	0.63
20	3372	93.8	5336	0.62

* The chosen antibody concentration is shown in bold font

Table 6.5: SI values generated in FlowJo to determine optimal antibody concentration for CXCR4 *(unfixed cells)*.

Concentration (µg/mL)	Median Positive	Median Negative	84th Percentile of Negative	SI
1.25	37.2	20.5	74.5	0.31
2.5	41.1	20.5	105	0.24
5	41.1	20.5	117	0.21
10	56.5	20.5	329	0.12
20	56.5	20.5	297	0.13

6.3.1.5 Compensation

When performing multicolour fluorescence studies using flow cytometry, spectral overlap between fluorophores can occur as they emit photons across a spectrum of energies and wavelengths that can be detected by multiple detectors within the machine. In order to account for this, compensation[35] is performed to determine the percentage of overspill between channels of interest, which can then be applied to files prior to analysis to ensure accurate data interpretation. To do this, two single stained compensation controls *(Live/Dead™ stained only and antibody stained/unstained)* were assessed in addition to an unstained control.

As seen in Figure *6.6*., density plots were generated in NovoExpress® before each control had an oval gate placed around each population of interest using parameters: FSC-A vs. SSC-A. To the unstained *(fixed)* control data set (Figure *6.6*a), a tight quadrant gate was placed at the edge of the population *(using parameters: FITC-A vs. APC-A)* to get a sense of where subsequent gates would be placed on single stained controls. A quadrant gate was then applied to the single stained control: Live/Dead™ stained only *(using parameters: FITC-A vs. APC-A)*. Since live cells take up some of the Live/Dead™ stain, but not to the same degree as dead cells do, two localised populations *(Figure 6.6b, FITC-A vs. APC-A)* were observed and the appropriate gating was applied to distinguish between them. Furthermore, the limited uptake of the stain by live cells meant brighter expression in the APC channel, when compared to the APC expression of the unstained cells *(Figure 6.6a, FITC-A vs. APC-A*), which was to be expected. A statistics table (Figure *6.6*b) was generated to show median-X values for the quadrants of interest: Q_1 *(APC^+)* and Q_3 *(APC^-),* where spillover was manually determined by adjusting the populations along the x-axis, such that they had almost identical values in the FITC-A channel, which equated to 0.15% compensation, indicating 0.15% spillover of APC into the FITC channel (Table *6.6*). To the second single stained compensation control: antibody stained/unstained (Figure *6.6*c), a quadrant gate was applied to separate $FITC^{+/-}$ populations. The antibody compensation percentage from the previous control was applied to the antibody stained/unstained control before a statistics table was generated to show median-Y values for quadrants Q_3 *($FITC^-$)* and Q_4 *($FITC^+$)*. Manual spillover was determined by adjusting the populations along the y-axis, such that they had identical values in the APC channel, which equated to 3.97% compensation indicating 3.97% spillover of FITC into the APC channel (Table *6.6*).

[35] A mathematical method where controls are used to measure the photons of a single fluorophore across multiple detectors used in the experiment.

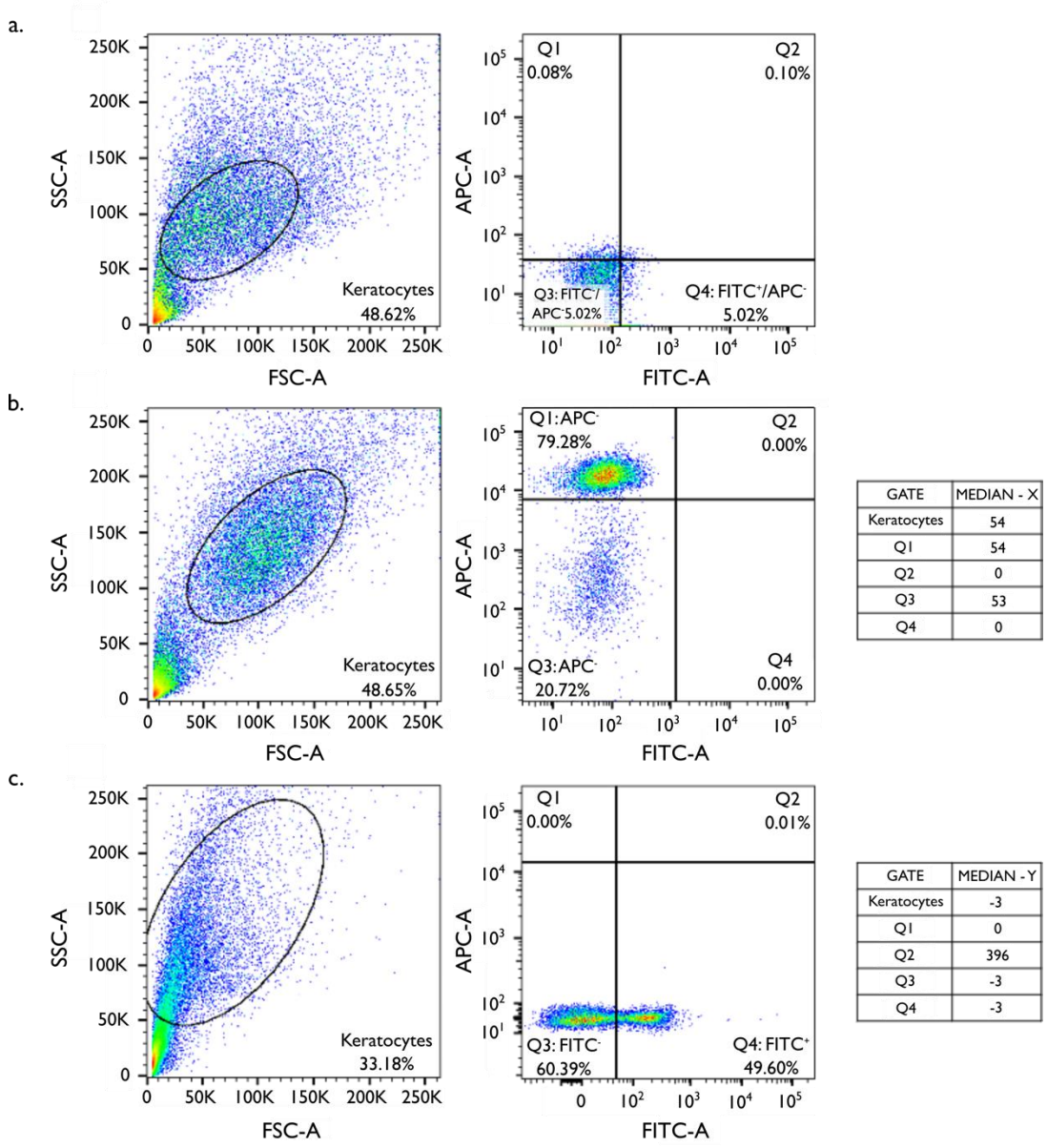

Figure 6.6: Gating strategies applied to samples for the compensation of spillover between FITC and APC channels. An oval gate was applied around keratocyte populations using the forwards scatter-area *(FSC-A)* vs. side scatter-area *(SSC-A)* parameter, followed by quadrant gates being applied to the FITC-A vs. APC-A parameters to separate positive and negative populations for the unstained control. (a.), Live/Dead™ stained only (b.), and antibody stained/unstained (c.).

Table 6.6: Compensation matrix of spillover percentages for FITC into APC channel and APC into FITC channel.

Source/Target	FITC	APC
FITC	100%	3.97%
APC	0.15%	100%

6.3.2 Evidence of Expression Location of Markers

Figure *6.7* displays flow cytometry plots with applied gating strategies to generate MedFI values indicative of expression for CX43, PAX6, and Bmi-1, obtained from cultured E_{18} keratocytes pre-treated with either, (a) fixative and permeabilising detergent, or (b) left untreated, prior to immunostaining. Following pre-treatment with both fixative and permeabilising detergent, greater MedFIs were reported for all three markers *(CX43 MedFI = 1902, PAX6 MedFI =139, Bmi-1 MedFI =2323)* in comparison to samples left untreated prior to immunostaining *(CX43 MedFI = 29.5, PAX6 MedFI =23.1, Bmi-1 MedFI =27)*. It should be noted that even without pre-treatment, expression of CX43, PAX6, and Bmi-1 was present, but at a minimal amount.

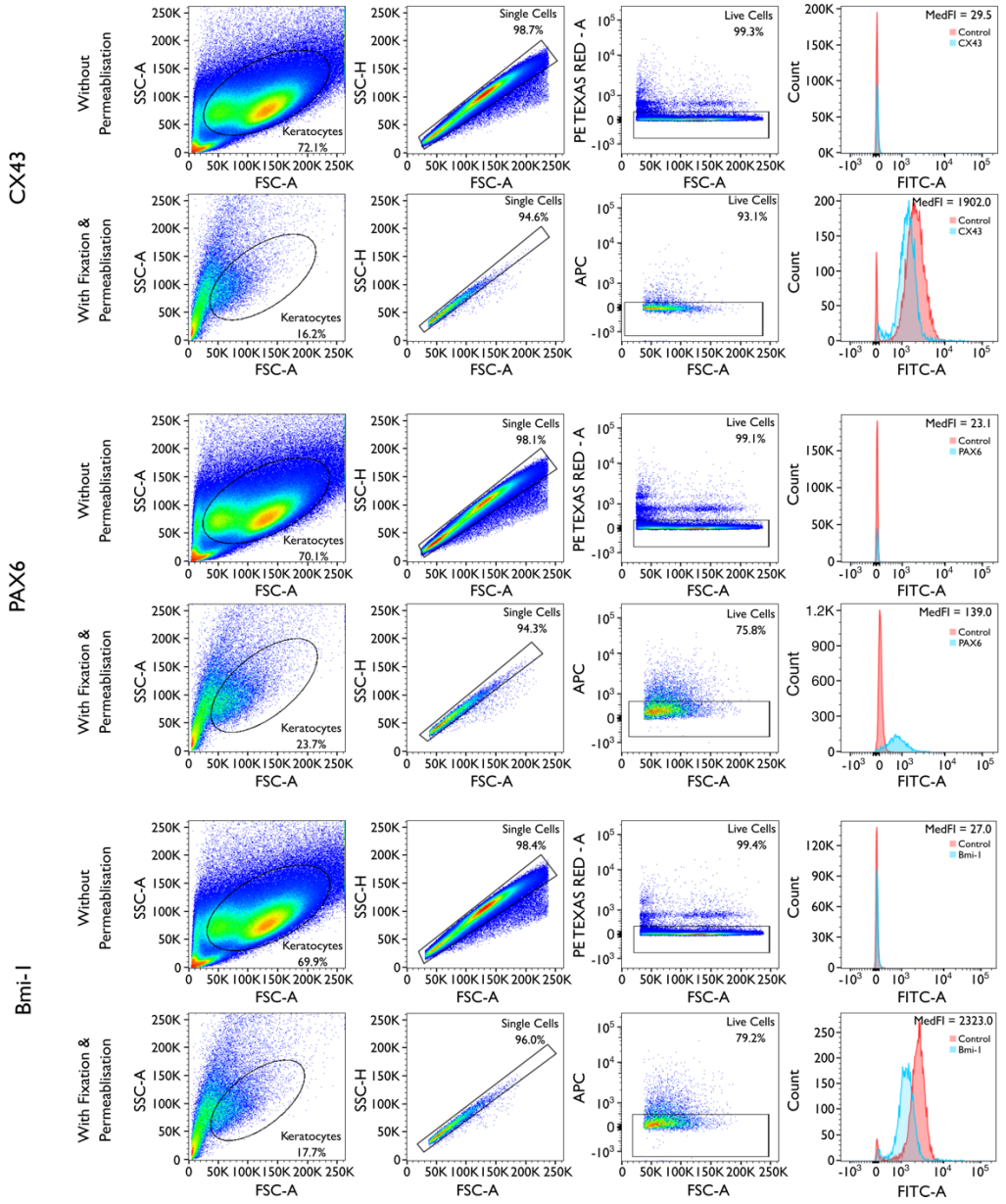

Figure 6.7: Comparison of median fluorescence intensity *(MedFI)* between untreated and treated *(fixed and permeabilised)* cells to assess antigen locations for CX43, PAX6, and Bmi-1. Prior to antibody staining, E_{18} keratocytes cultured to P_2 were either (a) untreated or (b) treated with 4% *(v/v)* paraformaldehyde and 0.2% *(v/v)* Tween® 20, prior to immunostaining with antibodies for CX43, PAX6, and Bmi-1. Flow cytometry plots show gating strategies applied to isolate cells of interest from debris *(FSC-A vs. SSC-A),* doublets *(FSC-A vs. SSC-H),* and dead cells *(FSC-A vs. PE Texas Red -A or APC)*, to generate histogram overlays of each sample and its corresponding control. The stated MedFI values on the histogram overlays correspond to the samples.

Overall, this shows that the antigen binding sites are primarily localised intracellularly for CX43, PAX6, and Bmi-1.

6.3.3 Expression of Putative Stromal Stem Cell Markers Using GAG Coated Culture Plates

Figure *6.8* shows micrographs taken at P_0 to document the pattern of E_{18} keratocyte growth on uncoated, crude CS-7D4/KS-5D4, and enhanced $6C3^{+++}/5D4^{-}$ coated culture plates. Keratocytes grown on uncoated dishes (Figure *6.8*a) grew in a non-specific, diffuse manner taking on average two to three full days to reach 100% confluency, whereas keratocytes growth on crude CS-7D4/KS-5D4 (Figure *6.8*b) and enhanced $6C3^{+++}/5D4^{-}$ coated (Figure *6.8*c) culture dishes formed multiple colony-like aggregates across the dish, taking greater than 7 days on average to reach 100% confluency.

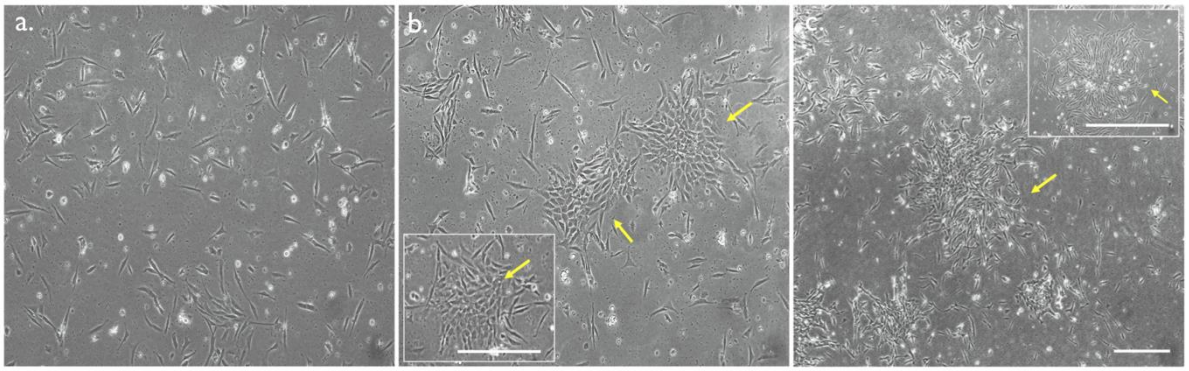

Figure 6.8: Phase contrast microscopy showing variation in growth pattern of cultured E_{18} keratocytes at P_0 *(Day 2)* with different coating conditions. Micrographs of cells cultured on uncoated dishes (a.) showed diffuse growth across the dish taking up to two days to reach 100% confluency, whereas cells cultured on crude CS-7D4/KS-5D4 (b.) and enhanced $6C3^{+++}/5D4^{-}$ (c.) coated culture dishes showed spherical colony growth *(arrows)* with 100% confluency being reached after seven days. Scale bars represents 20 μm.

Figure *6.9* shows micrographs of E_{18} keratocytes cultured to P_5 on uncoated, crude CS-7D4/KS-5D4 and enhanced $6C3^{+++}/5D4^{-}$ coated culture dishes. Differences in the morphology of cells cultured on crude CS-7D4/KS-5D4 and enhanced $6C3^{+++}/5D4^{-}$ coated culture dishes are evident when compared to cells cultured on uncoated dishes. Specifically, cells cultured on crude CS-7D4/KS-5D4 coating exhibited a spindle-shaped morphology with long, thin cytoplasmic processes extending from both ends of the cell (Figure *6.9*b). On the contrary, cells cultured on enhanced $6C3^{+++}/5D4^{-}$ coating had a mix of spindle-shaped cells *(red arrowheads)* and rectangular widespread cells *(yellow arrowheads)* (Figure *6.9*c).

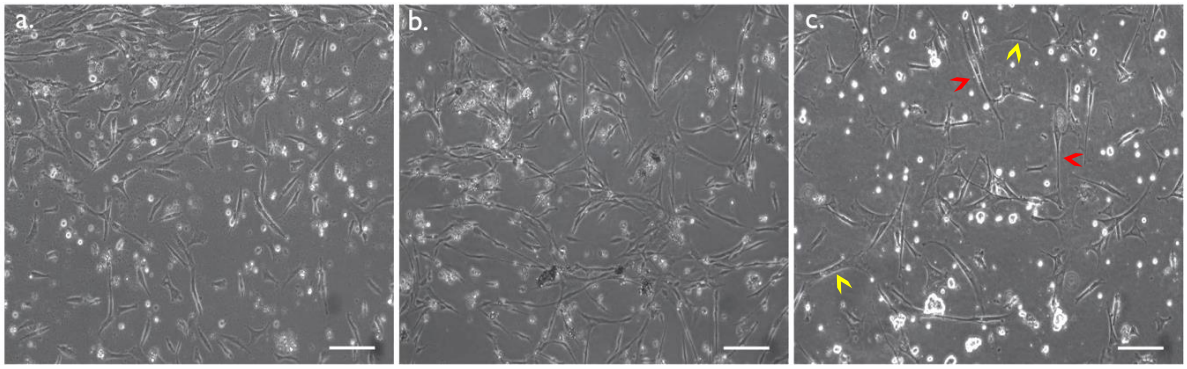

Figure 6.9: Phase-contrast microscopy of P_5 (Day 2) cultured E_{18} keratocytes across coating conditions. Micrographs of the cells exhibit a difference in phenotype presentation following growth on uncoated (a.), crude CS-7D4/KS-5D4 coated (b.), and Enhanced $6C3^{+++}/5D4^{-}$ (c.) coated dishes. Rectangular *cells (yellow arrowheads)*, Spindle-shaped cells *(red arrowheads)*. Scale bars represents 100 μm.

6.3.3.1 Marker Expression Between Coating Conditions

In the present study, repeat instrument measurements *(n=5)* of marker expression taken at each passage for each antibody and coating condition were included in the analysis. Table *6.7* displays marker expression *(nMedFI)* for each passage and antibody[36], in addition to the average marker expression across all passages for each antibody and coating condition. A repeated-measures ANOVA of marker expression obtained across coating conditions was significant for each antibody (Table *6.8*). Pair-wise post-hoc comparisons showed cell expression for CX43 significantly increased when cultured on crude CS-7D4/KS-5D4 coating and significantly decreased when cultured on enhanced $6C3^{+++}/5D4^{-}$ coating, compared to the cell expression of the uncoated control (Table *6.9*). However, marker expression by cells overall was significantly higher in the crude condition compared to the enhanced condition for CX43 (Table *6.9*). For markers PAX6, Bmi-1, and CXCR4, there was a significant increase in cell expression for both crude CS-7D4/KS-5D4 and enhanced $6C3^{+++}/5D4^{-}$ coatings, compared to the cell expression of the uncoated control (Table *6.9*). In contrast to CX43, marker expression by cells overall was significantly lower for the crude CS-7D4/KS-5D4 coating compared to the enhanced $6C3^{+++}/5D4^{-}$ coating for PAX6, Bmi-1, and CXCR4.

[36] The variability between repeated analyses of each sample for all passages and coating conditions never exceeded 14.6%.

Table 6.7: Summary of putative stromal stem cell marker expression *(nMedFI)* across passages for E_{18} keratocytes cultured on uncoated, crude CS-7D4/KS-5D4, and enhanced CS-6C3^{+++}/KS-5D4^{-} coated culture plates.

Antibody	P_0	P_2	P_3	P_4	P_5	Average *(Mean nMedFI ± SD)*
Uncoated *(Mean nMedFI)*						
n	5	5	5	5	5	
CX43	0.77	1.46	1.35	1.49	1.67	1.35 ± 0.34
PAX6	0.14	0.18	0.12	0.11	0.13	0.14 ± 0.03
Bmi-1	1.31	1.79	0.97	0.79	1.75	1.32 ± 0.45
CXCR4	0.29	0.38	1.67	1.62	1.55	1.10 ± 0.70
Crude CS-7D4/KS-5D4 *(Mean nMedFI)*						
CX43	0.77	3.81	1.39	2.35	1.95	2.05 ± 1.15
PAX6	0.14	0.48	0.20	0.19	0.27	0.26 ± 0.13
Bmi-1	1.31	3.17	1.41	1.36	1.98	1.85 ± 0.79
CXCR4	0.29	2.58	2.26	3.35	2.76	2.25 ± 1.16
Enhanced CS-6C3^{+++}/KS-5D4^{-} *(Mean nMedFI)*						
CX43	0.77	0.23	0.19	0.19	0.18	0.31 ± 0.26
PAX6	0.14	0.34	0.27	0.40	0.45	0.32 ± 0.12
Bmi-1	1.31	1.74	2.39	1.53	2.65	1.92 ± 0.57
CXCR4	0.29	3.36	3.70	2.37	3.58	2.66 ± 1.42

Table 6.8: Repeated-measures ANOVA of nMedFI across all passages for each putative stromal stem cell marker and coating condition.

Antibody	Repeated-measures ANOVA
CX43	$F_{2,4} = 2723.35$, $\eta_p^2 = 0.30$, 95% CI [0.12, 0.48], $p < 0.001$**
PAX6	$F_{2,4} = 117.26$, $\eta_p^2 = 0.30$, 95% CI [0.25, 0.41], $p < 0.001$**
Bmi-1	$F_{2,4} = 1508.91$, $\eta_p^2 = 0.36$, 95% CI [0.26, 0.48], $p < 0.001$**
CXCR4	$F_{2,4} = 241.13$, $\eta_p^2 = 0.18$, 95% CI [0.10, 0.29], $p < 0.001$**

*** p < 0.05, ** p < 0.001**

Table 6.9: Post-hoc comparisons *(Bonferroni)* of nMedFI's obtained with each PSSC marker from pairwise combinations of coating conditions.

Antibody	Post-hoc comparisons (p_{bonf})		
	Uncoated vs. Crude (CS-7D4/KS-5D4) Coated	**Uncoated vs. Enhanced (CS-6C3^{+++}/KS-5D4^{-}) Coated**	**Crude (CS-7D4/KS-5D4) Coated vs. Enhanced (CS-6C3^{+++}/KS-5D4^{-}) Coated**
CX43	< 0.001**	< 0.001**	< 0.001**
PAX6	< 0.001**	< 0.001**	< 0.001**
Bmi-1	< 0.001**	< 0.001**	< 0.001**
CXCR4	< 0.001**	< 0.001**	< 0.001**

*** p < 0.05, ** p < 0.001**

6.3.3.2 Marker Expression Across Passages (Within Each Coating Condition)

Figure *6.10* – Figure *6.13* display a regression line for marker expression *(nMedFI)* against passage for each coating condition and antibody. Table *6.10* summarises the regression coefficients for the relationships between nMedFI and passages for each coating condition and antibody. For CX43, the regression coefficients reported a significantly positive relationship between nMedFI and passage for the uncoated condition and a significantly negative relationship for the enhanced 6C3^{+++}/5D4^{-} coating condition (Figure *6.10*). In contrast, there was no significant relationship between expression of CX43 and passage for the crude CS-7D4/KS-5D4 coating condition. For PAX6, the regression coefficients reported a significantly negative relationship for the uncoated condition and a significantly positive relationship for the enhanced 6C3^{+++}/5D4^{-} coating condition (Figure *6.11*). Similar to CX43, there was no significant relationship between expression of PAX6 and passage for the crude CS-7D4/KS-5D4 coating condition. For Bmi-1, the regression coefficients reported a significantly positive relationship for the enhanced 6C3^{+++}/5D4^{-} coating condition only (Figure *6.12*). Whereas, for CXCR4, the regression coefficients reported a significantly positive relationship for all three coating conditions (Figure *6.13*).

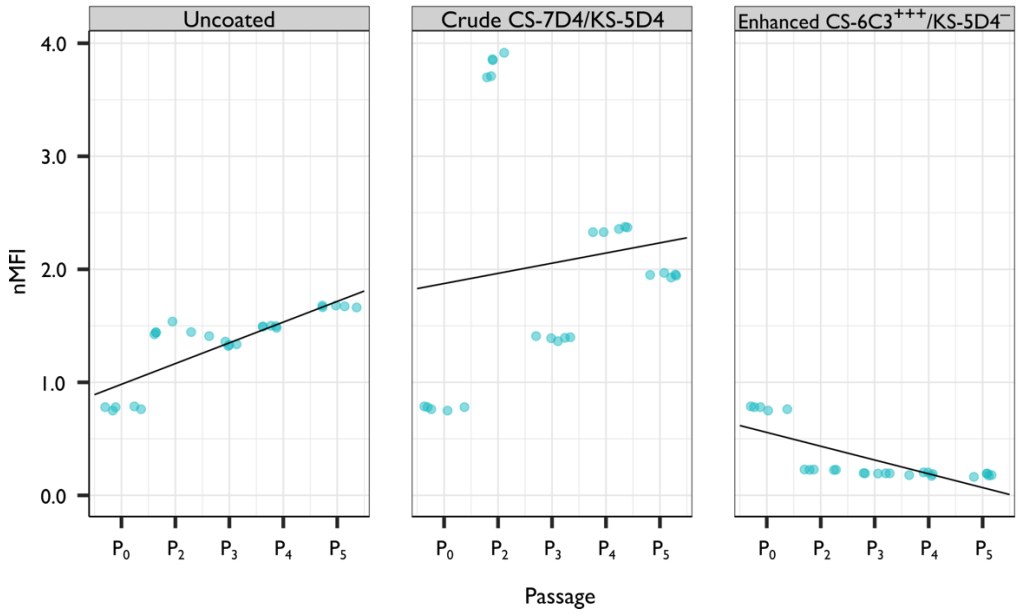

Figure 6.10: Linear regression showing the relationship between nMedFI and passage number in each coating condition for CX43 ***(each point represents a repeated instrument nMedFI measure).***

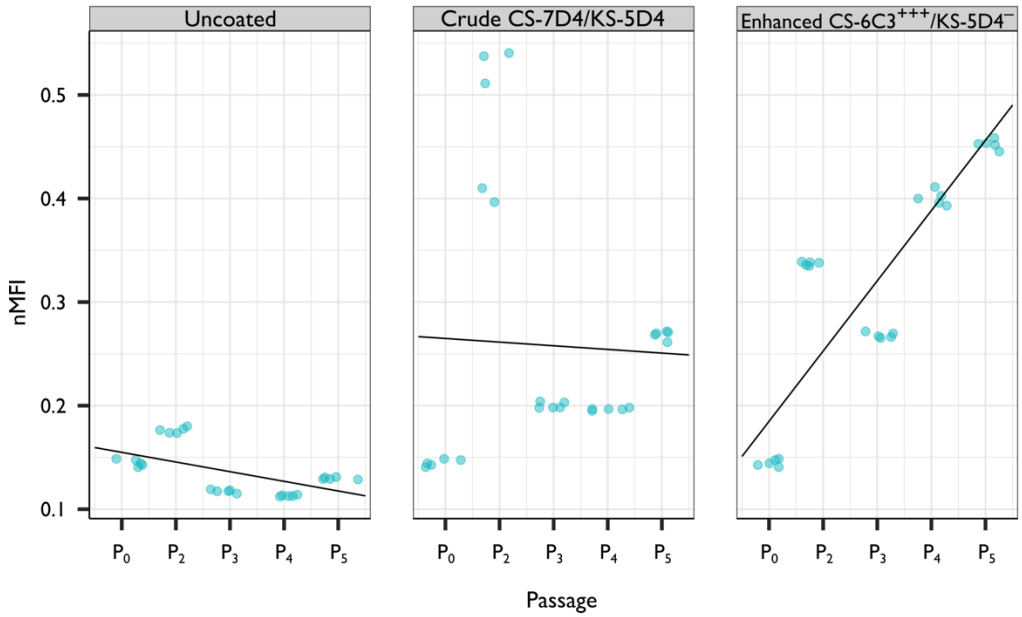

Figure 6.11: Linear regression showing the relationship between nMedFI and passage number in each coating condition for PAX6 ***(each point represents a repeated instrument nMedFI measure).***

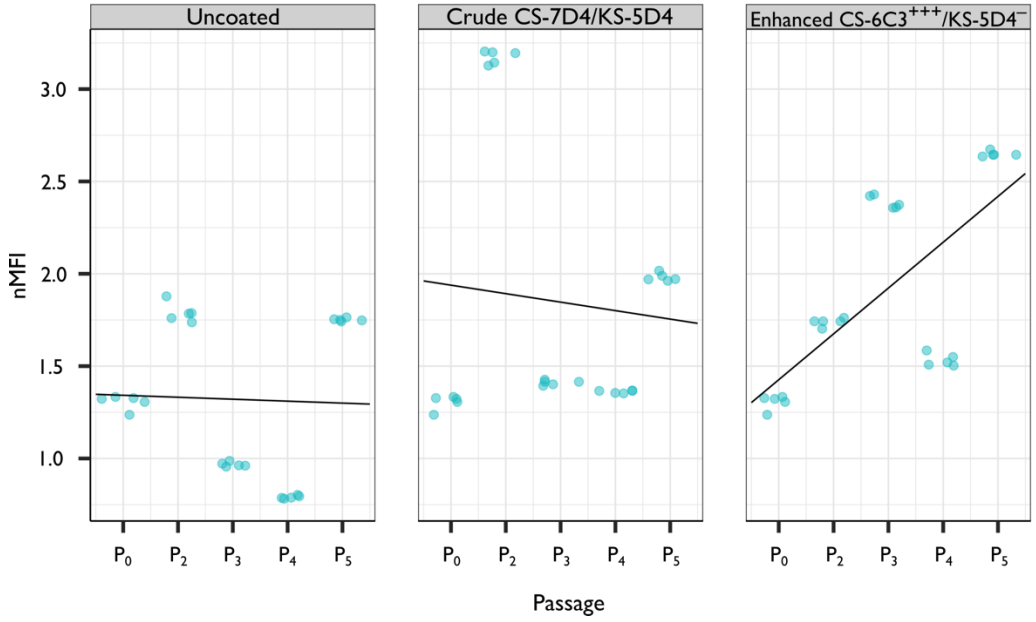

Figure 6.12: Linear regression showing the relationship between nMedFI and passage number in each coating condition for Bmi-1 ***(each point represents a repeated instrument nMedFI measure).***

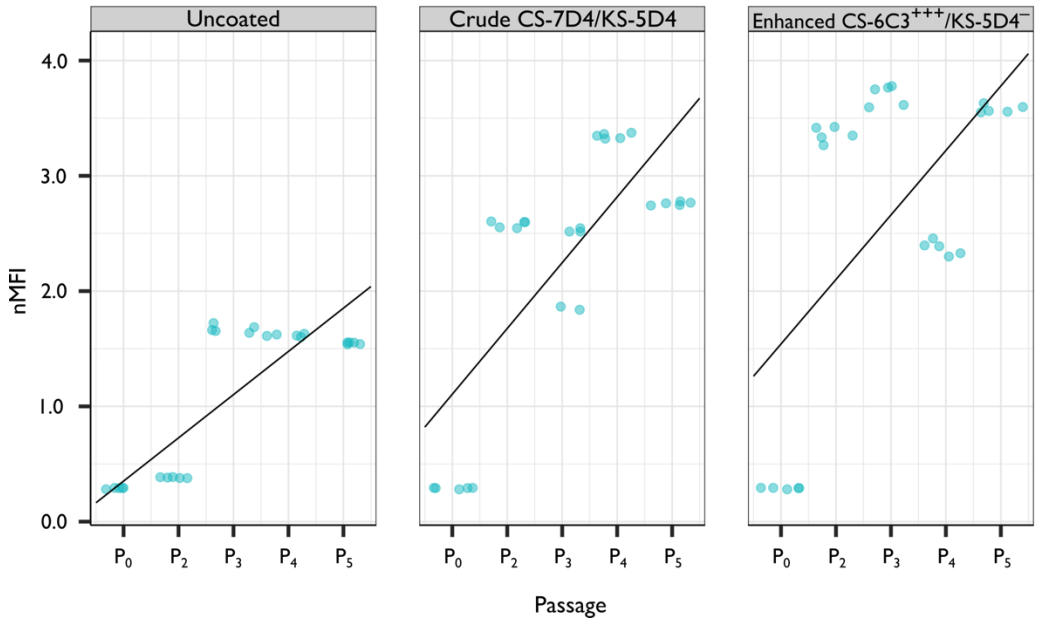

Figure 6.13: Linear regression showing the relationship between nMedFI and passage number in each coating condition for CXCR4 ***(each point represents a repeated instrument nMedFI measure).***

Table 6.10: Regression coefficients for the relationship between nMedFI and passages for each coating condition and putative stromal stem cell marker.

	Uncoated	Crude CS-7D4/KS-5D4	Enhanced CS-6C3^{+++}/KS-5D4^{-}
		CX43	
r	0.18	0.09	-0.12
R^2	0.70	0.03	0.54
p	<0.001**	0.55	<0.001**
F-stat	56.86	0.36	29.39
		PAX6	
r	-0.01	-0.004	0.06
R^2	0.30	0.04	0.78
p	0.002*	0.84	<0.001**
F-stat	11.37	0.04	90.09
		Bmi-1	
r	-0.01	-0.05	0.25
R^2	0.04	0.03	0.45
p	0.86	0.66	<0.001**
F-stat	0.03	0.19	20.26
		CXCR4	
r	0.38	0.57	0.56
R^2	0.70	0.57	0.36
p	<0.001**	<0.001**	<0.001**
F-stat	57.65	33.01	14.41

*** $p < 0.05$, ** $p < 0.001$**

The results of the above investigation show that both crude CS-7D4/KS-5D4 and enhanced 6C3^{+++}/5D4^{-} coatings have a morphological and phenotypical effect on cultured keratocytes. This suggests that cells are adopting a less differentiated state that is sustained across multiple passages.

6.4 Discussion

6.4.1 Optimisation of Experimental Design

In this study, a flow-cytometric method was specifically optimised for embryonic keratocytes extracted from E_{18} chick corneas. This method accounted for the main variables in the protocol required to generate reliable data, however, more minor aspects were exploited from literature so as to not lose sight of the scope of the experimental question. The developed protocol allowed for the quantification of PSSC marker expression by cells cultured on crude CS-7D4/KS-5D4 coated, enhanced CS-6C3^{+++}/KS-5D4^{-} coated, and uncoated culture plates over multiple passages. Initial attempts at performing flow cytometry used a pre-determined protocol provided by a

neighbouring research group that was specific to cell surface staining of live cells. The antibodies used in this study differed from the ones optimised in the provided protocol. The data *(not shown)*, therefore, did not account for location of target proteins, separation of live vs. dead cells, and antibody concentration. Realising the error, a series of sub-experiments were consequently performed on cells *(using the uncoated control condition)* to determine the concentrations, reagents, and compensations necessary for design optimisation.

6.4.1.1 Fixative

Earlier work treated cells with 4% *(v/v)* PFA solution made from a pre-existing reagent stored in the laboratory. Resultant data *(not shown)* exhibited significant amounts of debris when analysed using flow cytometry. Specifically, the plots *(FSC-A vs. SSC-A)* showed localisation of events at the intercept of the x- and y-axis with a dispersion of events also along the y-axis. These findings strongly suggest that cell-lysis, which was confirmed in micrographs taken of this sample, resulted from either old reagent that had polymerised, leading to inadequate fixation, or a damagingly high concentration of PFA. To test this, a fresh bottle of PFA was ordered and prepared such that the new reagent was depolymerised by heating, to generate a monomeric reagent prior to treating cells with a 4% *(v/v)* PFA solution. As a result, minimal debris was observed on the resultant cytometry plot, suggesting preservation of intact cells and thereby ruling out any uncertainty regarding the solutions concentration; it also confirmed that the likely cause of the earlier result was inadequate fixation resulting from a bottle of polymerised PFA. To further substantiate these findings, and future analyses, visual validation and subsequent image acquisition was performed on each sample prior to cytometric analysis.

A panel of aldehyde-based *(PFA)* and alcohol-based fixatives *(ethanol and methanol)*, commonly used in flow cytometry, were tested on cultured cells. PFA-fixed cells required subsequent treatment with permeabilising detergent, whereas those fixed with methanol and ethanol did not as these reagents simultaneously fix and permeabilise cells. PFA-fixed cells were subsequently treated with 0.2% Tween®20 to assess the ability of the fixative to protect cells from damage due to the dissolution of the lipid membrane in an attempt to generate entry points for antibody and dye perfusion. Glutaraldehyde, another aldehyde-based fixative, was omitted from the panel as its application is not wide-spread in flow cytometry. Reports have shown glutaraldehyde cross-links cells more effectively than PFA, whereby hampering the entry of antibodies and dyes into the cell (Prasadarao et al. 1990; Mrini et al. 1995; McKenzie et al. 2019). Furthermore, it has also been shown to markedly increase autofluorescence of the cell, which is problematic as it can hinder

quantification of true expression (Abay et al. 2019). The results of this study showed cells fixed with PFA had a similar profile to the control population, whereas, both alcohol-based fixatives resulted in dehydration of the cell *(a known outcome)* that in turn affected the FSC-A vs. SCA-A plot, indicative of cell shrinkage and aggregate formation. All fixatives did maintain the cells overall integrity, as shown in the corresponding micrographs of each sample, however, cells fixed with PFA maintained a similar profile to unfixed control cells and no cellular aggregates were observed when imaging the sample. The risk of cellular aggregation had to be avoided as it would reduce the reliability of the data set, with fewer cells included in the final analysis following doublet cells exclusion. As such, 4% *(v/v)* PFA was selected as the optimal fixative for the primary investigation into PSSC marker expression in keratocytes, as it retained a similar profile *(granularity and size)* to control cells and no cellular aggregates were seen.

6.4.1.1.1 Pre/Post- Fixation for Cell Surface Signalling

Unlike in the detection of intracellular epitopes, where fixation is the foremost step preceding permeabilisation and immunofluorescence staining, cell surface epitope detection can accommodate fixation prior to or after immunofluorescence staining. Both approaches require careful consideration as, in some instances, when fixation is performed prior to staining, antibody binding to target epitopes can be impaired due to the tendency of fixatives to alter antigen-epitope conformation, thus rendering it unreactive with an antibody (Dapson 2007; Scalia et al. 2016). Moreover, a dampening of the signal associated with the fluorophore of the conjugated antibody can occur when fixation is undertaken after staining (Stewart et al. 2007). The results of this experiment showed a considerably higher MedFI when immunofluorescence treatment followed fixation, as opposed to when performed before. However, based on these results it cannot be deduced if the fixative had altered the antigen-epitope structure. Conversely, the lower MedFI recorded when immunofluorescence treatment preceded fixation could have presumably resulted from antibody cross-linking multiple surface epitope binding sites, leading to a dampening of the resultant expression; again, this cannot be proven based on these findings alone. What can be determined is that for cell-surface staining, it was more appropriate to fix cells prior to immunostaining, as this yielded a remarkably elevated MedFI, over that seen with the reverse treatment sequence.

6.4.1.2 Permeabilising Detergent

Following the determination of the appropriate fixative, further work was done to establish a suitable permeabilising detergent that would yield the greatest amount of intracellular staining for

CX43, PAX6, and Bmi-1, as identified by the resultant MedFI. Three non-ionic detergents *(Tween®20, Saponin, and Triton X-100)* were used in preference to ionic detergents, as they are milder in their action of breaking protein-lipid and lipid-lipid associations with the added benefit of not denaturing proteins (Johnson 2013). In a study by Amidzadeh et al. (2014), Triton X-100, Tween®20, and Saponin were tested at varying concentrations and incubation times to determine the most appropriate protocol to yield the maximum fluorescence intensity for HeLA cells pre-fixed with PFA. Their results determined that permeabilisation using 0.2% Tween®20 for 30 minutes resulted in maximum fluorescence intensity. Moreover, all tested parameters for Tween®20 generated an expression that greatly exceeded the expressions obtained by any equivalent modification to Triton X-100 or Saponin parameters (Amidzadeh et al. 2014). Consequently, it was the protocol selected for use in this investigation with respect to Tween ®20. In contrast, a concentration of 0.1% *(v/v)* Triton X-100, at an incubation time of 10 minutes, was used based on the protocol recommended by Abcam; as Triton X-100 is a harsher detergent, compared to the other two, higher concentrations and incubation times can lead to excessive disruption of membrane proteins, which can affect staining results and for that reason a lower concentration and incubation time were used in this investigation (Abcam.com 2021). As for Saponin, which is a milder membrane solubiliser that creates large membrane pores, a concentration of 0.1% *(w/v),* with an incubation time of 15 minutes, was used according to the recommendation by Bio-Rad (Bio-Rad 2021b). From the results, it was apparent that Tween®20 produced the highest MedFI for all antibodies and presented no cellular aggregates, meaning that it would not lead to fewer cells in the final analysis, thereby reducing the reliability of the data set and any subsequent comparisons between passages.

6.4.1.3 Antibody Titration

Antibody titration is a key element of the larger process of panel optimization in flow cytometry. It is performed to empirically ascertain the smallest quantity of antibody needed to achieve antigen binding saturation, in addition to optimising the intensity of the fluorescence signal by minimizing background fluorescence. Through this process, robust data can be acquired by enhancing the resolution for population identification and the measurement of expression levels of target cells. Antibody concentrations ranged from 5-20 μg/mL with considerations being made to incorporate concentrations above and below the recommended amounts by each manufacturer. Titration curves were generated and the concentration that provided the highest SI was selected. In the case of Bmi-1, where two concentrations generated the same SI, the higher concentration was selected to ensure an excess of antibody was present in the event of higher-than-expected number of cells

in the sample. It was clear from the results that 10 μg/mL was the optimal concentration for antibodies CX43, PAX6, Bmi-1, and CXCR4. To answer an earlier question of whether cross-linking was a factor that led to a diminished MedFI in the post-fixation condition, a titration was also performed on unfixed cells. This showed that as antibody concentration increased, the SI decreased, indicating the antibody was most likely cross-linking on the membrane, resulting in reduced fluorescence, an adverse effect sometimes associated with using a polyclonal antibody on unfixed cells (Sulzer et al. 1996). These findings further substantiated that fixation of cells, with respect to CXCR4, was necessary to mitigate against cross-linking to expose the true fluorescence expression.

6.4.1.4 Data Analysis

6.4.1.4.1 Using Separation Index vs. Staining Index

To determine the optimal concentration for each antibody, a titration curve was generated from the SI between the negative control and each of the antibody-stained cell samples. Separation index and staining index are similar; however, the staining index uses the standard deviation, instead of percentiles, to estimate the difference between the positive signal of the fluorescing cells and the negative background noise (Telford et al. 2009). Both methods actively calculate the robust standard deviation. However, the staining index functions to minimise the relatively large error associated with the distribution of background fluorescence by weighting the right-hand slope of the control peak more heavily, so as to exclude events at the lowest point of the axis that would reduce the difference between positive and negative populations (Telford et al. 2009).

6.4.1.4.2 Using nMedFI vs. Percent Positive Cells

Flow cytometry is a well-established method that offers sensitive and repeatable identification of rare populations, assessment of marker expression, and tracking of cellular differentiation (Chan et al. 2013). The current approach for post-data acquisition analysis uses a gating strategy based on the negative control to set the threshold for determining positive events. For this method, the threshold of the gate is positioned such that it incorporates less than one percent of cells from the negative control. This gate can then be applied to corresponding samples and the cells included within the gate are termed as % positives, that is, the percentage of positively expressing cells (Chan et al. 2013). The reliance of this method on the negative control, however, draws attention to two of its major limitations. Firstly, the gate sums the number of events that fall within a range *(usually 3 logarithmic units)* of fluorescence intensity, resulting in a loss of resolution, as it does not

account for small shifts within the gating range. These seemingly inconsequential shifts are, however, important indicators of the cells state within the population of interest and provide insight into their progression through cell differentiation by the up- and down-regulation of marker expression (Chan et al. 2013). Secondly, this gating strategy is vulnerable to skewing because the threshold gate is placed to incorporate less than one percent of the positive cells from the negative control, which will often contain outliers (Chan et al. 2013). This poses a problem in circumstances where the number of outliers increases, as it will skew the gate more towards the right, thereby resulting in a percent positive value for the sample that is inaccurately low (Chan et al. 2013). This is problematic especially when investigating differences between two equivalent populations, as masking of expression is likely. That said, Chan et al. (2013) proposed an alternative method for data analysis based on MedFIs that are normalised to the negative control. They found that by normalising the MedFI of the sample to the MedFI of the corresponding control, they could accurately track the subtle changes that the percentage positive method could not, for pluripotent marker expression within the population of human embryonic stem cells (Chan et al. 2013). This method is growing in its application and is quickly becoming exploited by researchers within the stem cell field (Davies et al. 2016; El-Gamal et al. 2020). For these reasons, the data from this study was analysed using the nMedFI approach, to quantify and monitor the expressional changes of PSSC markers by embryonic keratocytes across multiple passages and coating condition more accurately.

6.4.2 Expression Location of CX43, PAX6, and Bmi-1

In the process of optimising a flow cytometry protocol for embryonic keratocytes, data was available for cells treated and untreated with permeabilising detergent prior to immunostaining. Cells subcultured to P_2 were immunostained using the same protocol for each treatment condition. Subsequent analysis using flow cytometry was done to generate MedFI values to contrast each condition, to further substantiate published reports by various researchers with respect to the immunolocalisation of cellular staining for CX43, PAX6, and Bmi-1. Flow cytometric data also provided validation for *in vitro* results of the aforementioned markers from Chapter 3. As expected, the result of this present study supports literature reporting localised CX43 immunostaining at the cell surface and within intracellular compartments of various cell types (Musil et al. 1990; Langlois et al. 2007; Johansen et al. 2011; Tittarelli et al. 2015; Xu et al. 2019; Au et al. 2020). Likewise, the results were also in agreement with earlier reports of nuclear and cytoplasmic staining for PAX6 and Bmi-1 (Voncken et al. 1999; Funderburgh et al. 2005; Reza et al. 2011; Robson et al. 2011; Sidney et al. 2015; Yogarajah et al. 2016; Ghoubay-Benallaoua et al. 2017; Chen et al. 2019). To

my knowledge, this is the first study using flow cytometry to show definitively that signalling of markers CX43, PAX6, and Bmi-1 is predominantly localised intracellularly as opposed to on the membrane surface.

6.4.3 The Effect of Coating Condition on Keratocyte Morphology *In Vitro*

In the current study, phase contrast images were acquired of embryonic keratocytes cultured on crude CS-7D4/KS-5D4 coated, enhanced CS-6C3^{+++}/KS-5D4^{-} coated, and uncoated culture plates. Qualitatively, the findings showed obvious morphological differences in the cells grown on the uncoated control plates versus both the crude and enhanced coated plates. Foundational work by Jester et al. (1994) documented the morphology of quiescent keratocytes as stellate in nature which was also shown to be maintained in serum-free culture conditions (Jester et al. 1994; Lakshman et al. 2010). However, in the presence of serum, keratocytes differentiated into active fibroblasts, as indicated by their adoption of a bipolar morphology (Dahl 1981; Hassel et al. 1992; Lakshman et al. 2010). It is apparent from the results of the present study that cells subcultured in serum did indeed adopt a classic bipolar morphology when grown on uncoated plastic, suggestive of an activated fibroblastic phenotype. However, when cells were cultured on crude CS-7D4/KS-5D4, they adopted a spindle-shaped morphology with thin cytoplasmic process, whereas cells cultured on enhanced CS-6C3^{+++}/KS-5D4^{-} coating adopted a mixture of both a spindle-shaped morphology in addition to a rectangular widespread morphology with an ample cytoplasm. The observation of these two distinct morphologies is similar to that made in De Schauwer et al.'s (2011) investigation of human and equine mesenchymal stem cells *in vitro*. They observed that equine mesenchymal stem cells exhibited either a slender and elongated morphology, or a more cuboidal morphology with shorter cytoplasmic extensions. Furthermore, work by other researchers has led to the categorisation of mesenchymal stem cells into two morphological shapes: (1) slowly replicating, flattened or cuboidal cells, indicative of mature mesenchymal stem cells or (2) rapidly self-renewing, spindle-shaped cells (Docheva et al. 2008; Marciel et al. 2014).

In addition to morphological differences between cells cultured on uncoated and CS-coated plates, differences in the adherence and pattern of cellular growth between coating conditions was also observed. Specifically, when keratocytes were cultured on crude CS-7D4/KS-5D4 and enhanced CS-6C3^{+++}/KS-5D4^{-} coatings, they formed multiple colony-like aggregates across the dish despite being in a single cell suspension, whereas, for cells cultured on uncoated control plates, diffuse adherence was observed without aggregate formation. Funderburgh et al. (2005) noted that keratocyte-derived fibroblasts lost the ability to form spheroids *in vitro* and regarded spheroid-

formation as a specialised characteristic maintained by cloned progenitor cells. From this viewpoint, it appears that cells cultured on the CS-based substrate are therefore, not taking on a differentiated keratocyte phenotype, but rather that of less-differentiated progenitor cells. However, while these observations are exciting, they do not allow for definitive conclusions to be made about the exact nature of these cells. In any case, they are encouraging, as they show to an extent that the crude CS-7D4/KS-5D4 and enhanced CS-6C3^{+++}/KS-5D4^{-} coatings are having an effect on cells *in vitro*. To determine what that effect is, supplementary immunostaining with various mesenchymal stem cell markers and keratocyte matrix markers is necessary.

6.4.4 Comparing the Effect of Coating Conditions on the Phenotypic Expression Profile of Keratocytes *In Vitro*

The results of this study showed a significant difference between the phenotypic profiles of PSSC markers expressed by embryonic keratocytes cultured on crude CS-7D4/KS-5D4-coated, enhanced CS-6C3^{+++}/KS-5D4^{-} coated, and uncoated culture plates. Notably, keratocytes cultured on enhanced CS-6C3^{+++}/KS-5D4^{-} coating revealed an expression profile for cells adopting a more stem cell-like phenotype, compared to the crude CS-7D4/KS-5D4 and uncoated culture conditions. This finding is novel and gives credence to the foremost hypothesis proposed by Hayes et al. (2008) asserting that differentially sulphated[37] CSPGs play a role in regulating the proliferation and differentiation potential of stem/progenitor cells within the stem cell niche. The data showed clearly that the expression profile of keratocytes cultured on the enhanced CS-6C3^{+++}/KS-5D4^{-} coating resulted in the lowest levels for CX43 expression combined with the highest levels of PAX6, Bmi-1, and CXCR4 expression, compared to both the crude CS-7D4/KS-5D4-coated and uncoated conditions.

CX43

Connexins play an integral role in directing cell-cell communications that mediate cellular processes like proliferation, differentiation, and apoptosis (Grueterich et al. 2002). In this study, an apparent down-regulation in phenotypic expression of CX43 by keratocytes was observed when cultured on the enhanced CS-6C3^{+++}/KS-5D4^{-} coating, but it was up-regulated by keratocytes cultured on the crude CS-7D4/KS-5D4 coating, compared to the expression of cells cultured on the uncoated control. Looking within the cornea, expression of CX43 has been well documented in the limbal suprabasal epithelium and anterior stroma *(by corneal fibroblasts)* but absent from the

[37] Minimally sulphated/non-sulphated CSPG isoforms were believed to form a protective barrier around stem/progenitor cells to prevent the binding of cell-signalling molecules which would lead to differentiation (Hayes et al. 2008)

limbal basal epithelium (Grueterich et al. 2002). Derived from various *in vitro* studies, Chen et al. (2006) was amongst the first to assert CX43 as a reliable, negative marker for stem cell populations. It was observed that primary limbal cultures harboured subpopulations of CX43-negative cells, characterised as being small, less-differentiated, and with a propensity for proliferation (Grueterich et al. 2002; Chen et al. 2006; Sikora et al. 2019). Isolated CX43-negative cells were later shown to represent, at very early stages in ocular development, precursors of basal and putative stem cells of the limbal epithelium (Wolosin et al. 2002: Chen et al. 2006). Correspondingly, Matic et al. (1997a; 2002) demonstrated both corneal epithelium and epidermis stem cells also lacked connexins, as did presumptive stem cells *(identified by their retention of tracer dye lucifer yellow)* within mice vibrissae. Given these findings, the evident down-regulation of CX43 by keratocytes cultured on enhanced CS-6C3^{+++}/KS-5D4^{-} coating could be viewed as cells adopting a less-differentiated phenotype. Matic speculated that the presence of CX43 would make a cell vulnerable to insult, which in turn would affect neighbouring cells, whereas the absence of CX43 would, therefore, confer survival advantageous to multipotent cells (Matic 1997a). Incidentally, the up-regulation of CX43 expression by cells cultured on crude CS-7D4/KS-5D4 coating does not therefore imply cells are terminally differentiated, when considering all other PSSC markers were also up-regulated by cells cultured on this coating. Haematopoietic stem cells within bone marrow have been seen to contain a CX43^{+} network of stromal cells that up-regulates CX43 to allow communication between stromal and stem cells before stem cell division (Rosendaal et al. 1994; Cancelas et al. 2000; Shanmuganathan et al. 2007). Human corneal epithelial cells were similarly seen to up-regulate CX43 expression in corneal fibroblasts in co-culture suggesting that the interaction between the two cell populations was linked to homeostasis of the corneal stroma (Ko et al. 2009). Since early eTACs are undifferentiated cells in transition between stem cells and differentiated cells, the up-regulation of CX43 together with the up-regulation of stem cell markers PAX6, Bmi-1 and CXCR4 might indicate an adoption of an eTAC phenotype on course to differentiate in the future. Similar speculations have been made by Joseph et al. (2004), who suggested that CX43 expression in the basal cornea was acquired during the differentiation of TACs. Secker and Daniels (2008) have also implied crosstalk between cells facilitated by CX43 were more readily utilised by eTACs, as demonstrated by the up-regulation of CX43 in the basal epithelium except at the limbus, which in turn has allowed for the differentiation between eTACs and limbal epithelial cells (Matic1997a; 1997b; Wolosin et al. 2000; Espana et al. 2003). Changes in CX43 expression were investigated in rabbit corneas by Ratkay-Traub et al. (2001) following excimer laser photorefractive keratectomy, revealing an up-regulation and relocation of CX43 expression to the upper cell layers of the stratified epithelium following surgery (Zhai et al. 2014). Further investigation by Laux-

Fenton (2003), using a rat corneal epithelial scrape wound model, showed down-regulation of CX43 in migrating epithelium at the site of the wound, however, dividing epithelium further back from the wounds edge showed an up-regulation in CX43 levels (Zhai et al. 2014). Though there were some parallels between the CS-based coatings, with respect to the expression trends for PAX6, Bmi-1, and CXCR4, the up-regulation in CX43 levels using the crude CS-7D4/KS-5D4 coating and down-regulation of CX43 using the enhanced CS-6C3^{+++}/KS-5D4^{-} coating was an interesting observation that would suggest differences in substrate composition *(i.e., epitope, whole GAG complex vs. only PGs)* is leading to distinct outcomes in phenotypic profiles.

PAX6

The paired-domain, transcription factor PAX6 is fundamental to the early development of much of the CNS, cerebral cortex, spinal cord, in addition to the eye (Hill et al. 1991; Glaser et al. 1994; Simpson and Price 2002; Sansom et al. 2009). Through phenotypic investigations of the gain- and loss-of-PAX6 function in neural stem cells, Sansom et al. (2009) established the important involvement of PAX6 in directing neural stem cell self-renewal, cell fate determination, and neurogenesis (Sansom et al. 2009). Interestingly, they found that the system was driven towards neurogenesis and basal progenitor cell genesis with an increase in PAX6 expression, whereas, the absence of PAX6 resulted in reduced stem cell renewal (Sansom et al. 2009). In relation to the eye, PAX6 is necessary for ocular development and is expressed by several embryonic ocular tissues but is absent from adult keratocytes (Collinson et al. 2003; Funderburgh et al. 2005). However, within the adult corneal stroma, reports have also shown a subpopulation of cells which retain the ability to divide extensively and generate adult keratocytes (Du et al. 2005; Funderburgh et al. 2005; West-Mays and Dwivedi 2006). These cells, referred to as progenitor cells, show strong nuclear immunostaining of PAX6 protein when cultured, whereas primary keratocytes cultured under the same conditions exhibit only a weak level of PAX6 protein expression (Funderburgh et al. 2005). *In situ* immunostaining also maintained that only rare cells were seen to express PAX6 in intact corneal stromas, making up roughly four percent of the total population (Funderburgh et al. 2005). In this study, PAX6 levels were elevated more for cells cultured on enhanced CS-6C3^{+++}/KS-5D4^{-} coating than crude CS-7D4/KS-5D4 coating however, both remained higher in expression compared to the uncoated condition, which saw a down-regulation of expression across passages. Funderburgh et al. (2005) established that progenitor cells and keratocytes could be distinguished on the basis of up-regulating known stem cells genes previously identified across multiple organ

systems. They determined that Bmi-1[38] was one of the markers that was distinctly up-regulated by keratocyte precursor cells. Indeed, this up-regulation was also noted here in both CS-based coating conditions; however, for the uncoated condition Bmi-1 was seen to decline throughout repeated passages. These findings, taken together with the conclusions from Du et al. (2005) and Funderburgh et al. (2005), provide strong evidence for cells cultured on both crude and enhanced coatings transitioning towards a less-differentiated state gaining both multipotentiality and self-renewal capabilities.

Bmi-1

Recent observations have identified Bmi-1, a polycomb complex protein, as an essential player in the self-renewal of stem cells in a number of organ systems (Park et al. 2003; Molofsky et al. 2003; Iwama et al. 2004; Biehs et al. 2013; Kalha et al. 2018). Notable investigations have shown both haematopoietic and neuronal stem cells to be highly expressive of the Bmi-1 protein (Lessard et al. 1999; Molofsky 2003; Park et al. 2003; 2004). In a knockout study by van der Lugt et al. (1994), postnatal, Bmi-1 null mutant mice were seen to exhibit defects in haematopoiesis, development of the cerebellum, neurological functions, and skeletal patterning. Furthermore, reports by Park et al. (2003) and Molofsky et al. (2003) supported the role of Bmi-1 for the efficient self-renewing cell division of both adult haematopoietic and peripheral/CNS stem cells, but showed that for the generation of differentiated progeny, Bmi-1 was less critical. In the cornea, Bmi-1 expression is well documented in the human, murine, and porcine limbus (Majo et al. 2006; Barbaro et al. 2007; Funderburgh et al. 2016; Kalha et al. 2019). In fact, subpopulations of human corneal stromal stem cells have been shown to positively express Bmi-1(Funderburgh et al. 2016). Conversely, in the murine model, Kalha et al. (2019) reported localisation of Bmi-1^{+} cells in the basal epithelium of the limbus and central cornea; using genetic mapping, the authors demonstrated that the subset of Bmi-1^{+} cells behaved as progenitor cells and renewed local corneal epithelium but did not participate in wound healing following ocular surface injury (Kalha et al. 2019). Interestingly, the findings of this present study clearly show elevated levels of Bmi-1 expression in stromal cells cultured on both enhanced CS-6C3^{+++}/KS-5D4^{-} and crude CS-7D4/KS-5D4 coating, compared to the uncoated control data. Moreover, the expression levels of Bmi-1 were significantly higher for the enhanced CS-6C3^{+++}/KS-5D4^{-} coating, compared to the crude CS-7D4/KS-5D4 coating. Looking at all the aforementioned studies, there is a clear link between Bmi-1 expression and undifferentiated cells, whether that is associated with stem cell or progenitor cell self-renewal, varies between organ and animal model. Nevertheless, the data from this study, when taken

[38] Bmi-1 has been linked to the self-renewal and maintenance of both mesenchymal and neural stem cell populations (Molofsky et al. 2003; Park et al. 2004).

together with the resultant phenotypic profile of stromal cells cultured on different CS-based substrates, are encouraging and suggestive of retention of self-renewal properties exhibited only by undifferentiated cells.

CXCR4

A number of studies have put forth compelling evidence that corneal stromal stem cells, in the limbal niche, provide a support system for the maintenance of native populations of active limbal epithelial stem cells (Zhang et al. 2010; Ainscough et al. 2011; Chen et al. 2011; Li et al. 2012; Xie et al. 2012; Hashmani et al. 2013). Limbal niche cells, in close association anatomically with limbal basal cells, have been shown to modulate limbal stem/progenitor cells via the CXCR4/SDF-1 receptor ligand axis, a connection which reduced differentiation of limbal epithelial stem cells (Chen et al. 2011; Xie et al. 2011; 2012; Li et al. 2014). Xie et al. (2011) also demonstrated that CXCR4, a surface chemokine receptor, was strongly expressed by human limbal stromal niche cells and when inhibited, it disrupted the consolidation of co-isolated populations in culture. What's more, epithelial spheres exhibited loss of holoclone formation and greater corneal differentiation (Xie et al. 2011). Their study provided for the first-time strong evidence that limbal stem cell function was linked to the close physical association with native niche cells via the CXCR4/SDF-1 axis (Xie et al. 2011). The CXCR4/SDF-1 axis has also been shown to be an obligatory component of pancreatic regeneration by way of maintaining duct cell survival and modulation of cell proliferation and migration (Kayali et al. 2003). More recent work by Funderburgh et al. (2016) has also substantiated the high levels of CXCR4 expression in subpopulations of human corneal stromal stem cells. In the present study, elevated levels of CXCR4 were observed in cells cultured on both the enhanced CS-6C3^{+++}/KS-5D4^{-} and crude CS-7D4/KS-5D4 coating, compared to the uncoated control condition. Similar to PAX6 and Bmi-1 expression, CXCR4 expression was also significantly higher for cells cultured on the enhanced CS-6C3^{+++}/KS-5D4^{-} coating, compared to the crude CS-7D4/KS-5D4 coating. The findings of this study, taken together with the aforementioned studies, further supports the assertion that cells cultured on CS-based substrates are likely adopting a less differentiated phenotype *in vitro* with the assistance of the CXCR4 receptor. Like many other chemokine receptors, CXCR4 couples a growing range of signalling molecules and pathways involved in stimulating stem cells expressing the receptor. However, for the purposes of better understanding the effect up-regulation of CXCR4 is having on cultured cells, further work must be done to firstly demonstrate the expression of SDF-1 by these cells and secondly, to perform more robust immunophenotyping, to provide a clearer picture as to what transdifferentiated state cells are adopting when cultured on various CS-based substrates.

6.4.5 Comparing the Effect of Serial Passage on Expression Levels of Putative Stromal Stem Cell Markers for Each Coating Condition

There has been a concerted effort by researchers to develop culture systems that are able to regulate stem cell function for the purposes of tissue engineering. Substrates are one of the more utilised approaches for this mission as they have been shown to influence stem cell functions, such as proliferation, induction or differentiation, self-renewal, and cellular attachments (Joddar et al. 2014). Current cultivation and expansion processes to generate transplantable corneal tissue have been reported by Szabo et al. (2015) to take upwards of three months, with some variability in duration between other research groups. Taking this into account and concurrent to the investigation into the effect crude CS-7D4/KS-5D4 coating, enhanced CS-6C3^{+++}/KS-5D4^{-} coating, and uncoated plastic culture plates had on the expression of PSSC marker expression, addressing the changes in expression over multiple subcultures was also pertinent. This in part was to address if the effects of the expression profiles were transient or sustainable over a longer duration. To my knowledge, it is unknown how long it takes for embryonic keratocytes to transdifferentiate between phenotypes, so it was important to assess expression over multiple subcultures in order to provide ample time for observable changes to occur. The baseline assumption was that expression would not change across passages, however, the results of this investigation showed otherwise for when the enhanced CS-6C3^{+++}/KS-5D4^{-} coating was used, there was a significant correlation between the resultant nMedFI and passage for all four PSSC markers. Specifically, as cells were repeatedly passaged, CX43 expression decreased and conversely, increased for PAX6, Bmi-1, and CXCR4. This is suggestive that cells were still in the process of transdifferentiating and any potential reversal or plateau in the expression profile was not observed in the timeframe of this investigation. However, for the crude CS-7D4/KS-5D4 coating, the relationship between nMedFI and passage was such that a significant increase was only seen for marker CXCR4, whereas for CX43, PAX6, Bmi-1 there was no significant change. Taken together with previous findings, this means that although there was a significant up-regulation in CX43, PAX6, and Bmi-1 expression, compared to the uncoated control, the expression levels remained stable across passages. The reason for this is not so apparent and had the subculturing of cells continued, perhaps more insight would have been gained into whether these findings would hold true, or if the influence of the coating would have gradually changed the expression profile. As this is the first study to examine the effect CS substrate on the multipotentiality of embryonic keratocytes, the findings nevertheless provide an exciting avenue for future investigative work and potential application in therapeutic corneal tissue engineering.

6.4.6 Limitations

One limitation of the present study was that only a single analysis could be performed for each coating condition and passage due to time and material constraints. As a result, the variability of the labelling could not be compared. However, for each coating condition, an instrument repeat of five MedFI measurements was taken for each PSSC at P_0 and P_2-P_5 to assess the variability of the instrument, but the number of cells available for the analysis of each marker and corresponding control restricted how many repeat measures could be performed. Nevertheless, significant differences were evident in the phenotypic expression of PSSC markers by keratocytes cultured on crude CS-7D4/KS-5D4 coated, enhanced CS-6C3^{+++}/KS-5D4^{-} coated, and uncoated culture plates, despite only one analysis being performed.

Moreover, the experimental protocol *(from dissociation of cells from culture plates to analysis on the flow cytometer)* was arduous and for the purposes of this thesis was capped at P_5 to provide an acceptable length of time within which to assess for changes in expression across passages. That being said, significant changes were detected for many of the markers for all coating conditions but nevertheless, if time permitted it would have been informative to see the effect of the coatings on cells over a longer duration. Additionally, due to the limitation in the yield of cells from a single cornea, flow cytometry and subsequent culturing could not be performed. As a result, a pooled sample of corneas was used to overcome this limitation, however, in doing so it has the potential of reducing the significance of any outliers and variability in the data, making the assessment in marker variability between individual corneas infeasible.

Another limitation of this study was the number of PSSC markers analysed using flow cytometry. In the review by Funderburgh et al. (2016), a robust selection of markers associated with pluripotent cells, mesenchymal stem cells, ocular precursor cells, and progenitor cells was analysed with respect to corneal stromal stem cells. However, when considering the time constraints associated with this thesis, the scope of the markers investigated were more realistic for the present framework. In addition, not all markers addressed in Funderburgh's review shared cross-reactivity in chickens, which was a major contributing factor to the initial selection of CX43, PAX6, Bmi-1, and CXCR4 for the study.

6.5 Summary

The results from this study can be summarised as follows:

- In the process of optimising the flow cytometric protocol for embryonic keratocytes, it was determined that 4% *(v/v)* PFA combined with 0.2% *(v/v)* Tween®20 maintained cell membrane integrity but also generated the highest MedFI for intracellular staining for CX43, PAX6, and Bmi-1. Furthermore, fixation prior to immunostaining with CXCR4 prevented cross-linking associated with antibody binding to cell-surface receptors to generate the highest MedFI. Moreover, a concentration of 10 μg/mL was determined to produce the greatest SI for all antibodies.
- Cells cultured on crude CS-7D4/KS-5D4 coating adopted a spindle shaped morphology with thin cytoplasmic processes, whereas cells cultured on enhanced $6C3^{+++}/5D4^{-}$ coating adopted a mixture of both a spindle-shaped morphology in addition to a rectangular widespread morphology with an ample cytoplasm. Both CS-based coatings were conducive to cells assuming a morphology comparable to mesenchymal stem cells, whereas cells cultured on uncoated plastic exhibited the classic bipolar morphology of activated fibroblasts in serum.
- Flow cytometric analysis of cells treated with permeabilising detergent were found to generate a MedFI greater than the MedFI of the untreated condition for CX43, PAX6, and Bmi-1. These findings support literature reports of immunolocalisation of all three markers intracellularly.
- The profile of PSSC markers expressed by cells cultured on crude CS-7D4/KS-5D4 and enhanced $6C3^{+++}/5D4^{-}$ coating significantly differed from the expression profile of the uncoated control. These findings are suggestive of cells cultured on CS-based substrate transdifferentiated to a stem-like phenotype.
- There was a positive correlation between the nMedFI of some markers and passage of cells cultured on uncoated, crude CS-7D4/KS-5D4 coated, and enhanced $6C3^{+++}/5D4^{-}$ coated culture plates.

The results of this study strongly suggest that both the crude CS-7D4/KS-5D4 and enhanced $6C3^{+++}/5D4^{-}$ coatings have a morphological and phenotypical effect on cultured keratocytes. Furthermore, the morphology and expression resulting from cultivation on the enhanced $6C3^{+++}/5D4^{-}$ substrate is suggestive of cells adopting a less differentiated state. Indeed, these results have important implications concerning the current approach for engineering transplantable corneal tissue, as well as translatable applications in various other organ systems following divergent streams of investigation. However further work is required, including a more robust phenotyping of cells cultured using both CS-based coatings, to better characterise them in

addition to assessing the expression over a longer period to determine reversal or plateau in the expression profiles.

Chapter 7: General Conclusions and Future Work

7.1 General Conclusions

The avian model was utilised in these investigations for its suitability as an animal model, its easy access, and rapid development. Extensive work by Hay and Revel (1969) documented the process of corneal development from preliminary events like the formation of the optical vesicle to the genesis of the primary stroma followed by mesenchymal cell invasion leading to differentiation into fibroblastic cells. The charted path of the cornea towards maturation allowed for key stages to be examined in relevant experimental chapters of this thesis in addition to facilitating what time point in corneal development would provide the highest yield of differentiating cells for primary cell culture. That said, the results of this thesis further substantiate the domestic chicken as a strong candidate for the study of a broad range of ocular surface diseases and conditions.

The overarching hypothesis of the research presented here was derived from the innovative work done by Hayes et al. (2008) who observed the localisation of differentially sulphated CSPGs in the stem cell niche of articular cartilage. Their findings led them to propose that CSPGs have a role in regulating the proliferation and differentiation potential of resident stem/progenitor cells. Given that a stem cell niche has also been identified in the human corneal limbus, this thesis applied the avian model to investigate the impact CS-based substrates have on keratocyte phenotype *in vitro*. Specifically, to determine assess if the phenotype of late-stage embryonic keratocytes cultured on different CS-based substrates would adopt a less differentiated state and if the resultant phenotype of cultured cells changed across multiple passages.

The overall aims of the research presented in this thesis were three-fold:

1. The first aim was to establish a baseline of qualitative data encompassing both *in vitro* labelling of matrix markers and PSSC markers in addition to *in situ* labelling of PSSC markers across key developmental points. This required the optimisation and development of relevant skills for primary cell culture and immunolabelling in order to successfully isolate E_{18} and adult keratocytes in addition to validating antibody expression in the avian cornea by using the murine cornea as a positive control.
2. The second aim was to examine the localisation of native CS sulphation motif epitopes *in situ* across selected time points in corneal development and *in vitro* cultures of embryonic keratocytes, with validation of epitope expression being performed on E_{14} chicken hindlimbs

as a positive control. This was formally undertaken to justify more advanced microscopic analyses later used to test the hypothesis of a presumptive stem cell niche in the avian cornea by identifying anatomical niche structures and cell-cell interactions analogous to those previously identified in the stem cell niche of the human corneal limbus by Shortt et al. (2007a) and Dziasko et al. (2016).

3. Finally, to optimise a flow cytometric protocol to investigate the effects culturing embryonic keratocytes on two different CS-based coatings would have on their resultant morphology and expression of PSSC markers.

This chapter summarises the main findings of each of the experiments detailed within this thesis, as well as the future work required to investigate these topics further.

Chapter one reviewed literature describing corneal ultrastructure and its cellular constituents in general, and then specifically focused on the literature concerned with detailing how the assembly of said components aided in the maintenance of corneal transparency. Following this, a review was presented of studies involving the manipulation of CSPG expression across multiple organ systems to illustrate the potential of CSPGs as a prospective therapeutic agent. The theory surrounding the involvement of CSPGs with the stem cell niche was also discussed. This chapter also highlighted the chicken cornea as a well-suited animal model with translatable, longer-term potential for new therapies to treat ocular surface disease. The end of Chapter one also discussed the components of the limbal stem cell niche and how limbal stem cells are a source for advancing current tissue engineering strategies to combat a broad spectrum of ocular surface disorders.

Chapter two detailed the adaptations made to established protocols and materials used to perform the necessary techniques for subsequent experimental chapters. Techniques for primary cell culture, immunostaining, cryo-sectioning, advanced microscopy, and flow cytometry were used, as appropriate, across four of the studies detailed within this thesis to investigate matrix and PSSC marker expression *in situ* and *in vitro*, where applicable. In addition, PSSC marker expression by embryonic keratocytes following culturing on a CS-based substrate was undertaken to assess CS-induced changes to the phenotypic profile of the cells. Furthermore, the basic principles that underpin each technique are also outlined.

In Chapter three, the immunolabelling of matrix markers was evaluated following *in vitro* culturing of embryonic keratocytes in addition to evaluating the immunolabelling of selected PSSC markers

CX43, PAX6, Bmi-1, and CXCR4 *in vitro* and *in situ* through various stages of corneal development. This was performed to provide a qualitative visualisation of labelling, more comprehensive than any previously reported, in relation to the chicken cornea, in addition to establishing a baseline for future experimental chapters. The results of this chapter showed E_{18} keratocytes could successfully be cultured as was seen by the positive immunolabelling of widely recognised matrix markers: pro-collagen type I, KS, and keratocan were seen in both embryonic and adult keratocyte cultures, which was indicative of an activated keratocyte phenotype. Furthermore, positive diffuse labelling of each PSSC marker was evident *in situ* throughout the corneal layers at all time points observed, except for PAX6 which was limited to the corneal epithelium. These findings were further corroborated with *in vitro* labelling and overall, these findings illustrated the breadth of activity cells within the developing cornea are undergoing to assemble a transparent ocular surface.

Chapter four investigated the localisation of antibodies that recognise native CS sulphation motif epitopes both *in vitro* and *in situ* through selected developmental stages. The results of this study provided the first evidence of immunolocalisation of native epitopes in the developing avian corneal limbus. They showed the gradual localisation of 4C3 and 6C3 in the stromal matrix towards the limbus, subjacent to the limbal epithelium, throughout development and into maturity. Furthermore, the CS epitopes revealed by these antibodies appeared to localise blow undulating folds of limbal epithelium and stroma – an area explored in the subsequent chapter using advanced microscopic techniques.

Chapter five investigated the presence of a limbal stem cell niche in the avian cornea using high-resolution imaging via SEM, SBF-SEM, and TEM. The results of this study showed some cell-cell interactions and anatomical features in the avian limbus analogous to those that previously reported in the human limbal stem cell niche. Using both SBF-SEM and TEM, distinct invaginations comparable to LCs and PoV were illustrated in the adult limbus. Small epithelial cells occupying the presumptive limbal crypts were also seen to have a high nucleus/cytoplasm ratio – a morphology suggestive of an epithelial stem cell. Notable 3D renderings on the developing avian cornea also showed evidence of cell-cell connections between basal epithelial cells and underlying stromal cells, in addition to matrix "cords" that allude to communications that may also be at play in the regulating corneal development.

Chapter six detailed the process by which a flow cytometry protocol was optimised for the quantification of PSSC markers CX43, PAX6, Bmi-1, and CXCR4 by embryonic keratocytes

cultured on either crude CS-7D4/KS-5D4, enhanced $6C3^{+++}/5D4^{-}$, and uncoated culture plates. The results strongly suggest that both the crude CS-7D4/KS-5D4 and enhanced $6C3^{+++}/5D4^{-}$ coatings have both a morphological and phenotypical effect on cultured keratocytes. Moreover, these findings suggest that cells are adopting a less differentiated state, however, a more robust assessment of immunophenotyping is required to identify the exact state of these cells in question and if the resultant phenotypic profile can be sustained over a longer period of subculturing, or if reversal or plateau of expressional changes exists.

The investigation undertaken in Chapter six details quantitative evidence regarding the resultant PSSC marker expression by keratocytes cultured on two different CS-based substrates vs. control. These findings reported a phenotypic profile indicative of elevated PSSC marker expression when cells were cultured on enhanced $6C3^{+++}/5D4^{-}$ substrate vs. control. These findings alone support the hypothesis that CSPGs have a function in preserving the stem/progenitor cell phenotype possibly through a mechanism by which stem/progenitor cells are protected from the binding of growth supplements that can directly influence the proliferation and differentiation potential of said cells. Though these findings are novel and exciting, there is a great deal to be done to fully appreciate them. The subsequent section aims to highlight some key areas that will benefit from additional investigation and to build the results obtained in this thesis

7.2 Future Work

From this study, further work is needed to demonstrate, with greater clarity, the effect CS-based coatings are having on the morphology and phenotypic profile of cultured cells. In addition, future work should examine the maturing limbal structure using advanced imaging techniques. For this thesis, only three timepoints were investigated *(E_{16}, E_{18}, and adult)* using SEM, TEM, and SBF-SEM which nevertheless detected changes in limbal architecture. However, in order to detect more subtle changes in limbal assembly, the examination of additional intermediate timepoints would be beneficial at both the embryonic level and following on from post-hatching to better document and understand the assembly of the limbus.

7.2.1 Immunophenotyping

Four putative stem cell markers were selected from a large repertoire of available markers to investigate phenotypic changes in cell expression across passages and treatment conditions. Despite the limited selection, it was apparent from the data that certain markers were favourably up-regulated and downregulated following treatment with CS-based substrates, suggesting the

coatings were having an effect on resultant phenotypic expression. Nevertheless, more robust immunophenotyping of cells, both *in situ* and *in vitro,* is required to provide a comprehensive understanding of their state throughout development and multiple subcultures. Together with the putative stromal stem cell markers assessed in this thesis, Funderburgh et al. (2016) also looked at pluripotent stem cell *markers (NANOG, REX1, SSEA4, SOX2, OCT4, KLF4)*, mesenchymal stem cell markers *(ABCG2)*, progenitor cell markers *(NGFR, CDH2, NESTIN)* and ocular precursor marker SIX6. Assessing these markers and many others across each coating condition will also support preliminary conclusions in regard to CS-based substates promoting a less differentiated state compared to cells cultured on standard plastic. It would also be pertinent to assess if similar effects could be achieved by culturing adult cells on each CS-based substrate. Incidentally, attempts were made at isolating corneal stromal stem cells using fibronectin coated dishes which had successful colony growth, but was abandoned due to the time constraints. It would be interesting to continue this study in relation to growing colonies on CS-based substrates to identify the expression of aforementioned markers and proliferation capacity in an effort to open up new avenues to enhance tissue engineering strategies.

A preliminary investigation was undertaken to assess the immunolabelling of matrix markers: pro-collagen type I, collagen type III, KS, and keratocan by E_{18} keratocytes cultured on crude CS-7D4/KS-5D4 and enhanced CS-6C3^{+++}/KS-5D4^{-} coated culture plates. As seen in Figure 7.14, weak labelling of the aforementioned markers was observed in some cells cultured on crude CS-7D4/KS-5D4, whereas, for cells cultured on enhanced CS-6C3^{+++}/KS-5D4^{-} coating, no labelling was observed. Results from Chapter 3 showed that keratocytes cultured on uncoated control plates did exhibit positive labelling for collagen type I, KS, and keratocan (Figure *3.2*). On the contrary, cells cultured on crude CS-based substrate displayed a weak, scattered labelling of the aforementioned markers, whereas cells cultured on enhanced CS-based substrate displayed no observable labelling, suggesting that CS has an effect on the phenotypic profile of keratocytes. Collectively, these findings support the conclusions drawn in Chapter 6, however further immunolabelling experiments will be necessary in future to substantiate these results.

An investigation by Xie et al. (2011) showed strong evidence that limbal stem cell function was dependent on the physical association with native niche cells through the SDF-1/CXCR4 axis. They found that SDF-1 was uniquely expressed by limbal epithelial progenitor cells, whereas CXCR4 was strongly expressed by surrounding limbal stromal niche cells and weakly expressed by limbal epithelial cells (Xie et al. 2011). A similar investigation of SDF-1 expression in the

chicken cornea will also need to be performed, in addition to assessing the expressional changes of any SDF-1, if any, on the CS-based substrates used in this thesis. The association between limbal basal progenitor cells and their subjacent mesenchymal stromal cells via SDF-1/CXCR4 signalling in the chicken cornea may also help to improve the future understanding of limbal stem cell self-renewal and regulation of fate decision in the limbal niche.

Incidentally, it would also be pertinent to further characterise the labelling of mAbs 4C3, 6C3, and 7D4 in the adult avian cornea with respect to sectional orientation. This was done in the porcine cornea by Hammond 2021), who characterised not only regional labelling within the cornea but also in relation to superior/inferior and nasal/temporal meridians. By performing a similar investigation in the avian cornea, it may provide more context and support for the relationship between CS and the presumptive stem cell milieu.

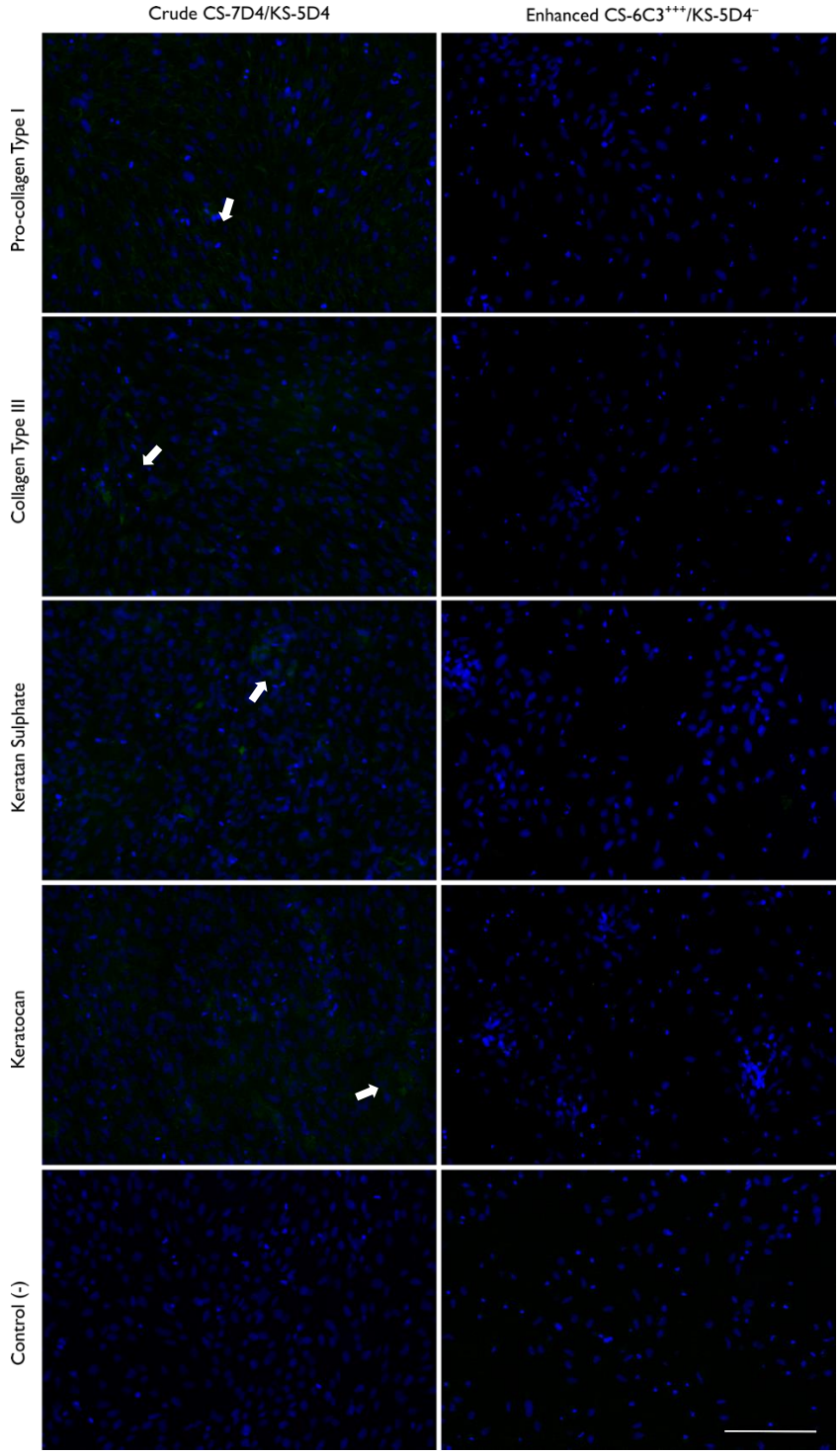

Figure 7.14: Immunolabeling of matrix markers in cultured E_{18} chicken corneal keratocytes on CS-based substrate. Very weak labelling *(green)* of pro-collagen type I, collagen type III, keratan sulphate, and keratocan by scattered cells *(arrows)* cultured on crude CS-7D4/KS-5D4 coated dishes. No observable labelling of pro-collagen type I, collagen type III, keratan sulphate, and keratocan was seen for cells cultured on enhanced CS-6C3^{+++}/KS-5D4^{-} coated culture plates. Nuclei counterstained with DAPI *(blue)*. The scale bar represents 100 μm.

7.2.2 Advanced Microscopy

As discussed previously, this thesis investigated the anatomical and cellular makeup of the corneal limbus at three developmental stages: E_{16}, E_{18}, and adult. Though marked differences were seen in the assembly of the limbus particularly for the formation of undulating folds, a comprehensive visualisation of the assembly would be better achieved with the analysis of samples from both earlier and intermediate timepoints using both TEM and SBF-SEM. Furthermore, the interaction of basal epithelial cells with underlying superficial stromal cells requires further analysis in addition to observing the cellular makeup surrounding the undulating folds as they become more pronounced. From a stem cell perspective, the current dogma suggests that an absence of CX43 expression in the stem cell niche functions to protect stem cells from pro-mitotic stimuli and the influence to differentiate. Work by Shanmuganathan et al. (2007) unexpectedly found expression of CX43 in human limbal epithelial crypts and adjacent palisades of Vogt which raised questions about the role CX43 plays with respect to the limbal stem cell niche. They proposed that $CX43^+$ cells act to support the niche and promote stem cell division when necessary. Despite their identification of $CX43^+$ cells using immunohistochemistry, they were unable to identify any gap junctions using TEM. That said, a parallel investigation of TEM data in the presumptive stem cell niche of the chicken may help clarify the position of whether or not the absence of CX43 is indeed necessary for the maintenance of the stem cell reservoir.

To supplement the evidence of novel anatomical structures in the avian limbus, comparable to the ones observed in the human limbal stem cell niche, further investigation is needed into the cellular activity within the limbus to support the assertion of a presumptive limbal stem cell niche in the chicken model. In this thesis, micrographs of basal cells with a high nucleus to cytoplasm ratio were documented in the undulating limbal folds of the adult corneal epithelium. These basal cells *(suggestive of stem cells residing within presumptive PoV)* would also need to demonstrate other characteristics of stem cells such as high proliferative capacity *in vitro* and show slow-cycling of [^{3}H] TdR- or BrdU-label *in vivo,* as evidenced in other animals (Rochat and Kobayashi 1994; Ebato et al. 1988; Lehrer et al. 1988; Cotsarelis et al. 1989 Pellegrini et al. 2001; 1999; Wang et al. 2011). In a study by Shanmuganathan et al. (2007) the immunochemical phenotype of limbal epithelial crypts was broadly seen to express $CX43^+/p63^+/Vimentin^+/Mib\text{-}1^-/CD34^-/CK3^-/CK19^+/CK14^+/ABCG2^+$, it would be interesting to verify this expression profile in the presumptive crypts of the avian limbus.

The presumptive avian limbal niche also requires investigation for the presence of associated cells, previously reported in connection with the human limbal stem cell niche, notably melanocytes, Langerhans cells, and early transient amplifying cells (Baum 1970; Davanger and Evensen 1971; Higa et al. 2005; Wang et al. 2011). Incidentally, the unique anatomical features of the limbus have previously been suggested to promote a close relationship between limbal epithelial stem cells and underlying limbal stromal cell evidenced by the preferential expression of α9 integrin, N-Cadherin, and an absence of CX43 by the limbal basement membrane (Stepp et al. 1995; Matic et al. 1997a; Shanmuganathan et al. 2007; Shortt et al. 2007b; Li et al. 2007; Hayashi et al. 2007; Wang et al. 2011). Investigating if this relationship also exists at the basement membrane along the limbus is warranted. Examining for the expression of putative stem cell markers p63α, ABCG2, and recently discovered corneal epithelial stem cell marker ABCB5 along the basement membrane in the limbus would also be valuable pursuits in supporting the presence of a stem cell reservoir at the limbus (de Paiva et al. 2005; Rama et al. 2010; Ksander et al. 2014; Singh et al. 2021).

7.2.3 Flow Cytometric Analysis

To further substantiate the findings outlined in Chapter six, it will be important to perform repeat analyses of PSSC marker expression across each passage and coating condition. As outlined in Section 7.2.1, expanding the study to include a wider range of PSSC marker expression is important to achieve a deeper understanding of the extent of the phenotypic changes of cells cultured on crude CS-7D4/KS-5D4 and enhanced $6C3^{+++}/5D4^{-}$ coatings. Another alternative for this analysis could be to use an ImageStream system to generate similar data for keratocytes extracted from a singular cornea to overcome the need for pooling samples for cell culture, due to limited cell numbers. This system, which combines microscopy and flow cytometry, would simultaneously provide multi-spectral imaging of cells *(brightfield, darkfield, and multiple fluorescence)* traveling in a fluidic stream, in addition to quantification of fluorescence and assessment of morphologic features *(e.g., texture, cell area, perimeter, spot counts, etc.)* (Zuba-Surma et al. 2007).

7.2.4 Culture Media

Traditionally, keratocytes have been cultured in DMEM and supplemented with FBS as it provides a source for attachment in addition to enhancing proliferation and expansion of cells in culture. However, there is a growing repertoire of media now in use that provide an avenue for culturing various cell types, such as keratinocyte serum-free medium *(K-SFM)*, medium 199, stem cell medium *(SCM)*, and many more. A study by Sidney et al. (2015) compared the properties of corneal stromal stem cells cultured in more widely applied media and found SCM had the most potential

for cell therapy application, based on its ability to promote markers associated with pluripotency and progenitor cells. It uses a knockout serum replacement in place of FBS and contains recombinant proteins b-FGF and LIF, in addition to a blend of additives *(vitamins, amino acids, insulin, lipid-rich albumin, etc.)* that have been shown to regulate pluripotency (Sidney et al. 2015). It would be interesting to assess the joint effect of culturing both adult and embryonic keratocytes in SCM on CS-based substrates to evaluate the impact of PSSC marker expression with the aim of moving towards more viable cell therapies to treat ocular surface disorders and beyond.

7.2.5 Wound Healing

Several studies have looked at corneal wound healing using genetic fate mapping and have shown the initiation of centripetal renewal of the corneal epithelium via the limbus (Kalha et al. 2019). However, the renewal patterns have been found to be species dependent. For example, Collinson et al. (2002) showed in the murine cornea that central corneal renewal was temporary and cells at this location were replaced by progeny generated at the limbus as the cornea progressively matures with clonal stripes stretching from the limbus to the central cornea. Whereas in the human cornea, Dua and Forrester (1990) observed unique circumferential movement of cells from the limbus following the infliction of a wound, with significant centripetal movement occurring only after complete re-establishment of complete limbal cover. That said, genetic fate mapping in the avian cornea would also be an interesting pursuit to better understand the limbal niche with respect to CS's involvement in the renewal mechanism in place to maintain corneal transparency. Work by Carlson et al. (2003) found a down-regulation of KS expression in mice following injury, however, to the author's knowledge the investigation into expressional changes to CS in the wounded cornea has not been examined. Additional work using a wound-healing assay would also be beneficial to investigate the effect of cell proliferation/viability on CS-coated substrate compared to uncoated surfaces to better understand the mechanism by which wound-healing occurs and how cell migration, proliferation, and differentiation is influenced (Lin et al. 2019).

7.2.6 CS-Based Substrates

In this thesis CS-based substrates of crude CS-7D4/KS-5D4 and enhanced $6C3^{+++}/5D4^{-}$ were used to investigate their respective influence of phenotypic expression of select PSSC markers by cultured cells. Our research collaborators are also in the process of purifying other substrates enhanced for specific CS-isoforms *(i.e., CS-7D4^{+}/CS-5D4^{-} and CS-6C3^{+++}/CS-5D4^{++})* which could be examined further using the methodology outlined in this thesis to assess effects on resultant expression. Moreover, it would allow for a more robust comparison between a greater sampling

of substrates to determine similarities and marked differences in their effect on the phenotypic profile of cultures cells, which could potentially improve our understanding of the involvement of CS as a potential modulated of the corneal limbal stem cell niche.

Appendix I - Antibody Validation

A1.1 Putative Stromal Stem Cell Marker Immunolabelling in the Murine Cornea

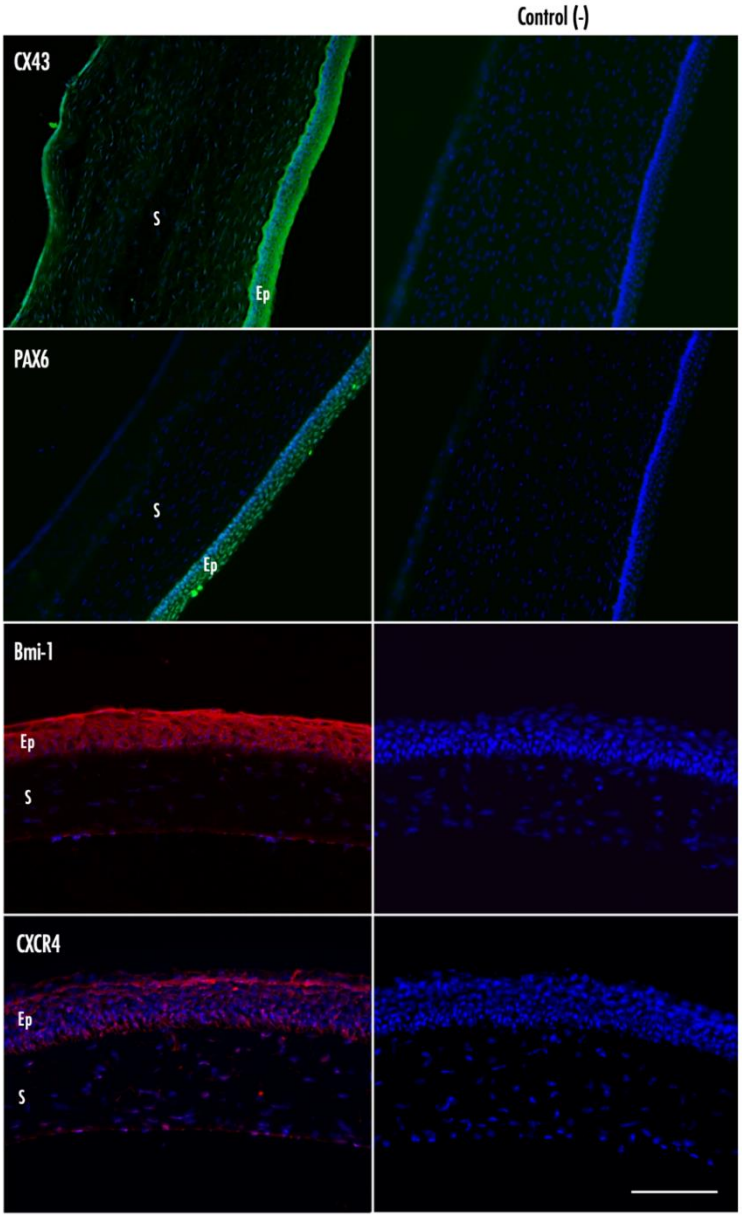

A1.1: Immunolocalisation of putative stromal stem cell markers in wild-type murine cornea. Positive control for fluorescence labelling of putative stromal stem cell marker antibodies CX43, PAX6, Bmi-1, and CXCR4 in the developing chicken cornea. Positive labelling of CX43 *(green)*, Bmi-1 *(red)*, and CXCR4 *(red)* was evident throughout the corneal layers, whereas PAX6 *(green)* was only observed in the epithelium. Nuclei counterstained with DAPI (*blue*). Epithelium (Ep), Stroma (S). Fluorescence was detected and images were acquired using the Olympus BX61 Upright Fluorescence Microscope, CellSens and ImageJ software. All images are representative from three individual experiments. Scale bar represents 100 μm.

Appendix II - FlowJo Software

A2.1 Calculating Separation Index Using FlowJo Software

A titration was performed to determine the appropriate antibody concentration required for complete saturation, that is, the lowest concentration of antibody where maximal signal staining was maintained. E_{18} keratocytes were isolated and cultured on uncoated dishes *(as described in Section 3.2.1.1)*. Flow cytometry was performed on P_2 cells *(as described in Section 6.2.2.1)* using primary antibody *(CX43, PAX6, Bmi-1, and CXCR4)* at concentrations of 5 µg/mL, 10 µg/mL, and 20 µg/mL in addition to lower concentrations where applicable. FSC files were imported into FlowJo v.10 and placed in corresponding antibody "**Groups**". Samples were gated as described in Section 6.2.2.3.2.

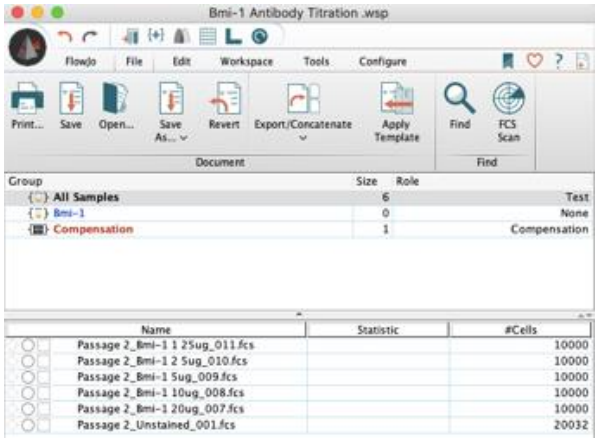

Calculating Separation Index in a Table

The separation index was used to calculate the difference in signal between positive and unstained *(negative)* populations while considering the spread of the negative population. The calculation below was applied:

$$\text{Separation Index} = \frac{Median_{(positive)} - Median_{(negative)}}{\left(\frac{84^{th} Percentile\ of\ median\ negative - Median_{(negative)}}{0.995}\right)}$$

The **Table Editor** was selected from the FlowJo ribbon and in the **Edit** ribbon "**Add Column**" was opened.

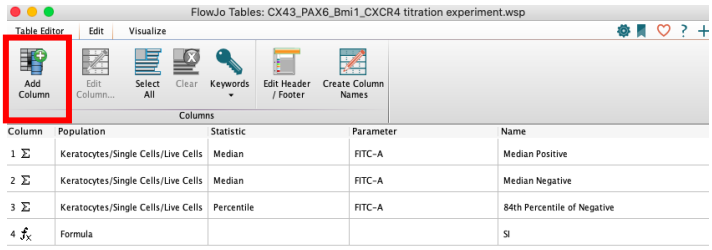

A column was added and named "Median Positive" where the median statistic was selected from the list. The "**Sample**" corresponded to any sample being analysed in the data set, "**Population**" corresponded to the gate from which the statistic was calculated *(e.g., Positive)*, "**Parameter**" pertained to the channel in which the antibody signal was collected *(i.e., FITC-A)*. This was repeated and adapted to create "Median Negative" and "84th Percentile of the Negative" columns.

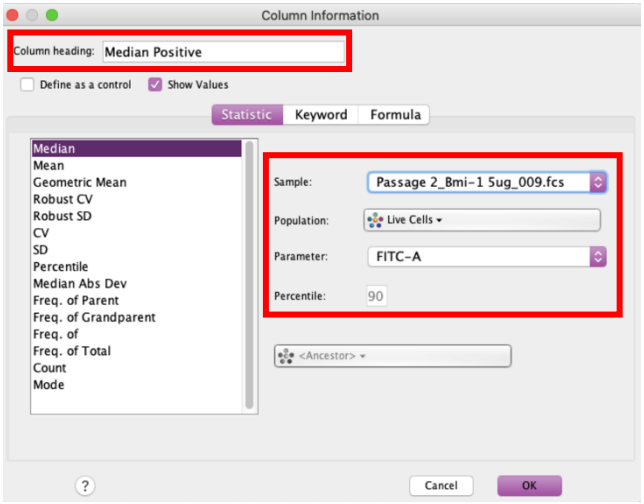

A fourth column was added to calculate the Separation index, the formula *(stated below)* was inputted into the text body and saved under the column heading of "SI" abbreviated for separation index.

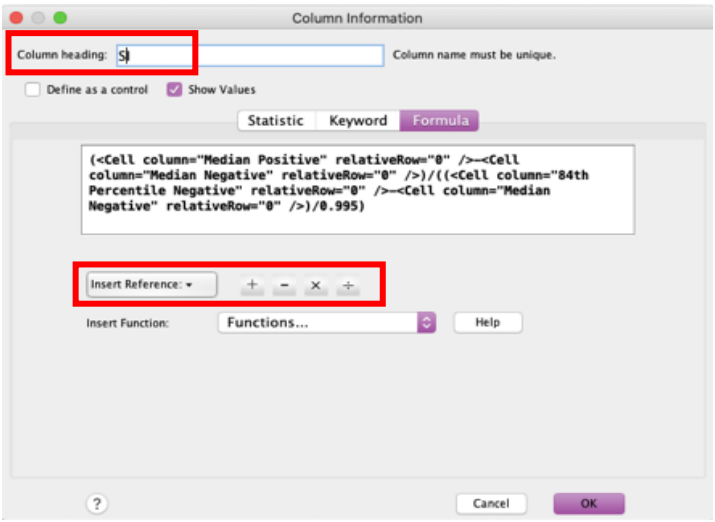

In the Iteration Section of the FlowJo Tables window, the **Group** was set to match the antibody in question and to **Iterate by** the sample, tables were created for each antibody using the **Create Table** icon.

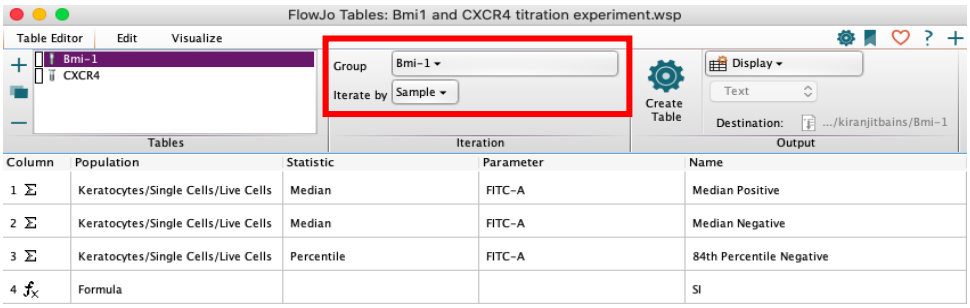

A2.2 Visual Validation of Samples Prior to Flow Cytometric Analysis

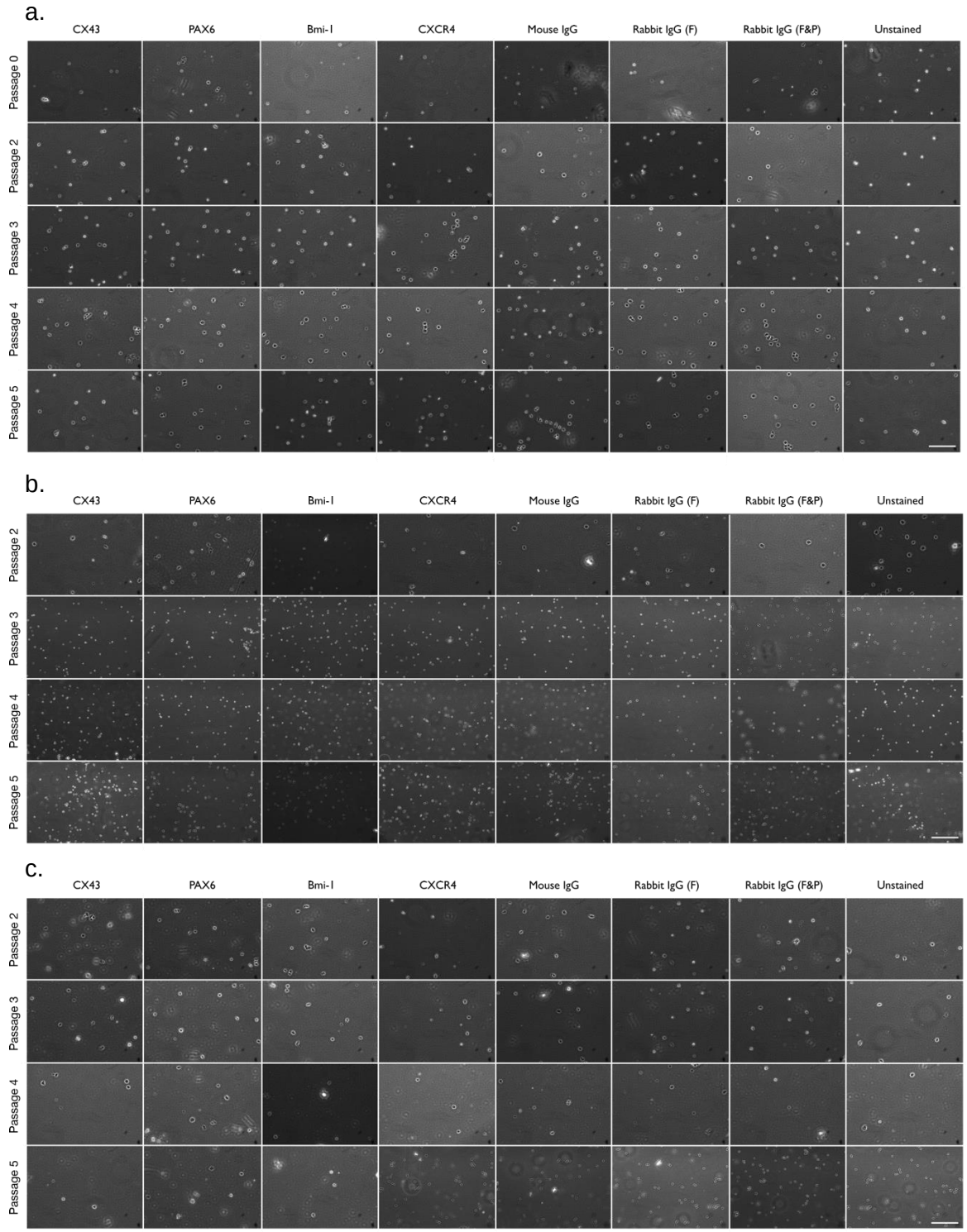

A2.2: Micrographs of keratocytes in cell suspension. Antibody-stained samples of E_{18} keratocytes cultured on (a.) uncoated, (b.) Crude *CS-7D4/KS-5D4* coated and (c.) Enhanced *CS-6C3*$^{+++}$*/KS-5D4*$^{-}$ coated culture plates at [1 μg/mL] from each passage were re-suspended as a single-cell suspension and imaged using an Olympus IX71 Inverted Fluorescence & Phase Contrast Tissue Culture Microscope prior to flow cytometric analysis. Images show round and intact cells following treatment with 4% *(v/v)* paraformaldehyde and 0.2% *(v/v)* Tween®20, where appropriate, for intracellular staining. F = Fixed, P = Permeabilised. Scale bars represent 100 μm.

A2.3 Summary of nMedFI Across Passages and Coating Conditions

A2.3: Summary of Putative stromal stem cell marker expression (nMedFI) across passages for E_{18} keratocytes cultured on uncoated, crude CS-7D4/KS-5D4, and enhanced CS-6C3^{+++}/KS-5D4^{-} coated culture plates.

Uncoated *(mean nMedFI ± SD)*						
Antibody	**P_0**	**P_2**	**P_3**	**P_4**	**P_5**	**Average**
n	5	5	5	5	5	
CX43	0.77 ± 0.015	1.46 ± 0.045	1.35 ± 0.035	1.49 ± 0.007	1.67 ± 0.008	1.35 ± 0.34
PAX6	0.14 ± 0.003	0.18 ± 0.003	0.12 ±0.002	0.11 ± 0.001	0.13 ± 0.001	0.14 ± 0.03
Bmi-1	1.31 ± 0.040	1.79 ± 0.054	0.97 ± 0.012	0.79 ± 0.008	1.75 ± 0.008	1.32 ± 0.45
CXCR4	0.29 ± 0.005	0.38 ± 0.004	1.67 ± 0.033	1.62 ± 0.011	1.55 ± 0.008	1.10 ± 0.70
Crude CS-7D4/KS-5D4 *(mean nMedFI ± SD)*						
CX43	0.77 ± 0.015	3.81 ± 0.097	1.39 ± 0.017	2.35 ± 0.022	1.95 ± 0.015	2.05 ± 1.15
PAX6	0.14 ± 0.003	0.48 ± 0.070	0.20 ± 0.003	0.19 ± 0.001	0.27 ± 0.004	0.26 ± 0.13
Bmi-1	1.31 ± 0.040	3.17 ± 0.036	1.41 ± 0.013	1.36 ± 0.007	1.98 ± 0.022	1.85 ± 0.79
CXCR4	0.29 ± 0.005	2.58 ± 0.028	2.26 ± 0.370	3.35 ± 0.022	2.76 ± 0.015	2.25 ± 1.16
Enhanced CS-6C3^{+++}/KS-5D4^{-} *(mean nMedFI ± SD)*						
CX43	0.77 ± 0.015	0.23 ± 0.002	0.19 ± 0.002	0.19 ± 0.014	0.18 ± 0.012	0.31 ± 0.26
PAX6	0.14 ± 0.003	0.34 ± 0.002	0.27 ± 0.003	0.40 ± 0.007	0.45 ± 0.005	0.32 ± 0.12
Bmi-1	1.31 ± 0.040	1.74 ± 0.022	2.39 ± 0.035	1.53 ± 0.034	2.65 ± 0.014	1.92 ± 0.57
CXCR4	0.29 ± 0.005	3.36 ± 0.065	3.70 ± 0.088	2.37 ± 0.061	3.58 ± 0.033	2.66 ± 1.42

Appendix III – Optimisation of CS-Based Substrate

GAGs are a class of biomolecules present ubiquitously on cell surfaces and within the ECM, where they interface with an assortment of signalling and structural proteins (Bishop et al. 2007, Hof et al. 2019). Through these interactions, GAGs are able to influence physiological processes like immune response, ECM, remodelling, and blood clotting (Gray et al. 2008; Divya and Krishnan 2009; Gill et al. 2010; Hof et al. 2019). The underlying mechanisms by which they exert their biological roles largely remain to be elucidates (Hof et al. 2019). One obstacle in studying these interactions stems from the inherent negative charge of GAGs which results in poor adhesion to apolar surfaces like standard culture polystyrene plates. To overcome this, various GAG immobilisation methods have been developed by modifying the surface to which GAGs adhere (Satoh et al. 1998; Marson et al. 2009; Dickinson and Gerecht 2010; Takada et al. 2013). Hof et al. (2019) demonstrates that salt-based immobilisation of GAGs could easily and efficiently adhere unmodified GAGs onto plastic surfaces using high concentrations of salt solution. Furthermore, they determined 80% *(v/v)* saturated ammonium sulphate: $(NH_4)_2SO_4$ produced the highest immobilization efficiency for CS GAGs out of all the salts tests (Hof et al. 2019).

A3.1 Coating Density of GAGs (µg/cm^2) Determined Using ELISA

Both crude CS-7D4/KS-5D4 and enhanced CS-6C3^{+++}/KS-5D4$^-$ substrate in 80% saturated ammonium sulphate solution *(provided by Sean Ashworth, MSc., Cardiff University School of Optometry and Vision Sciences, UK)* underwent a serial dilution to generate coating densities of 0.5 µg/cm^2, 0.25 µg/cm^2, 0.125 µg/cm^2, 0.05 µg/cm^2, and 0.025 µg/cm^2. Each of the five solutions was coated in a 96-well cell culture plate (ThermoFisher Scientific, Cat. # 167008) at 100 µl/well with the addition of two repeats done for each solution to determine reliability. The plates were covered with parafilm and stored at 4°C overnight.

The following day, coated wells were washed twice with TSA buffer *(see Table A3.1 for specifications)* and then blocked with 5% BSA/TSA for one hour at 37°C. Following incubation, wells were again washed twice with TSA buffer before instillation of sulphation motif-specific primary antibody (CS-7D4 1:500, CS-6C3 1:5, and KS-5D4 1:1000) in 5% BSA/TSA (leaving controls in just 5% BSA/TSA). The 96-well plate was covered with parafilm and incubated at 37°C for one hour. The plate was subsequently washed three times with 200 µl/well of TSA. Then 100 µl/well of AP-conjugated secondary antibody (0.2 µg/mL, Promega Anti-Mouse IgG, Cat. # S3721) in 5% BSA/TSA was instilled and the plate was incubated at 37°C for one hour. The plate was

subsequently washed four times before alkaline phosphate (ThermoFisher Scientific, Cat. # 34047) in DEA buffer *(see table A3.2 for specification)* was added at 100 µl/well before being incubated at 37°C for one hour.

The plate was subsequently placed in a CLARIOstar monochromator microplate reader and using the CLARIOstar Software (BMG Labtech, Aylesbury, UK) the microplate absorbance was measured, and the data was exported into excel for processing.

A3.1: Tris/Saline/Azide (TSA) buffer specifications.

Compound	Quantity (g/L)	Catalogue #
50mM TRIZMA	24.23	Sigma-Aldrich T1503
200mM NaCl	46.76	Sigma-Aldrich S7653
0.02% NaN_3	0.8	Sigma-Aldrich S2002
0.05% Tween	2.0mL	Sigma-Aldrich P1379

A3.2: DEA substrate buffer.

Compound	Quantity	Catalogue #
MilliQ Water	400mL	N/A
$MgCl_2$	12.8mg	Sigma-Aldrich M8266
Diethanolamine	48mL	Sigma-Aldrich D8885

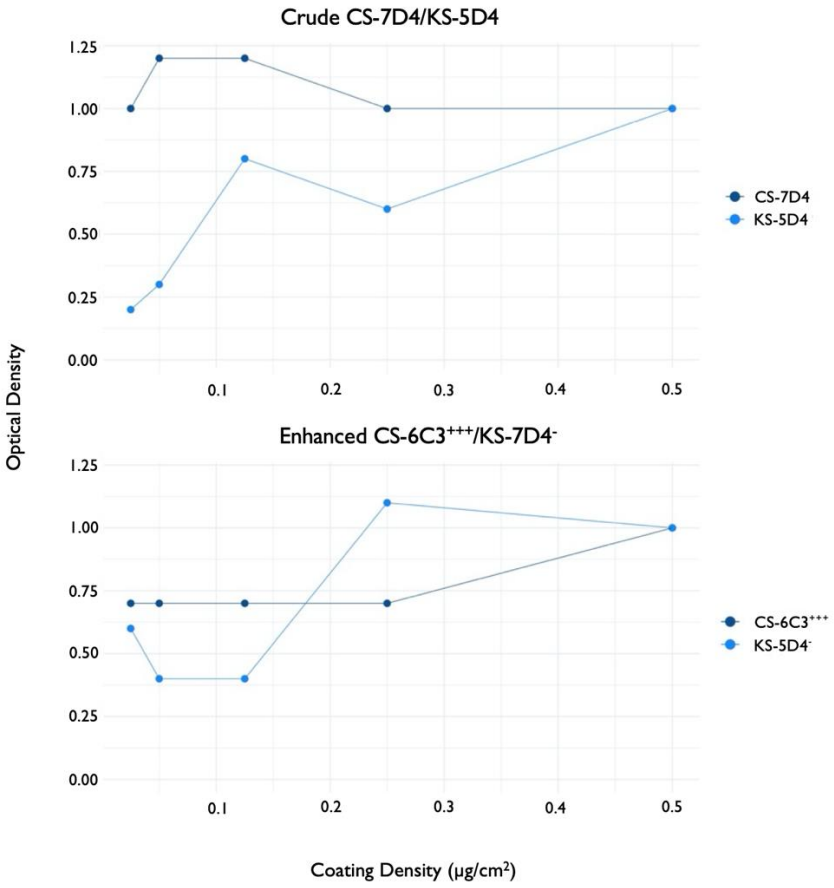

A3.3: Binding of sulphation motif-specific antibodies CS-7D4, KS-5D4, and CS-6C3 to Nunclon™ Delta plates coated with crude CS-7D4/KS-5D4 and enhanced CS-6C3^{+++}/KS-5D4^{-} substrates to determine optimum coating density using indirect-ELISA. A series of coating density dilutions *(0.5, 0.25, 0.125, 0.05, and 0.025 µg/cm²)* in 80% *(v/v)* saturated ammonium sulphate were tested. Dilution of the second antibody (AP-conjugated anti-mouse IgG) was 1:10,000 (0.2 µg/mL). Data points represent normalised mean optical densities *(n=3)*.

A3.4: Effects of coating density on binding of chondroitin *(7D4)* and keratan sulphate *(5D4)* sulphation motif-specific antibodies to crude CS-7D4/KS-5D4 substrate.

			7D4		
Coating Density (µg/cm²)	**0.5**	**0.25**	**0.125**	**0.05**	**0.025**
Sample 1	1.0	1.0	1.2	1.1	1.0
Sample 2	1.1	1.0	1.3	1.1	1.0
Sample 3	1.1	1.1	1.2	1.2	1.0
Mean ± SD	1.0 ± 0.074	1.0 ± 0.026	1.2 ± 0.048	1.2 ± 0.042	1.0 ± 0.025
			5D4		
Coating Density (µg/cm²)	**0.5**	**0.25**	**0.125**	**0.05**	**0.025**
Sample 1	1.0	0.5	0.7	0.3	0.2
Sample 2	1.0	0.7	0.8	0.4	0.2
Sample 3	1.0	0.6	0.9	0.4	0.2
Mean ± SD	1.0 ± 0.02	0.6 ± 0.12	0.8 ± 0.06	0.3 ± 0.08	0.2 ± 0.02

A3.5: Effects of coating density on binding of chondroitin (6C3) and keratan sulphate (5D4) sulphation motif-specific antibodies to enhanced CS-6C3^{+++}/KS-5D4^{-} substrate.

			6C3		
Coating Density (µg/cm²)	**0.5**	**0.25**	**0.125**	**0.05**	**0.025**
Sample 1	1.0	0.8	0.7	N/A	0.7
Sample 2	1.0	0.6	0.7	0.8	0.7
Sample 3	1.0	0.7	0.8	0.7	0.7
Mean ± SD	1.0 ± 0.00	0.7 ± 0.07	0.7 ± 0.05	0.7 ± 0.06	0.7 ± 0.02
			5D4		
Coating Density (µg/cm²)	**0.5**	**0.25**	**0.125**	**0.05**	**0.025**
Sample 1	1.0	1.1	0.4	0.4	0.7
Sample 2	0.9	1.1	0.4	0.3	0.7
Sample 3	1.2	1.2	0.4	0.4	0.4
Mean ± SD	1.0 ± 0.14	1.1 ± 0.04	0.4 ± 0.00	0.4 ± 0.05	0.6 ± 0.14

References

Abay, A., Simionato, G., Chachanidze,R., Bogdanova, A., Hertz, L., Bianchi, P., van den Akker, E. *et al.* (2019). Glutaraldehyde – A Subtle Tool in the Investigation of Healthy and Pathologic Red Blood Cells. *Frontiers in Physiology* **10**.

Abcam.com. (2021). *Flow cytometry intracellular staining protocol | Abcam*. [online] Available at: <https://www.abcam.com/protocols/flow-cytometry-intracellular-staining-protocol> [Accessed 17 June 2021].

Abcam.com. 2019b. *Flow cytometry introduction | Abcam*. Available at: https://www.abcam.com/protocols/introduction-to-flow-cytometry [Accessed 19 Sep. 2019].

Abu El-Asrar, A.M., Struyf, S., Al-Mosallam, A.A., Missotten, L. Damme, J.V., Geboes, K. (2001). Expression of chemokine receptors in vernal keratoconjunctivitis. *British Journal of Opthalmology* **85**(11), pp. 1357-1361

Aguas, A.P. (1982). The use of osmium tetroxide-potassium ferrocyanide as an extracellular tracer in electron microscopy. *Biotechnic and Histochemistry* **57**(2), pp. 69-73.

Ainscough, S.L., Linn, M.L., Barnard. Z., Schwab, I.R. and Harkin, D.G. (2011). Effects of fibroblast origin and phenotype on the proliferative potential of limbal epithelial progenitor cells. *Experimental Eye Research* **92**(1), pp. 10–19.

Akama, T.O., Misra, A.K., Hindsgaul, O. and Fukuda, M.N. (2002). Enzymatic synthesis in vitro of the disulfated disaccharide unit of corneal keratan sulfate. *Journal of Biological Chemistry* **277**(45), pp. 42505–42513.

Akhtar, S., Bron, A., Hayes, A.J., Meek, K.M.A. and Caterson, B. (2010). Role of keratan sulphate (sulphated poly-N-acetyllactosamine repeats) in keratoconic cornea, histochemical, and ultrastructural analysis. *Graefe's Archive for Clinical and Experimental Ophthalmology* **249**(3), pp.413-420.

Akiyama, H., Sakai, S., Linhardt, R.J, Goda, Y., Toida, T. and Maitani, T. (2004). Chondroitin sulphate structure affects its immunological activities on murine splenocytes sensitized with ovalbumin. *Biochemical Journal* **382**(Pt 1), pp. 269-278.

Albert, R., Veren, Z., Csomos, K., Moe, M.C., Johnsen, E.O, Olstad, O.K., Nicolaissen, B. *et al.* (2012). Cultivation and characterization of cornea limbal epithelial stem cells on lens capsule in animal material-free medium. *PLoS One* **7**(10), pp. 1-12.

Alberts, B., Johnson, A., Lewis, J., Raff, M., Roberts, K. and Walter, P. (2002). *In: Molecular Biology of the Cell. 4th ed.* New York, NY: Garland Science; 2002. The extracellular matrix of animals.

Amano, S., Yamagami, S., Mimura, T., Uchida, S. and Yokoo, S. (2006). Corneal stromal and endothelial cell precursors. *Cornea*, 25S73-S77.

Amidzadeh, Z., Behbahani, A.B., Erfani, N., Sharifzadeh, S., Ranjbaran, R., Moezi, L., Aboualizadeh, F. *et al.* (2014). Assessment of different permeabilization methods of minimizing damage to the adherent cells for detection of intracellular RNA by flow cytometry. *Avicenna Journal of Medical Biotechnology* **6** (1), pp. 38-46.

Angyal, A., Egelston, C., Kobezda, T., Olasz, K., Laszlo, A., Gland, T.T. and Mikecz, K. (2010). Development of proteoglycan-induced arthritis depends on T cell-supported autoantibody production but does not involve significant influx of T cells into the joints. *Arthritis Research & Therapy* **12**(2): R44.

Archer, C.W., McDowell, J., Bayliss, M.T., Stephens, M.D. and Bentley, G. (1990). Phenotypic modulation in sub-populations of human articular chondrocytes in vitro. *Journal of Cell Biology* **97**, pp. 361-371.

Ashworth, S., Harrington, J., Hammond, G.M., Bains, K.K., Koudouna, E., Hayes, A.J., Ralphs, J.R. *et al.* (2021). Chondroitin sulfate as a potential modulator of the stem cell niche in cornea. *Frontiers in Cell and Developmental Biology* **8**, e567358.

Aspberg, A., Miura, R., Bourdoulous, S., Shimonaka, M., Heinegard, D., Schachner, M., Ruoslahti, E. *et al.* (1997). The C-type lectin domains of lecticans, a family of aggregating chondroitin sulfate proteoglycans, bind tenascin-R by protein– protein interactions independent of carbohydrate moiety. *Proceedings of the National Academy of Sciences of the United States of* America **94**(19), pp. 10116–10121.

Au, A., Shao, Q., White, K.K., Lucaciu, S.A., Esseltine, J.L., Barr, K. and Laird, D.W. (2020). *Comparative Analysis of Cx31 and Cx43 in differentiation-competent rodent keratinocytes* **10**(10), 1143

Azuma, N., Nishina, S., Yanagisawa, H., Okuyama, T. and Yamada, M. (1996). PAX6 missense mutation in isolated foveal hypoplasia. *Natural Genetics* **13**(2), pp.141-142.

Bains, K.K., Fukuoka, H., Hammond, G.M., Sotozono, C. and Quantock, A.J. (2019). Recovering vision in corneal epithelial stem cell deficient eyes. *Contact Lens and Anterior Eye* **42**(4), pp.350-358.

Barbaro, V., Testa, A., Di Lorio, E., Mavilio, F., Pellegrini, G. and De Luca, M. (2007). C/EBPdelta regulates cell cycle and self-renewal of human limbal stem cells. *Journal of Cell Biology* **177**(6), pp. 1037-1049.

Bard, J.B.L. and Higginson, K. (1977). Fibroblast-collagen interaction in the formation of the secondary stoma of the chick cornea. *Journal of Cell Biology* **74**(3), pp. 816-827.

Basu, S., Hertsenberg, A.J., Funderburgh, M.L., Burrow, M.K, Mann, M.M, Du, Y., Lathrop, K.L. *et al.* (2014). Human limbal biopsy-derived stromal stem cells prevent corneal scarring. *Science Translational Medicine* **6**(266), 266ra172.

Baulmann, D.C. (2002). Pax6 heterozygous eyes show defects in chamber angle differentiation that are associated with a wide spectrum of other anterior eye segment abnormalities. *Mechanisms of Development* **118**(1-2), pp. 3–17.

Baum, J.L. (1970). Melanocyte and langerhans cell population of the corneal and limbus in the albino animal. *American Journal of Ophthalmology* **69**, pp. 669-676.

Beales, M.P., Funderburgh, J.L., Jester, J.V. and Hassell, J.R. (1999). Proteoglycan synthesis by bovine keratocytes and corneal fibroblast: maintenance of the keratocyte phenotype in culture. *Investigative Opthalmology & Visual Science* **40**(8), pp. 1658-1663.

Bee, J.A., Kuhl, U., Edgar, D. and von der Mark, K (1988). Avian corneal nerves: co- distribution with collagen type IV and acquisition of substance P immunoreactivity. *Investigative Ophthalmology & Visual Science* **29**(1), pp. 101-107.

Belmadani, A., Tran, P.B., Ren, D., Assimacopoulos, S., Grove, E.A. and Miller, R.J. (2005). The chemokine stromal cellderivedfactor-1 regulates the migration of sensory neuron progenitors. *Journal of Neuroscience*, **25**(16), pp.3995-4003.

Benedek, G.B. (1971). Theory of Transparency of the Eye. *Applied Optics* **10**(3), pp. 459-473.

Berardi, N., Pizzourusso, T., Ratto, G.M. and Maffei, L. (2003). Molecular basis of plasticity in the visual cortex. *Trends Neurosciences* **26**(7), 369–378.

Bergmanson, J.P., Horne, J., Doughty, M.J., Garcia, M. and Gondo, M. (2005). Assessment of the number of lamellae in the central region of the normal human corneal stroma at the resolution of the transmission electron microscope. *Eye Contact Lens* **31**(6), pp. 281–287.

Bettelheim, F.A. and Plessy, B. (1975). The hydration of proteoglycans of bovine cornea. *Biochimica et Biophysics Acts* **381**(1), pp. 203–214.

Beuerman, R. and Pedroza, L. (1996). Ultrastructure of the human cornea. *Microscopy Research and Technique*, **33**(4), pp.320-335.

Biehl, J. and Russell, B. (2009). Introduction to stem cell therapy. *The Journal of Cardiovascular Nursing* **24**(2), pp.98-103.

Biehs, B., Hy, J.K.-H., Strauli, N.B., Sangiorgi, E., Jung, H., Heber, R-F, Ho., S. *et al.* (2013). BMI1 represses Ink4a/Arf and Hox genes to regulate stem cells in the rodent incisor. *Nature Cell Biology* **15**(7), pp. 846-852.

Bio-Rad. (2021a). *Permeabilization & Fixation – Flow Cytometric Guide | Bio-Rad.* [online] Available at: <https://www.bio-rad-antibodies.com/flow-cytometry-fix-and-perm.html> [Accessed 24 July 2021].

Bio-Rad. (2021b). *Intracellular Staining Flow Cytometry Protocol using Saponin | Bio-Rad.* [online] Available at: <https://www.bio-rad-antibodies.com/direct-staining-of-intracellular-antigens-by-flow-cytometry-paraformaldehyde-method.html> [Accessed 17 June 2021].

Biochemistry for Medics - Lecture Notes. 2017. *Triple helical structure of collagen*. [online] Available at:http://www.namrata.co/structure-of-collagen-solution-to-problem-based-on-osteogenesis-imperfecta/triple-helical-structure-of-collagen/ [Accessed 11 Dec. 2017].

Biolegend.com. (2021). *Protocol - Cell Fixation and Permeabilization Protocol using 70% Ethanol.* [online] Available at: <https://www.biolegend.com/en-us/protocols/cell-fixation-and-permeabilization-protocol-using-70ethanol#:~:text=Prepare%2070%25%20Ethanol%20and%20chill%20to%20%2D20%C2%B0C.&text=Add%203ml%20cold%2070%25%20ethanol,%C2%B0C%20for%201%20hour.> [Accessed 24 July 2021].

Birk, D.E. and Trelstad, R.L (1984). Extracellular compartments in matrix morphogenesis: collagen fibril, bundle, and lamellar formation by corneal fibroblasts. *Journal of Cell Biology* **99**(6), pp. 2024-2033.

Birk, D.E., Fitch, J.M. and Linsenmayer, T.F. (1986). Organization of collagen types I and V in the embryonic chicken cornea. *Investigative Ophthalmology & Visual Science* **27**(10), pp 1470-1477.

Birk, D.E., Fitch, J.M., Babiarz, J.P., Doane, K.J. and Linsenmayer, T.F. (1990). Collagen fibrillogenesis in vitro: interaction of types I and V collagen regulates fibril diameter. *Journal of Cell Science* **95**, pp. 649-657.

Birk, D.E., Lande, M.A. and Fernandez-Madrid, F.R. (1981). Collagen and glycosaminoglycan synthesis in aging human keratocyte cultures. *Experimental Eye* Research **32**, pp. 331-339.

Bishop, J.R., Schuksz, M. and Esko, J.D. (2007). Heparan sulphate proteoglycans fine-tune mammalian physiology. *Nature: New Biology* **446**(7139), pp. 1030–1037

Bizheva, K., Tan, B., MacLellan, B., Hosseinaee, Z., Mason, E., Hileeto, D. and Sorbara, L. (2017). In-vivo imaging of the palisades of Vogt and the limbal crypts with sub-micrometer axial resolution optical coherence tomography. *Biomedical Optics* Express **8**(9), pp. 4141-4151.

Blochberger, T.C., Vergnes, J.P., Hempel, J. and Hassell, J.R. (1992). cDNA to chick lumican (corneal keratan sulfate proteoglycan) reveals homology to the small interstitial proteoglycan gene family and expression in muscle and intestine. *The Journal of Biological Chemistry* **267**(1), pp. 347-352.

Bock, H., Michaeli, P., Bode, C., Schultz, W., Kresse, H., Herken, R. and Miosge, N. (2001). The small proteoglycans decorin and biglycan in human articular cartilage of late-stage osteoarthritis. *Osteoarthritis and Cartilage* **9**(7), pp.654-663.

Bonanno, J. (2012). Molecular mechanisms underlying the corneal endothelial pump. *Experimental Eye Research* **95**(1), pp. 2-7.

Borcherding, M.S., Blacik, L.J., Sittig, R.A., Bizzell, J.W., Breen, M. and Weinstein, H.G. (1975). Proteoglycans and collagen fibre organization in human corneoscleral tissue. *Experimental Eye Research* **2**1, pp. 59–70.

Boulais, P.E. and Frenette, P.S. (2015). Making sense of hematopoietic stem cell niches. *Blood* **125**(17), pp. 2621-2629.

Boulton, M. and Albon, J. (2004). Stem cells in the eye. *The International Journal of Biochemistry & Cell Biology* **36**, pp. 643-657.

Bourcier, T., Berbar, T., Paquet, S., Rondeau, N., Thomas, F., Borderie, V., Rostene, W. *et al.* (2003). Characterization of functionality of CXCR4 chemokine receptor and SDF-1 in human corneal fibroblasts. *Molecular Vision* **9**, pp. 96-102.

Bourin, M.C., Lundgren-Akerlund, E. and Lindahl, U. (1990). Isolation and characterization of the g1ycosaminoglycan component of rabbit thrombomodulin proteoglycan. *Journal of Biological Chemistry* **265**(26), pp. 15424-15431.

Bozzola, J.J. and Russell, L.D. (1998). *Electron microscopy: principles and techniques for biologists*. 2nd ed. Toronto: Jones and Bartlett Publishers, pp. 19-22.

Bradbury, E.J., Moon, L.D.F., Popat, R.J., King, V.R., Bennett, G.S., Patel, P.N., Fawcett, J.W. *et al.* (2002). Chondroitinase ABC promotes functional recovery after spinal cord injury. *Nature* **416**(6881), pp. 636-640.

Bradbury, S., Joy, D.C. and Ford, B.J. (2019). *Transmission electron microscope*. *Encyclopedia Britannica.* https://www.britannica.com/technology/transmission-electron-microscope

Bron, A., Tripathi, R. and Tripathi, B. (2001). *Wolff's anatomy of the eye and orbit*. London: Arnold.

Bron, A.J. (2001). The architecture of the corneal stroma. *British Journal of Ophthalmology* **85**, pp. 379-281.

Buchwald, G., Van der Stoop, P., Weichenrieder, O., Perrakis, A., Van Lohuizen, M., Sixma, T.K. (2006). Structure and E3-ligase activity of the Ring-Ring complex of polycomb proteins Bmi1 and Ring1b. E*MBO Journal* **25**(11), pp. 2465–2474.

Buchwalow, I., Samoilova, V., Boecker, W. and Tiemann, M. (2011). Non-specific binding of antibodies in immunohistochemistry: fallacies and facts. *Scientific Reports* **1**(28), pp. 1-6.

Buijtenhuijs, P., Buttafoco, L., Poot. A.A., Daamen, W.F., van Kuppevelt, T.H., Dijkstra, P.J., de Vos, R.A. *et al.* (2004). Tissue engineering of blood vessels: characterization of smooth-muscle cells for culturing on collagen-and-elastin-based scaffolds. *Biotechnology and Applied Biochemistry* **39**(Pt 2), pp. 141–149.

Burman, S. and Sangwan, V. (2008). Cultivated limbal stem cell transplantation for ocular surface reconstruction. *Clinical Opthalmology* **2**(3), pp. 489-502.

Byers, B. and Porter, K. (1964). Oriented microtubules in elongating cells of the developing lens rudiment after induction. *Proceedings of the National Academy of Sciences* **52**(4), pp.1091-1099.

Calabro, A., Midura, R.J. and Hascall, V.C. (2000). 'Structure and biosynthesis of chondroitin sulfate and hyaluronan', In: Iozzo, RV. (eds.) *Proteoglycans: Structure, Biology, and molecular interactions*. New York: Marcel Dekker Inc, pp. 5-26.

Campbell, S.C., Krueger, R.C. and Schwartz, N.B. (1990). Deglycosylation of chondroitin sulfate proteoglycan and derived peptides. *Biochemistry* **29**(4), pp. 907–14.

Cancelas, J.A., Koevoet, W.L.M, de Konig, A.E., Mayen, A.E.M., Rombouts, E.J.C. and Ploemacher, R.E. (2000). Connexin-43 gap junctions are involved in multiconnexin-expressing stromal support of hemopoietic progenitors and stem cells. *Blood* **96**(2), pp. 498-505.

Candela, M.E., Yasuhara, R., Iwamoto, M. and Enomoto-Iwamoto, M. (2014). Resident Mesenchymal progenitors of articular cartilage. *Matrix Biology* **39**, pp. 44-49.

Canning, D.R., Brelsford, N.R. and Lovett, N.W. (2015). Chondroitin sulfate effects on neural stem cell differentiation. *In vitro Cellular and Developmental Biology* – Animal. **52**, pp. 35-44.

Canoll, P., Petanceska, S., Schlessinger, J. and Musacchio, J.M. (1996). Three forms of RPTP-? are differentially expressed during gliogenesis in the developing rat brain and during glial cell differentiation in culture. *Journal of Neuroscience Research* **44**(3), pp.199-215.

Cao, H-M., Ye, X-P., Ma, J-H., Jiang, H., Li, S-X., Li, R-Y., Li, X-S. *et al.* (2015). Mimecan, a hormonal abundantly expressed in adipose tissue, reduced food intake independently of leptin signalling. *EBioMedicine* **2**(11), pp. 1718-1724.

Cao, R., Tsukada, Y. and Zhang, Y. (2005). Role of Bmi-1 and Ring1A in H2A ubiquitylation and Hox gene silencing. *Molecular Cell* **20**(6), pp. 845-854.

Carlson, E.C., Liu, C.Y., Chikama, T., Hayashi, Y., Kao, C.W.C., Birk, D.E., Funderburgh, J.L. *et al.* (2005). Keratocan, a cornea-specific keratan sulfate proteoglycan, is regulated by lumican. *The Journal of Biological Chemistry* **250**(27), pp. 15541-15547.

Carlson, E.C., Wang, I-J., Liu, C-Y., Brannan, P., Kao, C.W-C. and Winston, W.Y. (2003). Altered KSPG expression by keratocytes following corneal injury. *Molecular Vision* **9**, pp. 615-623.

Caterson, B. (2012). Fell-Muir Lecture: Chondroitin sulphate glycosaminoglycans: fun for some and confusion for others. *International Journal of Experimental Pathology* **93**(1), pp. 1-10.

Caterson, B., Christner, J.E. and Baker, J.R. (1983). Identification of a monoclonal antibody that specifically recognizes corneal and skeletal keratan sulfate. *The Journal of Biological Chemistry* **258**(14), pp. 8848-8864.

Caterson, B., Christner, J.E., Baker, J.R. and Couchman, J.R. (1985). Production and characterization of monoclonal antibodies directed against connective tissue proteoglycans. *Federation of American Societies for Experimental Biology* **44**(2), pp. 386-393.

Caterson, B., Flannery, C.R., Hughes, C.E. and Little, C.B. (2000). Mechanisms involved in cartilage proteoglycan catabolism. *Matrix Biology* **19**(4), pp. 333-44.

Caterson, B., Griffin, J., Mahmoodian, F. and Sorrell, J.M. (1990b). Monoclonal antibodies against chondroitin sulfate isomers: their use as probes for investigating proteoglycan metabolism. *Biochemical Society Transactions* **18**(5), pp. 820–823.

Caterson, B., Hughes, C.E., Roughley, P. and Mort, J.S. (1995). Anabolic and catabolic markers of proteoglycan metabolism in osteoarthritis. *Acta Orthopaedica Scadinavica Supplementum* **266**, pp. 121-124.

Caterson, B., Mahmoodian, F., Sorrell, J.M., Hardingham. (1990a). Modulation of native chondroitin sulphate structure in tissue development and in disease. *Journal of Cell Science* **97**(Pt 3), pp. 411-417.

Cell Signaling Technology. (2021). *Flow Cytometry Protocol (Flow) | Cell Signaling Technology*. [online] Available at: <https://www.cellsignal.co.uk/learn-and-support/protocols/protocol-flow> [Accessed 24 July 2021].

Chakravarti, S., Magnuson, T., Lass, J.H., Jepsen, K.J., LaMantia, C. and Carroll, H. (1998). Lumican regulates collagen fibril assembly: skin fragility and corneal opacity in the absence of lumican. *Journal of Cell Biology* **141**(5), pp. 1277–1286.

Chan, L.Y., Yim, E.K.F. and Choo, A.B.H. (2013). Normalized median fluorescence: an alternative flow cytometry analysis method for tracking human embryonic stem cells states during differentiation. *Tissue Engineering Part C* **19**(2), pp. 156- 165.

Chao, J.R., Bronner, M.E., Lwigale, P.Y. (2013). Human fetal keratocytes have multipotent characteristics in the developing avian embryo. *Stem Cells and Development* **22**(15), pp. 2186-2195.

Chao, L.Y., Huff, V., Strong, L.C. and Saunders, G.F. (2000). Mutation in the PAX6 gene in twenty patients with aniridia. *Human Mutation* **15**(4), pp.332–339.

Chao, Y.H., Wu, K.H., Chiou, S.H., Chiang, S.F., Huang, C.Y., Yang, C.Y., Chan, C.K. *et al.* (2015). Downregulated CXCL12 expression in mesenchymal stem cells associated with severe aplastic anemia in children. *Annals of Hematology* **94**(1), pp. 13-22.

Chen, C., Michelini-Norris, B., Stevens, S., Rowsey, J., Ren, X., Goldstein, M. and Shultz, G. (2000). Measurement of mRNAs for TGFβ and extracellular matrix proteins in corneas of rats after PRK. *Investigative Opthalmology & Visual Science* **41**(13), pp. 4108-4116.

Chen, S. and Birk, D.E. (2011). Focus on molecules: decorin. *Experimental Eye Research* **92**, pp. 444-445.

Chen, S., Mienaltowski, M.J. and Birk, D.E. (2015). Regulation of corneal stroma extracellular matrix assembly. *Experimental Eye Research* **133**, pp. 69–80.

Chen, S.Y., Cheng, A.M.S., Zhang, Y., Zhu, Y.T., He, H., Mahabole, M. and Tseng, S.C.G. (2019). Pax 6 controls neural crest potential of limbal niche cells to support self-renewal of limbal epithelial stem cells. *Scientific Reports* **9**(1), pp. 9763.

Chen, S.Y., Hayashida, Y., Chen, M.Y., Xie, H.T. and Tseng S.C.G. (2011). A new isolation method of human limbal progenitor cells by maintaining close association with their niche cells. *Tissue Engineering Part C Methods* **17**(5), pp. 537–548.

Chen, Z., de Paiva, C.S., Luo, L., Kretzer, F.L., Pflugfelder, S.C. and Li, D-Q. (2004). Characterization of putative stem cell phenotype in human limbal epithelia. *Stem Cells* **22**(3), pp. 355-366.

Chen, Z., Evans, H., Pflugfelder, S.C. and Li, D-Q. (2006). Gap junction protein connexin 43 serves as a negative marker for stem cell-containing population of human limbal epithelial cells. *Stem Cells* **24**, pp. 1265-1273.

Cheng, X., Wang, H., Zhang, X., Zhao, S., Zhou, Z., Mu, X., Zhao, C. *et al.* (2017). The role of SDF-1/CXCR4/CXCR7 in neuronal regeneration after cerebral ischemia. *Frontiers in Neuroscience* **11**(590), pp.1-13.

Chiu, M.L., Goulet, D.R., Teplyakov, A. and Gilliland, G.L. (2019). Antibody structure and function: the basis for engineering therapies. Antibodies **8**(4), e55.

Church, R.L. (1980). Procollagen and collagen produced by normal bovine corneal stroma fibroblasts in cell culture. *Investigative Opthalmology & Visual Science* **19**(2), pp. 192-202.

Cintron, C., Hong, B.S., Covington, H.I., Macarak, E.J. (1988). Heterogeneity of collagens in rabbit cornea: type III collagen. *Investigative Opthalmology & Visual Science* **29**, pp. 767-775.

Cocks, E., Taggart, M., Rind, F.C. and White, K. (2018). A guide to analysis and reconstruction of serial block face scanning electron microscopy data. *Journal of Microscopy* **270**(2), pp. 217-234.

Collinson, J.M., Morris, L., Reid, A.I., Ramaesh, T., Keighren, M.A., Flockhart, J.H., Hill, R.E. *et al.* (2002). Clonal analysis of patterns of growth, stem cell activity, and cell movement during the development and maintenance of the murine corneal epithelium. *Developmental Dynamics* **224**(4), pp. 432-440.

Collinson, J.M., Quinn, J.C., Hill, R.E. and West, J.D. (2003). The roles of Pax6 in the cornea, retina, and olfactory epithelium of the developing mouse embryo. *Developmental Biology* **255**(2), pp. 303–312.

Conrad, G.W., Dessau, W. and von der Mark, K. (1980). Synthesis of type iii collagen by fibroblasts from the embryonic chick cornea. *Journal of Cell Biology* **84**, pp. 501-512.

Cooper, M. and Lummas, S. (2007). Antibodies for Immunochemistry. In: Renshaw, S. *Immunohistochemistry*. Oxfordshire: Scion Publishing Ltd., pp. 1-24.

Corpuz L.M., Funderburgh, J.L., Funderburgh, M.L., Bottomley, G.S., Prakash, S. and Conrad, G.W. (1996). Molecular cloning and tissue distribution of keratocan. *Journal of Biological Chemistry* **271**(16), pp. 9759-9763.

Corradetti, B., Taraballi, F., Minardi, S., Van Eps, J., Cabrera, F., Francis, L.W., Gazze, S.A. *et al.* (2016). Chondroitin sulfate immobilized on a biomimetic scaffold modulates inflammation while driving chondrogenesis. *Stem Cell Translational Medicine* **5**(5), pp. 670-682.

Cotsarelis, G., Cheng, S.Z., Dong, G., Sun, T.T. and Lavker R.M. (1989). Existence of slow cycling limbal epithelial basal cells that can be preferentially stimulated to proliferate: Implications on epithelial stem cells. *Cell* **57**(2), pp. 201-209.

Couchman, J.R., Caterson, B., Christner, J.E. and Baker, J.R. (1984). Mapping by monoclonal antibody detection of glycosaminoglycans in connective tissue. *Nature* **307**, pp. 650-652.
Crane, I.J., Wallace, C.A., McKillop-Smith, S. and Forrester, J.V. (2000). CXCR4 receptor expression on human retinal pigment epithelial cells from the blood-retina barrier leads to chemokine secretion and migration in response to stromal cell-derived factor 1alpha. *Journal of Immunology* **165**(8), pp.4372-4378.
Daniels, J., Secker, G. and Shortt, A. (2010). Ocular surface restoration. *Ocular Disease*, pp.83-90.
Daniels, J.T., Dart, J.K., Tuft, S.J. and Khaw, P.T. (2001). Corneal stem cell in review. *Wound Repair and Regeneration* **9**, pp. 483-494.
Daniels, J.T., Notara, M., Shortt, A.J., Secker, G., Harris, A. and Tuft, S.J. (2007). Limbal epithelial stem cell therapy. *Expert Opinion on Biological Therapy* **7**, pp. 1-3.
Dapson, R.W. (2007). Macromolecular changes caused by formalin fixation and antigen retrieval. *Biotechnic & Histochemistry* **82**(3), pp. 133-140.
Davanger, M. and Evensen, A. (1971). Role of the pericorneal papillary structure in renewal of corneal epithelium. *Nature* **229**, pp. 560-561.
Davies S.J., Fitch, M.T., Memberg, S.P., Hall, A.K., Raisman, G. and Silver, J. (1997). Regeneration of adult axons in white matter tracts of the central nervous system. *Nature* **390**(6661), pp. 680–683.
Davies, R., Vogelsand, P., Jonsson, R. and Appel, S. (2016). An optimized multiplex flow cytometry protocol for the analysis of intracellular signaling in peripheral blood mononuclear cells. *Journal of Immunological Methods* **436**, pp. 58-63.
Davies, S.B., Chui, J., Madigan, M.C., Provis, J.M., Wakefield, D. and Di. Girolamo, N. (2009). Stem cell activity in the developing human cornea. *Stem Cells* **27**(11), pp. 2781-2792.
Davis, J., Duncan, M.K., Robison, W.G. and Piatigorsky, J. (2003). Requirement for Pax6 in corneal morphogenesis: a role in adhesion. *Journal of Cell Science* **116**(Pt 11), pp. 2157–2167.
Daya, S.M., Watson, A., Sharpe, J.R., Giledi, O., Rowe, A., Martine, R. and James, S.E. (2005). Outcomes and DNA analysis of ex vivo expanded stem cell allograft for ocular surface reconstruction. *Opthalmology* **112**(3), pp. 470-477.
de Assumpcao Pereira-da-Silva, M., and Ferri, F.A. (2017). Scanning Electron Microscopy. In: Róz, A., Ferreira, M., Leite, F. and Oliveira, O. *Nanocharacterization techniques*. Oxford: William Andrew: Applied Science Publishers, pp.1-35.
de Paiva, C.S., Chen, Z., Corrales, R.M., Pflugfelder, S.C. and Li, D.Q. (2005). ABCG2 transporter identifies a population of clonogenic human limbal epithelial cells. *Stem Cells* **23**, pp. 63-73.
De Schauwer, C., Meyer, E., Van de Walle, G. and Van Soom, A. (2011). Markers of stemness in equine mesenchymal stem cells: a plea for uniformity. *Theriogenology* **75**(8), pp. 1431-1443.
Deerinck, T., Bushong, E., Thor, A. and Ellisman, M.H. (2010). NCMIR methods for 3D EM: A new protocol for preparation of biological specimens for serial blockface scanning electron microscopy. *Microscopy*, pp. 6-8.
Dickinson, L.E. and Gerecht, S. (2010). Micropatterned surfaces to study hyaluronic acid interactions with cancer cells. *Journal of Visualized Experiments* (46), e2413.
Divya, P. and Krishnan, L.K. (2009). Glycosaminoglycans restrained in a fibrin matrix improve ECM remodelling by endothelial cells grown for vascular tissue engineering. *Journal of Tissue Engineering and Regenerative Medicine* **3**(5), pp. 377–388.
Doane, K.J., Ting, W., McLaughlin, J.S. and Birk, D.E. (1996). Spatial and temporal variations in extracellular matrix of periocular and corneal regions during corneal stromal development. *Experimental Eye Research* **62**(3), pp. 285–292.
Docheva, D., Padula, D., Popov, C., Mutschler, W., Clausen-Schaumann, H. and Schieker, M.J. (2008) Researching into the cellular shape, volume and elasticity of mesenchymal stem cells, osteoblasts and osteosarcoma cells by atomic force microscopy. *Journal of Cell Molecular Medicine* **12**(2), pp. 537-552.
Dong, Y., Roos, M., Gruijters, T., Donaldson, P., Bullivant, S., Beyer, E. and Kistler, J. (1994). Differential expression of two gap junction proteins in corneal epithelium. *European Journal of Cell Biology* **64**(1), pp. 95-100.
Dora, N., Ou, J., Kucerova, R., Parisi, I., West, J.D. and Collinson, J.M. (2008). PAX6 dosage effects on corneal development, growth, and wound healing. *Developmental Dynamic* **237**(5), pp. 1295-1306.
Dowthwaite, G.P., Bishop, J.C., Redman, S.N., Ilyas, M.K., Rooney, P., Evans, D.R.J., Haughton, L. *et al.* (2004). The surface of articular cartilage contains a pro-genitor cell population. *Journal of Cell Science* **117**(6), pp. 889–897.
Du, Y. and Funderburgh, J.L. (2010). Stem cells of the ocular surface. *Encyclopedia of the Eye*, pp. 212-218.
Du, Y., Funderburgh, M.L., Mann, M.M., SundarRaj, N. and Funderburgh, J.L. (2005). Multipotent stem cells in human corneal stroma. *Stem Cells* **23**(9), pp.1266-1275.
Dua, H.S. and Forrester, J.V. (1990). The corneoscleral limbus in human corneal epithelial wound healing. *American Journal of Opthalmology* **110**(6), pp. 646-656.
Dua, H.S., Shanmuganathan, V.A., Powell-Richards, A.O., Tighe, P.J. and Joseph, A. (2005). Limbal epithelial crypts: a novel anatomical structure and a putative limbal stem cell niche. *British Journal of Opthalmology* **89**(5), pp. 529-532.
Duan, Y. and Giger, R.J. (2010). A new role for RPTPsigma in spinal cord injury: signaling chondroitin sulfate proteoglycan inhibition. *Science Signal* **3**(110), pe6.

Dudakovic, A.D, Camilleri, E., Riester, S.M., Lewallen, E.A., Kvasha, S., Chen, X., Radel, D.J. *et al.* (2014). High-resolution molecular validation of self-renewal and spontaneous differentiation in adipose-tissue derived human mesenchymal stem cells cultured in human platelet lysate. *Journal of Cell Biochemistry* **115**(10), pp. 1816-1828.

Dunlevy, J., Beales, M.P., Berryhill, B.L., Cornuet, P.K. and Hassell, J.R. (2000). Expression of the keratan sulfate proteoglycans lumican, keratocan and osteoglycin/mimecan during chick corneal development. *Experimental Eye Research* **70**(3) pp. 349-362.

Dziasko, M.A. and Daniels, J.T. (2016). Anatomical features and cell-cell interactions in the human limbal epithelial stem cell niche. *The Ocular Surface* **14**(3), pp. 322-330.

Dziasko, M.A., Armer, H.E., Levis, H.J., Shortt, A.J., Tuft, S. and Daniels, J.T. (2015). Localisation of epithelial cells capable of holoclone formation in vitro and direct interaction with stromal cells in the native human limbal crypt. *PLoS One* **9**(4), e94283.

Ebato, B., Friend, J. and Thoft, R.A. (1989). Comparison of limbal and peripheral human corneal epithelium in tissue culture. *Investigative Ophthalmology and Visual Science* **29**, pp. 1533-1537.

Ebrahimi, M., Taghi-Abadi, E. and Baharvand, H. (2009). Limbal stem cells in review. *Journal of Ophthalmic & Vision Research* **4**(1), pp. 40-58.

Egerton, R. (2008). *Physical principles of electron microscopy*. New York, NY: Springer, pp. 125-153.

El-Gamal, R., Hashem, A., Habashy, D., Abou Elwafa, M. and Boshnak, N. (2020). Flow cytometry in detection of Nucleophosmin 1 mutation in acute myeloid leukemia patients: A reproducible tertiary hospital experience. *International Journal of Laboratory Hematology* **43**(1), pp.68-75.

Engel, M., Maurel, P., Margolis, R.U. and Margolis, R.K. (1996). Chondroitin sulfate proteoglycans in the developing central nervous system. I. Cellular sites of synthesis of neurocan and phosphacan. *The Journal of Comparative Neurology* **366**(1), pp.34-43.

Epstein, J.A., Glaser, T., Cai, J., Jepeal, L., Walton, D.S. and Maas, R.L. (1994). Two independent and interactive DNA-binding subdomains of the Pax6 paired domain are regulated by alternative splicing. *Genes Development* **8**(17), pp. 2022–2034.

Eroschenko, V. (2012). *Difiore's Atlas of Histology: With Functional Correlations*. Philadelphia: Wolters Kluwer Health.

Esko, J.D., Kimata, K. and Lindahl, U. (2009). 'Proteoglycans and Sulfated Glycosaminoglycans,' In: Varki A, Cummings RD, Esko JD, et al. (eds) Essentials of Glycobiology. New York: Cold Spring Harbor Laboratory Press (NY): Cold Spring Harbor Laboratory Press, Chapter 16.

Espana, E.M., Kawakita, T., Romano, A., Di Pascuale, M., Smiddy, R., Liu, C-Y. and Tseng, S.C.G. (2003). Stromal niche controls the plasticity of limbal and corneal epithelial differentiation in a rabbit model of recombined tissue. *Investigative Opthalmology and Visual Science* **44**(12), pp. 5130- 5135.

Etheredge, L.T., Kane, B.P and Hassell, J.R. (2009). The effect of growth factor signalling of keratocytes in vitro and its relationship to the phases of stromal wound repair. *Investigative Ophthalmology & Visual Science* **50**(7), pp. 3128-3136.

Fasolo, A., Pedrotti, E., Passilongo, M., Marchini, G., Monterosso, C., Zampini, R., Bohm, E. *et al.* (2017). Safety outcomes and long-term effectiveness of ex vivo autologous cultured limbal epithelial transplantation for limbal stem cell deficiency. *British Journal of Ophthalmology* **101**(5), pp. 640-649.

Fedarko, N. (1993). Isolation and purification of proteoglycans. *Experientia* **49**(5), pp.369-383.

Feneck, E.M., Lewis, P.N. and Meek, K.M. (2020). Identification of a primary stroma and novel endothelial cell projections in the developing human cornea. *Cornea* **6**(1), pp. 1-5.

Feng, Y.F., Guo, H., Yuan, F. and Shen, M. (2015), Lipopolysaccharide promotes choroidal neovascularization by up-regulation of CXCR4 and CXCR7 expression in choroid endothelial cell. *PLoS One* **10**(8), pp. 1-18.

Ferraro, F., Lo Celso, C. and Scadden, D. (2010). Adult stem cells and their niches. *Advances in Experimental Medicine and Biology*, pp.155-168.

Fini, M. and Stramer, B. (2005). How the Cornea Heals. *Cornea* **24**(Supplement 1), pp. S2-S11.

Fischer, E.R., Hansen, B.T., Nair, V., Hoyt, F.H. and Dorward, D.W. (2013). Scanning Electron Microscopy. *Current Protocols Microbiology* **25**(1), pp. 2B.2.1-2B.2.47.

Fischer, O. and Schoenemann, B. (2019). Why are bones in vertebrate eyes? morphology, development and function of scleral ossicles in vertebrate eyes-a comparative study. *Journal of Anatomy and Physiological Studies* **3**(2), pp. 1-26.

Fitzgerald, J. and Bateman, J. (2001). A new FACIT of the collagen family: COL21A1. *FEBS Letters* **505**(2), pp.275-280.

Flannery, C.R., Lark, M.W. and Sandy, J.D. (1992). Identification of a stromelysin cleavage site within the interglobular domain of human aggrecan: Evidence for proteolysis at this site in vivo in human articular cartilage. *The Journal of Biological Chemistry* **267**(2), pp. 1008–1014.

Fowler, W.C., Chang, D.H., Roberts, B.C., Zarovnaya, E.L. and Proia, A.D. (2004). A new paradigm for corneal wound healing research: The white leghorn chicken (Gallus gallus domesticus). *Current Eye Research* **28**(4), pp.241-250.

Fox, K. and Caterson, B. (2002). Neuroscience - freeing the brain from the perineuronal net. *Science* **298**(5596), pp. 1187–1189.

Franz-Odendaal, T.A. (2011). The ocular skeleton through the eye of evo-devo. *Journal of Experimental Zoology Part B: Molecular and Developmental Evolution* **316B**(6), pp. 393-401.
Freegard, T. (1997). The physical basis of transparency of the normal cornea. *Eye* **11**(4), pp.465-471.
Freeman, I.L (1978). Collagen polymorphism in mature rabbit cornea. *Investigative Opthalmology & Visual Science* **17**, pp. 171-177.
Friedlander, D.R., Milev, P., Karthikeyan, L., Margolis, R.K., Margolis, R.U. and Grumet, M. (1994). The neuronal chondroitin sulfate proteoglycan neurocan binds to the neural cell adhesion molecules Ng-CAM/L1/NILE and N-CAM and inhibits neuronal adhesion and neurite outgrowth. *Journal of Cell Biology* **125**(3), pp. 669–680.
Fuchs, E. and Segre, J. (2000). Stem cells: a new lease of life. *Cell* **100**(1), pp.143–55.
Fukagawa, K., Okada, N., Fujishima, H., Nakajima, T., Tsubota, K., Takano, Y., Kawasaki, H. *et al.* (2002). CC-chemokine receptor 3: a possible target in treatment of allergy-related corneal ulcer. *Investigative Opthalmology & Visual Science* **43**, pp. 58-62.
Fukuta, M., Inazawa, J., Torii, T., Tsuzuki, K., Shimada, E. and Habuchi, O. (1997). Molecular cloning and characterization of human keratan sulfate Gal-6-sulfotransferase. *Journal of Biological Chemistry* **272**(51), pp. 32321–32328.
Funderburgh, J.L. (2000). Keratan sulfate: structure, biosynthesis, and function. *Glycobiology* **10**(10), pp. 951–958.
Funderburgh, J.L. (2002). Keratan sulfate biosynthesis. *International Union of Biochemistry and Molecular Biology: Life* **54**(4), pp.187-194.
Funderburgh, J.L. (2010). The corneal stroma. *Encyclopedia of the Eye,* pp.515-521.
Funderburgh, J.L., Caterson, B. and Conrad, G.W. (1986). Keratan sulfate proteoglycan during embryonic development of the chicken cornea. *Developmental Biology* **116**(2), pp. 267–277.
Funderburgh, J.L., Corpus, L.M., Roth, M.R., Funderburgh, M.L., Tasheva, E.S. and Conrad, G.W. (1997). Mimecan, the 25-kDa corneal keratan sulfate proteoglycan, is a product of the gene producing osteoglycin. *Journal of Biological Chemistry* **272**(44), pp. 28089-28095.
Funderburgh, J.L., Funderburgh, M.L. and Du, Y. (2016). Stem cells in the limbal stroma. *The Ocular Surface* **14**(2), pp. 113-120.
Funderburgh, J.L., Funderburgh, M.L., Mann, M.M., Prakash, S. and Conrad, G.W. (1996). Synthesis of corneal keratan sulfate proteoglycans by bovine keratocytes in vitro. *Journal of Biological Chemistry* **271**(3), pp. 31431-41436.
Funderburgh, J.L., Funderburgh, M.L., Rodrigues, M.M., Krachmer, J.H. and Conrad, G.W. (1990). Altered antigenicity of keratan sulfate proteoglycan in selected corneal diseases. *Investigative Opthalmology & Visual Science* **31**, pp. 419-428.
Funderburgh, J.L., Mann, M.M. and Funderburgh, M.L. (2003). Keratocyte phenotype mediates proteoglycan structure: a role for fibroblasts in corneal fibrosis. *Journal of Biological Chemistry* **278**(46), pp. 45629-45637.
Funderburgh, M.L., Du, Y., Mann, M.M., SundarRaj, N. and Funderburgh, J.L. (2005). PAX6 expression identifies progenitor cells for corneal keratocytes. *The Federation of American Societies for Experimental Biology Journal* **19**(10), pp. 1371-1373.
Galtrey, C.M. and Fawcett, J.W. (2007). The role of chondroitin sulfate proteoglycans in regeneration and plasticity in the central nervous system. *Brain Research Reviews* **54**(1), pp.1–18.
Garrett, D.M. and Conrad, G.W. (1979). Fibroblast-like cells from embryonic chick cornea, heart, and skin are antigenically distinct. *Developmental Biology* **70**(1), pp. 50-70.
Gatzioufas, Z., Charalambous, P. and Thanos, S. (2007). Reduced expression of the gap junction protein Connexin 43 in keratoconus. *Nature* **22**, pp.294-299.
Gealy, C., Hayes, A.J., Buckwell, R., Young, R.D., Caterson, B., Quantock, A.J. and Ralphs, J.R. (2009). Actin and type I collagen propeptide distribution in the developing chick cornea. *Investigative Opthalmology & Visual Sciences* **50**(4), pp. 1653-1658.
Ghoubay-Benallaoua, D., de Sousa, C., Martos, R., Latour, G., Schanne-Klein, M.C., Dupin, E. and Borderie, V. (2017). Easy xeno-free and feeder-free method for isolating and growing limbal stromal and epithelial stem cells of the human cornea. *PLOS ONE* **12**(11), e0188398.
Giglia-Mari, G., Zotter, A. and Vermeulen, W. (2011). DNA damage response. *Cold Spring Harbor Prospectives in Biology* **3**(1), a000745.
Gill, S., Wight, T.N. and Frevert, C.W. (2010). Proteoglycans: key regulators of pulmonary inflammation and the innate immune response to lung infection. *The Anatomical Record (Hoboken)* **293**(6), pp. 968–981.
Gipson, I.K.(1989). The epithelial basement membrane zone of the limbus. *Eye* **3**, pp. 132-40.
Givan, A. (2010). *Flow cytometry*. 2nd ed. New York: Wiley-Liss, pp.15-114.
Glaser, T., Jepeal, L., Edwards, J.G., Young, S.R., Favor, J. and Mass, R.L. (1994). PAX6 gene dosage effect in a family with congenital cataracts, aniridia, anophthalmia and central nervous system defects. *Nature Genetics* **7**(4), pp. 463-471.
Godbey, W. (2014). Fluorescence. *An Introduction to Biotechnology: The science, technology and medical applications*, pp.173-186.
Goldberg, M.F. and Bron, A.J. (1982). Limbal palisades of Vogt. *Transactions of the American Ophthalmological Society* 80, pp. 155-171.
Goldman, J.N. and Benedek, G.B. (1967). The relationship between morphology and transparency in the nonswelling

comeal stroma of the shark. *Investigative Ophthalmology* **6**(6), pp. 574-600.
Goldstein, J.I., Newburt, D.E., Micheal, J.R., Ritchie, N.W.M., Scott, J.H.J. and Joy, D.C. (2018). *Scanning electron microscopy and x-ray microanalysis*. 4th ed. New York: Springer Nature, pp.65-91.
González, S. and Deng, S. X. (2013). Presence of native limbal stromal cells increases the expansion efficiency of limbal stem/progenitor cells in culture. *Experimental Eye Research* 116, pp. 169-176.
Goodhew, P., Humphreys, J. and Beanland, R. (2017). *Electron microscopy and analysis*. 3rd ed. London: CRC Press, pp. 122-167.
Gopalakrishnan, S.M., Teusch, N., Imhof, C., Bakker, M.H.M., Schurdak, M., Burns, D.J. and Warrior, U. (2008). Role of Rho kinase pathway in chondroitin sulfate proteoglycan-mediated inhibition of neurite outgrowth in PC12 cells. *Journal of Neuroscience Research* **86**(10), pp. 2214-2226.
Gordon, M. and Hahn, R. (2010). Collagens. *Cell and Tissue Research* **339**(1), pp.247-257.
Gordon, M.K., Foley, J.W., Birk, D.E., Fitch, J.M. and Linsenmayer, T.F. (1994). Type V collagen and Bowman's Membrane: quantitation of mRNA in corneal epithelium and stroma. *Journal of Biological Chemistry* **269**(40), pp. 24959-24966.
Graves, B. (1934). Certain clinical features of the normal limbus. *British Journal of Ophthalmology* **18**(6), pp. 305–341.
Gray, E., Mulloy, B. and Barrowcliffe, T.W. (2008). Heparin and low molecular-weight heparin. *Thrombosis and Haemostasis* **99**(5), pp. 807–818.
Gray, F., Cho, H.J., Shukla, S., He, S., Harris, A., Boytsov, B., Jaremko, L. *et al.* (2016). BMI1 regulates PRC1 architecture and activity through homo- and hetero-oligomerization. *Nature Communications* **9**(7), pp.1-12.
Green, C.A., Green, C.R., Dickinson, M.E., Johnson, V. and Sherwin, T. (2016). Keratocytes are induced to produce collagen type II: A new strategy for in vivo corneal matrix regeneration. *Experimental Cell Research* **347**(1), pp. 241-249.
Grieve, K., Ghoubay, D., Georgeon, C., Thouvenin, O., Bouheraoua, N., Paques, M. and Borderie, V.M. (2015). Three-dimensional structure of the mammalian limbal stem cell niche. *Experimental Eye Research* **140**, pp. 75-84.
Grogan, S.P., Miyaki, S., Asahara, H., D'Lima, D.D. and Lotz, M.K. (2009). Mesenchymal progenitor cell markers in human articular cartilage: normal distribution and changes in osteoarthritis. *Arthritis Research & Therapy* **11**(3), R85.
Gross, J. (1974). Collagen biology: structure, degradation, and disease. In: *The Harvey Lectures*. New York: Academic Press, pp. 351–432.
Grueterich, M., and Tseng, S.C.G. (2002). Human limbal progenitor cells expanded on intact amniotic membrane ex vivo. *Archives of Ophthalmology* **120**(6), pp. 783-790.
Grueterich, M., Espana, E.M., Touhami, A., Ti, S.E. and Tseng, S.C.G. (2002). Phenotypic study of a case with successful transplantation of ex vivo expanded human limbal epithelium for unilateral total limbal stem cell deficiency. *Ophthalmology* **109**(8), pp.1547-1552.
Grueterich, M., Espana, E. and Tseng, S.C.G. (2002). Connexin 43 expression ad proliferation of human limbal epithelium on intact and denuded amniotic membrane. *Investigative Opthalmology and Visual Science* **43**(1), pp. 63-71.
Grumet, M., Milev, P., Sakurai, T., Karthikeyna, L., Bourdon, M., Margolis, R.K. and Margolis R.U. (1994). Interactions with tenascin and differential effects on cell adhesion of neurocan and phosphacan, two major chondroitin sulfate proteoglycans of nervous tissue. *Journal of Biological Chemistry* **269**(16), pp. 12142-12146.
Grupcheva, C.N., Laux, W.T, Rupenthal, I.D., McGhee, J., McGhee, C.N.J. and Green, C.R. (2012). Improved corneal wound healing through modulation of gap junction communication using connexin43-specific antisense oligodeoxynucleotides. *Investigative Opthalmology & Visual Science* **53**, pp. 1130-1138.
Hamburger, V. and Hamilton, H. (1951). A series of normal stages in development of the chick embryo. *Journal of Morphology* **88**(1), pp. 49–92.
Hamilton, W.J. (1953). Lillie's development of the chick—an introduction to embryology. *Journal of Anatomy* **87**(Pt 2), pp. 217.
Hammond, G.M. (2021). 'Characterisation of the porcine corneal epithelial stem/progenitor cell niche', PhD thesis, Cardiff University School of Optometry and Vision Sciences, UK.
Hardingham, T.E., Fosang, A.J., Hey, N.J., Hazell, P.K., Kee, W.J. and Ewins, R.J.F. (1994). The sulphation pattern in chondroitin sulphate chains investigated by chondroitinase ABC and ACII digestion and reactivity with monoclonal antibodies. *Carbohydrate Research* **255**, pp. 241-254.
Hart, G. (1976). Biosynthesis of glycosaminoglycans during corneal development. *Journal of Biological Chemistry* **251**(21), pp. 6513–6521.
Hart, R.W. and Farrell, R.A. (1969). Light scattering in the cornea. *Journal of the Optical Society of American* **59**(6), pp. 766-774.
Hashmani, K., Branch, M.J., Sidney, L.E., Dhillon, P.S., Verma, M., McIntosh, O.W., Hopkinson, A. *et al.* (2013). Characterization of corneal stromal stem cells with the potential for epithelial transdifferentiation. *Stem Cell Research Therapy* **4**(3), pp. 75.
Hassell, J., Kane, B.P., Etheredge, L.T., Valkov, N. and Birk, D.E. (2008). Increased stromal extracellular matrix synthesis and assembly by insulin activated bovine keratocytes cultured under agarose. *Experimental Eye Research* **87**(6), pp. 604-611.
Hay, E. and Revel, J. (1969). *Fine structure of the developing avian cornea*. Basel, New York: Karger.

Hay, E.D., Linsenmayer, T.F., Trelstad, R.L. and Von der Mark, K. (1979). Origin and distribution of collagens in the developing avian cornea. *Current Topics in Eye Research* **1**, pp.1-35.

Hayashi, R., Ishikawa, Y., Sasamoto, Y., Katori, R., Nomura, N., Ichikawa, T., Araki, S. *et al.* (2016). Co-ordinated ocular development from human iPS cells and recovery of corneal function. *Nature* **531**, pp. 376–380.

Hayashi, R., Yamato, M., Sugiyama, H., Sumide, T., Yang, J., Okano, T., Tano, Y. *et al.* (2007). N- Cadherin is expressed by putative stem/progenitor cells and melanocytes in the human limbal epithelial stem cell niche. *Stem Cells* **25**(2), pp. 289–296.

Hayes, A., Hughes, C.E., Smith, S.M., Caterson, B., Little, C.B. and Melrose, J. (2016). The CS sulfation motifs 4C3, 7D4, 3B3[−]; and perlecan identify stem cell populations and their niches, activated progenitor cells and transitional areas of tissue development in the fetal human elbow. *Stem Cells and Development* **25**(11), pp. 836-847.

Hayes, A., Sugahara, K., Farrugia, B., Whitelock, J.M., Caterson, B. and Melrose, J. (2018). Biodiversity of CS–proteoglycan sulphation motifs: chemical messenger recognition modules with roles in information transfer, control of cellular behaviour and tissue morphogenesis. *Biochemical Journal* **475**(3), pp. 587-620.

Hayes, A., Tudor, D., Nowell, M.A., Caterson, B. and Hughes, C.E. (2008). Chondroitin sulfate sulfation motifs as putative biomarkers for isolation of articular cartilage progenitor cells. *Journal of Histochemistry & Cytochemistry* **56**(2), pp.125-138.

Hayes, A.J., Hughes, C.E., Ralphs, J. and Caterson, B. (2011). Chondroitin sulphate sulphation motif expression in the ontogeny of the intervertebral disc. *European Cells and Materials* **21**, pp. 1-14.

Hayes, A.J., Hughes, C.E., Smith, S.M., Caterson, B., Little, C.B. and Melrose, J. (2016). The CS sulfation motifs 4C3, 7D4, 3B3[–]; and perlecan identify stem cell populations and their niches, activated progenitor cells and transitional areas of tissue development in the fetal human elbow. *Stem Cells and Development* **25**, pp. 836-847.

Hayes, A.J., MacPherson, S., Morrison, H., Dowthwaite, G. and Archer, C.W. (2001). The development of articular cartilage: evidence for an appositional growth mechanism. *Anatomy and Embryology* **203**, pp. 469-479.

Hayes, A.J., Tudor, D., Nowell, M.A., Caterson, B. and Hughes, C.E. (2008). Chondroitin sulfate sulfation motifs as putative biomarkers for isolation of articular cartilage progenitor cells. *Journal of Histochemical and Cytochemistry* **56**, pp. 125-138.

Hayes, S., Lewis, P., Islam, M.M., Doutch, J., Sorensen, T., White, T., Griffith, M. *et al.* (2015). The structural and optical properties of type III human collagen biosynthetic corneal substitutes. *Acta Biomaterialia* **25**, pp.121-130.

Haylock-Jacobs, S., Keough, M.B., Lau, L. and Yong, V.W. (2011). Chondroitin sulphate proteoglycans: Extracellular matrix proteins that regulate immunity of the central nervous system. *Autoimmunity Reviews* **10**(12), pp. 766-772.

He, Z., Jia, M., Yu, Y., Yuan, C. and Wang, J. (2018). Roles of SDF-1/CXCR4 axis in cartilage endplate stem cells mediated promotion of nucleus pulposus cells proliferation. *Biochemical and Biophysical Research Communications* **506**(1), pp. 94-101.

Hedbys, B. (1961). The role of polysaccharides in corneal swelling. *Experimental Eye Research* **1**(1), pp. 81-91.

Hegyi, J. and Hegyi, V. (2016). New developments in fluorescence diagnostics. *Imaging in Dermatology*, pp. 89-94.

Heinegård, D. (2009). Fell-Muir Lecture: Proteoglycans and more - from molecules to biology. *International Journal of Experimental Pathology* **90**(6), pp. 575-586.

Hertsenberg, A.J. and Funderburgh, J.L. (2015). Stem Cells in the Cornea. *Progress in Molecular Biology and Translational Science* **134**, pp. 25-41.

Higa, K., Kato, N., Yoshida, S., Ogawa, Y., Shimazaki, J., Tsubota, K. and Shimmura, S. (2013). Aquaporin 1-positive stromal niche-like cells directly interact with N-cadherin-positive clusters in the basal limbal epithelium. *Stem Cell Research* **10**(2), pp. 147-155.

Higa, K., Shimmura, S., Miyashida, H., Shimazaki, J. and Tsubota, K. (2005). Melanocytes in the corneal limbus interact with K19-positive basal epithelial cells. *Experimental Eye Research* **81**, pp. 218-223.

Hill, R.E., Favor, J., Hogan, B.L., Ton, C.C., Saunders, G.F., Handon, I.M., Prosser, J. *et al.* (1991). Mouse small eye results from mutations in a paired-like homeobox-containing gene. *Nature* **354**(6354), pp. 522-525.

Hirose J., Kawashima, H., Yoshie, O., Tashiro, K. and Miyasaka, M. (2001). Versican interacts with chemokines and modulates cellular responses. *Journal of Biological Chemistry* **276**, pp. 5228–5234.

Ho, L.T.Y., Harris, A.M., Tanioka, H., Tagi, N., Kinoshita, S., Caterson, B., Quantock, A.J. *et al.* (2014). A comparison of glycosaminoglycan distributions, keratan sulphate sulphation patterns and collagen fibril architecture from central to peripheral regions of the bovine cornea. *Matrix Biology* **38**, pp. 59-68.

Hof, D.J., Versteeg, E.M.M., van de Lest, C.H.A., Daamen, W.F. and van Kuppevelt, T.H. (2019). A versatile salt-based method to immobilize glycosaminoglycans and create growth factor gradients. *Glycoconjugate Journal* **36**, pp. 227-236.

Holland, E.J. (2015). Management of limbal stem cell deficiency: a historical perspective, past, present, and future. *Cornea* **34**(10), S9-15.

Hollander, A., Dickinson, S.C. and Kafienah, W. (2010). Stem cells and cartilage development: complexities of a simple tissue. *Stem Cells* **28**(11), pp. 1992-1996.

Holmes, D.F. and Kadler, K.E. (2005). The precision of lateral size control in the assembly of corneal collagen fibrils. *Journal of Molecular Biology* **345**(4), pp. 773-784.

Höög, J.L., Gluenz, E., Vaughan, S. and Gull, K. (2010). *Ultrastructural investigation method for Trypanosoma brucei*. In: Müller-Reichert, T. Electron Microscopy of Model Systems. Amsterdam: Elsevier, Academic Press, pp. 175-196.

Huang, K. and Wu, L.D. (2008). Aggrecanase and aggrecan degradation in osteoarthritis: a review. *Journal of International Medical Research* **36**, pp,1149–1160.

Hughes, L., Hawes, C., Monteith, S. and Vaughan, S. (2013). Serial block face scanning electron microscopy—the future of cell ultrastructure imaging. *Protoplasma* **251**(2), pp.395-401.

Hulmes, D.J.S. (2008). Collagen diversity, synthesis and assembly. In: Fratzl, P., Ed, Collagen, Structure and Mechanics, Springer, New York, Chapter 2, pp. 15-47.

Ida, M., Shuo, T., Hirano, K., Tokita, Y., Nakanishi, K., Matsui, F., Aono, S. *et al.* (2005). Identification and functions of chondroitin sulfate in the milieu of neural stem cells. *Journal of Biological Chemistry* **281**(9), pp. 5982-5991.

Ihanamäki, T., Pelliniemi, L.J. and Vuorio, E. (2004). Collagens and collagen-related matrix components in the human and mouse eye. *Progress in Retinal and Eye Research* **23**(4), pp. 403-434.

Inatomi, T., Nakamura, T., Koizumi, N., Sotozono, C. and Kinoshita, S. (2005). Current concepts and challenges in ocular surface reconstruction using cultivated mucosal epithelial transplantation. *Cornea* **24**(8), pp. 32–38.

Iozzo, R.V. (1997). The family of the small-leucine-rich proteoglycans: key regulators of matrix assembly and cellular growth. *Critical Reviews in Biochemistry and Molecular Biology* **32**(2), pp. 141-174.

Iozzo, R.V. (1998). Matrix proteoglycans: from molecular design to cellular function. *Annual Review of Biochemistry* **67**, pp. 609-652.

Iozzo, R.V. and Schaefer, L. (2015). Proteoglycan form and function: A comprehensive nomenclature of proteoglycans. *Matrix Biology* **42**, pp.11-55.

Iwama, A., Oguro, H., Negishi, M., Kato, Y., Morita, Y., Tsukui, H., Ema, H. *et al.* (2004). Enhanced self-renewal of hematopoietic stem cells mediated by the polycomb gene product bmi-1. *Immunity* **21**(6), pp. 843-851.

Izumikawa, T., Kanagawa, N., Watamoto, Y., Okada, M., Saeki, M., Sakano, M., Sugahara, K. *et al.* (2010). Impairment of embryonic cell division and glycosaminoglycan biosynthesis in glucuronyltransferase-i-deficient mice. *Journal of Biological Chemistry* **285**(16), pp. 12190-12196.

Izumikawa, T., Sato, B. and Kitagawa, H. (2014). Chondroitin sulfate is indispensable for pluripotency and differentiation of mouse embryonic stem cells. *Scientific Reports* **4**(1), e3701.

Jacobson, O. and Weiss, I.D. (2013). CXCR4 chemokine receptor overview: biology, pathology and applications in imaging and therapy. *Theranostic*s **3**(1), pp.1-2.

Jakus, M. (1956). Studies on the cornea -The fine structure of Descemet's membrane. *The Journal of Cell Biology* **2**(4), pp. 243-252.

Jassal, B., Matthews, L., Viteri, G., Gong, C., Lorente, P., Fabregat, A., Sidiropoulos, K. *et al.* (2020). The reactome pathway knowledgebase. *Nucleic Acids Research* **48**(D1), pp. D498- D503.

Jenkins, R.B., Hall, T. and Dorfman, A. (1981). Chondroitin 6-sulfate oligosacharides as immunological determinants of chick proteoglycans. *Journal of Biological Chemistry* **256**(16), pp. 8279-8282.

Jester, J.V. and Ho-Chang, J. (2003). Modulation of cultured corneal keratocyte phenotype by growth factors/cytokines control in vitro contractility and extracellular matrix contraction. *Experimental Eye Research* **77**(5), pp. 581-592.

Jester, J.V., Barry, P.A., Lind, G.J., Petroll, W.M., Garana, R. and Cavanagh, H.D. (1994). Corneal keratocytes: In situ and in vitro organization of cytoskeletal contractile proteins. *Investigative Opthalmology and Visual Science* **35**(2), pp. 730–743.

Jester, J.V., Petroll, W.M., Barry, P.A. and Cavanagh, H.D. (1995). Expression of alpha smooth muscle (alpha-SM) actin during corneal stromal wound healing. *Investigative Opthalmology & Visual Science* **36**(5), pp. 809-819.

Joddar, B., Hoshiba, T., Chen, G. and Ito, Y. (2014). Stem cell culture using cell-derived substrates. *Biomaterials Science* **11**(2), pp. 1595-1603.

Johansen, D., Cruciani, V., Sundset, R., Ytrehus, K. and Mikalsen, S.O. (2011). Ischemia Induces Closure of Gap Junctional Channels and Opening of Hemichannels in Heartderived Cells and Tissue. *Cellular Physiology and Biochemistry* **28**, pp. 103-114.

Johnson, M. (2013). Detergents: Triton X-100, Tween-20, and more. *Materials and Methods* **3**, pp. 163.

Jones, L.L., Margolis, R.U. and Tuszynski, M.H. (2003). The chondroitin sulfate proteoglycans neurocan, brevican, phosphacan, and versican are differentially regulated following spinal cord injury. *Experimental Neurology* **182**(2), pp. 399-411.

Jones, L.L., Sajed, D. and Tuszynski, M.H. (2003). Axonal regeneration through regions of chondroitin sulfate proteoglycan deposition after spinal cord injury: a balance of permissiveness and inhibition. *Journal Neuroscience* **23**(28), pp. 9276-9288.

Kalha, S., Shrestha, B., Navarro, M.S., Jones, K.B., Klein, O.D. and Michon, F. (2018). Bmi1+ progenitor cell dynamics in murine cornea during homeostasis and wound healing. *Stem Cells* **36**(4), pp. 562-573.

Kawakami, A., Kimura-Kawakami, M., Nomura, T. and Fujisawa, H. (1997). Distributions of PAX6 and PAX7 proteins suggest their involvement in both early and late phases of chick brain development. *Mechanisms of Development* **66**(1-2), pp.119-130.

Kawashima, H., Hirose, M., Hirose, J., Nagakubo, D., Plaas, A.H. and Miyasaka, M. (2000). Binding of a large chondroitin sulfate/dermatan sulfate proteoglycan, versican, to L-selectin, P-selectin, and CD44. *Journal of Biological Chemistry* **275**(45), pp. 35448-3556.

Kayali, A.G., Van Gunst, K., Campbell, I.L., Stotland, A., Kritzik, M., Liu, G., Flodstrom-Tullberg, M. *et al.* (2003). *The Journal of Cell Biology* **163**(4), pp. 859- 869.

Kerdcharoen, T. and Wongchoosuk, C. (2013). "Carbon nanotube and metal oxide hybrid materials for gas sensing," In: Jaaniso, R. and Tan, O.K. *Semiconductor Gas Sensors*, Cambridge: Woodhead Publishing, pp. 386-407.

Khan, A.A., Riemersma, J.C. and Booij, H.L. (1961). The reactions of osmium tetroxide with lipids and other compounds. *Journal of Histochemical Cytochemistry* **9**, pp. 560-563.

King, T.J. and Lampe, P.D. (2005). Temporal regulation of connexin phosphorylation in embryonic and adult tissues. *Biochimica et Biophysica Acta* **1719**(1-2), pp. 24-35.

Kinoshita, S. Friend, J. and Thoft, R.A. (1981). Sex chromatin of donor corneal epithelium in rabbits. *Investigative Opthalmology & Visual Science* **21**, pp. 438-441.

Kinoshita, S., Adachi, W., Sotozono, C., Nishida, K., Yokoi, N., Quantock, A.J. and Okubo, K. (2001). Characteristics of the human ocular surface epithelium. *Progress in Retinal Eye Research* **20**(5), pp. 639-673.

Kinoshita, S., Friend, J. and Thoft, R.A. (1981). Sex chromatin of donor corneal epithelium in rabbits. *Investigative Opthalmology & Visual Science* **21**(3), pp. 434–441.

Kinoshita, S., Koizumi, N.K. and Nakamura, T. (2004). Transplantable cultivated mucosal epithelial sheet for ocular surface reconstruction. *Experimental Eye Research* **78**(3), pp. 483-491.

Kirschner, S.E., Ciaccia, A. and Ubels, J.L. (1990). The effect of retinoic acid on thymidine incorporation and morphology of corneal stromal fibroblasts. *Current Eye Research* **9**(11), pp. 1121-1125.

Kiselev, Y., Eriksen, T.J., Forsdahl, S., Nguyen, L.H.T. and Mikkola, I. (2012). 3T3 cell lines stably expressing Pax6 or Pax6(5a)–a new tool used for identification of common and isoform specific target genes. *PLoS One* **7**(2): e31915.

Kitazawa, K., Hikichi, T., Nakamura, T., Sotozono, C., Kinoshita, S. and Masui, S. (2017). PAX6 regulates human corneal epithelium cell identity. *Experimental Eye Research* **154**, pp.30-38.

Kiyono, T., Foster, S.A., Koop, J.I., McDougall, J.K., Galloway, D.A. and Klingelhutz, A.J. (1998). Both Rb/p16INK4a inactivation and telomerase activity are required to immortalize human epithelial cells. *Nature* **396**(6706), pp. 84–88.

Kluppel, M., Wright, T.N., Chan, C., Hinek, A. and Wrana, J.L. (2005). Maintenance of chondroitin sulfation balance by chondroitin-4-sulfotransferase 1 is required for chondrocyte development and growth factor signalling during cartilage morphogenesis. *Development* **132**, pp. 3989-4003.

Ko, J-A., Yanai, R., Morishige, N., Takezawa, T. and Nishida, T. (2009). Upregulation of connexin43 expression in corneal fibroblasts by corneal epithelial cells. *Investigative Opthalmology and Visual Science* **50**(5), pp. 2054- 2060.

Kobe, B. and Kajava, A.V. (2001). The Leucine-rich repeat as a protein recognition motif. *Current Opinion in Structural Biology* **11**(6), pp. 725-732.

Koizumi, N., Inatomi, T., Quantock, A.J., Fullwood, N.J., Dota, A. and Kinoshita, S. (2000). Amniotic membrane as a substrate for cultivating limbal corneal epithelial cells for autologous transplantation in rabbits. *Cornea* **19**(1), pp. 65-71.

Kokovay, E., Goderie, S., Wang, Y., Lotz, S., Lin, G., Sun, Y., Roysam, B., Shen, Q. and Temple, S. (2010). Adult SVZ lineage cells home to and leave the vascular niche via differential responses to SDF1/CXCR4 signalling. *Cell Stem Cell* **7**(2), pp. 163–173.

Kolli, S., Ahman, S., Mudhar, H.S., Meeny, A., Lako, M. and Figueiredo, F.C. (2014). Successful application of ex vivo expanded human autologous oral mucosal epithelium for the treatment of total bilateral limbal stem cell deficiency. *Stem Cells* **32**(8), pp. 2135-2146.

Komai, Y. and Ushiki, T. (1991). The three-dimensional organization of collagen fibrils in the human cornea and sclera. *Investigative Opthalmology & Visual Science* **32**(8), pp. 2244-2258.

Koroma, B.M., Yang, J.M. and Sundin, O.H. (1997). The Pax-6 homeobox gene is expressed throughout the corneal and conjunctival epithelia. *Investigative Opthalmology & Visual Science* **38**(1), pp. 108-120.

Kotini, M., Barriga, E.H., Leslie, J., Gentel, M., Rauschenberger, V., Schambony, A. and Mayor, R. (2018). Gap junction protein connexin-43 is a direct transcriptional regulator of N-cadherin in vivo. *Nature Communications* **9**(1), e3846.

Koudouna, E., Spurlin, J., Babushkina, A., Quantock, A.J., Jester, J.V. and Lwigale, P. (2020). Recapitulation of normal collagen architecture in embryonic wounded corneas. Scientific Reports **10**(1), e13815.

Kozmik, Z., Czerny, T. and Busslinger, M. (1997). Alternatively, spliced insertions in the paired domain restrict the DNA sequence specificity of Pax6 and Pax8. *EMBO Journal* **16**(22), pp. 6793–6803.

Kronenberg, H.M. (2007). The role of the perichondrium in fetal bone development. *Annals of the New York Academy of Science* **1116**, pp. 59-64.

Ksander, B.R., Kolovou, P.E., Wilson, B.J., Saab, K.R., Guo, Q., Ma, J., McGuire, S.P. *et al.* (2014). ABCB5 is a limbal stem cell gene required for corneal development and repair. *Nature* **511**(7509), pp. 353-357.

Kuberka, M., Heschel, I., Glasmacher, B. and Rau, G. (2002). Preparation of collagen scaffolds and their applications in tissue engineering. *Biomedizinische Technik* **471**(Suppl 1 Pt), pp. 485–187.

Kubilus, J.K., Morales, C.Z. and Linsenmayer, T.F. (2017). The corneal epithelial barrier and its developmental role in isolating corneal epithelial and conjunctival cells from one another. *Investigative Opthalmology & Visual Science* **58**(3), pp. 1665-1672.

Kuhn, K. (1987). The classical collagens: types I, II, and III, ed. R. Mayne and R. E. Burgeson, pp. 1–42. Academic Press: Orlando.
Kumagai, N., Fukuda, K., Ishimura, Y. and Nishida, T. (2000). Synergistic induction of eotaxin expression in human keratocytes in TNF-alpha and IL-4 or IL-13. *Investigative Opthalmology & Visual Science* **41**(6), pp. 1448-1453.
Kumar, P., Pandit, A. and Zeugolis, D.I. (2016). Progress in corneal stromal repair: from tissue grafts and biomaterials to modular supramolecular tissue-like assemblies. *Advanced materials* **28**, pp. 5381-5399.
Kumar, P.S., Pavithra, K.G. and Naushad, M. (2019). "Characterization techniques for nanomaterials," In: Thomas, S., Sakho, E.H.M., Kalarikkal, N., Oluwafemi, S.O. and Wu, J. *Nanomaterials for solar cell applications* Amsterdam: Elsevier, pp 97-124.
Kurtz, S., Ong, K., Lau, E., Mowat, F. and Halpern, M. (2007). Projections of primary and revision hip and knee arthroplasty in the United States from 2005 to 2030. *Journal of Bone and Joint Surgery* **89**(4), pp. 780-785.
Laird, D.W. and Lamp, P.D. (2018). Therapeutic strategies targeting connexins. *Nature* **17**(12), pp. 905- 921.
Lakshman, N., Kim, A. and Petroll, W.M. (2010). Characterization of Corneal Keratocyte Morphology and Mechanical Activity within 3-D Collagen Matrices. *Experimental Eye Research* **90**(2), pp. 350-359.
Lamari, F.N. and Karamanos, N.K. (2006). Structure of chondroitin sulfate. *Advances in Pharmacology* **53**, pp. 33-48.
Langlois, S., Maher, A.C., Manias, J.L., Shai, Q. and Kidder, G.M. (2007). Connexin levels regulate keratinocyte differentiation in the epidermis. *The Journal of Biological Chemistry* **282**(41), 00. 30171-30180.
Lauder, R.M., Huckerby, T.N. and Nieduszynski, I.A. (2000). A fingerprinting method for chondroitin/dermatan sulfate and hyaluronan oligosaccharides. *Glycobiology* **10**(4), pp.393-401.
Laux-Fenton, W. (2012). The role of connexins in corneal homeostasis and repair: mastering the connexions to improve repair (PhD thesis). University of Auckland, Auckland, New Zealand.
Lavker, R. and Sun, T. (2003). Epithelial stem cells: the eye provides a vision. *Eye* **17**(8), pp.937-942.
Lavker, R.M., Tseng, S.C.G and Sun, T.T. (2004). Corneal epithelial stem cells at the limbus: looking at some old problems from a new angle. *Experimental Eye Research* **78**(3), pp. 433-446.
Le Marchand, S. and Dalva, M. (2020). "New imaging tools to study synaptogenesis," In: Rakic, P., Rubenstein, J., Chen, B. and Kwan, K., 2nd edition *Synapse Development and Maturation*, Oxfordshire: Academic Press, pp. 119-148.
Lehrer, M.S., Sun, T.T. and Lavker, R.M. (1998). Strategies of epithelial repair: modulation of stem cell and transient amplifying cell proliferation. *Journal of Cell Science* **111**(Pt 19), pp. 2867-2875.
Leiper, L.J., Walczysko, P., Kucerova, R., Ou, J., Shanley, L.J., Lawson, D., Forrester, J.V. *et al.* (2006). The roles of calcium signalling and ERK1/2 phosphorylation in a Pax6+/- mouse model of epithelial wound-healing delay. *BMC Biology* **4**(27), pp.1-14.
Lessard, J., Baban, S. and Sauvageau, G. (1999). Stage-specific expression of Polycomb group genes in human bone marrow cells. *Blood* **91**(4), pp.1216–1224.
Levanon, D. and Stein, H. (1993). Evaluation of the use of tannic acid in preparation of the rabbit knee meniscus for scanning electron microscopy. *Scanning Microscopy* **7**(2), pp.741-748.
Levine, J.M. and Nishiyama, A. (1996). The NG2 chondroitin sulfate proteoglycan: a multifunctional proteoglycan associated with immature cells. *Perspective on Developmental Neurobiology* **3**(4), pp. 245–259.
Levis, H. and Daniels, J. (2016). Recreating the human limbal epithelial stem cell niche with bioengineered limbal crypts. *Current Eye Research* **41**(9), pp.1153-1160.
Lewis, P.N., Pinali, C., Young, R.D., Meek, K.M., Quantock, A.J. and Knupp, C. (2010). Structural interactions between collagen and proteoglycans are elucidated by three-dimensional electron tomography of bovine cornea. *Structure* **18**(2), pp. 239–245.
Li, G.G, Zhu, Y.T., Xie, H.T., Chen, S.Y. and Tseng, S.C.G. (2012). Mesenchymal stem cells derived from human limbal niche cells. *Investigative Opthalmology and Visual* **53**, pp. 5686–5697.
Li, W., Chen, Y-T., Hayashida, Y., Blanco, G., Kheirkah, A., He, H., Chen, S-Y. *et al.* (2008). Down-regulation of Pax6 in association with abnormal differentiation of corneal epithelial cells in severe ocular surface disease. *Journal of Pathology* **214**(1), pp. 114-122.
Li, W., Hayashida, Y., Chen, Y.T., Tseng, S.C.G. (2007). Niche regulation of corneal epithelial stem cell at the limbus. *Cell Research* **17**(1), pp. 26–36.
Li, Y., Inoue, T., Takamatsu, F., Kobayashi, T., Shiraishi, A., Maeda, N., Ohashi, Y. *et al.* (2014). Difference between niche cells and limbal stromal cells in maintenance of corneal limbal stem cells. *Cornea* **55**, pp. 1453-1362.
Li, Z., Cao, R., Wang, M., Myers, M.P., Zhang, Y. and Ming, R-M. (2006). Structure of Bmi-1-Ring1B polycomb group ubiquitin ligase complex. *Journal of Molecular Chemistry* **281**(29), pp.20643-20649.
Liang, W-H., Kienitz, B.L., Penick, K.J., Welter, J.F., Zawadozinski, T.A. and Baskaran, H. (2011). Concentrated collagen-chondroitin sulfate scaffolds for tissue engineering application. *Journal of Biomedical Materials Research* **94**(4), pp. 1050-1060.
Lima, F., Vieira, L., Santos, A., De Simone, S., Hirano, L., Silva, J. and Romão, M. (2009) Anatomy of the scleral ossicles in Brazilian birds. *Brazilian Journal of Morphological Science* **26**, pp. 165-169.
Lin, J-Y., Lo, K-Y. and Sun, Y-S. (2019). Effects of substrate-coating materials on the wound-healing process. *Materials (Basel)* **12**(17), pp. 2775.
Lindahl, U., Couchman, J., Kimata, K. and Esko, J.D. (2015-2017). Proteoglycans and Sulfated Glycosaminoglycans. 2017. In: Varki A, Cummings RD, Esko JD, et al., editors. Essentials of Glycobiology [Internet]. 3rd edition. Cold

Spring Harbor (NY): Cold Spring Harbor Laboratory Press; 2015-2017. Chapter 17. Available from: https://www.ncbi.nlm.nih.gov/books/NBK453033/doi: 10.1101/glycobiology.3e.017
Linsenmayer, T.F. (2012). 'Collagen,' In: Hay, E.D. *Cell biology of extracellular matrix*. 2nd edition. New York: Springer, pp.7-44.
Linsenmayer, T.F., Fitch, J.M., Gordon, M.K., Cai, C.X., Igoe, F., Marchant, J.K. and Birk, D.E. (1998). Development and roles of collagenous matrices in the embryonic avian cornea. *Progress in Retinal and Eye Research* **17**(2), pp. 231-265.
Linsenmayer, T.F., Fitch, J.M., Schmid, T.M., Zak, N.B., Gibney, E., Sanderson, R.D. and Mayne, R. (1983). Monoclonal antibodies against chicken type V collagen: production, specificity, and use for immunocytochemical localization in embryonic cornea and other organs. *Journal of Cell Biology* **96**(1) pp.124–132.
Linsenmayer, T.F., Gibney, E. and Fitch, J.M. (1986). Embryonic avian cornea contains layers of collagen with greater than average stability. *Journal of Cell Biology* **103**(4), pp. 1587-1593.
Liu, C., Shiraishi, A., Kao, C.W., Converse, R.L., Funderburgh, J.L., Corpuz, L.M., Conrad, G.W. *et al.* (1998). The cloning of mouse keratocan cDNA and genomic DNA and the characterization of its expression during eye development. *Journal of Biological Chemistry* **273**(35), pp. 22584-22588.
Lohmander, L.S., Shinomura, T., Hascall, V.C. and Kimura, J.H. (1989). Xylosyl transfer to the core protein precursor of the rat chondrosarcoma proteoglycan. *Journal of Biological Chemistry* **264**(31), pp. 18775-18780.
Lopez-Arribillaga, E., Rodilla, V., Pellegrinet, L., Guiu, J., Iglesias, M., Roman, A.C., Gutarra, S. *et al.* (2014). Bmi1 regulates murine intestinal stem cell proliferation and self-renewal downstream of Notch. *Development* **142**, pp. 41-50.
Lopez, M.J., Seyed-Razavi, Y., Jamali, A., Harris, D.L. and Hamrah, P. (2018). The chemokine receptor CXCR4 mediates recruitment of $CD11c^{+}$ conventional dendritic cells into the inflamed murine cornea. *Cornea* **59**(13), pp.5671-5681.
Lwigale, P., Cressy, P.A. and Bronner-Fraser, M. (2005). Corneal keratocytes retain neural crest progenitor cell properties. *Developmental Biology* **288**(1), pp. 284-293.
Ma, L., Gao, C., Mao, Z., Zhou, J., Shen, J., Hu, X. and Han, C. (2003). Collagen/chitosan porous scaffolds with improved biostability for skin tissue engineering. *Biomaterials* **24**(26), pp. 4833–4841.
Maciel, B.B., Rebelatto, C.L.K., Brofman, P.R.S., Brito, H.F.V., Patricio, L.F.L., Cruz, M.A. and Locatelli-Dittrich, R. (2014). Morphology and morphometry of feline bone marrow-derived mesenchymal stem cells in culture. *Pesquisa Veterinária Brasileira* **34**(11), pp. 1127-1134.
Maeda, N., Ichihara-Tanaka, K., Kimura, T., Kadomatsu, K., Muramatsu, T. and Noda, M. (1999). A receptor-like protein-tyrosine phosphatase PTPζ/RPTPβ binds a heparin-binding growth factor midkine: involvement of arginine 78 of midkine in the high affinity binding to PTPζ *Journal of Biological Chemistry* **274**(18), pp. 12474-12479.
Maeda, N., Nishiwaki, T., Shintani, T., Hamanaka, H. and Noda, M. (1996). 6B4 proteoglycan/phosphacan, an extracellular variant of receptor-like protein-tyrosine phosphatase ζ/RPTPβ, binds pleiotrophin/heparin-binding growth-associated molecule (HB-GAM). *Journal of Biological Chemistry* **271**, pp. 21446-21452.
Majo, F., Rochat, A., Nicolas, M., Jaoude, G.A. and Barrandon, Y. (2008). Oligopotent stem cells are distributed throughout the mammalian ocular surface. *Nature* **456**(7219), pp. 250-254.
Mantovani, V., Maccari, F. and Volpi, N. (2016). Chondroitin sulfate and glucosamine as disease modifying anti-osteoarthritis drugs (DMOADs). *Current Medicinal Chemistry* **23**(11), pp.1139-1151.
Mark, M.P., Butler, W.T. and Ruch, J.V. (1989). Transient expression of a chondroitin sulfate-related epitope during cartilage histomorphogenesis in the axial skeleton of fetal rats. *Developmental Biology* **133**(2), pp. 475-488.
Marson, A., Robinson, D.E., Brookes, P.N., Mulloy, B., Wiles, M., Clark, S.J., Fielder, H.L. *et al.* (2009). Development of a microtiter plate-based glycosaminoglycan array for the investigation of glycosaminoglycan-protein interactions. *Glycobiology* **19**(12), pp. 1537–1546
Matic, M., Evans, W.H., Brink, P.R. and Simon, M. (2002). Epidermal stem cells do not communicate through gap junctions. *Journal of Investigative Dermatology* **118**(1), pp. 110-116.
Matic, M., Petrov, I.N., Chen, S., Wang, C., Dimitrijevich, S.D. and Wolosin, J.M. (1997a) Stem cells of the corneal epithelium lack connexins and metabolite transfer capacity. *Differentiation* **61**(4), pp. 251–260.
Matic, M., Petrov, I.N., Rosenfeld, T., Wolosin, J.M. (1997b). Alterations in connexin expression and cell communication in healing corneal epithelium. *Investigative Opthalmology and Visual Science* **38**(3), pp. 600-609.
Matsumoto, K. (2006). Identification and characterization of versican/PG-M aggregates in cartilage. *Journal of Biological Chemistry* **281**(26), pp.18257-18263.
Maurice, D.M. (1957). The structure and transparency of the cornea. *The Journal of Physiology* **136**(2), pp.263-286.
Maurice, D.M. (1981). The Cornea and Sclera. In Davson H ed. The Eye, Academic Press, New York. pp. 489-599.
McKenzie, A.T. (2019). Glutaraldehyde: A review of its fixative effects on nucleic acids, proteins, lipids, and carbohydrates.
McKeon, R.J., Schreiber, R.C., Rudge, J.S. and Silber, J. (1991). Reduction of neurite outgrowth in a model of glial scarring following CNS injury is correlated with the expression of inhibitory molecules on reactive astrocytes. *Journal of Neuroscience* **11**(11), pp.3398-3411.
Meek, K.M. (2009). Corneal collagen—its role in maintaining corneal shape and transparency. *Biophysical Reviews* **1**(2), pp. 83-93.

Meek, K.M. and Boote, C. (2004). The organization of collagen in the corneal stroma. *Experimental Eye Research* **78**(3), pp. 503-512.
Meek, K.M. and Fullwood, N. (2001). Corneal and scleral collagens—a microscopist's perspective. *Micron* **32**(3), pp. 261-272.
Meek, K.M. and Holmes, D.F. (1983). Interpretation of the electron microscopical appearance of collagen fibrils from corneal stroma. *International Journal of Biological Macromolecules* 5(1), pp. 17–25.
Meek, K.M. and Knupp, C. (2015). Corneal structure and transparency. *Progress in Retinal and Eye Research* **49**, pp. 1-16.
Meek, K.M. and Leonard, D.W. (1993). Ultrastructure of the corneal stroma: a comparative study. *Biophysical Journal* 64(1), pp. 273-280.
Meek, K.M., Quantock, A.J., Boote, C., Liu, C.Y. and Kao, W.W.-Y. (2003). An X-ray scattering investigation of corneal structure in keratocan-deficient mice. *Matrix Biology* **22**(6), pp.467-475.
Melrose, J., Chaung, C. and Whitelock, J. (2008). Tissue engineering of cartilages using biomatrices. *Journal of Chemical Technology & Biotechnology* **83**(4), pp. 444-463.
Melrose, J., Isaacs, M.D., Smith, S.M., Hughes, C.E., Little, C.B., Caterson, B. and Hayes, A.J. (2012). Chondroitin sulphate and heparan sulphate sulphation motifs and their proteoglycans are involved in articular cartilage formation during human foetal knee joint development. *Histochemistry and Cell Biology* **138**, pp. 461-475.
Melrose, J., Smith, S.M., Hughes, C.E., Little, C.B., Caterson, B. and Hayes, A.J. (2016). The 7D4, 4C3 and 3B3 (-) chondroitin sulphation motifs are expressed at sites of cartilage and bone morphogenesis during foetal human knee joint development. *Journal of glycobiology* **5**(1), e118.
Menon, V., Thomas, R., Ghale, A.R., Reinhard, C. and Pruszak, J. (2014). Flow cytometry protocols for surface and intracellular antigen analyses of neural cell types. *Journal of Visualized Experiments* **94**, e52241.
Meselson, M., Stahl, F.W. and Vinograd, J. (1957). Equilibrium Sedimentation of Macromolecules in Density Gradients. *Proceedings of the National Academy of Science of the United States of America* **43**(7), pp. 581-588.
Meyer, D.B. and O'Rahilly, R. (1959). The Development of the Cornea in the Chick. *Development* **7**(2), pp. 303-315.
Michelacci, Y. (2003). Collagens and proteoglycans of the corneal extracellular matrix. *Brazilian Journal of Medical and Biological Research* **36**(8), pp. 1037-1046.
Midura, R.J. and Hascall, V.C. (1989). Analysis of the proteoglycans synthesized by corneal explants from embryonic chicken. II. Structural characterization of the keratan sulfate and dermatan sulfate proteoglycans from corneal stroma. *Journal of Biological Chemistry* **264**(3), pp. 1423–1430.
Mikami, T. and Kitagawa, H. (2013). Biosynthesis and function of chondroitin sulfate. *Biochemica Biophysica Acta* **1830** (10), pp. 4719-4733.
Milev, P., Chiba, A., Haring, M., Rauvala, H., Schachner, M., Ranscht, B., Margolis, R.K. *et al.* (1998a). High affinity binding and overlapping localization of neurocan and phosphacan/protein-tyrosine phosphatase-zeta/beta with tenascin-R, amphoterin, and the heparin-binding growth-associated molecule. *Journal of Biological Chemistry* **273**(12), pp. 6998-7005.
Milev, P., Friedlander, D.R., Sakurai, T., Karthikeyan, L., Flad, M., Margolis, R.K., Grumet, M. *et al.* (1994). Interactions of the chondroitin sulfate proteoglycan phosphacan, the extracellular domain of a receptor-type protein tyrosine phosphatase, with neurons, glia, and neural cell adhesion molecules. *Journal of Cell Biology* **127**(6), pp. 1703–1715.
Milev, P., Maurel, P., Haring, M., Margolis, R.K. and Margolis, R.U. (1996). TAG-1/Axonin-1 Is a High-affinity Ligand of Neurocan, Phosphacan/Protein-tyrosine Phosphatase-ζ/β, and N-CAM. *Journal of Biological Chemistry* **271**, pp. 15716–15723.
Milev, P., Monnerie, H., Popp, S., Margolis, R.K. and Margolis, R.U. (1998b). The Core Protein of the Chondroitin Sulfate Proteoglycan Phosphacan Is a High-affinity Ligand of Fibroblast Growth Factor-2 and Potentiates Its Mitogenic Activity. *Journal Biological Chemistry* **273**(34), pp. 21439-21442.
Mirshahi, F., Pourtau, J., Li, H., Muraine, M., Trochon, V., Legrand, E., Vannier, J. *et al.* (2000). SDF-1 activity on microvascular endothelial cells: consequences on angiogenesis in in vitro and in vivo models. *Thrombosis Research* **99**(6), pp. 587-594.
Moller-Pedersen, T. (1997). A comparative study of human corneal keratocyte and endothelial cell density during aging. *Cornea* **16**, pp. 333-338.
Moller-Pedersen, T. (2004). Keratocyte reflectivity and corneal haze. *Experimental Eye Research* **78**(3), pp. 553-560.
Moller-Pedersen, T. and Ehlers, N. (1995). A three-dimensional study of the human corneal keratocyte density. *Current Eye Research* **14**(6), pp. 459-464.
Molofsky, A.V., Pardal, R., Iwashita, T., Park, I-K., Clarke, M.F. and Morison, S.J. (2003). Bmi-1 dependence distinguishes neural stem cell self-renewal from progenitor proliferation. *Nature* **425**, pp. 962-967.
Mort, R.L., Douvaras, P., Morley, S.D. Dora, N., Hill, R.E., Collinson, J.M. and West, J.D. (2012). Stem cell and corneal maintenance – insights from the mouse and other animal models. *Results and Problems in Cell Differentiation* **55**, pp. 357-394.
Mourao, P.A.S. (1988). Distribution of chondroitin 4-sulfate and chondroitin 6-sulphate in human articular and growth cartilage. *Arthritis & Rheumatology* **31**(8), pp. 1028-1033.
Mrini, A., Moukhles, H., Jacomy, H., Bosler, O. and Doucet, G. (1995). Efficient immunodetection of various protein antigens in glutaraldehyde-fixed brain tissue. *The Journal of Histochemistry and Cytochemistry* **43**, pp. 1285–1291.

Muller, L.J., Pels, L. and Vrensen, G.F. (1995). Novel aspects of the ultrastructural organization of human corneal keratocytes. *Investigative Ophthalmology & Visual Science*, **36**(13), pp. 2557-2567.

Murdoch, C. and Finn, A. (2000). Chemokine receptors and their role in inflammation and infectious disease. *The American Society of Hematology* **95**(10), pp.3032-3043.

Murtey, M. and Ramasamy, P. (2016). Sample preparations for scanning electron microscopy – life sciences. *Modern Electron Microscopy in Physical and Life Sciences*, pp.161-185.

Musil, L.S., Cunningham, B.A., Edelman, G.M. and Goodenough, D.A. (1990). Differential phosphorylation of the gap junction protein connexin43 in junctional communication-competent and -deficient cell lines. *Journal of Cell Biology* **111**(5 Pt 1), pp. 2077-2088.

Narisawa, Y., Kohda, H. and Tanaka, T. (1997). Three-dimensional demonstration of melanocyte distribution of human hair follicles: special reference to the bulge area. *Acta Dermoato-Venereologica* **77**(2), pp. 97-101.

Nadig, R. (2009). Stem cell therapy - Hype or hope? A review. *Journal of Conservative Dentistry* **12**(4), p.131-138.

Nakamura, T., Inatomi, T., Sotozono, C., Amemiya, T., Kanamura, N. and Kinoshita, S. (2004). Transplantation of cultivated autologous oral mucosal epithelial cells in patients with severe ocular surface disorders. *British Journal of Opthalmology* **88**(10), pp. 1280-1284.

Nakamura, T., Inatomi, T., Sotozono, C., Ang, L.P.K., Koizumi, N., Yokoi, N. and Kinoshita, S. (2006). Transplantation of autologous serum-derived cultivated corneal epithelial equivalents for the treatment of severe ocular surface disease. *Opthalmology* **113**(10), pp. 1765-1772.

Nakayasu, K., Tanaka, M., Konomi, H. Hayashi, T. (1986). Distribution of types I, II, III, IV and V collagen in normal and keratoconus corneas. *Ophthalmic Research* **18**(1), pp.1-10.

Nakazawa, K., Takahashi, I. and Yamamoto, Y. (1998). Glycosyltransferase and sulfotransferase activities in chick corneal stromal cells before and after in vitro culture. *Archives of Biochemistry and Biophysics* **359**(2), pp. 269-282.

Newsome, D.A., Foidart, J.M., Hassell, J.R., Krachmer, J.H., Rodrigues, M.M. and Katz, S.I. (1981). Detection of specific collagen types in normal and keratoconus corneas. *Investigative Opthalmology & Visual Science* **20**(6), pp. 738-750.

Newsome, D.A., Gross, J. and Hassell, J.R. (1982). Human corneal stroma contains three distinct collagens. *Investigative Opthalmology and Visual Science* **22**, pp. 376-381.

Nigro, J., Wang, A., Mukhopadhyay, D., Lauer, M., Midura, R.J., Sackstein, R. and Hascall, V.C. (2009). Regulation of heparan sulfate and chondroitin sulfate glycosaminoglycan biosynthesis by 4-fluoro-glucosamine in murine airway smooth muscle cells. *Journal of Biological Chemistry* **284**(25), pp. 16832-16839.

NIH Stem Cell Information Home Page. In *Stem Cell Information* [World Wide Web site]. Bethesda, MD: National Institutes of Health, U.S. Department of Health and Human Services, 2016 [cited July 17, 2019] Available at < //stemcells.nih.gov/info/2001report/appendixE.htm>

Nikitovic, D., Katonis, P., Tsatsakis, A., Karamanos, N.K. and Tzanakaksi, G.N. (2008). Lumican, a small leucine-rich proteoglycan. *International Union of Biochemistry and Molecular Biology: Life* **60**(12), pp. 818-823.

Nishida, K., Kinoshita, S., Ohashi, Y., Kuwayama, Y. and Yamamoto, S. (1995). Ocular surface abnormalities in aniridia. *American Journal of Ophthalmology* **120**(3), pp. 368-375.

Nishida, K., Yamato, M., Hayashida, Y., Watanabe, K., Yamamoto, K., Adachi, E., Nagai, S., Kikuchi, A., Maeda, N., Watanabe, H., Okana, T. and Tano, Y. (2004a). Corneal reconstruction with tissue-engineered cell sheets composed of autologous oral mucosal epithelium. *New England Journal of Medicine* **351**(12), pp. 1187-1196.

Nishida, K., Yamato, M., Hayashida, Y, Watanabe, K., Maeda, N., Watanabe, H., Yamamoto, K., Nagai, S., Kikuchi, A., Tano, Y. and Okano, T. (2004b). Functional bioengineered corneal epithelial sheet grafts from corneal stem cells expanded ex vivo on a temperature-response cell culture surface. *Transplantation* **77**(3), pp. 379-385.

Nishida, T., Ueda, A., Fukuda, M., Mishima, H., Yasumoto, K. and Otori, T. (1988). Interactions of extracellular collagen and corneal fibroblasts: morphologic and biochemical changes of rabbit corneal cells cultured in a collagen matrix. *In Vitro Cell Developmental Biology* **24**, pp. 1009-1014.

Nishida, T., Yasumoto, K., Otori, T. and Desaki, J. (1987). The network structure of corneal fibroblasts in the rat as revealed by scanning electron microscopy. *Investigative Ophthalmic & Visual Science* **29**(12), pp.1887-1890.

Nishina, S., Kohsaka, S., Yamaguchi, Y., Handa, H., Kawakami, A., Fujisawa, H. and Azuma, N. (1999). PAX6 expression in the developing human eye. *British Journal of Opthalmology* **83**(6), pp. 723-727.

Nishiyama, A., Lin, X.H., Giese, N., Heldin, C.H. and Stallcup, W.B. (1996). Co-localization of NG2 proteoglycan and PDGF ?-receptor on O2A progenitor cells in the developing rat brain. *Journal of Neuroscience Research* **43**(3), pp. 299-314.

Notara, M., Schrader, S. and Daniels, J,T. (2011). The porcine epithelial stem cell niche as a new model for the study of transplanted tissue-engineered human limbal epithelial cells. *Tissue Engineering Part A* **17**, pp. 741-50.

Novus Biologicals (2021). *General Flow Cytometry Protocol Using Detergents*. [online] Available at: <https://www.novusbio.com/support/support-by-application/flow-cytometry/protocol.html> [Accessed 17 June 2021].

Nowell, C.S. and Radtke, F. (2017). Corneal epithelial stem cells and their niche at a glance. *Journal of Cell Science* **130**, pp. 1021-1025.

Nunez, R. (2001). *Flow cytometry for research scientists*. Wymondham, Norfolk, U.K.: Horizon Press, pp.1-27.

Nuttall, R.P. DNA synthesis during the development of the chick cornea. Journal of Experimental Zoology **198**(2), pp. 193-208.
Odriozola, A., Llodra, J., Radecke, J., Ruegsegger, Tschanz, S., Saxena, S., Stephan, R. *et al.* (2017). High contrast staining for serial block face scanning electron microscopy without uranyl acetate. BioRxiv, pp. 1-11.
Oeben, M., Kelle, R., Stuhlsatz, H.W. and Greiling, H. (1987). Constant and variable domains of different disaccharide structure in corneal keratan sulphate chains. *Biochemical Journal* **248**(1), pp. 85-93.
Ohtani, O. (1992). The maceration technique in scanning electron microscopy of collagen fiber frameworks: its application in the study of human livers. *Archives of Histology and Cytology* **55**, pp. 225-232.
Omata, T., Itokazu, Y., Inoue, N. Segawa, Y. (2000). Effects of chondroitin sulfate-C on articular cartilage destruction in murine collagen-induced arthritis. *Arzneimittelforschung* **50**(2), pp. 148-153.
Ong-Chai, S. (1999). Investigation of the epitope in chondroitin sulphate chains recognised by monoclonal antibody 7D3. PhD Dissertation. School of Biological Sciences, University of Manchester, UK.
Onley, C. (2007). Antibodies for Immunochemistry. In: Renshaw, S. *Immunohistochemistry*. Oxfordshire: Scion Publishing Ltd., pp. 35-103.
Oohira, A., Matsui, F., Tokita, Y., Yamauchi, S. and Aono, S. (2000). Molecular interactions of neural chondroitin sulfate proteoglycans in the brain development. *Archives of Biochemistry and Biophysics* **374**(1), pp. 24-34.
Osborne, C.S., Reid, W.H. and Grant, M.H. (1998). Investigation into the biological stability of collagen/chondroitin-6-sulphate gels and their contraction by fibroblasts and keratinocytes: the effect of crosslinking agents and diamines. *Biomaterials* **20**, pp. 283-290.
Oyster, C. (2006). *The human eye*. Sunderland, Mass.: Sinauer Associates, pp. 1-50.
Panayi, G.S., Lanchbury, J.S. and Kingsley, G.H. (1992). The importance of the T cell in initiating and maintaining the chronic synovitis of rheumatoid arthritis. *Arthritis & Rheumatology* **35**(7), pp. 729-735.
Parfitt G.J., Pinali, C., Akama, T.O., Young, R.D., Nishida, K., Quantock A. J. and Knupp, C. (2011). Electron tomography reveals multiple self-association of chondroitin sulphate/dermatan sulphate proteoglycans in Chst5-null mouse corneas. *Journal of Structural Biology* **174**, pp. 536–541.
Parish, C., Castelo-Branco, G., Rawal, N., Tonnesen, J., Sorensen, A.T., Salto, C., Kokaia, M. *et al.* (2008). Wnt5a-treated midbrain neural stem cells improve dopamine cell replacement therapy in parkinsonian mice. *Journal of Clinical Investigation* **118**(1), pp. 149-160.
Park I.K., Qian, D., Kiel, M., Becker, M., Pihalja, M., Weissman, I.L., Morrison, S.J. *et al.* (2003). Bmi-1 is required for the maintenance of adult self-renewing hematopoietic stem cells. *Nature* **423**, pp. 302-305.
Park, C.Y., Lee, J.K., Zhang, C. and Chuck, R.S. (2015). New details of the human corneal limbus revealed with second harmonic generation imaging. *Investigative Opthalmology & Visual Science* **56**(10), pp. 6058-6066.
Park, I.K., Morrison, S.J., Clarke, M.F. (2004). Bmi1, stem cells, and senescence regulation. *The Journal of Clinical Investigation* **113**(2), pp. 175-179.
Park, I.K., Qian, D., Kiel, M., Becker, M.W., Pihalja, M. and Weissman, I.L. (2003). Bmi-1 is required for maintenance of adult self-renewing haematopoietic stem cells. *Nature* **423**(6937), pp.302-305.
Peles, E., Nativ, M., Campbell, P.L., Sakurai, T., Martinex, R., Levt, S., Clary, D.O. *et al.* (1995). The carbonic anhydrase domain of receptor tyrosine phosphatase beta in a functional ligand for the axonal cell recognition molecule contactin. *Cell* **82**(2), pp. 251–260.
Pellegrini, G. (2001). p63 identifies keratinocyte stem cells. *Proceedings of the National Academy of Sciences of the United States of America* **98**(6), pp.3156–3161.
Pellegrini, G., Dellambra, E., Golisano, O., Martinelli, E., Fantozzi, I., Bondanza, S., Ponzin, D. *et al.* (2001). P63 identifies keratinocyte stem cells. *Proceedings of the National Academy of Science* **98**(6), pp. 3156-3161.
Pellegrini, G., Golisano, O., Paterna, P., Lambiase, A., Bonini, S., Rama, P. and De Luca, M. (1999). Location and clonal analysis of stem cells and their differentiated progeny in the human ocular surface. *Journal of Cell Biology* **145**(4), pp. 769-782.
Pellegrini, G., Traverso, C.E., Franzi, A.T., Zingirian, M., Cancedda, R. and De Luca, M. (1997). Long-term restoration of damaged corneal surfaces with autologous cultivated corneal epithelium. *Lancet*, **349**(9057), pp. 990-993.
Persi, M.A. and Burnham, J.C. (1981). Use of tannic acid as a fixative-mordant to improve the ultrastructural appearance of *Candida albicans* blastospores. *Journal of Medical and Veterinary Mycology* **19**(1), pp.1-8.
Petersen, F., Bock, L., Flad, H.D. and Brandt, E. (1998). A chondroitin sulfate proteoglycan on human neutrophils specifically binds platelet factor 4 and is involved in cell activation. *Journal Immunology* **161**(8), pp. 4347-4355.
Petroll, W.M. and Miron-Mendoza, M. (2015). Mechanical interactions and crosstalk between corneal keratocytes and the extracellular matrix. *Experimental Eye Research* **133**, pp. 49-57.
Pinnamaneni, N. and Funderburgh, J.L. (2012). Concise Review: Stem cells in the corneal stroma. *Stem Cells* **30**, pp. 1059-63.
Pizzorusso, T., Medini, P., Berardi, N., Chierzi, S. Fawcett, J.W. and Maffei, L. (2002). Reactivation of ocular dominance plasticity in the adult visual cortex. *Science* **298**(5596), pp. 1248–1251.
Pizzorusso, T., Medini, P., Landi, S., Baldini, S., Berardi, N. and Maffei, L. (2006). Structural and functional recovery from early monocular deprivation in adult rats. *Proceedings of the National Academy of Sciences of the United States of* America **103**(22), pp. 8517–8522.
Polack, F.M. (1961). Morphology of the cornea. 1. Study with silver stains. *American Journal Ophthalmology* **51**, pp. 1051-

1056.
Pot, S.A., Liliensiek, S.J., Myrna, K.E., Bentley, E., Jester, J.V., Nealey, P.F. and Murphy, C.J. (2010). Nanoscale topography-induced modulation of fundamental cell behaviours of rabbit corneal keratocytes, fibroblasts, and myofibroblasts. *Investigative Opthalmology & Visual Science* **51**(3), pp. 1373-1381.
Prasadarao, N., Tobet, S.A. and Jungalwala, F.B. (1990). Effect of different fixatives on immunocytochemical localization of HNK-1-reactive antigens in cerebellum: a method for differentiating the localization of the same 1758carbohydrate epitope on proteins vs lipids. *The Journal of Histochemistry and Cytochemistry* **38**, pp. 1193–1200.
Quantock, A.J. (2003). Collagen organization in the secondary chick cornea during development. *Investigative Opthalmology & Visual Science* **44**(1), pp.130-136.
Quantock, A.J. and Young, R.D. (2008). Development of the corneal stroma, and the collagen-proteoglycan associations that help define its structure and function. *Developmental Dynamics* **237**(10), pp. 2607-2621.
Quantock, A.J., Boote, C., Siegler, S. and Meek, K.M. (2003). Collagen organization in the secondary chick cornea during development. *Investigative Opthalmology & Visual Science* **44**(1), p. 130-136.
Quantock, A.J., Meek, K.M. and Chakravarti, S. (2001). An X-ray diffraction investigation of corneal structure in lumican-deficient mice. *Investigative Ophthalmology & Visual Science* **42**(8), pp. 1750-1756.
Quantock, A.J., Young, R.D. and Akama, T.O. (2010). Structural and biochemical aspects of keratan sulphate in the cornea. *Cellular and Molecular Life Sciences* **67**(6), pp. 891-906.
Queiroz de K (1982). The scleral ossicles of sceloporine iguanids: a reexamination with comments on their phylogenetic significance. *Herpetologica* **38**, pp. 302-311.
R Core Team (2019). R: A Language and Environment for Statistical Computing. R Foundation for Statistical Computing, Vienna, Austria.
Radner, W. and Mallinger, R. (2002). Interlacing of collagen lamellae in the midstroma of the human cornea. *Cornea* **21**(6), pp. 598-601.
Radner, W., Zehetmayer, M., Aufreiter, R. and Mallinger, R. (1998). Interlacing and cross-angle distribution of collagen lamellae in the human cornea. *Cornea* **17**(5), pp. 537-543.
Rama, P., Matuska, S., Paganoni, G., Spinelli, A., de Luca, M. and Pellegrini, G. (2010). Limbal stem-cell therapy and long-term corneal regeneration. *The New England Journal of Medicine* **363**, pp. 147-155.
Ramaesh, T. (2003). Corneal abnormalities in Pax6+ /− small eye mice mimic human aniridia-related keratopathy. *Investigative Ophthalmology & Visual Science* **44**(5), pp.1871–1878.
Ramaesh, T. (2006). Increased apoptosis and abnormal wound-healing responses in the heterozygous Pax6+/- mouse cornea. *Investigative Ophthalmology & Visual Science* **47**(5), pp.1911–1917.
Rankin, S.M. (2012). Chemokines and adult bone marrow stem cells. Immunology *Letters* **145**, pp. 47-54.
Ratajczak, M.Z., Serwin, K. and Schneider, G. (2012). Innate immunity derived factors as external modulators of the CXCL12-CXCR4 axis and their role in stem cell homing and mobilization. *Theranostics* **3**(1), pp. 3-10.
Ratkay-Traub, I., Hopp, B., Bor, Zs., Dux, L., Becker, D.L. and Krenacs, T. (2001). Regeneration of rabbit cornea following excimer laser photorefractive keratectomy: a study of gap junctions, epithelial junctions and epidermal growth factor receptor expression in correlation with cell proliferation. *Experimental Eye Research* **73**(3), pp. 291-302.
Ratliff, B.B., Singh, N., Yasuda, K., Park, H-C., Addabbo, F., Ghaly, T., Rajdev, M. *et al.* (2010). Mesenchymal stem cells, used as bait, disclose tissue binding sites: A tool in the search for the niche? *American Journal of Pathology* **177**(2), pp.873–883.
recognition motif. Curr. Opin. Struct. Biol. 11, 725–732.
Reed, C.C. and Iozzo, R.V. (2002). The role of decorin in collagen fibrillogenesis and skin homeostasis. *Glycoconjugate Journal* **19**, pp. 249–55.
Ren, R., Hutcheon, A.E.K., Guo, X.Q., Saeidi, N., Melotti, S.A., Ruberti, J.W., Zieske, J.D. *et al.* (2008). Human primary corneal fibroblasts synthesize and deposit proteoglycans in long-term 3-D cultures. *Developmental Dynamics* **237**(10), pp.2705-2715.
Reza, H.M., Ng, B.Y., Gimeno, F.L., Phan, T.T. and Ang, L.P.K. (2011). Umbilical cord lining stem cells as a novel and promising source for ocular surface regeneration. *Stem Cell Reviews and Reports* **7** (4), pp. 935-947.
Ribeiro-Rodrigues, T.M., Martins-Marques, T., Morel, S., Kwak, B.R. and Girao, H. (2017). Role of connexin 43 in different forms of intercellular communication – gap junctions, extracellular vesicles and tunnelling nanotubes. *Journal of Cell Science* **130**(21), pp.3619-3630.
Ritchey, E.R., Code, K., Zelinka, C., Scott, M. and Fischer, A. (2011). The chicken cornea as a model of wound healing and neuronal reinnervation. *Molecular Vision* **17**, pp.2440-2454.
Robson, L.G., Di Foggia, V., Radunovic, A., Bird, K. Zhang, X. and Marino, S. (2011). Bmi1 is expressed in postnatal myogenic satellite cells, controls their maintenance and plays an essential role in repeated muscle regeneration. *PLOS ONE* **6**(11), e27116.
Rochat, A. and Kobayashi, K. (1994). Location of stem cell of human hair follicles by clonal analysis. *Cell* **76**, pp. 1063-1073.
Rodrigues, M., Nirankari, V., Rajagopalan, S., Jones, K. and Funderburgh, J.L. (1992). Clinical and histopathological changes in the host cornea after epikeratoplasty for keratoconus. *American Journal of Opthalmology* **114**(2), pp. 161-170.

Rolls, A., Cahalon, L., Bakalash, S., Avidan, H., Lider, O. and Schwartz, M. (2006). A sulfated disaccharide derived from chondroitin sulfate proteoglycan protects against inflammation-associated neurodegeneration. *FASEB Journal* **20**(3), pp.547-549.

Rolls, A., Shechter, R. and Schwartz, M. (2008a). The bright side of the glial scar in CNS repair. *Nature Reviews Neuroscience* **10**(3), pp. 235–241.

Rolls, A., Shechter, R., London, A., Segev, Y., Jacob-Hirsch, J., Amariglio, N., Rechavi, G. *et al.* (2008b). Two faces of chondroitin sulfate proteoglycan in spinal cord repair: a role in microglia/macrophage activation. *PLoS Medicine* **5**(8): e171.

Romano, A.C. Espana, E.M., Yoo, S.H., Budak, M.T., Wolosin, M. and Tseng, S.C.G. (2003). Different cell sizes in human limbal and central corneal basal epithelia measured by confocal microscopy and flow cytometry. *Investigative Ophthalmology and Visual Science* **44**, pp. 5125–5129.

Rosendaal, M., Green, C.R., Rahman, A. and Morgan, D. (1994). Up-regulation of the connexin43+ gap junction network in haemopoietic tissue before the growth of stem cells. Journal of Cell Science **107**(Pt. 1), pp. 29 – 37.

Sajdera, S. and Hascall, V. (1969). Proteinpolysaccharide Complex from Bovine Nasal Cartilage: A Comparison of Low and High Shear Extraction Procedures. *Journal of Biological Chemistry* **24**(1), pp. 77-87.

Sakai, K., Kimata, K., Sato, T., Gotoh, M., Narimatsu, H., Shinomiya, K. and Watanabe, H. (2007). Chondroitin sulfate N-acetylgalactosaminyltransferase-1 plays a critical role in chondroitin sulfate synthesis in cartilage. *Journal of Biological Chemistry* **282**(6), pp. 4152-4161.

Salzmann, M. (1912). *The anatomy and histology of the human eyeball in the normal state, its development and senescence*. Chicago: [University Press], pp. 191-203.

Sanchez-Pulido, L., Devos, D., Sung, Z.R., and Calonje, M. (2008). RAWUL: a new ubiquitin-like domain in PRC1 ring finger proteins that unveils putative plant and worm PRC1 orthologs. *BMC Genomics* **9**(308), pp.1-11.

Sandvig, A., Berry, M., Barrett, L.B., Butt, A. and Logan, A. (2004). Myelin-, reactive glia-, and scarderived CNS axon growth inhibitors: expression, receptor signaling, and correlation with axon regeneration. *Glia* **46**(3), pp. 225-251.

Sandy, J.D. (1992). The structure of aggrecan fragments in human synovial fluid. Evidence for the involvement in osteoarthritis of a novel proteinase which cleaves the Glu 373\Ala 374 bond of the interglobular domain. *Journal of Clinical Investigation* **89**(5), pp. 1512-1516.

Sangwan, V., Basu, S., Vemuganti, G.K., Sejpal, K., Subramaniam, S.V., Bandyopadhyay, S., Krishnaiah, S. *et al.* (2011). Clinical outcomes of xeno-free autologous cultivated limbal epithelial transplantation: a 10-year study. *British Journal of Opthalmology* **95**(11), pp. 1525-1529.

Sansom, S.N., Griffiths, D.S., Faedo, A., Kleinjan, D.J., Ruan, Y., Smith, J., van Heyningen, V. *et al.* (2009). The level of the transcription factor Pax6 is essential for controlling the balance between neural stem cell self-renewal and neurogenesis *PLOS Genetics* **5**(6), e1000511.

Sasamoto, Y., Hayashi, R., Park, S-J., Saito-Adachi, M., Suzuki, Y., Kawasaki, S., Quantock, A.J. *et al.* (2016). PAX6 isoforms, along with reprogramming factors, differentially regulate the induction of cornea-specific genes. *Scientific Reports* **6**(1), pp.1-14.

Sasamoto, Y., Ksander, B.R., Frank, M.H. and Frank, N.Y. (2018). Repairing the corneal epithelium using limbal stem cells or alternative cell-based therapies. *Expert Opinion of Biological Therapy* **18**(5), pp. 505-513.

Sato, Y. and Oohira, A. (2009). Chondroitin sulfate, a major niche substance of neural stem cells, and cell transplantation therapy of neurodegeneration combined with niche modification. *Current Stem Cell Research & Therapy* **4**(3), pp. 200-209.

Satoh, A., Kojima, K., Koyama, T., Ogawa, H. and Matsumoto, I. (1998). Immobilization of saccharides and peptides on 96-well microtiter plates coated with methyl vinyl ether–maleic anhydride copolymer. *Analytical Biochemistry* **260**(1), pp. 96–102.

Sauerland, K., Plaas, A.H.K., Raiss, R.X. and Steinmeyer, J. (2003). The sulfation pattern of chondroitin sulfate from articular cartilage explants in response to mechanical loading. *Biochimica et Biophysica Acta - Molecular Basis of Disease* **1638**(3), pp. 241-248.

Scalia, C.R., Boi, G., Bolognesi, M.M., Riva, L., Manzoni, M., DeSmedt, L., Bosisio, F.M. *et al.* (2016). Antigen masking during fixation and embedding, dissected. *Journal of Histochemistry & Cytochemistry* **65**(1), pp. 5-20.

Schermer, A., Galvin, S., and Sun, T.T. (1986). Differentiation-related expression of a major 64K corneal keratin in vivo and in culture suggest limbal location of corneal epithelial stem cells. *Journal of Cell Biology* **103**(1), pp. 49-62.

Schlotzer-Schrehardt, U. and Kruse, F.E. (2005). Identification and characterization of limbal stem cells. *Experimental Eye Research* **81**(3), pp. 247-364.

Schlotzer-Schrehardt, U., Dietrich, T., Saito, K., Sorokin, L., Sasaki, T., Paulsson, M., and Kruse, F.E. (2007). Characterisation of extracellular matrix components in the limbal epithelial stem cell compartment. Experimental eye research **85**(6), pp. 845-860.

Schmut, O. (1977). The identification of type III collagen in calf and bovine cornea and sclera. *Experimental Eye Research* **25**(5), pp. 505-509.

Schwartz, N.B. (1977). Regulation of chondroitin sulfate synthesis. Effect of beta-xylosides on synthesis of chondroitin sulfate proteoglycan, chondroitin sulfate chains, and core protein. *Journal of Biological Chemistry* **252**, pp. 6316–6321.

Scott, J.E. (1975). Composition and structure of the pericellular environment. Physiological function and chemical

composition of pericellular proteoglycan (an evolutionary view). *Philosophical Transactions of the Royal Society London B: Biological Science* **271**(912), pp. 135-142.
Scott, J.E. (1991). Proteoglycan: collagen interactions in connective tissues. Ultrastructural, biochemical, functional and evolutionary aspects. *International Journal of Biological Macromolecules* **13**(3), pp. 157-61.
Scott, J.E. (1995). Extracellular matrix, supramolecular organisation and shape. *Journal of Anatomy* **187**(Pt 2), pp. 259-269.
Scott, J.E. (2001). Structure and function in extracellular matrices depend on interactions between anionic glycosaminoglycans. *Pathology Biology* **49**(4), pp. 284-289.
Scott, J.E. and Haigh, M. (1988). Identification of specific binding sites for keratan sulphate proteoglycans and chondroitin-dermatan sulphate proteoglycans on collagen fibrils in cornea by the use of cupromeronic blue in 'critical-electrolyte-concentration' techniques. *Biochemical Journal* **253**(2), pp. 607-610.
Scott, S-G., Jun, A.S. and Chakravarti, S. (2011). Sphere formation from corneal keratocytes and phenotype specific markers. *Experimental Eye Research* **93**(6), pp. 898-905.
Secker, G.A. and Daniels, J.T. (2008). Corneal epithelial stem cells: deficiency and regulation. *Stem Cell Reviews* **4**(3), pp. 159-168.
Secker, G.A. and Daniels, J.T. (2009). *Limbal Epithelial Stem Cells of the Cornea* [Online]. Massachusetts: The Stem Cell Research Community. Available at: http://www.stembook.org/node/588.html [Accessed: 10 December 2017].
Seligman, A.M., Wasserkrug, H.L. and Hanker, J.S. (1996). A new staining method (OTO) for enhancing contrast of lipid-containing membranes and droplets in osmium-tetroxide-fixed tissue with osmiophilic thiocarbohydrazide (THC). *Journals of Cell Biology* **30**(2), pp. 424-432.
Shanmuganathan, V.A., Foster, T., Kulkarni, B.B., Hopkinson, A., Gray, T., Powe, D.G., Lowe, J. *et al.* (2007). Morphological characteristics of the limbal epithelial crypts. *British Journal of Ophthalmology* **91**(4), pp. 514-519.
Sharma, A. and Coles, W. H. (1989). Kinetics of corneal epithelial maintenance and graft loss. A population balance model. *Investigative Ophthalmology & Visual Science* **30**(9), pp. 1962-1971.
Sherwin, T. (2016). Defining the limbal stem cell niche. Journal of Cell Signalling **1**(3), e1000119.
Shibata, S., Hayashi, R., Okubo, T., Kudo, Y., Katayama, T., Ishikawa, Y., Toga, J. *et al.* (2018). Selective laminin-directed differentiation of human induced pluripotent stem cells into distinct ocular lineages. *Cell Reports* **25**(6), pp. 1668–1679.
Shintani, T., Watanabe, E., Maeda, N. and Noda, M. (1998). Neurons as well as astrocytes express proteoglycan-type protein tyrosine phosphatase ζ/RPTPβ: analysis of mice in which the PTPζ/RPTPβ gene was replaced with the LacZ gene. *Neuroscience Letters* **247**(2-3), pp.135-138.
Shortt, A.J., Secker, G.A., Munro, P.M., Khaw, P.T., Tuft, S.J. and Daniels, J.T. (2007a). Characterization of the limbal epithelial stem cell niche: Novel imaging techniques permit in vivo observation and targeted biopsy of limbal epithelial stem cells. *Stem Cells* **25**(6), pp. 1402–1409.
Shortt, A.J., Secker, G.A., Notara, M.D., Limb, G.A., Khaw, P.T., Tuft, S.J. and Daniels, J.T. (2007b). Transplantation of ex vivo cultured limbal epithelial stem cells: a review of techniques and clinical results. *Survey of Ophthalmology* **52**(5), pp. 483-502.
Sidney, L.E., Branch, M.J., Dua, H.S. and Hopkinson, A. (2015). Effect of culture medium on propagation and phenotype of corneal stroma-derived stem cells. *Cytotherapy* **17**, pp. 1706-1722.
Sikora, B., Skubis-Sikora, A., Kimsa-Furszik, M., Ciszek, W., Kostrzewski, M., Stojko, J., Mazurek, U. *et al.* (2019). Adipose-derived ste cells undergo differentiation after co-culture with porcine limbal epithelial stem cells. *Stem Cell Research* **41**, e101609.
Silbert, J.E. and Sugumaran, G. (2002). Biosynthesis of Chondroitin/Dermatan Sulfate. *Journal of the International Union of Biochemistry and Molecular Biology* **54**(4), pp 177-186.
Simpson, T.I. and Price, D.J. (2002). Pax6; a pleiotropic player in development. *Bioessays* **24**(11), pp. 1041-1051.
Singh, V., Tiwari, A., Kethiri, A.R. and Sangwan, V.S. (2021). Current perspectives of limbal-derived stem cells and its application in ocular surface regeneration and limbal stem cell transplantation. *Stem Cells Translational Medicine* **10**, pp. 1121-1128.
Sirko, S., Von Hoist, A., Wizenmann, A., Gotx, M. and Faissner, A. (2007). Chondroitin sulfate glycosaminoglycans control proliferation, radial glia cell differentiation and neurogenesis in neural stem/progenitor cells. *Development* **134**(15), pp. 2727-2738.
Sivak, J.M., Mohan, R., Rinehart, W.B., Xu, P.X., Maas, R.L., and Fini, M.E. (2002). Pax-6 expression and activity in the reepithelialising cornea control activity of the transcriptional promoter for matrix metalloproteinase gelatinase B. *Developmental Biology* **222**(1), pp.41–54.
Sivak, J.M., West-Mays, J.A., Yee, A., Williams, T. and Fini, M.E. (2004). Transcription factors Pax6 and AP-2alpha interact to coordinate corneal epithelial repair by controlling expression of matrix metalloproteinase Gelatinase B. *Molecular Cell Biology* **24**(1), pp.245–257.
Smith, D. and Starborg, T. (2019). Serial block face scanning electron microscopy in cell biology: Applications and technology. *Tissue and Cell* **57**, pp.111-122.
Soares, A.R., Martines-Marques, T., Ribeiro-Rodrigues, T., Ferreira, J.V.,Cararino, S., Pinho, M.J., Zuzarte, M. *et al.* (2015). Gap junctional protein Cx43 is involved in the communication between extracellular vesicles and mammalian cells. *Scientific Reports* **5**, e13243.

Sobel, R.A. and Ahmed, A.S. (2001). White matter extracellular matrix chondroitin sulfate/dermatan sulfate proteoglycans in multiple sclerosis. *Journal of Neuropathology & Experimental Neurology* **60**(12), pp. 1198-1207.
Song, R.H., Tortorella, M.D., Malfait, A.M. Alston, J.T., Yang, Z. Arner, E.C. and Griggs, D.W. (2007). Aggrecan degradation in human articular cartilage explants is mediated by both ADAMTS-4 and ADAMTS-5. *Arthritis & Rheumatology* **56**(2), pp. 575-585.
Sorgen, P.L., Trease, A.J., Spagnol, G., Delmar, M. and Nielsen, M.S. (2018). Protein-protein interactions with connexin 43: regulation and function. *International Journal of Molecular Science* **19**(5): e1428.
Sorrell J.M., Carrino, D.A. and Caplan, A.I. (1996). Regulated expression of chondroitin sulfates at sites of epithelial mesenchymal interaction: spatio-temporal patterning identified with anti-chondroitin sulphate monoclonal antibodies. *International Journal of Developmental Neuroscience* **14**(3), pp. 233-248.
Sorrell J.M., Mahmoodian, F., Schafer, I.A., Davis, B. and Caterson, B. (1990). Identification of monoclonal antibodies that recognize novel epitopes in native chondroitin/dermatan sulphate glycosaminoglycan chains: their use in mapping functionally distinct domains of human skin. *Journal of Histochemical Cytochemistry* **38**(3), pp. 393-402.
Sorrell, J.M., Carrino, D.A. and Caplan, A.I. (1993). Structural Domains in Chondroitin Sulfate Identified by Anti-Chondroitin Sulfate Monoclonal Antibodies. Immunosequencing of Chondroitin Sulfates. *Matrix* **13**(5), pp. 351-361.
Sorrell, J.M., Lintala, A.M., Mahmoodian, F. and Caterson, B. (1988). Epitope-specific changes in chondroitin sulphate/dermatan sulphate proteoglycans as markers in the lymphopoietic and granulopoietic compartments of developing bursae of Fabricius. *Journal of Immunology* **140**(12), pp. 4263-4270.
Spanakis, S.G., Petridou, S. and Masur, S.K. (1998). Functional gap junctions in corneal fibroblasts and myofibroblasts. *Investigations in Opthalmology & Visual Science* **39**(8), pp. 1320-1328.
Stanton, H., Rogerson, F.M., East, C.J., Golub, S.B., Lawlor, K.E., Meeker, C.T., Little, C.B. *et al.* (2005). ADAMTS5 is the major aggrecanase in mouse cartilage in vivo and in vitro. *Nature* **434**(7033), pp. 648-652.
Stearns, M.L. (1940). Studies of the development of connective tissue in transparent chambers in the rabbit's ear. *American Journal of Anatomy* **66**(1), pp. 133-176.
Stepp, M.A., Zhu, L., Sheppard, D. and Cranfill, R.L. (1995). Localized distribution of alpha 9 integrin in the cornea and changes in expression during corneal epithelial cell differentiation. *Journal of Histochemistry and Cytochemistry* **43**(4), pp. 353–362.
Stewart, J.C., Villasmil, M.L. and Frampton, M.W. (2007). Changes in fluorescence intensity of selected leukocyte surface markers following fixation. *Cytometry Part A* **71A**(6), pp. 379-385.
Stoesser, T.R., Church, R.L., and Brown, S.I. (1978). Partial characterization of human collagen and procollagen secreted by human corneal stromal fibroblast in cell culture. *Investigative Opthalmology & Visual Science* **17**(3), pp. 264-271.
Stoykova, A. and Gruss, P. (1994). Roles of Pax-6 genes in developing and adult brain as suggested by expression patterns. *Journal of Neuroscience* **14** (3 Pt 2), pp. 1395-1412.
Sugahara, K. and Mikami, T. (2007). Chondroitin/dermatan sulfate in the central nervous system. *Current Opinion in Structural Biology* **17**(5), pp. 536-545.
Sulzer, B., De Boer, R.J. and Perelson, A.S. (1996). Cross-linking reconsidered: binding and cross-linking fields and the cellular response. *Biophysical Journal* **70**, pp. 1154-1168.
Sun, T.T. (1984). Classification, expression, and possible mechanisms of evolution of mammalian epithelial keratins: A unifying model. In: *Levine, A. et al. . Classification, expression and possible mechanisms of evolution of mammalian epithelial keratins: A unifying mode*. New York: Cold Spring Harbor, pp. 169-176.
Sun, T.T. and Lavker, R.M. (2004). Corneal epithelial stem cells: past, present, and future. *The Journal of Investigative Dermatology* **9**(3), pp.202-207.
Suzuki, E. (2002). High-resolution scanning electron microscopy of immunogold-labelled cells by the use of plasma coating of osmium. *Journal of Microscopy* **208**(3), pp.153-157.
Suzuki, M. (1939). Biochemical studies on carbohydrates: L. Prosthetic group of corneamucoid. *Journal of Biochemistry* **30**(2), pp. 185-191.
Takada, W., Fukushima, M., Pothacharoen, P., Kongtawelert, P. and Sugahara, K. (2013). A sulfated glycosaminoglycan array for molecular interactions between glycosaminoglycans and growth factors or anti-glycosaminoglycan antibodies. *Analytical Biochemistry* **435**(2), pp. 123– 130.
Tang, X., Davies, J.E. and Davies, S.J. (2003). Changes in distribution, cell associations, and protein expression levels of NG2, neurocan, phosphacan, brevican, versican V2, and tenascin-C during acute to chronic maturation of spinal cord scar tissue. *Journal of Neuroscience Research* **71**(3), pp. 427-444.
Telford, W.G., Babin, S.A., Khorev, S.V. and Rowe, S.H. (2009). Green fiber lasers: an alternative to traditional DPSS green lasers for flow cytometry. *Cytometry Part A* **75A**(12), pp. 1031-1039.
Thakur, S.D., Obradovic, M., Dillon, J.R., Ng, S.G. and Wilson, H.L. (2019). Development of flow cytometry based adherence assay for Neisseria gonorrhoeae using 5'-carboxyfluorosceinsuccidyl ester. *BMC Microbiology* **19**(67).
Thale, A. and Tillmann, B. (1993). The collagen architecture of the sclera – SEM and immunohistochemical studies. *Annals of Anatomy* **175**(3), pp. 215-220.
Thavarajah, R., Mudimbaimannar, V.K., Elizabeth, J., Rao, U.K. and Ranganathan, K. (2012). Chemical and physical basics of routine formaldehyde fixation. *Journal of Oral and Maxillofacial Pathology* **16**(3), pp. 400-405.

Thoft, R.A. and Friend, J. (1983). The X, Y, Z hypothesis of corneal epithelial maintenance. *Investigative Ophthalmology & Visual Science* **24**(10), pp. 1442-1443.

Tittarelli, A., Guerrero, I., Tempio, F., Gleisner, M.A., Avalos, I., Sabanegh, S., Ortiz, C. *et al.* (2015). Overexpression of connexin 43 reduces melanoma proliferative and metastatic capacity. *British Journal of Cancer* **113**, pp. 259-267.

Ton, C.C.T, Miwa, H. and Saunders, G.F. (1991). Small eye (Sey): Cloning and Characterization of the Murine Homolog of the Human Aniridia Gene. *Genomics* **13**, pp. 251-256.

Townsend, W.M. (1991). The limbal palisades of Vogt. *Transactions of the American Ophthalmological Society* **89**, pp. 721–756.

Tribble, J.R, Williams, P.E., Caterson, B., Sengpiel, F. and Morgan, J.E. (2018). Digestion of the glycosaminoglycan extracellular matrix by chondroitinase ABC supports retinal ganglion cell dendritic preservation in a rodent model of experimental glaucoma. *Molecular Brain* **11**, e69.

Tsai, R., Li, L.M. and Chen, J.K. (2000). Reconstruction of damaged corneas by transplantation of autologous limbal epithelial cells. *New England Journal Medicine*, **343**(2), pp. 86-93.

Tseng, S.C. (1989). Concept and application of limbal stem cells. *Eye* **3**(Pt 2), pp. 141-157.

Tseng, S.C., Jarvinen, M.J., Nelson, W.G., Huang, J.W., Woodcock-Mitchell, J. and Sun, T.T. (1982). Correlation of specific keratins with different types of epithelial differentiation: monoclonal antibody studies. *Cell* **30**(2), pp. 361-372.

Tseng, S.C.G. (1996). Regulation and clinical implications of corneal epithelial stem cells. *Molecular Biology Reports* **23**, pp.47-58.

Tsubota, K., Satake, Y., Kaido, M., Shinozaki, N., Shimmura, S., Bissen-Miyajima, H. and Shimazaki, J. (1999). Treatment of Severe Ocular-Surface Disorders with Corneal Epithelial Stem-Cell Transplantation. *New England Journal of Medicine* **340**(22), pp.1697-1703.

Turque, N., Plaza, S., Radvanyi, F., Carriere, C. and Saule, S. (1994). Pax-QNR/Pax-6, a paired box- and homeobox-containing gene expressed in neurons, is also expressed in pancreatic endocrine cells. *Molecular Endocrinology* **8** (7), pp. 929-938.

van der Lugt, N.M., Domen, J., Linder, K., van Room, M., Robanus-Maandag, E., te Riele, H., van der Valk, M., Deschamps, J., Sofroniew, M. and van Lohuizen, M. (1994). Posterior transformation, neurological abnormalities, and severe hematopoietic defects in mice with a targeted deletion of the bmi-1 proto-oncogene. *Genes and Development* **8**(7), pp. 757-769.

van der Lugt, N.M.T., Alema, M., Berns, A. and Deschamps, J. (1996). The Polycomb-group homolog Bmi-1 is a regulator of murine Hox gene expression. *Mechanisms of Development* **58**(1-2), pp.153–164.

Vertel, B.M., Walters, L.M., Flay, N., Kearns, A.E. and Schwartz, N.B. (1993). Xylosylation in an endoplasmic reticulum to Golgi even. *Journal of Biological Chemistry* 268(15), pp. 11105-11112.

Victor, X.V., Nguyen, T.K.N., Ethirajan, M., Tran, V.M., Nguyen, K.V. and Kuberan, B. (2009). Investigating the elusive mechanism of glycosaminoglycan biosynthesis. *Journal of Biological Chemistry* **284**(38), pp. 25842-25853.

Vogel, K.G., Paulsson, M. and Heinegard, D. (1984). Specific inhibition of type I and type II collagen fibrillogenesis by the small proteoglycan of tendon. *Biochemical Journal* **223**(3), pp. 587-597.

Vogt, A. (1977). *Atlas of slit Lamp microscopy of the living eye*. Berlin: J. Springer, pp. 6-23.

von der Mark, K., von der Mark, H., Timpl, R. and Trelstad, R.L. (1977). Immunofluorescent localization of collagen types I, II, and III in the embryonic chick eye. *Developmental Biology* **59**, pp. 75-85.

Voncken, J. W., Schweizer, D., Aagaard, L., Sattler, L., Jantsch, M.F. and van Lohuizen, M. (1999). Chromatin-association of the Polycomb group protein BMI1 is cell cycleregulated and correlates with its phosphorylation status. *Journal of Cell Science* **112**, pp. 4627-4639.

Wagoner, M. D. (1997). Chemical injuries of the eye: current concepts in pathophysiology and therapy. *Survey of Ophthalmology* **41**(4), pp. 275-313.

Walther, C. and Gruss, P. (1991). Pax-6, a murine paired box gene, is expressed in the developing CNS. *Development* **113**(4), pp.1435–1449.

Wang, G., Wang, L., Erdjument-Bromage, H., Vidal, M., Tempst, P., Jones, R.S. and Zhang, Y. (2004). Role of histone H2A ubiquitination in polycomb silencing. *Nature* **431**(7010), pp.873-878.

Wang, I-J., Tsai, R.J-F., Yeh, L-K., Tsai, R.Y-N., Hu, F-R., Kao, W.W.Y. (2011). Changes in corneal basal epithelial phenotypes in an altered basement membrane. *PLOS ONE* **6**(1), e145537.

Wang, K., Hoshino, M., Uesugi, K., Yagi, N., Young, R.D., Frost, B.E., Regini, J.W. et al. (2020). Cell compaction is not required for the development of gradient refractive T index profiles in the embryonic chick lens. *Experimental Eye Research* **197**, 108112.

Wang, X., Veruki, M.L., Bukoreshtliev, N.V., Hartveit, E. and Gerdes, H.H. (2010). Animal cells connected by nanotubes can be electrically coupled through interposed gap-junction channels. *Proceedings of the National Academy of Sciences of the Unite States of America* **107**(40), pp.17194-17199.

Wang, Y., Zang, X., Wang, Y. and Chen, P. (2012). High expression of $p16^{INK4a}$ and low expression of Bmi1 are associated with endothelial cellular senescence in the human cornea. *Molecular Vision* **18**, pp. 803-8165.

Ward, A.C., Dowthwaite, G.P. and Pitsillides, A.A. (1999). Hyaluronan in joint cavitation. *Biochemical Society Transactions* **27**(2), pp. 128.135.

Waring, G., Bourne, W.M., Edelhauser, H.F. and Kenyon, K.R. (1982). The Corneal Endothelium: Normal and Pathologic Structure and Function. *Opthalmology* **89**(6), pp. 531-590.
Watanabe, H., Yamada, Y. and Kimata, K. (1998). Roles of aggrecan, a large chondroitin sulfate proteoglycan, in cartilage structure and function. *Journal of Biochemistry* **124**(4), pp.687-693.
Wei, Z., Sun, T.T. and Lavker, R.M. (1996). Rabbit conjunctival and corneal epithelial cells belong to two separate lineages. *Investigative Ophthalmology & Visual Science* **37**(4), pp. 523-533.
Weiss, P. and Jackson, S. (1961). Fine-structural changes associated with lens determination in the avian embryo. *Developmental Biology* **3**(4), pp. 532-554.
West-Mays, J.A. and Dwivedi, D. (2006). The keratocyte: corneal stromal cell with variable repair phenotypes. *The International Journal of Biochemistry & Cell Biology* **38**(10), pp.1625-1631.
West-Mays, J.A., Strissel, K.J., Sadow, P.M. and Fini, M.E. (1995). Competence for collagenase gene expression by tissues fibroblasts requires activation of an IL-1α autocrine loop. *Proceedings of the National Academy of Sciences of the United States of America* **92**(15), pp. 6768-6772.
Wickham, H. (2009). ggplot2. New York: Springer.
Williams, R., Khan, I.M., Richardson, K., Nelson, L., McCarthy, H.E., Analbelsi, T., Singhrao, S.K. *et al.* (2010). Identification and clonal characterisation of a progenitor cell sub-population in normal human articular cartilage. *PLos One* **5**, e13346.
Willingham, M.C. and Rutherford, A.V. (1983). The use of osmium-thiocarbohydrazide-Osmium (OTO) and ferrocyanide-reduced osmium methods to enhance membrane contrast and preservation in cultured cells. *The Journal of Histochemistry and Cytochemistry* **32**(4), pp. 455-460.
Wilson, S. and Hong, J. (2000). Bowman's Layer Structure and Function. *Cornea* **19**(4), pp.417-420.
Wilson, S.E. (2012). Corneal myofibroblast biology and pathobiology: generation, persistence, and transparency. *Experimental Eye Research* **99**(1), pp. 78-88.
Wilson, S.E., Netto, M. and Ambrosio, R. (2003). Corneal cells: chatty in development, homeostasis, wound healing, and disease. *American Journal of Ophthalmology* **136**(3), pp. 530-536.
Winkler, M., Shoa, G., Tran, S.T., Xie, Y., Thomasy, S., Raghunathan, V.K., Murphy, C. *et al.* (2015). A comparative study of vertebrate corneal structure: the evolution of a refractive lens. *Investigative Ophthalmology & Visual Science* **56**(4), pp. 2764-72.
Wisely, C., Sayed, J.A., Tamez, H., Zelinka, C., Abdel-Rahman, M.H., Fischer, A.J. and Cebulla, C.M. (2018). The chick eye in vision research: An excellent model for the study of ocular disease. *Progress in Retinal and Eye Research* **61**, pp.72-97.
Wolosin, J.M., Schutte, M., Zieske, J.D. and Badak, M.T. (2002). Changes in connexin 43 in early ocular surface development. *Current Eye Research* **24**(6), pp. 430-438.
Wolosin, J.M., Xiong, X., Schutte, M., Stegman, Z., Tient, A. (2000). Stem cells and differentiation stages in the limbo-corneal epithelium. *Progress in Retinal and Eye Research* **19**(2), pp. 223-255.
Wright, B., Mi, S. and Connon, C.J. (2013). Towards the use of hydrogels in the treatment of limbal stem cell deficiency. *Drug Discovery Today* **18**(1-2), pp.79-86.
Wu, J.J. (1992). Identification of cross-linking sites in bovine cartilage type IX collagen reveals an antiparallel type II–type IX molecular relationship and type IX to type IX bonding. *Journal of Biological Chemistry* **267**(32), pp. 23007–23014.
Wu, J.J. and Eyre, D.R. (1995). Structural analysis of cross-linking domains in cartilage type XI collagen: Insights on polymeric assembly. *Journal Biological Chemistry* **270**(32), pp. 18865–18870.
Wylde, V., Dieppe, P., Hewlett, S. and Learmonth, I.D. (2007). Total knee replacement: Is it really an effective procedure for all? *Knee* **14**(6), pp. 417-423.
Xiao, Z.C., Bartsch, U., Margolis, R.K., Rougon, G., Montag, D. and Schachner, M. (1997). Isolation of a Tenascin-R binding protein from mouse brain membranes: A phosphacan-related chondroitin sulfate proteoglycan. *Journal of Biological Chemistry* **272**(51), pp. 32092-32101.
Xie, H., Chen, S., Li, G. and Tseng, S. C. G. (2012). Isolation and expansion of human limbal stromal niche cells. *Investigative Ophthalmology and Visual Science* **53**(1), pp. 279-286.
Xie, H., Chen, S.Y., Li, G.G. and Tseng, S.C.G (2011). Limbal epithelial stem/progenitor cells attract stromal niche cells by SDF-1/CXCR4 signalling to prevent differentiation. *Stem Cells* **29**(11), pp.1874-1885.
Xu, C.Y., Zhang, W.S., Zhang, H., Cao, Y. and Zhou, H.Y. (2019). The role of connexin-43 in the inflammatory process: a new potential therapy to influence keratitis. *Journal of Opthalmology* **2019**, pp. 1-13.
Yadav, A.K., Sahasrabuddhe, A.A., Dimr, M., Bomi, P.V., Sainger, R. and Dimri, G.P. (2010). Deletion analysis of BMI1 oncoprotein identifies its negative regulatory domain. *Molecular Cancer* **9**(158), pp.1-13.
Yamada, K., Young, R.D., Lewis, P.N., Shinomiya, K., Meek, K.M., Kinoshita, S., Caterson, B. *et al.* (2015). Mesenchymal-epithelial cell interactions and proteoglycan matrix composition in the presumptive stem cell niche of the rabbit corneal limbus. *Molecular Vision* **21**, pp. 1328-1339.
Yamagami, S., Miyazaki, D., Ono, S.J. and Dana, M.R. (1999). Differential chemokine gene expression in corneal transplant rejection. *Investigative Opthalmology & Visual Science* **40**(12), pp. 2892-2897.

Yamagata, M., Kimata, K., Oike, Y., Tani, K., Maeda, N., Yoshida, K., Shimomura, Y. *et al.* (1987). A monoclonal antibody that specifically recognizes a glucuronic acid 2-sulfate-containing determinant in intact chondroitin sulfate chain. *Journal of Biological Chemistry* **262**(9), pp. 4161-4152.

Yamakoshi, Y. (2014). Dental and Oral Biology, Biochemistry. *Reference Module in Biomedical Sciences*, pp. 1-15.

Yamashita, M., Konishi, T. and Sato, T. (2015). Sclerotic rings in Mosasaurs (Squamata: Mosasauridae): structures and taxonomic diversity. *PloS one* 10, pp. 1-16.

Yanagashita, M., Midura, R.J. and Hascall, V.C. (1987). Proteoglycans: isolation and purification from tissue cultures, in: Methods in Enzymology: Academic Press: San Diego 138: pp. 279-287.

Yannas, I.V., Burke, J.F., Gordon, P.L., Huang, C. and Rubenstein, R.H. (1980). Design of an artificial skin. II. Control of chemical composition. *Journal of Biomedical Materials Research* **14**(2), pp. 107-132.

Yeung, A.M., Tint, N.L., Kulkarni, B.B., Mohammed, I., Suleman, H., Hopkinson, A. and Dua, H.S. (2009). Infant limbus: An immunohistochemical study. Experimental Eye Research **88**(6), pp. 1161–1164.

Yick, L., So, K.F., Cheung, P.T. and Wu, W.T. (2004). Lithium chloride reinforces the regeneration-promoting effect of chondroitinase ABC on rubrospinal neurons after spinal cord injury. *Journal of Neurotrauma* **21**(7), pp. 932-943.

Yick, LW., Cheung, P.T., So, K.F. and Wu, W. (2003). Axonal regeneration of Clarke's neurons beyond the spinal cord injury scar after treatment with chondroitinase ABC. *Experimental Neurology* **182**(1), pp. 160-168.

Yiu, G. and He, Z. (2006). Glial inhibition of CNS axon regeneration. *Nature Reviews Neuroscience* **7**, pp. 617-27.

Yogarajah, M., Matarin, M., Vollmar, C., Thompson, P.J., Duncan J.S., Symms, M., Moore, A.T. *et al.* (2016). PAX6, brain structure and function in human adults: advanced MRI in aniridia. *Annals of Clinical and Translational Neurology* **3**(5), pp. 314-330.

Yoon, J.J., Ismail, S. and Sherwin, T. (2014). Limbal stem cells: central concepts of corneal epithelial homeostasis. *World Journal of Stem Cells* **6**(4), pp. 391-403.

Yoshida, A., Kaburagi, Y. and Hishiyama, Y. (2016). Scanning Electron Microscopy. *Materials Science and Engineering of Carbon*, pp.71-93.

Yoshida, S., Shimmura, S., Nagoshi, N., Fukuda, K., Matsuzaki, Y., Okano, H. and Tsubota, K. (2006). Isolation of multipotent neural crest-derived stem cells from the adult mouse cornea. *Stem Cells* **24**(12), pp. 2714-2722.

Yoshida, S., Shimmura, S., Shimazaki, J., Shinozaki, N. and Tsubota, K. (2005). Serum-free spheroid culture of mouse corneal keratocytes. *Investigative Ophthalmology and Visual Science* **46**(5), pp. 1653-1658.

Young, R.D., Knupp, C., Koudouna, E., Ralphs, J.R., Ma, Y., Lwigale, P.Y. and Jester J.V. (2020). Observations of nascent matrix structures in embryonic cornea: important in cell interactions, or merely vestiges of the lens surface? *Archives of Clinical and Experimental Opthalmology* **2**(2), pp. 67-72.

Yu, Y-R., O'Koren, E.G., Hotten, D.F. and Kan, M.J. (2016). A protocol for the comprehensive flow cytometric analysis of immune cells in normal and inflamed murine non-lymphoid tissues. *PLos ONE* **11**(3), e015060.

Yuan, X., Chen, Z., Yang, Z., Gao, J., Zhang, A., Wu, S.M. and Jacoby, R. (2009). Expression pattern of connexins in the corneal and limbal epithelium of primates. *Cornea* **28**(2), pp. 194-199.

Zeiss.com. 2019. *ZEISS SIGMA field emission scanning electron microscope*. Available at: https://www.zeiss.com/microscopy/int/products/scanning-electron-microscopes/sigma.html [Accessed 16 Sep. 2019].

Zhai, J., Wang, Q., Tao, L. (2014). Connexin expression patterns in diseased human corneas. *Experimental and Therapeutic Medicine* **7**(4), pp.791-798.

Zhang, X., Huang, C.T., Pankratz, M.T., Xi, J., Li, J., Yang, Y., Lavaute, T.M. *et al.* (2010a). Pax6 is a human neuroectoderm cell fate determinant. *Cell Stem Cell* **7**(1), pp.90-100.

Zhang, X., Sun, H., Li, X., Yuan, X., Zhang, Lei. And Zhao, S. (2010b). Utilization of human limbal mesenchymal cells as feeder layers for human limbal stem cells cultured on amniotic membrane. *Journal of Tissue Engineering and Regenerative Medicine* **4**(1), pp.38–44

Zhang, Y., Conrad, A.H., Tasheva, E.S., An, K., Corpus, L.M., Kariya, Y., Suzuki, K. *et al.* (2005). Detection and quantification of sulfated disaccharides from keratan sulfate and chondroitin/dermatan sulfate during chick corneal development by ESI-MS/MS. *Investigative Ophthalmology and Visual Science* **46**(5), pp. 1604 –1614.

Zhao, Y. and Ma, L. (2015). Systematic review and meta-analysis on transplantation of ex vivo cultivated limbal epithelial stem cell on amniotic membrane in limbal stem cell deficiency. *Cornea* **34**(5), pp. 592-600.

Zhou, J., Nagarkatti, P., Zhong, Y. and Nagarkatti, M. (2010). Immune modulation by chondroitin sulfate and its degraded disaccharide product in the development of an experimental model of multiple sclerosis. *Journal of Neuroimmunology* **223**(1-2), pp. 55-64.

Zuba-Surma, E.K., Kucia, M., Abdel-Latif, A., Lillard, J.W. and Ratajczak, M.Z. (2007). The ImageStream System: a key step to a new era in imaging. *Folia Histochemica et Cytobiologica* **45**(4), pp. 279-290.